Photoactive Platinum Azide Anticancer Complexes

A Thesis Submitted for the Degree of

Doctor of Philosophy

by

Fiona S. Mackay, *MChem.*

School of Chemistry

Faculty of Science and Engineering

University of Edinburgh

May 2006

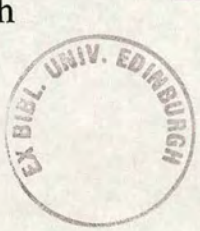

Abstract

Photoactive platinum compounds have the potential to reduce some of the debilitating side-effects associated with conventional chemotherapeutics, such as cisplatin. Stable, inert platinum(IV) compounds which are reduced to active platinum(II) species only upon irradiation, could provide a site-specific treatment.

The Pt^{IV} azide complexes, *cis, trans, cis*-$[Pt(N_3)_2(OH)_2(NH_3)_2]$ and *cis, trans*-$[Pt(en)(N_3)_2(OH)_2]$, have previously been shown to be stable in the dark but reduced to Pt^{II} upon irradiation. The synthesis and characterisation of new platinum azide compounds, designed to improve important properties such as solubility and wavelength of absorbance are described here. Complexes which have azide ligands in a *trans* position were synthesised, the general formula is *trans, trans, trans*-$[Pt(N_3)_2(OH)_2(NH_3)R]$ where R is NH_3, pyridine, methylamine, ethylamine, thiazole, 2-picoline, 3-picoline, 4-picoline or cyclohexylamine. Several Pt^{IV} diazido compounds containing chelating aromatic ligands, such as 2,2′-bipyridine and 1,10-phenanthroline were also prepared. Many of the novel compounds synthesised were characterised by X-ray structure determination. The complexes with *trans* azides generally showed improved water solubility as well as a shift of the main absorbance band towards the visible region, compared to their *cis* analogues.

The photochemistry of these Pt^{IV} azide compounds was investigated by UV-visible spectroscopy, NMR spectroscopy and mass spectrometry. Several compounds were synthesised with ^{15}N-labels which allowed the reactions to be followed by 2D $[^1H,^{15}N]$ HSQC NMR spectroscopy. Photoreactions in the presence of nucleotides such as 5′-GMP and d(GpG) were also studied. Reduction and binding to 5′-GMP was observed after only 1 min of irradiation for some complexes.

A transcription mapping study of a fragment of pSP73KB plasmid DNA treated with *cis, trans*-$[Pt(en)(N_3)_2(OH)_2]$ and visible light, has shown that platination mainly occurs at consecutive guanine bases. The major binding sites were similar to those of cisplatin. No platination was seen in an identical sample which was not irradiated.

Two-photon excitation (TPE) involves the simultaneous absorption of two photons to produce an excited state which corresponds to absorption of a single photon of approximately twice the energy (half the wavelength). This technique could potentially enable the use of red light to activate compounds which mainly absorb in the blue / UV region. The two-photon photochemistry of an azo-dye was investigated to determine the optimum experimental conditions. The *trans* to *cis* photoisomerisation was followed by ^{1}H NMR spectroscopy. The rate constants for the one- and two-photon reactions are of a similar magnitude, which suggests that the two-photon induced reaction closely mimics the one-photon process. Attempts were made to apply TPE to photoactive platinum compounds.

Acknowledgements

I would like to thank Professor Peter J. Sadler for his supervision and encouragement throughout my project. I am grateful to him for all his help and advice, and for everything he has taught me.

I would also like to thank Dr. Philippe Müller who started this project and introduced me to the subject. I am very grateful for the time and effort he kindly took to do this.

Many thanks are due to Dr. Simon Parsons and his group members, especially Dr. Stephen Moggach, for their efficient X-ray structure determination service.

Thanks are also due to Dr. Steven Magennis and Dr. Anita Jones who were involved in the multiphoton work and taught me many new things about this technique. I am very grateful to Dr. Steven Magennis whose ideas and interest helped further the project.

I would also like to thank Dr. Julie Woods and Dr. Karen Harper for the *in vitro* cell testing results, and all the hard work this involved. Thanks are also due to Professor Patrick Bednarski, for both his enthusiasm for the project which has helped to produce some new exciting results and also for his warm hospitality when I visited his laboratory in 2002. I would also like to thank Professor Viktor Brabec and Dr. Jana Kašpárková for stimulating discussions and for carrying out some very important DNA studies.

I would like to thank Juraj Bella for assistance with NMR experiments, and the whole of the PJS group for all their friendship, help and support. Special thanks are due to Dr. Abraha Habtemariam for all his advice and encouragement throughout my project. I would also like to express my thanks to Anna Peacock, Dr. Tina Hunter and Dr. Ana Pizarro who have all been a constant source of support and fun, I am very grateful for their friendship over the years.

I would like to thank the EPSRC and the University of Edinburgh for financial support, and also the EC COST programme for giving me the opportunity to present my work at conferences. I would also like to thank the University of Edinburgh Development Trust which enabled me to present work at a conference in the United States.

Very special thanks are due to my parents for their invaluable support and constant encouragement along the way, and finally my sincere thanks go to Damien for all his patience and for always being there for me.

Contents

Abbreviations

bpy	2,2′-bipyridine
bp	base pair
c-HexNH_2	cyclohexylamine
CT	calf thymus
CTTS	charge-transfer-to-solvent
d(GpG)	2′-deoxyguanylyl (3′ → 5′) -2′-deoxyguanosine
EBSS	Earle's balanced salt solution
en	ethylenediamine
ESI-MS	electrospray ionisation mass spectrometry
9-EtG	9-ethylguanine
EtNH_2	ethylamine
FAAS	flameless atomic absorption spectroscopy
fs	femtosecond
FWHM	full width half maximum
5′-GMP	guanosine 5′-monophosphate
GSH	reduced glutathione
GSSG	oxidised glutathione
HMG	high mobility group
HOMO	highest occupied molecular orbital
HSQC	heteronuclear single-quantum coherence
IC	internal conversion
IL	intraligand
ISC	intersystem crossing
LF	ligand field
LMCT	ligand-to-metal charge-transfer
LUMO	lowest unoccupied molecular orbital
MeNH_2	methylamine
MLCT	metal-to-ligand charge-transfer
MO	molecular orbital
mol eq	molar equivalent

OAc	acetate
OPE	one-photon excitation
OPO	optical parametric oscillator
PDT	photodynamic therapy
phen	1,10-phenanthroline
pic	picoline
py	pyridine
TPE	two-photon excitation
tz	thiazole
Watergate	water suppression by gradient-tailored excitation

Chapter 1

Introduction

This thesis is concerned with platinum(IV) azide complexes as potential photoactivated anticancer drugs. An introduction to the coordination chemistry of platinum, platinum anticancer drugs and platinum photochemistry is given in this chapter.

1.1 Platinum

Platinum is in group 10 of the periodic table, it has atomic number 78 and is found in six naturally occurring isotopes (Table 1.1). ^{195}Pt has a nuclear spin quantum number ½ and is therefore NMR active.

Table 1.1 Atomic and physical properties of platinum.

Atomic Number	78
Isotopes	^{190}Pt (0.01 %) ^{192}Pt (0.78 %) ^{194}Pt (32.9 %) ^{195}Pt (33.8 %) ^{196}Pt (25.3 %) ^{198}Pt (7.21 %)
Atomic Weight	195.078(2)
Electronic Configuration	[Xe] $4f^{14}$ $5d^{9}$ $6s^{1}$
Electronegativity	2.2
Effective Ionic Radius (Oxidation State)	0.57 Å (V) 0.63 Å (IV) 0.80 Å (II)

The abundance of platinum in the earth's crust is approximately 0.01 ppm. Platinum is usually recovered from nickel or copper sulphide ores, and then has to be selectively extracted from other "Platinum Group" metals (ruthenium, rhodium, palladium, osmium and iridium). Although these metals occur together, the cost of the individual metals varies widely, as their consumption is not proportional to their abundance. The world's major deposits are found in Bushveld in South Africa, Sudbury in Canada and Noril'sk Talnakh in Russia.

Platinum compounds in the +2 and +4 oxidation states are by far the most common, although complexes in the 0, +1, +3, +5 and +6 states are also known. Compounds in the 0 oxidation state often contain π-acceptor ligands, such as PR_3 or CO. The higher oxidation states (+5 and +6) have only been found in a few fluoro and oxyfluoro compounds.[1]

1.1.1 Coordination Chemistry of Platinum

Platinum(II) complexes are d^8, diamagnetic and virtually always square-planar due to the strong splitting of the d-orbitals (Figure 1.1). All eight electrons can be placed in the four lower energy orbitals which leaves the uppermost orbital ($d_{x^2-y^2}$) empty. As a third row transition metal, the d-orbital splitting is sufficient to offset the energy required to pair-up two electrons (Figure 1.1). Pt^{II} shows class-b / soft characteristics and therefore prefers heavy donor atoms such as PR_3 or I^-.

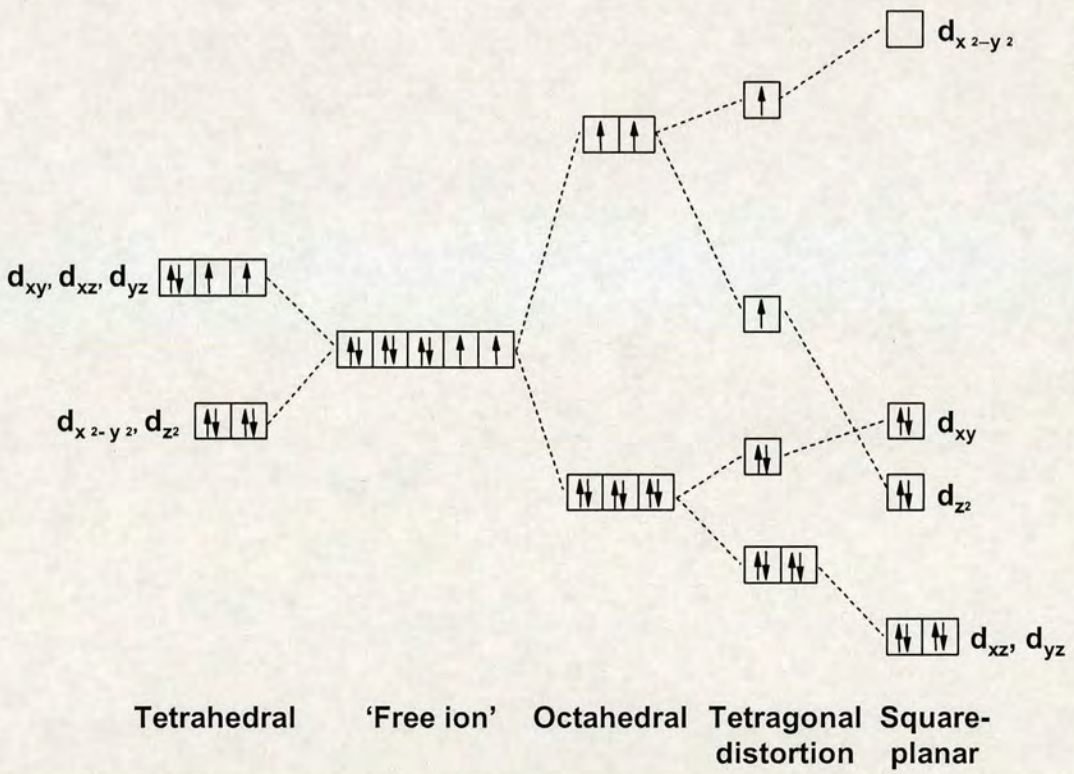

Figure 1.1 Splitting of the d-orbitals in crystal fields of different symmetries, and the resulting electronic configurations of a d^8 ion.

An important feature of coordination chemistry, which is widely used in the synthesis of square-planar complexes is the *trans* effect. The *trans* effect is defined as the effect of the ligand on the rate of substitution of the group *trans* to it.[2] By comparison with a large number of reactions, it is possible to set up a *trans*-directing series. The ordering of ligands in this series is as follows:[3]

$$CO, CN^-, C_2H_4 > PR_3, H^- > CH_3^- > C_6H_5^-, NO_2^-, I^-, SCN^- > Br^-, Cl^- > py, NH_3, OH^-, H_2O$$

This order roughly correlates with the degree of increasing overlap of the ligand orbitals with either a σ or a π Pt 6*p* orbital, therefore the greater the overlap the stronger the *trans* effect.[4] The trans effect is kinetically controlled as the thermodynamically most stable isomer is not always produced. Synthetic use of the *trans* effect is illustrated later in the preparation of square-planar Pt^{II} starting materials (Chapter 3).

Another important phenomenon is the thermodynamic *trans* influence. This effect is greatest for ligands which are strong σ-donors and the ordering of the ligands in the series is as follows:

$$H^- > PR_3 > SCN^- > I^-, CH_3^-, CO, CN^- > Br^- > Cl^- > NH_3 > OH^-$$

The *trans* influence is the extent to which a ligand weakens the bond *trans* to itself, and can affect properties such as metal-ligand bond lengths and NMR coupling constants.

Pt^{IV} complexes are octahedral, diamagnetic and have a low-spin t_{2g}^6 electron configuration. They generally display class-a or hard characteristics, and compounds containing halides, pseudohalides and N-donors are particularly abundant. Compared to Pt^{II}, Pt^{IV} complexes are generally more thermodynamically stable and kinetically inert.

1.2 Platinum Anticancer Drugs

1.2.1 Cisplatin

Cis-[$Pt^{II}Cl_2(NH_3)_2$] (Figure 1.2), now better known as cisplatin, was first synthesised in 1845, but its biological activity was not discovered until the 1960's.[5] It was approved for clinical use in 1978 and has gone on to be one of the most widely used and effective anticancer drugs in the world. Cisplatin is used to treat various types of cancer, including testicular, ovarian, cervical, bladder and head and neck cancers.[6] Its use against testicular cancer has turned this disease from one which killed about 80 % of patients, to one which is now more than 90 % curable.[7]

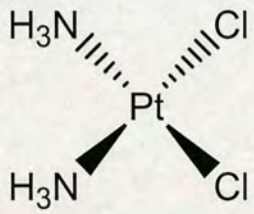

Figure 1.2 Structure of cisplatin.

There are, however, some serous drawbacks associated with cisplatin chemotherapy, these include (i) severe toxicity (e.g. nausea, ear damage, vomiting, loss of sensation in hands and kidney toxicity), (ii) poor solubility in saline and (iii) resistance to the drug, either intrinsic or acquired. Cisplatin is also only effective in quite a narrow range of tumours. The design of new platinum drugs to circumvent some of these problems has been the subject of a great deal of research (Section 1.2.2).

Cisplatin is administered by injection or infusion, and while it is transported in the blood stream hydrolysis is inhibited due to the relatively high chloride concentration in blood (ca. 100 mM). The precise mechanism of cellular uptake still remains unclear. There are some data to suggest that cisplatin enters the cell via passive diffusion,[8] although there is also evidence for an additional pathway involving active transport, and an altered expression of some membrane proteins has been reported for cisplatin-resistant cells.[9,10] Upon entering the cell the chloride concentration drops to 4 – 25 mM, and cisplatin is hydrolysed to *cis*-$[PtCl(NH_3)_2(H_2O)]^+$ and *cis*-$[Pt(NH_3)_2(H_2O)_2]^{2+}$, which are more active forms of the

drug.[11] These aqua species go on to react with DNA mainly at the N7 position of consecutive guanine bases to form 1,2-intrastrand cross-links.[12] It is now generally accepted that cisplatin exerts it cytotoxic effect by forming these bifunctional DNA-adducts. These adducts are capable of blocking replication and inhibiting transcription. The *cis*-$\{Pt(NH_3)_2\}^{2+}$ moiety can also bind to proteins.[12] Some of the important events relating to the mechanism of action of cisplatin and cellular resistance are summarised in Figure 1.3.

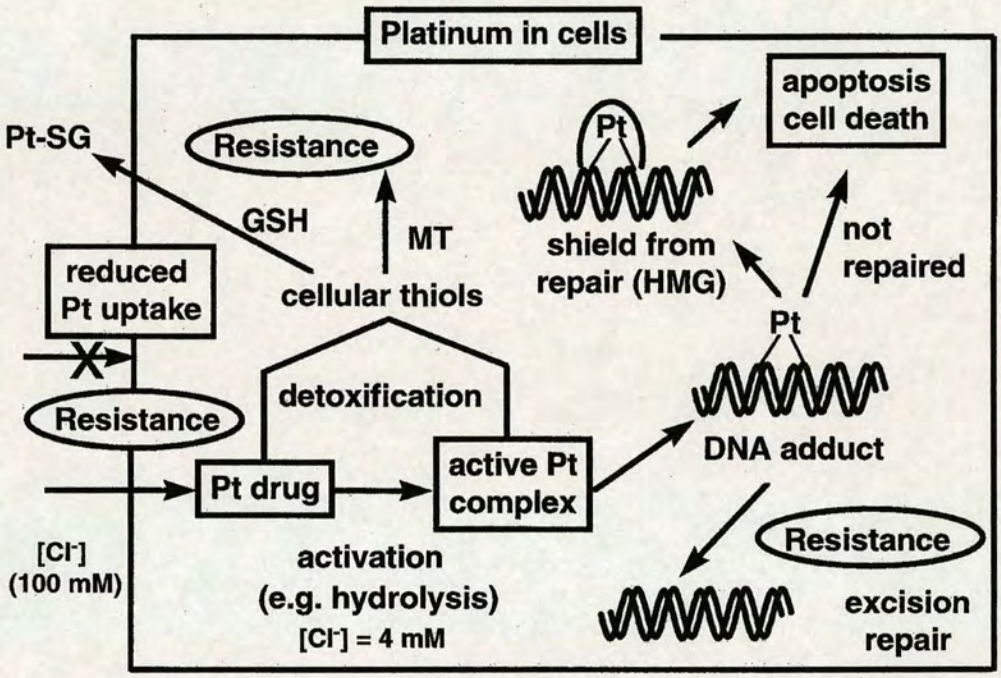

Figure 1.3 Schematic representation of the reactions of cisplatin in the cell. Based on reference 13.

Hydrolysis is known to be the rate limiting step in the binding of cisplatin to DNA.[14] A summary of the hydrolysis reactions, including half lives of aquation,[15] and pK_a values[16] is given in Figure 1.4.

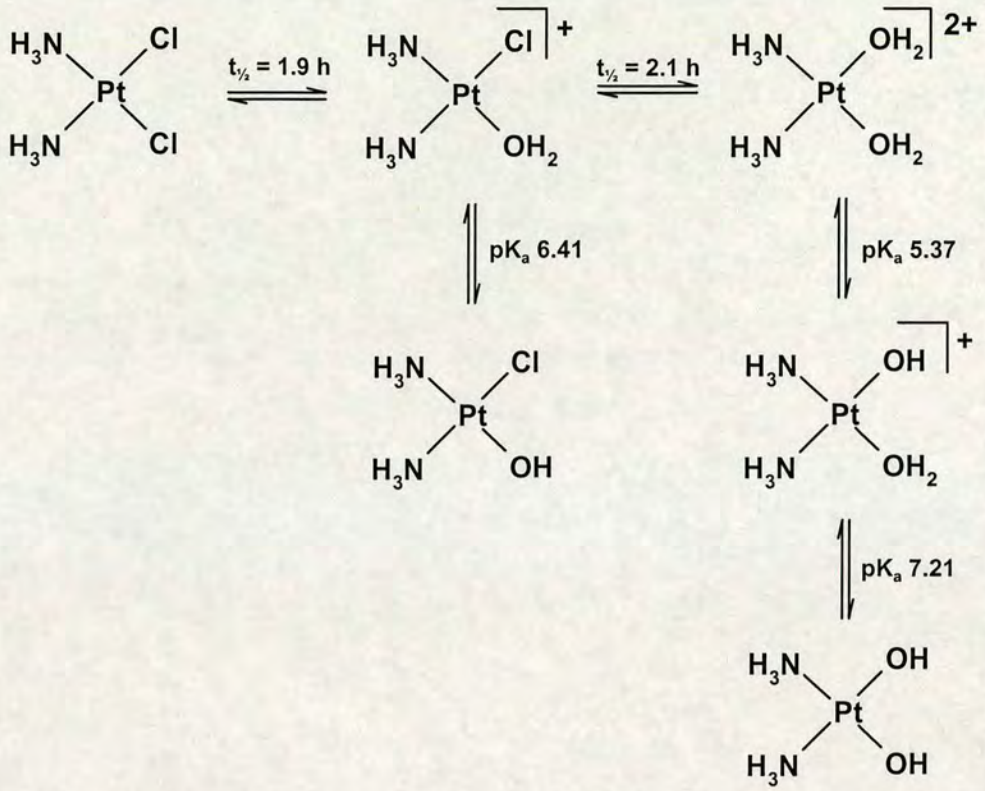

Figure 1.4 Hydrolysis of cisplatin in aqueous solution with half-lives for hydrolysis (310 K)[15] and pK_a values (300 K)[16] of its aqua adducts.

There are a large number of potential biological targets for platinum compounds. The hard-soft acid-base principle indicates S-donor ligands in proteins would bind strongly and give very stable bonds, however binding to nitrogen lone pairs would also be expected to be strong. Such bonds could be formed with the amino acid side chains of cysteine, methionine, histidine, and also the solvent-exposed N7 atoms of adenine and guanine in double-stranded DNA. The N3 atoms of cytosine and N1 of adenine would be additionally accessible in single-stranded DNA and RNA.[17]

Approximately 1 % of intracellular cisplatin reacts with genomic DNA and produces a variety of mono-adducts and intra- and interstrand cross-links. The most nucleophilic site in duplex DNA is the N7 position of a guanine residue located adjacent to a second guanine residue.[18] It has been shown that binding at N7 of two adjacent guanines to form intrastrand d(GpG) cross-links is the preferred binding site of cisplatin.[19] Besides GG intrastrand cross-links (70 %), the other major DNA adducts of cisplatin are intrastrand AG (but not GA) cross-links (15 %). Minor

adducts include 1,3-intrastrand and interstrand cross-links involving two non-neighbouring guanines.[19]

Many structural studies have been carried out to determine the nature of this 1,2-intrastrand cisplatin adduct on double and single-stranded DNA fragments, both by X-ray crystallography,[20-22] and NMR spectroscopy.[23-25] The X-ray structure of the Pt adduct of a double-stranded dodecamer has been determined and is shown in Figure 1.5. The basic structure is kinked with a significant bend towards the major groove (ca. 45 °), and the dihedral angle between the guanine bases is 30 °. A consequence of the platinum binding is a widened shallow minor groove, a feature which may be important for protein recognition and anticancer activity.

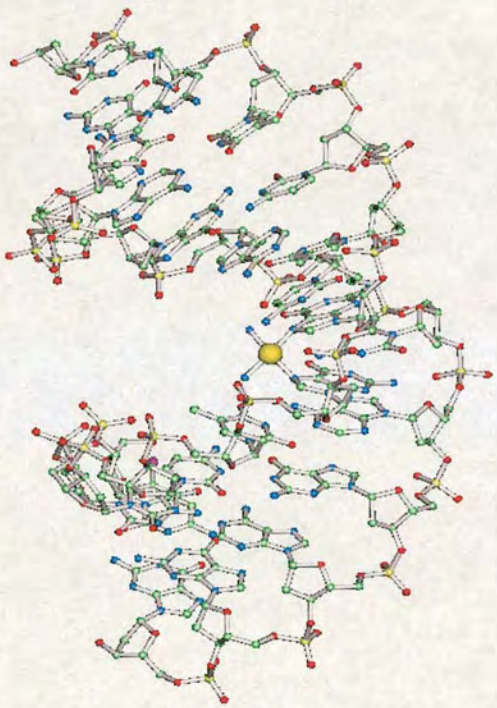

Figure 1.5 X-ray crystal structure of a dodecamer platinated with $\{Pt(NH_3)_2\}^{2+}$. The sequence of the duplex is d(CCTCTG*G*TCTCC), d(GGAGACCAGAGG); where G* indicates the G residue is platinated at N7.[21]

The discovery of a protein that preferentially binds to cisplatin-damaged DNA, the high mobility group (HMG) protein,[26] has led to the identification of many more such proteins which have similar binding affinities towards cisplatin-modified

DNA.[12] An X-ray crystal structure of HMG1 protein domain A bound to a 16-mer strand of duplex DNA containing a *cis*-GG adduct has been determined.[27] It is thought that the HMG protein specifically recognises locally bent and unwound DNA, and that this protein binding could shield DNA repair and ultimately lead to cell apoptosis.

Drug resistance is a major complication in cancer chemotherapy. Cisplatin resistance exists in two forms: acquired resistance, in which a drug is initially beneficial but becomes ineffective over time, and intrinsic resistance, in which the drug is ineffective from the outset. Drug resistance can operate by a number of mechanisms, none of which is fully understood. Suggested mechanisms of cisplatin drug resistance include decreased intracellular accumulation of cisplatin, increased intracellular levels of certain sulfur-containing macromolecules, and increased DNA repair.[28,29]

1.2.2 Development of New Platinum Anticancer Drugs

The design of new platinum drugs to circumvent some of the problems associated with cisplatin, such as toxic side effects, resistance and poor solubility in saline, has been the subject of a great deal of research. Indeed over 3000 platinum compounds have been synthesised and tested for antitumour activity,[12] but of these only a few have made it into clinical trials,[30] and there are currently six platinum drugs approved (in at least one country) for clinical use.[31]

1.2.2.1 Cisplatin Derivatives

Carboplatin (Figure 1.6a), like cisplatin, has achieved routine clinical use. It is more stable towards biomolecules because of the chelating 1,1-cyclobutanedicarboxylato ligand, and this stability is believed to be the reason carboplatin can be tolerated in higher doses than cisplatin (2000 mg / dose compared to 100 mg / dose for cisplatin).[17] Carboplatin shows an identical spectrum of activity to that of cisplatin, but lacks nephrotoxicity in standard doses; neurotoxicity, ototoxicity and gastrointestinal effects are also less pronounced.

Oxaliplatin (Figure 1.6b), was approved for clinical use in major European countries in 1999.[31] It has shown some potency in tumours that are resistant to cisplatin and carboplatin, and is now the standard first line treatment for metastatic colorectal cancer.[32] The dose-limiting toxicity of oxaliplatin is neurotoxicity.

Nedaplatin (Figure 1.6c) has been approved for clinical use in Japan, and like carboplatin myleosuppression is the dose-limiting toxicity. Unlike oxaliplatin, nedaplatin shows cross-resistance with cisplatin and carboplatin.[33] This can be attributed to the fact that these drugs all form the same type of DNA adducts.

Loboplatin (Figure 1.6d) and heptaplatin (Figure 1.6e) have been approved in China and South Korea, respectively.[31] Loboplatin is used against small cell lung cancer, breast tumours and chronic myelogenous leukaemia. Heptaplatin is used to treat gastric cancer, but nephrotoxicity is a major dose-limiting factor.

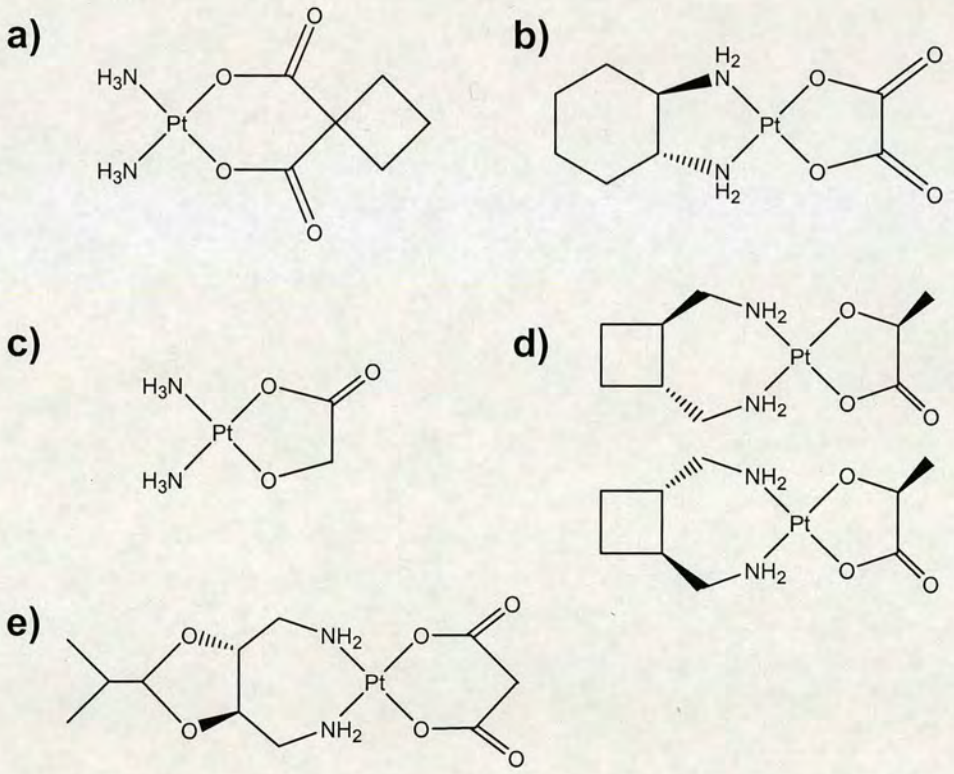

Figure 1.6 Structures of platinum drugs approved for clinical use.[31] a) Carboplatin, b) oxaliplatin, c) nedaplatin, d) lobaplatin and e) heptaplatin.

NX473 (formerly AMD473, ZD0473, Figure 1.7a) is currently in Phase I / II clinical trials, and has shown promising activity against a range of tumour types, including ovarian, lung and breast. Interestingly it has also shown significantly reduced cross resistance with cisplatin. The steric hindrance caused by the methyl group is believed to destabilize the trigonal bipyramidal transition state formed during substitution reactions. This reduces the rate of deactivation by biological thiols,[34,35] and is also believed to result in the formation of DNA-adducts which are recognised differently from those of cisplatin by the excision repair system.[36]

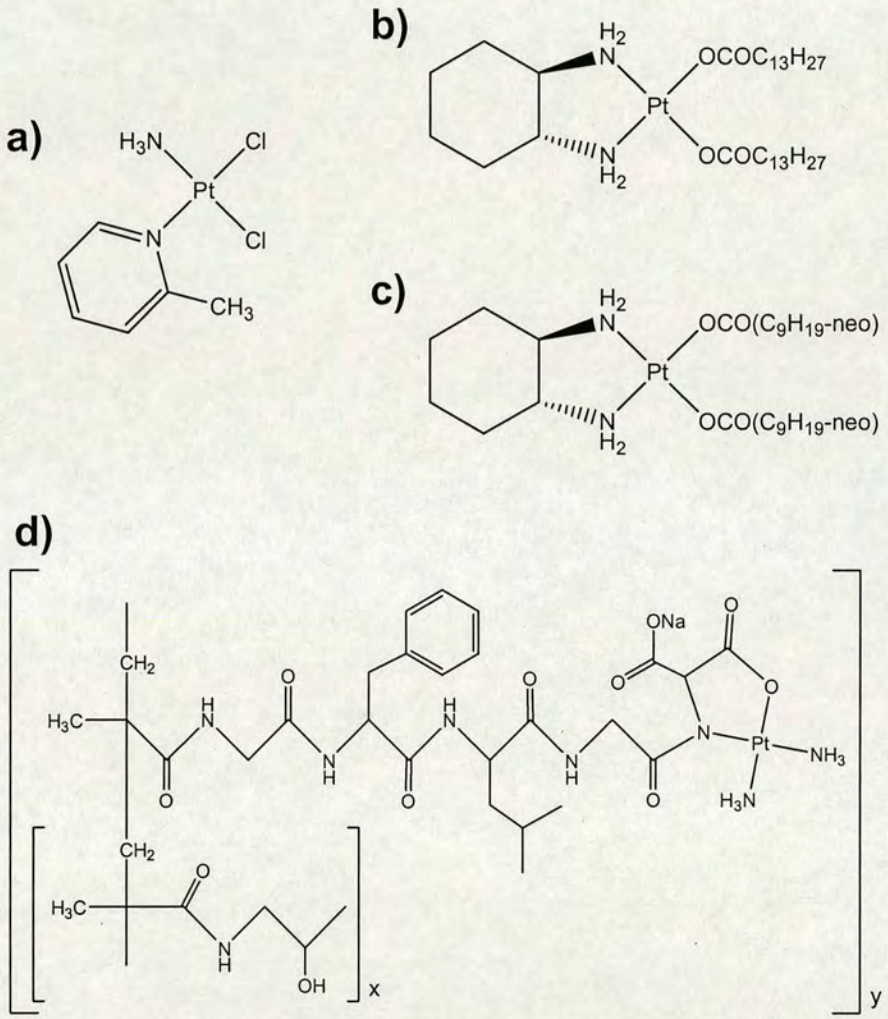

Figure 1.7 Structures of some platinum(II) complexes currently in clinical trials. a) NX473, b) SM-11355, c) aroplatin (L-NDDP) and d) AP5280.

Several other platinum(II) compounds are currently in clinical trials, including three which are based on a targeted therapy approach, where the aim is for the platinum to be selectively accumulated in the tumour. These compounds are SM11355, aroplatin (L-NDDP) and AP5280, and their structures are shown in Figure 1.7. For a comprehensive review of the current state of preclinical platinum anticancer complexes see reference 31.

1.2.2.2 Pt^{IV} Complexes

Platinum(IV) complexes, such as *cis*-$[PtCl_4(NH_3)_2]$ (Figure 1.8a), have been known to have anticancer activity since the early studies by Rosenberg and co-workers.[37,38] It is generally accepted that reduction of Pt^{IV} complexes to their Pt^{II} counterparts is required for activity, this has been discussed in detail in a recent review.[39] Pt^{IV} complexes offer several advantages over their Pt^{II} analogues, these include (i) the possibility of oral administration, (ii) reduced side-effects, (iii) reduced reactivity, (iv) more possibilities of structural variations and (v) reduction to more reactive platinum(II) compounds. It is therefore surprising that only three Pt^{IV} anticancer complexes have entered clinical trials; satraplatin (JM216), tetraplatin (ormaplatin) and iproplatin (Figure 1.8). Trials of tetraplatin and iproplatin were abandoned due to severe neurotoxicity and lack of superior performance, respectively.[40] Satraplatin entered clinical trials in 1992; it is a lipophilic complex which can be administered orally. Oral administration opens the possibility for an outpatient treatment, which is also beneficial in terms of cost. *In vitro*, satraplatin is capable of circumventing both intrinsic and acquired cisplatin resistance; interestingly this has been shown to occur by a mechanism not related to the initial extent of DNA platination.[41] The lipophilic nature of satraplatin could help overcome resistance caused by reduced platinum accumulation.[30] Phase III studies comparing satraplatin plus prednisone (a corticosteroid), with prednisone alone are underway. Phase I / II trials combining satraplatin with radiation therapy have also begun.[31]

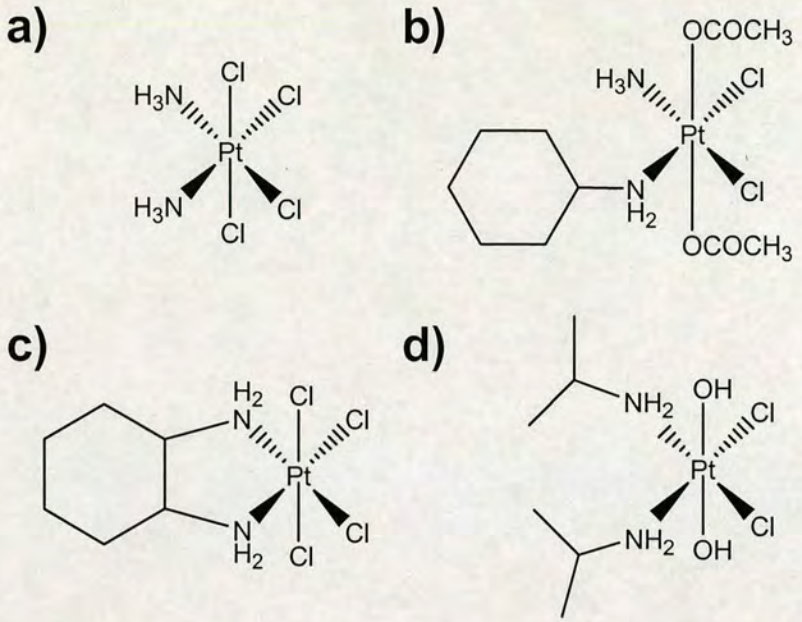

Figure 1.8 Structures of antitumour active Pt^{IV} complexes. a) *cis*-$[PtCl_4(NH_3)_2]$, b) satraplatin (JM216), c) tetraplatin (ormaplatin) and d) iproplatin.

Pt^{IV} complexes are much more inert to ligand substitution than Pt^{II} complexes.[42] This kinetic inertness means that loss of the drug through deactivating reactions with biomolecules could be reduced, and unwanted side reactions which lead to toxic side-effects could potentially be avoided. It is not yet known whether Pt^{IV} complexes are reduced extra- or intra-cellularly *in vivo*. Upon reduction the axial ligands are lost and the resulting Pt^{II} complex will be less lipophilic (decreased cell uptake) and much more reactive (increased toxicity). Therefore the *in vivo* anticancer activity of Pt^{IV} complexes is difficult to predict from *in vitro* studies.

Pt^{IV} 5′-GMP adducts have been reported in the literature, but only as minor products.[43] Evidence was found of an intermediate 5′-GMP adduct of tetraplatin which was then rapidly reduced to a Pt^{II} adduct by 5′-GMP. More recently, Galanski *et al.* described the formation of a Pt^{IV}-5′-GMP adduct from the reaction of $[Pt(en)(OAc)_4]$ with 5′-GMP, this adduct was reported to be stable over several weeks without reduction.[44]

If reduction is necessary for activity, it seems logical that the ease of reduction of a Pt^{IV} complex influences its biological behaviour. The reduction potentials of many Pt^{IV} compounds have been compared,[39] and a general trend established. Complexes containing chlorides in the axial position are easily reduced, whereas if these are replaced by hydroxides the analogous complex becomes significantly harder to reduce. The reduction potentials of complexes with axial carboxylato ligands fall somewhere in between those of chloride and hydroxide. Changing these ligands also affects the lipophilicity of the complexes. Cyclic voltammetry (CV) is generally used to measure reduction potentials (E_p) of platinum (IV) complexes, but reduction results in loss of ligands and so the process is irreversible, and the E_p values obtained by CV are not thermodynamic. However, a correlation between E_p and reduction rates has been established.[39]

Biomolecules in blood and cells are numerous and diverse, in both structure and chemical activity. Many of these small molecules, proteins and enzymes have the potential to react with Pt^{IV} complexes and reduce them. Glutathione (GSH) is a tripeptide found in cells at concentrations of up to 10 mM.[45] GSH is one of the primary defenses against toxins and oxidants in cells, and can deactivate chemotherapeutic drugs such as cisplatin by coordinating to them and thereby reducing the amount of active species that arrives at the target site (DNA). It is therefore important to understand the kinetics and mechanisms of reduction of Pt^{IV} complexes by thiols (e.g. GSH) and other biomolecules; several such studies have been published.[46-50]

1.2.2.3 Trans Platinum Complexes

All the complexes approved for clinical use so far, adhere to a set of structure-activity relationships which were derived by Cleare and Hoeschele over 30 years ago.[51] These relationships were formulated from early systematic studies, and state that for a platinum complex to show antitumour activity it has to have the following features.

1. *Cis* geometry of the form $PtX_2(amine)_2$ for Pt^{II}, and $PtX_2(amine)_2Y_2$ for Pt^{IV}, (with Y ligands *trans*).

2. The X ligand (leaving group) should be an anion with intermediate binding strength such as Cl^-, citrate, oxalate, and other carboxylic acid residues. The Y ligands can be Cl^-, OH^- or $O(CO)C_nH_{2n+1}$.
3. The complex should be neutral, as passive transport through the lipophilic cell wall is believed to be the mechanism of cell uptake, a pathway which is less available to charged compounds.
4. The amine should possess at least one NH moiety, necessary for H-bonding interactions with DNA.

These structure-activity relationships dominated platinum drug design for over 20 years. However, recently so-called "non-classical" platinum complexes have been developed which violate and in some cases invert these rules. Such complexes include those with *trans* geometry, charged complexes, complexes with more than two coordinated nitrogens, multinuclear complexes, compounds with sulphur ligands and platinum complexes with tertiary amine ligands.[31] Some of these are discussed below with particular attention paid to *trans* complexes due to the relevance to this work.

The *trans* isomer of cisplatin, *trans*-$[PtCl_2(NH_3)_2]$ (transplatin, Figure 1.9a) is relatively non-toxic to cancer cells.[52] The first chloride of transplatin is very labile, and so monofunctional adducts are quickly formed. However, removal / substitution of the second chloride to form bifunctional adducts is much more difficult. The rapid formation of monofunctional adducts with biomolecules could lead to deactivation of transplatin before it reaches the cell nucleus. The *trans* geometry also prevents the formation of GG intrastrand cross-links of the type formed by cisplatin.

There are four known classes of antitumour active mononuclear *trans* compounds.[53] These are Pt^{II} complexes with planar aromatic ligands (Figure 1.9b), with asymmetric aliphatic amine ligands (Figure 1.9c), iminoether compounds (Figure 1.9d), and Pt^{IV} mixed amine complexes.

For the complexes with planar aromatic ligands, three different series of *trans*-

$[PtCl_2(L)(L')]$ have been investigated as potential anticancer agents.[54] i) L = L′ = pyridine, *N*-methylimidazole, or thiazole, ii) L = quinoline and L′ = RR′SO (R = Me, R′ = Me, Benzyl or Phenyl), and iii) L = NH_3 and L′ = quinoline or thiazole. The cytotoxicity of all the *trans* complexes examined was approximately one-order of magnitude larger than that of transplatin, and was also generally at least as cytotoxic as the *cis* analogues. The *trans* complexes were generally not cross-resistant with cisplatin. The planar ligands are likely to hinder the approach of incoming nucleophiles to the axial positions of the platinum centre, which may have some effect not only on DNA binding, but also on deactivation by glutathione and other sulphur-containing biomolecules.

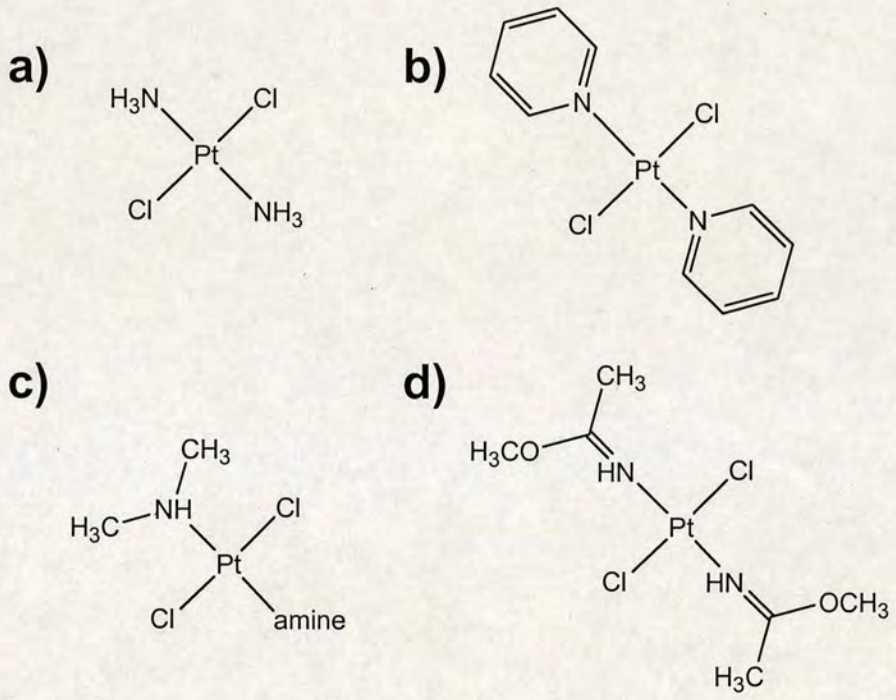

Figure 1.9 Structures of *trans*-Pt^{II} complexes. a) transplatin, b) *trans*-$[PtCl_2(py)_2]$, c) *trans*-[$PtCl_2$(dimethylamine)(amine)] and d) *trans*-$[PtCl_2(iminoether)_2]$.

Trans platinum(II) complexes containing asymmetric aliphatic amines, such as *trans*-[$PtCl_2$(amine)(isopropylamine)], have shown cytotoxic activity comparable to that of cisplatin.[55,56] In HL-60 leukaemic cells these compounds have IC_{50} values lower than that of cisplatin.

The *trans* iminoether complexes reported by Coluccia and Natile have the general formula *trans*-[$PtCl_2$(iminoether)$_2$] or *trans*-[$PtCl_2$(iminoether)(NH_3)] (iminoether, HN=C(OR)R′).[57-59] Iminoether ligands are planar, like aromatic amines, but have one hydrogen linked to the nitrogen like aliphatic amines. The hydrogen is suitable for hydrogen-bond formation. There is also the possibility of isomerisation within the ligand, *E* or *Z* configurations around the C=N double bond can exist. The *trans*-iminoether complexes have shown growth inhibitory activity similar to that of cisplatin in various cell lines, and were also active against a cisplatin resistant cell line.[60]

Trans-Pt^{IV}-mixed amine complexes have also been found to be antitumour active.[61] An extensive investigation into the activity of over forty complexes with *trans* geometry, half Pt^{II} and half Pt^{IV}, has been carried out. [61] Many of these compounds were found to have an activity comparable to cisplatin against a panel of human cell lines, some also overcame cisplatin resistance. Fourteen complexes were also active *in vivo*, all of which were Pt^{IV}, and all except one contained axial hydroxide ligands.[61]

1.2.2.4 Multinuclear Platinum Complexes

Dinuclear and trinuclear compounds are a relatively new class of platinum anticancer complex. They provide multiple binding sites to DNA, which can be separated by linkers of variable lengths. Farrell and co-workers developed BBR3005 (Figure 1.10a) which contains two monofunctional platinum moieties with a hexane-1,6-diamine linker. BBR3005 was found to be active in cisplatin-resistant cell lines, and this work led to the synthesis of the trinuclear complex, BBR3464 (Figure 1.10b). The third platinum unit is unreactive, but it improves the solubility and electrostatic interactions of the drug with DNA. The DNA intrastrand adducts formed by BBR3464 do not lead to DNA bending and are not recognised by high mobility group (HMG) proteins. This could be a major factor in the ability of multinuclear complexes to overcome cisplatin resistance. BBR3464 is approximately 40-fold more potent than cisplatin on a molar basis in tumour models, but so far the phase II trials have yielded a poor response rate (~ 6 %) and a short time to progression.[31]

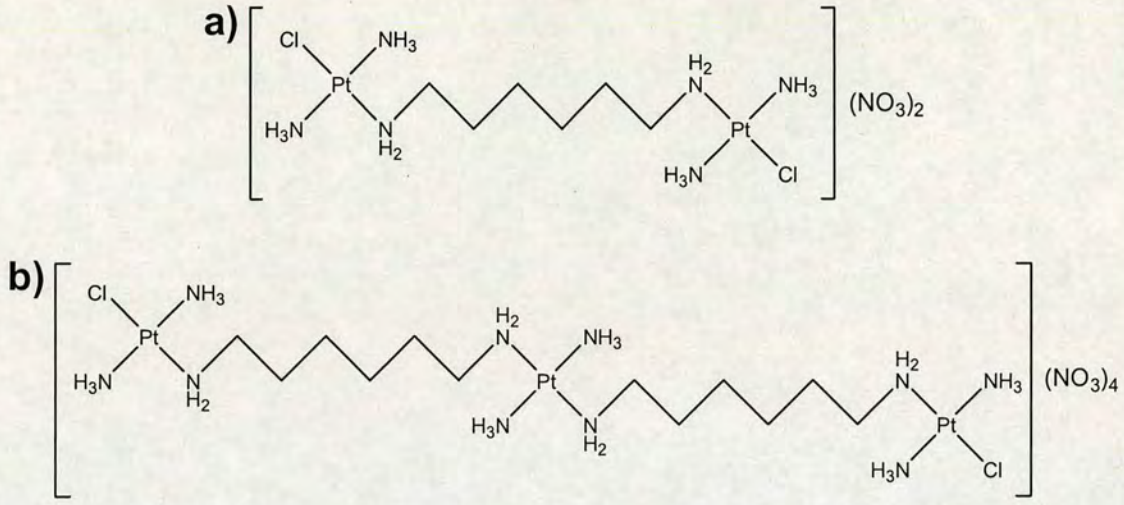

Figure 1.10 Structures of multinuclear Pt^{II} complexes, a) BBR3005 and b) BBR3464.

1.3 Photochemistry of Coordination Compounds

Photochemistry is the branch of chemistry concerned with the chemical effects of light. A photochemical reaction is a term generally used to describe a chemical reaction caused by the absorption of ultraviolet, visible or infrared radiation.[62]

This section describes the individual processes which take place during a photochemical reaction, with focus on coordination compounds. The formation of excited states by photoexcitation, the different types of electronic transitions, and photophysical and photochemical deactivation reactions are discussed. This is followed by a detailed look at the photochemistry of platinum complexes.

In most photochemical processes, excitation takes place by interaction of radiation with the complex,[63] i.e. by photoexcitation:

$$A + h\nu \rightarrow A^*$$

where A is a complex in the ground state and A* is a complex in an excited state. The term photoexcitation describes the electric dipole transition, other types of transitions (magnetic dipole or electric quadrupole transitions) are not relevant to

photochemistry. Photoexcitation is a resonance process which can occur if the difference between the energy of an excited state (E_{ES}) and the ground state (E_{GS}) is equal to the energy of a photon ($h\upsilon$) interacting with the complex:

$$E_{ES} - E_{GS} = h\upsilon$$

The probability of light absorption for a certain transition is expressed by means of the oscillator strength f (μ, transition dipole moment; m_e, mass of an electron; e, charge of an electron; $\Psi_{GS/ES}$, wavefunction of ground / excited state; $\hat{R}$, dipole moment operator):

$$f \equiv \frac{8\pi^2 m_e \nu |\mu|^2}{3he^2} \qquad \mu \equiv \int \Psi_{GS} \hat{R} \Psi_{ES} d\tau$$

The transition dipole moment can have a value of zero for certain transitions. Transitions for which the transition dipole moment is zero are called forbidden transitions. Conditions under which the transition dipole moment adopts a value of zero are expressed by selection rules:

- electric dipole transitions between states of different multiplicity are forbidden (spin-forbidden transitions).
- electric dipole transitions between states of equal parity (g $\rightarrow$ g, u $\rightarrow$ u) are forbidden (orbitally forbidden transitions).
- electric dipole transitions involving the simultaneous excitation of two or more electrons are forbidden.

The amount of light absorbed in a homogeneous medium is defined by the Beer-Lambert law:

$$I = I_0 \, 10^{-\varepsilon c l}$$

where I_0 is the incident light intensity, I is the transmitted light intensity, ε is the extinction coefficient ($M^{-1}cm^{-1}$), c is the concentration (M) and l is the path length of the light beam (cm). The absorbance is defined as:

$$A = \log_{10}(I/ I_0) = \varepsilon\, c\, l$$

and is therefore proportional to the concentration and the path-length.

The quantum yield or quantum efficiency of a photochemical reaction is normally defined as the fraction of photoactivated molecules that undergo some change. This is also called the overall quantum yield of products. The quantum yield (Φ) of any stable product X from the photodecomposition of a compound M ($M + h\nu \rightarrow X$), for example, is defined by:

$$\Phi_X = \frac{d[X]/dt}{I_a} = \frac{\text{No. of molecules or ions of X formed / cm}^3\text{s}}{\text{No. of quanta absorbed by M / cm}^3\text{s}}$$

The above quantum yield is measured irrespective of whether X is formed directly in a primary process, or in a secondary thermal reaction involving free radicals or atoms.[64]

1.3.1 Types of Electronic Transition

The excitation process is characterised according to the localisation of the electron density transfer. These transfers can occur within a complex, or an electron may be exchanged between the complex and its environment. Although electron transfer is described as occurring between molecular orbitals, it is important to note that the whole electron system of the complex is always changed (i.e. interelectronic repulsion, degeneration of levels, energy of orbitals etc.).

Four fundamental types of electronic transition exist.

1) Transitions between molecular orbitals (MOs) localised on the central atom. These can be divided into:

- ligand-field (LF) transitions (electron density transfer between d- or f-orbitals of the same principal quantum number)
- Rydberg transitions (transfer between orbitals differing in principal quantum number)
- inter-valence charge transfer (IT) transitions (transfer from one to the other

central atom in polynuclear bridged complexes)

2) Transitions between MOs localised on ligands. These can be either intraligand (IL) transitions (electron density transfer between MOs localised on one ligand) or ligand-to-ligand (LLCT) transitions (electron transfer from one ligand's HOMO to the other ligand's LUMO).

3) Transitions between MOs of different localisation. Depending on the direction of electron density transfer, there are:

- metal-to-ligand charge transfer (MLCT) transitions
- ligand-to-metal charge transfer (LMCT) transitions

4) Transfer of an electron between the complex and an environmental particle. Such transitions are called charge-transfer-to-solvent (CTTS) transitions.

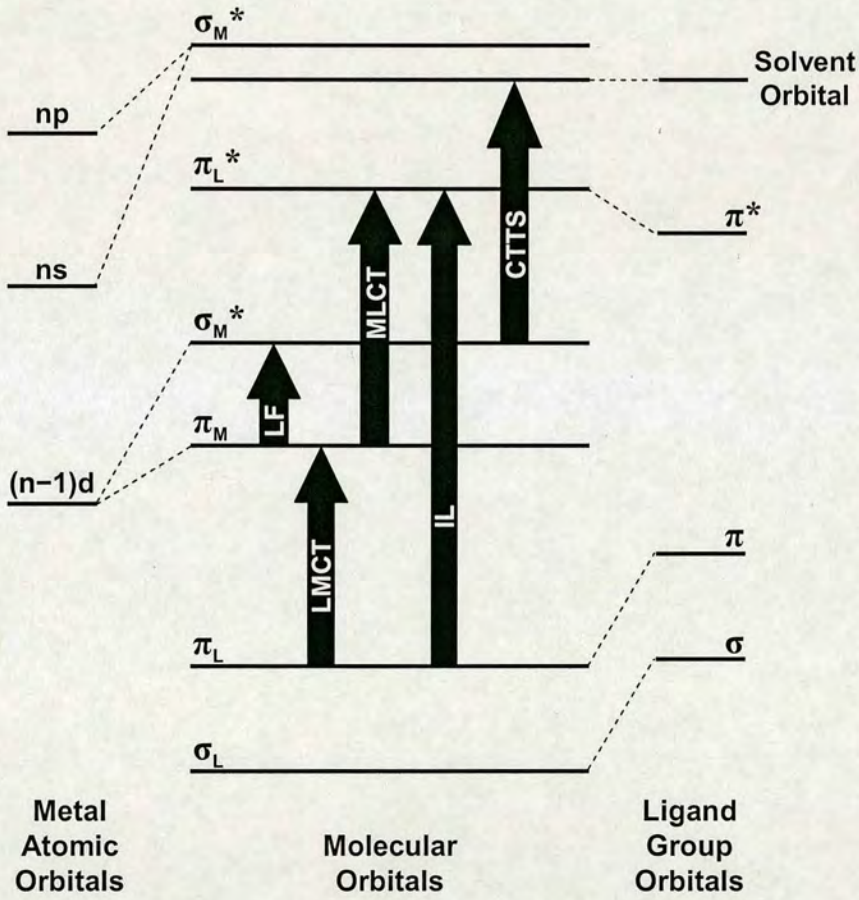

Figure 1.11 Molecular orbital diagram for an octahedral coordination complex and the various kinds of electronic transitions that may occur between the orbitals.

The different types of transitions that can occur in an octahedral coordination

complex are shown in Figure 1.11. These transitions are discussed further in the following sections.

1.3.1.1 Ligand Field Transitions

Transitions between different energy levels corresponding to a redistribution of electrons in the partially filled d-orbitals are referred to as ligand field (LF) or d → d transitions. In an octahedral field, the d-orbitals of a metal split into two sets of energetically different orbitals; the d_{xy}, d_{xz} and d_{yz} orbitals (the t_{2g} set) decrease in energy and the energy of the $d_{x^2-y^2}$ and d_{z^2} orbitals (the e_g set) increases (Figure 1.12a). By absorbing a photon of energy corresponding exactly to the t_{2g}-e_g energy gap Δ_o, a single electron can, in theory, be promoted from the lower set of orbitals to the upper ones (Figure 1.12b).

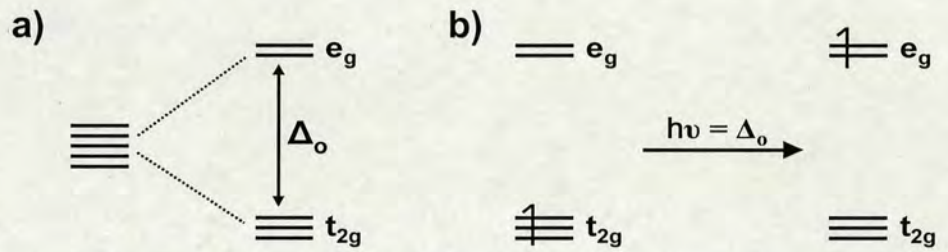

Figure 1.12 Energy level splitting for octahedral complexes. a) The two sets of orbitals (e_g and t_{2g}) are split by energy Δ_o. b) Promotion of an electron from the t_{2g} orbital set to the e_g orbitals requires the absorption of light of energy Δ_o.

Selection rules determine which transitions are formally allowed. The Laporte or parity selection rule forbids transitions between energy levels with the same symmetry with respect to the centre of inversion, therefore all d → d transitions in O_h complexes are Laporte forbidden. The Laporte rule can be relaxed under certain circumstances, either the molecule is not totally symmetric due to the presence of different ligands, or as the molecule vibrates the centre of symmetry is temporarily removed. Therefore d → d transitions for O_h complexes are observed but are often not very intense.

1.3.1.2 Charge-Transfer Transitions

Charge transfer transitions are formally allowed by the selection rules, and are therefore much more intense (often by a factor of a thousand or more) compared to the forbidden d → d transitions. All ligands possess molecular orbitals which may be of σ-, σ*-, π-, π*- or non-bonding character. If these orbitals are filled, and those on the metal are empty, then charge transfer may occur from the ligand-based orbitals to the metal d-orbitals (LMCT). If the ligand has low-lying empty orbitals and the metal is in a low oxidation state and hence electron rich, then metal-to-ligand charge transfer (MLCT) transitions occur.

Fully allowed electronic transitions have high molar extinction coefficients, whereas Laporte and spin-forbidden d-d transitions in centrosymmetric molecules generally have relatively weak absorptions. The intensities of the different types of electronic transitions of transition metal complexes are summarised in Table 1.2.

Table 1.2 Intensities of different types of electronic transitions in metal complexes.

Transition Type	ε_{max} **($M^{-1}cm^{-1}$)**
Spin-forbidden	< 1
Laporte-forbidden d-d	20 - 100
Laporte-allowed d-d	~ 500
Symmetry-allowed (e.g. CT)	1000 – 50,000

1.3.1.3 Intraligand and Charge-Transfer to Solvent Transitions

Intraligand (IL) transitions occur in complexes that contain organic ligands with a multiple bond(s), such as pyridine, 2,2′-bipyridine or 1,10-phenanthroline. IL transitions are usually orbitally and spin-allowed, and they occur in the spectra as intense bands in the visible and UV regions with values of $\varepsilon_{max} \approx 10^3 - 10^5$ $M^{-1}cm^{-1}$. Unlike MLCT and LMCT transitions, with which they frequently overlap, the bands of IL transitions depend only slightly on the character of the central atom and on the presence of other ligands in the coordination sphere.

Charge-transfer to solvent (CTTS) transitions can take place if the oxidation number

of the complexes central atom is low, if with an increase in the oxidation number of the central atom the structure of the coordination sphere is unchanged, and if the central atom has a higher oxidation state which is stable. CTTS transitions are usually allowed. The CTTS transition bands appear in the UV region of the spectrum, and have values of $\varepsilon_{max} \approx 10^1 - 10^3$ $M^{-1}cm^{-1}$. The positions of the bands and the values of ε_{max} are markedly influenced by the solvent reduction potential, with the easier the reduction the lower the transition energy.

1.3.2 Deactivation Processes from Excited States

Two types of deactivation processes exist – photophysical and photochemical. Photophysical processes result in the system returning to the ground state, whereas photochemical processes lead to different products. The variety of pathways through which an excited system can dissipate the energy gained by absorbing a photon are outlined in Figure 1.13.

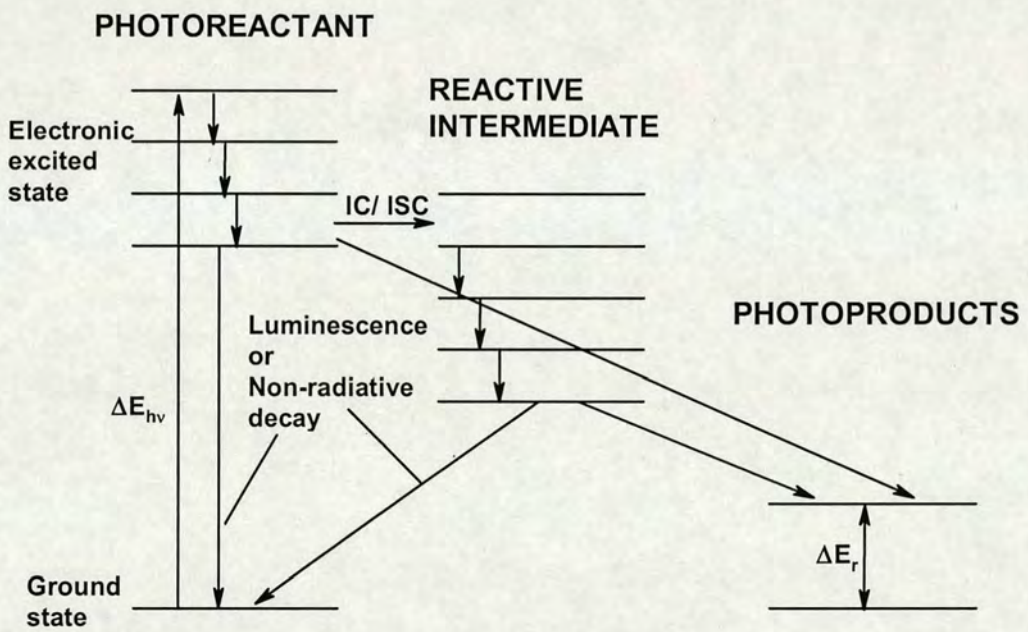

Figure 1.13 Jablonski diagram summarising the various pathways available to an excited molecule or complex, (IC, internal conversion; ISC, intersystem crossing).

Vibrational relaxation, as shown in Figure 1.13 by the short downward arrows, is the process by which most molecules drop back to the lowest vibrational level of the

excited electronic state. This is caused by the photoactive species undergoing a rapid thermal equilibration with their surroundings, and results in a Boltzman population distribution. After vibrational relaxation, the excited molecules can decay back to the ground state by luminescent emission or non-radiative decay. Alternatively the formation of photoproducts can occur, either directly or via a reactive intermediate.

Internal conversion (IC) is a transition between two excited states with identical multiplicitiy, whereas intersystem crossing (ISC) occurs between excited states of different multiplicity. Non-radiative deactivation of an excited state results in the energy being released into the environment in the form of heat. The excited state can also be deactivated by interacting with a quencher (Q). A quencher is another particle in the medium that can absorb the energy difference between the excited and ground states.

1.3.3 Photochemical Reactions of Coordination Compounds

The photochemical pathways compete with the various photophysical decay processes (Section 1.3.2), and this controls the extent to which photochemical products are formed. The reactivity of the excited state, which is chemically different from the ground state, influences the pathways taken. The following sections discuss photoredox, photoisomerisation and photosubstitution reactions with respect to coordination compounds.

1.3.3.1 Photoredox

Photoredox reactions can be divided into three types:

(a) reactions producing changes in the constitution of the complex, e.g. elimination and addition reactions,

(b) reactions where an electron is transferred between the complex and particles of the environment, the complex constitution and structure are preserved, and

(c) reactions where the structure is changed but the overall composition of the complex is preserved, e.g. inner-complex rearrangements.

Reactions in group (a) include reductive eliminations and oxidative additions, these

are the most important reactions when considering the photochemistry of platinum complexes.

Oxidative addition results in an increase in the oxidation number of the central atom, and is usually accompanied by an increase in coordination number. The opposite applies to reductive eliminations where a decrease in oxidation state and coordination number is generally seen. Charge-transfer from ligands to central atoms, and vice versa are involved in these types of reactions. LMCT transitions (Section 1.3.1.2) can often lead to reductive elimination of a ligand. Photoinduced reductive elimination reactions of Pt^{IV} complexes are discussed with specific examples in section 1.3.4. Oxidative addition photoreactions of platinum compounds are less common, but have been reported, and are also mentioned briefly later.

1.3.3.2 Photoisomerisation

Photoisomerisation reactions are light-induced processes where the composition of the compound is preserved, but the structure and properties are changed.[63] There are several different types of photoisomerisation reaction, but only the photoisomerisation of geometrical isomers will be considered here.

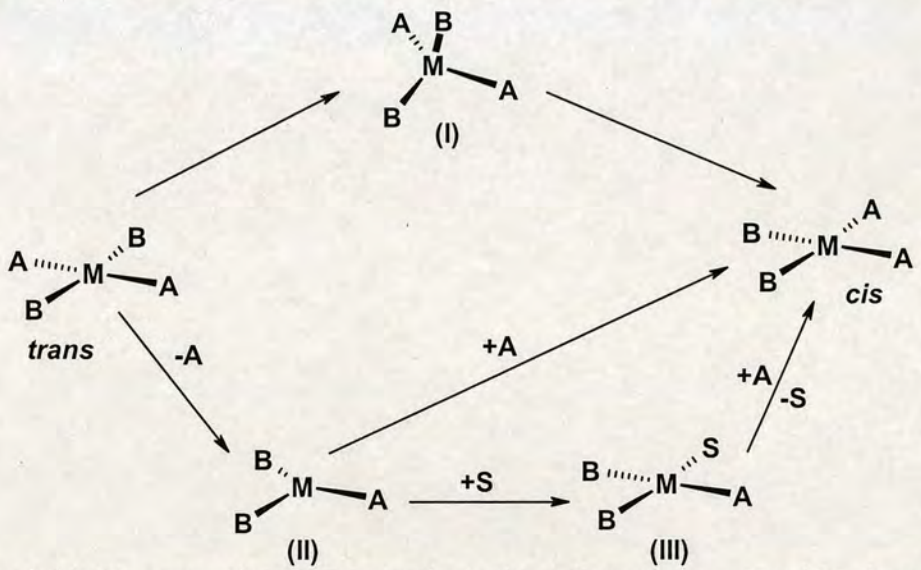

Figure 1.14 *Cis-trans* photoisomerisation of a square-planar complex. A and B are different ligands, S denotes solvent molecules, or another molecule present in solution in excess. I and II represent intermediates, I is tetrahedral, II is trigonal-planar and III is square-planar.

Photoisomerisation of geometrical isomers results in a change in symmetry of the complex. Investigations into the mechanism of *cis* → *trans* photoisomerisations of square-planar [MA_2B_2] and octahedral [MA_4B_2] complexes have been carried out, M is the central metal and A and B are the ligands. A proposed mechanism is shown in Figure 1.14.[63] The mechanism is believed to be the same for both square-planar and octahedral complexes.

1.3.3.3 Photosubstitution

Photosubstitution reactions are non-redox photochemical transformations, during which a ligand (or ligands) is exchanged between the primary and secondary coordination sphere. Photosubstitution reactions are generally different from thermal substitutions in their kinetics, products and stereochemistry. Photosubstitutions usually take place more rapidly than thermal substitutions (up to 14 orders of magnitude).[65] Further examples of these differences can be found in reference 66.

Photosubstitutions typically take place from ligand-field (Section 1.3.1.1) excited states. LF excitation leads to labilisation of the ligands due to population of the σ_d^* orbitals which can subsequently lead to substitution.

1.3.4 Platinum Photochemistry

The photochemistry of platinum is extensive and varied, and so is briefly summarised here. Several relevant reviews which cover the topic of platinum photochemistry have been published.[67-69]

The nature of photochemical reactions depends to a large extent on the type of electronic transition. LF transitions are usually associated with photoisomerization and photosubstitution reactions,[68] whereas LMCT generally causes photoreduction (i.e., Pt^{IV} to Pt^{II} and Pt^{II} to Pt^0).[67] However it should be noted that LF transitions can also result in photoredox reactions,[70,71] and LMCT can also cause ligand substitutions and isomerisations. The nature of the leaving ligand and the solvent play an important role in determining the pathway. The photochemistry of platinum complexes is not easy to predict, and the photoproducts must therefore be

investigated carefully to establish the pathway(s).

1.3.4.1 Platinum Halide Photochemistry

An example of the solvent dependence of reaction pathways can be seen upon irradiation (λ = 254 nm) into the LMCT band of $[Pt^{IV}(CN)_4Cl_2]^{2-}$.[72] The photoreaction in ethanol leads to efficient reduction to $[Pt^{II}(CN)_4]^{2-}$, but in aqueous solution the photoredox reactivity is almost negligible, and instead photoaquation is observed. Similar photoreactivity was found for the corresponding ammino compound $[Pt^{IV}(NH_3)_4Cl_2]^{2+}$.[73] Often a mixture of photosubstitution / aquation and photoreduction products are formed.[67]

Photoredox reactions upon irradiation into ligand field bands have been reported for chloro and azido complexes.[70,71] The photoinduced reduction of $[PtCl_6]^{2-}$ occurs at all wavelengths at which the complex absorbs light. Irradiation at energies as low as 514 nm yield platinum metal.[70] The photoreactions of platinum azide complexes are discussed in Section 1.3.4.2.

The first photoactivatable Pt^{IV} complexes designed with anticancer applications in mind contained iodide ligands. Kratochwil *et al.* prepared *trans, cis*-$[Pt(en)(OAc)_2I_2]$, which has iodide ligands in the *cis* position and gives rise to a LMCT band at relatively long wavelengths (ca. 400 nm).[74] Upon irradiation (> 375 nm) this complex was reduced to Pt^{II}, and bound covalently to DNA. However, in the absence of nucleobases, no direct photoreduction of Pt^{IV} to Pt^{II} was observed, and the photoreaction in the presence of nucleobases proved not to be a simple photoreductive elimination.[75] These iodo complexes were also found to be easily reduced by thiols (e.g. glutathione) to cytotoxic Pt^{II} species,[76] and so were deemed unsuitable for development as photoactive anticancer drugs.

The oxidative addition of Cl_2 to $[Pt^{II}(bpy)Cl_2]$ upon irradiation (λ = 280 nm) has been reported. The mechanism is believed to go via a Pt^{III} species:

$$[Pt^{II}(bpy)Cl_2] + CHCl_3 \xrightarrow{h\upsilon} [Pt^{III}(bpy)Cl_3] + \cdot CHCl_2$$

$$[Pt^{III}(bpy)Cl_3] + \cdot CHCl_2 \longrightarrow [Pt^{IV}(bpy)Cl_3]^+ + CHCl_2^-$$

$$[Pt^{IV}(bpy)Cl_3]^+ + CHCl_2^- \longrightarrow [Pt^{IV}(bpy)Cl_4] + :CHCl$$

$[Pt^{IV}(bpy)Cl_4]$ is a stable end-product, but the monochlorocarbene goes on to react further with another solvent molecule to give 1,1,2,2-tetrachloroethane.

Photoisomerisation reactions of square-planar Pt^{II} and octahedral Pt^{IV} complexes can be found in the literature. Examples include the *cis* → *trans* isomerisation of $[PtCl_2(PEt_3)_2]$, which occurs via intermediate I (Figure 1.14), this mechanism is called the intramolecular "twisting" mechanism.[77] The *cis* → *trans* isomerisation of $[Pt^{II}Cl_2(py)_2]$ takes place by a solvent-assisted mechanism and involves intermediate III (Figure 1.14).[78] A photoinduced isomerisation of *trans, trans, trans*-$[Pt^{IV}Cl_2(OAc)_2NH_3(c\text{-}HexNH_2)]$ to *cis, cis, trans*-$[Pt^{IV}Cl_2(OAc)_2NH_3(c\text{-}HexNH_2)]$ has been reported more recently, although no mechanism has been proposed.[79]

1.3.4.2 Platinum Azide Photochemistry

It has been stated that almost any transition metal azide complex is light sensitive, regardless of oxidation state.[80] Metal azides have been found to undergo a variety of different photoreactions, which include: (i) photosubstitution of the azide ligand,[81,82] (ii) photoreduction of an oxidising metal,[80,83-92] (iii) the generation of metal-nitrenes,[93-99] and (iv) production of singlet oxygen.[100,101] General azide photochemistry has also been covered in several reviews.[67,102-104]

The main focus of this work is the photoredox chemistry of platinum azide complexes. The first photoreductive elimination of azide from a platinum centre was reported by Vogler *et. al.* in 1978.[83] The electronic absorption spectrum of the complex *trans*-$[Pt(N_3)_2(CN)_4]^{2-}$ contains a maximum at 302 nm with an extinction coefficient (ε) of 18,300 $M^{-1}cm^{-1}$. This absorption is assigned as a ligand-to-metal

(N_3 → Pt) charge-transfer transition. Irradiation of this CT band led to the *trans* elimination of azide, and was found to proceed via the formation of two azide radicals ($N_3^{\bullet}$) without the production of a Pt^{III} intermediate.

$$[Pt(N_3)_2(CN)_4]^{2-} \xrightarrow{h\upsilon} [Pt(CN)_4]^{2-} + 3N_2$$

This was also later confirmed by Weber and van Eldik, who found evidence to support the theory that the scission of both Pt-N_3 bonds occurs simultaneously.[92]

The electronic absorption spectrum of the homoleptic azide complex $[Pt(N_3)_6]^{2-}$ has a maximum at 305 nm (ε = 36,300 $M^{-1}cm^{-1}$) in water. Excitation of this LMCT band yields $[Pt(N_3)_4]^{2-}$.[84,86] Ligand field (LF) transitions of $[Pt(N_3)_6]^{2-}$ are present above 400 nm, but irradiation of these bands does not lead to any chemical change. The complex $[Pt(N_3)_4]^{2-}$ has LF absorptions above 300 nm, and LMCT absorptions at 255 and 211 nm. Charge-transfer excitation again leads to reductive elimination and platinum is produced in its zero oxidation state.

The mechanism for photoactivation of the Pt^{II} azide complex *cis*-$[Pt(N_3)_2(PPh_3)_2]$ has been investigated by many techniques including ESR, luminescence spectroscopy,[85] spin trapping of radicals,[105] and IR and UV-visible spectroscopy,[106] The overall reaction is:

$$[Pt(N_3)_2(PPh_3)_2] \xrightarrow{h\upsilon} [Pt^0(PPh_3)_2] + 3N_2$$

An interesting feature of the photochemical behaviour of this compound is that it undergoes reduction of the metal centre upon irradiation with $\lambda > 350$ nm. At these wavelengths only ligand field transitions are present, and so internal conversion or intersystem crossing to a lower lying LMCT state must occur.[106] Reduction upon irradiation into ligand-field transitions has also been reported for the Pt^{IV} complex $[PtCl_6]^{2-}$.[70]

To photoreduce Pt^{IV} to Pt^{II}, two azide ligands are required. One possible mechanism is that upon irradiation the azides leave in the form of radicals ($^{\bullet}N_3$) (Figure 1.15).

Azide radicals are very unstable, and decompose in water rapidly into molecular nitrogen (N_2), which prevents reoxidation of the platinum centre. This fast decomposition is believed to be the reason for the efficiency of photoredox reactions involving complexes containing azide ligands. Halogen radicals do not decompose in water, and therefore recombination to generate the starting material is an efficient process.[84]

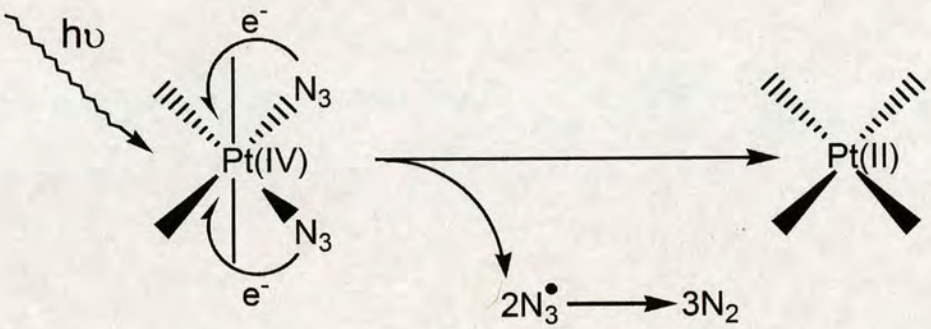

Figure 1.15 Possible mechanism for the photoreduction of a Pt^{IV}-diazido complex.

Two photoactive Pt^{IV} azido complexes based on the structures of cisplatin and its ethylenediamine analogue [Pt(en)Cl_2] have previously been synthesised.[107,108] *Cis, trans, cis*-[Pt(N_3)$_2$(OH)$_2$(NH_3)$_2$] and *cis, trans*-[Pt(en)(N_3)$_2$(OH)$_2$] contain axial hydroxo ligands, which enhance aqueous solubility, and stabilize the Pt^{IV} oxidation state.[39,47] Changing the am(m)ine ligands does not significantly alter the reduction potential of Pt^{IV} compounds, so it was thought that these ligands could be varied to improve properties such as lipophilicity, without affecting the stability.[39] The stability, photoreactions and nucleotide / DNA binding of these two compounds were investigated using visible light.[107,108] The results were promising; the complexes proved to be very stable, even to high concentrations of glutathione, and binding to nucleotides and DNA was observed upon irradiation, but not in the dark. This class of compounds therefore warranted further investigation as potential photoactivatable anticancer drugs (Section 1.5).

1.4 Photoactivated Drugs

The use of light, in combination with photoactive compounds to treat various diseases dates back as far as the Ancient Egyptians, who used sunlight and Bishop's Weed or Bullwort, which contain psoralens, to treat vitiligo. Today vitiligo and other skin disorders, such as psorisis are still treated in much the same way. Phototherapy with synthetic psoralens (e.g. 8-methoxypsoralen), which are applied orally or topically is a standard treatment.[109]

Illumination of the skin is clearly not difficult, but applying light to other parts of the body is one of the major problems of phototherapy. Recent advances in laser and fibre optic technologies have prompted the development of new medical applications based on the use of light. It is now possible to irradiate various parts of the body (e.g. oesophagus, head and neck, lung, bladder, cervix and colon); this is useful for treating cancer, as many solid tumours grow in these areas. The significant advantage of treating cancer by locally activating an anticancer agent with light, is the potential to avoid the major side-effects associated with chemotherapy.

The wavelength of light used to activate the compounds once they are inside the body is important. Red and near infrared light (Figure 1.16) are preferred, mainly because of the increased depth of penetration into tissue. It has been established that light in the 600 – 1000 nm spectral region (also known as the "phototherapeutic window") possesses the maximum penetration into most human tissues. This is due to the low absorbance of the normal cell constituents (e.g. melanin, cytochromes, haemoglobin) at these wavelengths, and can also be attributed to inefficient scattering of red light by cell organelles.[110] The penetration depth is defined as the depth in the tissue at which the intensity of incident light is reduced to 1 / e, or 37 % of its initial intensity. The penetration depth can be as large as 2 cm for lightly pigmented tissue with light above 700 nm, and can reach 1.5 cm at 900 nm for heavily pigmented tissues.[110] Further experiments on the penetration of light into various tissues can be found in reference 111 and references therein.

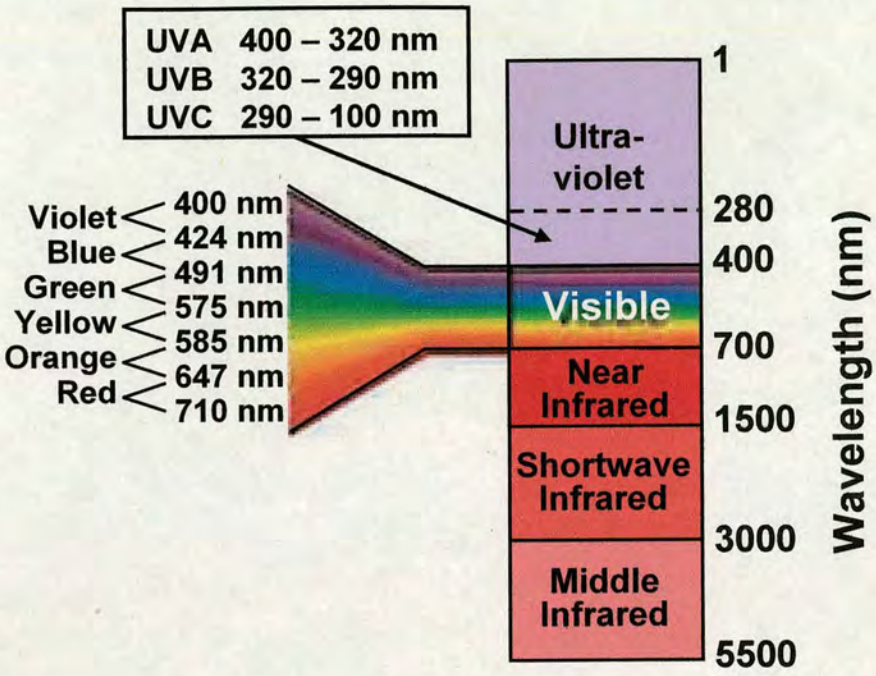

Figure 1.16 UV, visible and infrared regions of the electromagnetic spectrum.

Several other important properties, besides wavelength, have to be considered when designing photoactive drugs. An ideal compound would also be selective for tumours over healthy tissues, produce controllable cell death, and have minimal dark toxicity.

1.4.1 Photodynamic Therapy

PDT involves the selective damage of target tissue by using a photosensitizing drug and light. PDT is currently used to treat cancers such as lung, superficial gastric, cervical and bladder cancer, as well as cancer of the head and neck, and is also effective against age-related macular degeneration. The recent availability of relatively low-cost, efficient lasers has led to this form of treatment becoming much more wide-spread. In turn, the success of PDT has led to the development of new non-laser light sources, such as light-emitting diodes and various types of filtered lamps especially designed for treating skin lesions.[112]

The mechanism of action of photosensitizers involves oxygen. The photosensitizer absorbs energy from a light source and becomes excited to an energetically higher electronic state. Further reactions, which are classed as having type I or type II mechanisms, then take place (Figure 1.17). Reactions with a type I mechanism

transfer electrons to biological substrates, this forms radicals and radical ions which interact with oxygen to generate products such as the superoxide ion O_2^-. In type II reactions, the energy is transferred to oxygen which converts it from a triplet ground state ($^3O_2$) to a singlet excited state ($^1O_2$). The photosensitizer is then regenerated and so works catalytically. Singlet oxygen ($^1O_2$) is a short-lived but highly reactive molecule and reacts rapidly with cellular components. These reactions cause damage to the cell that ultimately leads to cell death. The lifetime of singlet oxygen is so short (~ 0.6 μs in a lipid cell membrane)[113] that it can only diffuse across a single cell membrane, and therefore cannot escape into the rest of the body and cause damage to healthy tissue. However, the requirement for oxygen is a major drawback as many malignant and most aggressive cancer cells are hypoxic.[114]

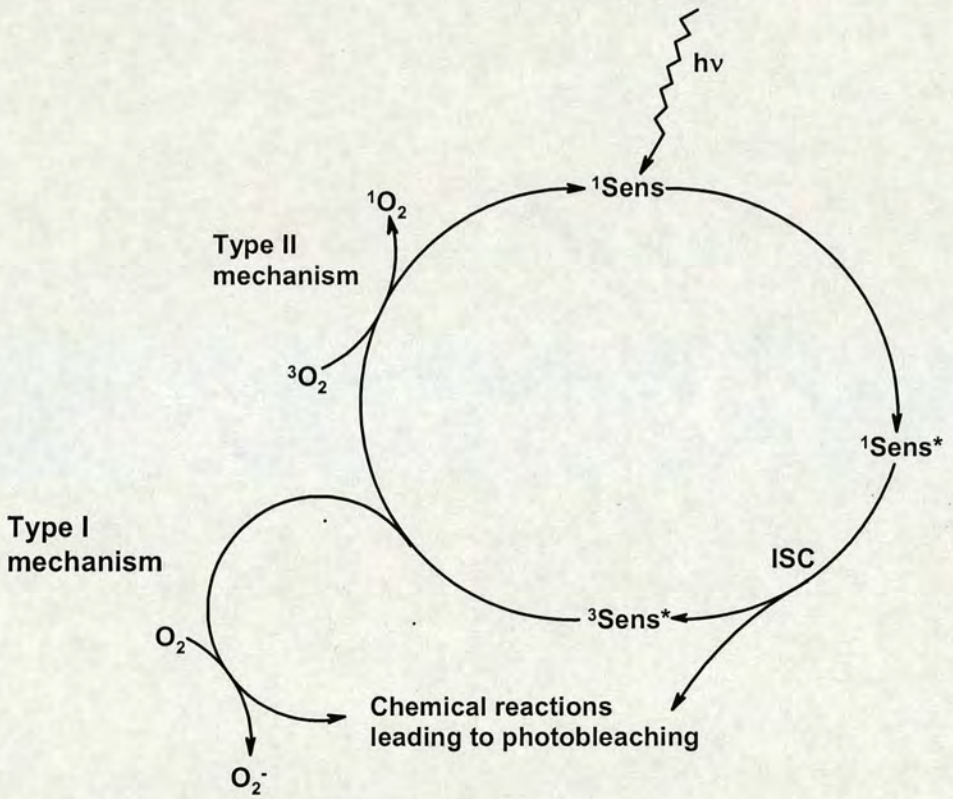

^{1}Sens	sensitiser in singlet electronic ground state
^{1}Sens*	sensitiser in singlet electronic excited state
^{3}Sens*	sensitiser in triplet electronic excited state
$^3O_2$	oxygen in triplet electronic ground state
$^1O_2$	oxygen in singlet electronic excited state
ISC	intersystem crossing

Figure 1.17 Photophysical mechanisms involved in photodynamic therapy (PDT) based on reference 115.

The main advantage of photodynamic therapy over surgery is that it is relatively non-invasive, and so can often be done in an out-patient or day-case setting (Figure 1.18). Repeating the dose is possible as there are no total-dose limitations unlike radiotherapy. The treatment is also accurately targeted and so side-effects like those associated with chemotherapy can be avoided.

Figure 1.18 Patients undergoing PDT whilst reading, demonstrating the non-invasive nature of this treatment. Picture courtesy of Dr Sam Eljamel, Consultant Neurosurgeon, Ninewells Hospital, Dundee.

The photosensitizer porfirmer sodium (Photofrin) was approved for clinical use in 1995. It is a complex mixture of porphyrins, haematoporphyrin derivatives (HpD) (Figure 1.19a), and is currently used against various cancers, including advanced and early-stage lung cancer.[112] Photofrin is one of only two photosensitzers approved for systemic administration, the other is temoporfrin (Foscan; Figure 1.19b), which entered the clinic in 2001. Foscan is used against palliative head and neck cancer, and is a highly active photosensitzer which requires a much lower dose of both drug and light compared to Photofrin.[116] Aminolevulinic acid (Levulan; Figure 1.19c) and methyl aminolevulinate (Metvix; Figure 1.19d) have been approved for topical use, and are used for the treatment of actinic keratosis (a precancerous skin growth).[112] These are precursors of protoporphyrin IX (Figure 1.19a) and so the porphyrin photosensitizer is generated *in situ* before light is applied.

PDT is unable to cure advanced disseminated cancers because it is not possible to irradiate the entire body with the required dose of light. However it can improve a

patient's quality of life and lengthen survival time. The main side-effect of PDT is light sensitivity. Intravenously administered photosensitzers stay in the body for some time after treatment (Photofrin ~ 5 - 6 weeks)[113] and patients can sometimes experience severe skin reactions to strong light.

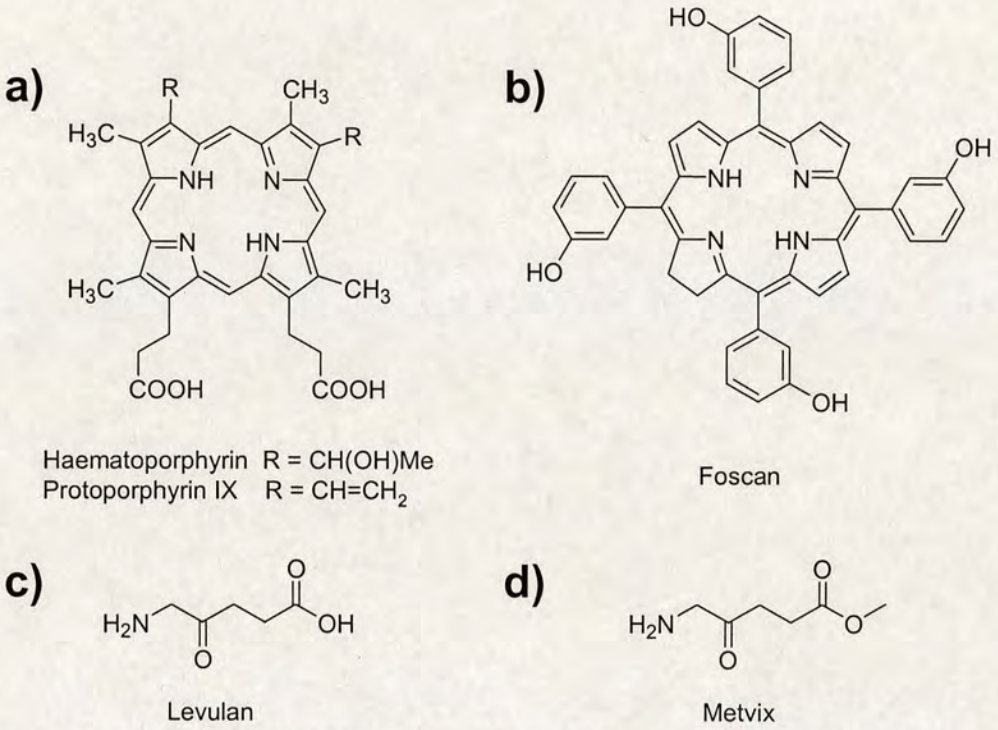

Figure 1.19 Structures of drugs approved for photodynamic therapy.

A large amount of research is currently devoted to the design of new photosensitizers which have (i) a strong absorbance at longer wavelengths, (ii) accumulate selectively in tumor tissue, and (iii) are quickly cleared from the body. However due to the mechanism of action of PDT the presence of oxygen will still be essential, which is not ideal due to the oxygen-deficient nature of many tumors. This is a major advantage that photoactivated platinum compounds could have over currently-used photosensitizers.

1.4.2 Phototoxic Metal Compounds

Recently, there has been a great deal of research into the development of photoactive metal complexes with potential medical applications, and a lot of this work has involved the platinum group metals. [117]

The *cis* and *trans* isomers of $[RuCl_2(DMSO)_4]$ have recently been reported to be phototoxic in human melanoma cell lines.[118] Covalent binding of the ruthenium complexes to the N7 position of guanines can be induced with UVA light. Photoactive rhodium(III) 1,10-phenanthroline dichloride complexes have been developed which are not only toxic to cancer cells upon irradiation, but have also been shown to inactivate an intracellular alphavirus Sindbis (SINV).[119] Other photoactive complexes include the ruthenium(II) bipyridine compound *cis*-$[Ru(bpy)_2(NH_3)_2]^{2+}$ which is phototoxic to human skin fibroblasts (Hs-27);[120] and mixed metal Ru^{II}-Rh^{III} complexes which bind to DNA upon irradiation.[121] As yet no *in vitro* testing has been reported for these mixed-metal complexes.

Pt^{II}-haematoporphyrin complexes have been designed as dual drugs to take advantage of the fact that cancer cells accumulate porphyrins. These complexes are technically not photoactivated Pt^{II} complexes, because they are supposed to show dark toxicity as well as phototoxicity. The cytotoxic and phototoxic efficacies of some of these Pt^{II}-porphyrin complexes have been reported to exceed the sum of the phototoxicity of the corresponding porphyrin ligand and the cytotoxicity of cisplatin.[122] These complexes along with others are described in more detail in recent reviews.[123,124]

1.5 Aims of this Work

The general aims of this work were to develop new Pt^{IV} azide complexes, investigate the photoactivation mechanism of existing and new Pt^{IV} azide complexes, and to extend the wavelength of absorption towards the red region of the visible spectrum.

It is important to elucidate the mechanism of photoactivation of these diazido-complexes to gain further insight into possible *in vitro* phototoxicity pathways. DNA is the major target of Pt^{II} drugs in the body, and so the interaction of Pt^{IV} azide complexes with nucleobases and DNA upon irradiation is also of interest. It is not yet clear if these complexes react in the same way when light of different wavelengths is used; higher energy light may open up new activation routes.

Ideally a photoactivated drug should absorb between 700 – 1000 nm, this is the region where light can penetrate deepest into tissue. Pt^{IV} azide complexes typically absorb in the UV region due to the high energy N_3 → Pt LMCT band. However, by careful choice of the other substituents, it may be possible to shift this band far enough into the visible region to give sufficient absorbance for photoactivation at longer wavelengths.

Another possible way to overcome the short wavelength of absorbance is to use multiphoton techniques. This involves femtosecond pulsed lasers which can activate a molecule which absorbs in the UV region (e.g. 350 nm) by irradiation with red light (e.g. 700 nm). Two-photons are absorbed almost simultaneously allowing access to an excited state which is roughly double the energy of that achieved by one-photon absorbance.

1.6 References

[1] Greenwood, N.N.; Earnshaw, A. In *Chemistry of the Elements*, 2nd Edition, Reed Educational and Professional Publishing Ltd., Oxford, **1997**.

[2] Basolo, F.; Pearson, R.G. *Prog. Inorg. Chem.* **1962**, *4*, 381.

[3] Cotton, F.A.; Wilkinson, G. In *Advanced Inorganic Chemistry*, 5th Edition, John Wiley and Son, New York, **1988**.

[4] Shriver, D.F.; Atkins, P.W.; Langford, C.H. In *Inorganic Chemistry*, 2nd Edition, Oxford University Press, Oxford, **1996**.

[5] Rosenberg, B.; van Camp, L.; Krigas, T. *Nature* **1965**, *205*, 698.

[6] Barnard, C.F.J. *Plat. Met. Rev.* **1989**, *33*, 162.

[7] Lippert, B.E. Ed. *Chemistry and Biology of a Leading Anticancer Drug*, Verlag Helvetica Chimica Acta, Zürich, **1999**.

[8] Andrews, P.A.; Albright, K.D. In *Platinum and Other Metal Coordination Compounds in Cancer Chemotherapy*, Plenum Press, New York, **1991**, pp. 151.

[9] Kawai, K.; Kamatani, N.; Georges, E.; Ling, V. *J. Biol. Chem.* **1990**, *265*, 13137.

[10] Gately, D.P.; Howell, S.B. *Br. J. Cancer* **1993**, *67*, 1171.

[11] Jennerwein, M.; Andrews, P.A. *Drug Metab. Dispos.* **1995**, *23*, 178.

[12] Jamieson, E.R.; Lippard, S.J. *Chem. Rev.* **1999**, *99*, 2467.

[13] Guo, Z.; Sadler, P.J. *Adv. Inorg. Chem.* **2000**, *49*, 183.

[14] Johnson, N.P.; Hoeschele, J.D.; Rahn, R.O. *Chem. Biol. Interact.* **1980**, *30*, 151.

[15] Bancroft, D.P.; Lepre, C.A.; Lippard, S.J. *J. Am. Chem. Soc.* **1990**, *112*, 6860.

[16] Berners-Price, S.J.; Frenkiel, T.A.; Frey, U.; Ranford, J.D.; Sadler, P.J. *J. Chem. Soc., Chem. Commun.* **1992**, 721.

[17] Reedijk, J. *J. Chem. Soc., Chem. Commun.* **1996**, 801.

[18] Saito, I.; Takayama, M.; Sugiyama, H.; Nakatani, K. *J. Am. Chem. Soc.* **1995**, *117*, 6406.

[19] Fichtinger-Schepman, A.M.J.; van der Veer, J.L.; den Hartog, J.H.J.; Lohman, P.H.M.; Reedijk, J. *Biochemistry* **1985**, *24*, 707.

[20] Gelasco, A.; Lippard, S.J. In *Metallopharmaceuticals: DNA Interactions*, Springer-Verlag, Berlin, **1999**, pp. 2.

[21] Takahara, P.M.; Rosenzweig, A.C.; Frederick, C.A.; Lippard, S.J. *Nature* **1995**,

377, 649.

[22] Takahara, P.M.; Frederick, C.A.; Lippard, S.J. *J. Am. Chem. Soc.* **1996**, *118*, 12309.

[23] Herman, F.; Kozelka, J.; Stoven, V.; Guittet, E.; Girault, J.-P.; Huynk-Dinh, T.; Igolen, J.; Lallemand, J.-Y.; Chottard, J.-C. *Eur. J. Biochem.* **1990**, *194*, 119.

[24] Yang, D.; van Boom, S.S.G.E.; Reedijk, J.; van Boom, J.H.; Wang, A.H.-J. *Biochemistry* **1995**, *34*, 12912.

[25] Gelasco, A.; Lippard, S.J. *Biochemistry* **1998**, *37*, 9230.

[26] Toney, J.H.; Donahue, B.A.; Kellett, P.J.; Bruhn, S.L.; Essigmann, J.M.; Lippard, S.J. *Proc. Natl. Acad. Sci. USA* **1989**, *86*, 8328.

[27] Ohndorf, U.M.; Rould, M.A.; He, Q.; Pabo, C.O.; Lippard, S.J. *Nature* **1999**, *399*, 708.

[28] Pil, P.; Lippard, S.J. In *Encyclopedia of Cancer*, Bertino, J.R. Ed. Academic Press, San Diego, CA, **1997**, *1*, pp. 392-410.

[29] Chu, G. *J. Biol. Chem.* **1994**, *269*, 787.

[30] Wong, E.; Giandomenico, C.M. *Chem. Rev.* **1999**, *99*, 2451.

[31] Galanski, M.; Jakupec, M.A.; Keppler, B.K. *Curr. Med. Chem.* **2005**, *12*, 2075.

[32] Graham, J.; Muhsin, M.; Kirkpatrick, P. *Nat. Rev. Drug Discov.* **2004**, *3*, 11.

[33] Ita, M.; Okafuji, M.; Fukuda, K.; Mitsuoka, K.; Hanakita, T.; Hayatsu, Y. *Oral Oncol.* **2003**, *39*, 144.

[34] Chen, Y.; Guo, Z.; Parsons, S.; Sadler, P.J. *Chem. Eur. J.* **1998**, *4*, 672.

[35] Chen, Y.; Guo, Z.; Parkinson, J.A.; Sadler, P.J. *J. Chem. Soc., Dalton Trans.* **1998**, 3577.

[36] Chen, Y.; Parkinson, J.A.; Guo, Z.; Brown, T.; Sadler, P.J. *Angew. Chem. Int. Ed.* **1999**, *38*, 3577.

[37] Rosenberg, B.; van Camp, L.; Krigas, T. *Nature* **1965**, *205*, 698.

[38] Rosenberg, B.; van Camp, L.; Trosko, J.E.; Mansour, V.H. *Nature* **1969**, *222*, 385.

[39] Hall, M.D.; Hambley, T.W. *Coord. Chem. Rev.* **2002**, *232*, 49.

[40] Lebwohl, D.; Canetta, R. *Eur. J. Cancer* **1998**, *34*, 1522.

[41] Fokkema, E.; Groen, H.J.M.; Helder, M.N.; de Vries, E.G.E.; Meijer, C.

Biochem. Pharmacol. **2002**, *63*, 1989.

[42] Hartley, F.R. *Coord. Chem. Rev.* **1981**, *35*, 143.

[43] Roat, R.M.; Reedijk, J. *J. Inorg. Biochem.* **1993**, *52*, 263.

[44] Galanski, M.; Keppler, B.K. *Inorg. Chim. Acta* **2000**, *300-302*, 783.

[45] Neumann, C.; Boubakari; Grünert, R.; Bednarksi, P.J. *Anal. Biochem.* **2003**, *320*, 170.

[46] Shi, T.; Berglund, J.; Elding, L.I. *Inorg. Chem.* **1996**, *35*, 3498.

[47] Lemma, K.; Berglund, J.; Farrell, N.; Elding, L.I. *J. Bioinorg. Chem.* **2000**, *5*, 300.

[48] Lemma, K.; Shi, T.; Elding, L.I. *Inorg. Chem.* **2000**, *39*, 1728.

[49] Lemma, K.; Sargeson, A.M.; Elding, L.I. *J. Chem. Soc., Dalton Trans.* **2000**, 1167.

[50] Chen, L.; Lee, P.F.; Ranford, J.D.; Vittal, J.J.; Wong, S.Y. *J. Chem. Soc., Dalton Trans.* **1999**, 1209.

[51] Cleare, M.J.; Hoeschele, J.D. *Bioinorg. Chem.* **1973**, *2*, 187.

[52] Blisard, K.S.; Harrington, D.A.; Long, D.A.; Jackson, J.E. *J. Comp. Pathol.* **1991**, *105*, 367.

[53] Natile, G.; Coluccia, M. *Met. Ions Biol. Syst.* **2004**, *42*, 209.

[54] van Beusichem, M.; Farrell, N. *Inorg. Chem.* **1992**, *31*, 634.

[55] Montero, E.I.; Diaz, S.; Gonzàlez-Vadillo, A.M.; Pèrez, J.M.; Alonso, C.; Navarro-Ranninger, C. *J. Med. Chem.* **1999**, *42*, 4264.

[56] Pèrez, J.M.; Montero, E.I.; Gonzalez, A.M.; Alvarez-Valdes, A.; Alonso, C.; Navarro-Ranninger, C. *J. Med. Chem.* **1999**, *77*, 37.

[57] Coluccia, M.; Nassi, A.; Loseto, F.; Boccarelli, A.; Mariggiò, M.A.; Giordano, D.; Intini, F.P.; Caputo, P.A.; Natile, G. *J. Med. Chem.* **1993**, *36*, 510.

[58] Coluccia, M.; Boccarelli, A.; Mariggiò, M.A.; Caputo, P.A.; Intini, F.P.; Natile, G. *Chem. Biol. Interact.* **1995**, *98*, 251.

[59] Coluccia, M.; Mariggiò, M.A.; Boccarelli, A.; Loseto, F.; Cardellicchio, N.; Caputo, P.A.; Intini, F.P.; Pacifico, C.; Natile, G. In *Platinum and Other Metal Coordination Compounds in Cancer Chemotherapy 2*, Pinedo, H.M.; Schornagel, J.H. Editors, Plenum Press, New York, **1996**.

[60] Boccarelli, A.; Coluccia, M.; Intini, F.P.; Natile, G.; Locker, D.; Leng. M. *Anti-Cancer Drug Des.* **1999**, *14*, 253.

[61] Kelland, L.R.; Barnard, C.F.J.; Evans, I.G.; Murrer, B.A.; Theobald, B.R.C.; Wyer, S.B.; Goddard, P.M.; Jones, M.; Valenti, M.; Bryant, A.; Rogers, P.M.; Harrap, K.R. *J. Med. Chem.* **1995**, *38*, 3016.

[62] Braslavsky, S.E.; Houk, K.N.; Verhoeven, J.W. Eds. *Glossary of terms used in Photochemistry*, 2nd Edtion, IUPAC, **1996**.

[63] Sykora, J.; Sima, J. *Coord. Chem. Rev.* **1990**, *107*.

[64] Calvert, J.G.; Pitts, J.N. Jr. In *Photochemistry* Wiley & Sons, New York, 1966.

[65] Bergkamp, M.A.; Watts, R.J.; Ford, P.C. *J. Am. Chem. Soc.* **1980**, *102*, 2627.

[66] Kirk, A.D. *J. Chem. Educ.* **1983**, *60*, 834.

[67] Horvath, O.; Stevenson, K.L. In *Charge Transfer Photochemistry of Coordination Compounds*, VCH, Weinheim, Germany, **1993**.

[68] Ferraudi, G.J. In *Elements of Inorganic Photochemistry*, Wiley-Interscience, NY, **1988**.

[69] Roundhill, D.M. In *Photochemistry and Photophysics of Metal Complexes*. Plenum Press, NY, **1994**.

[70] Cameron, R.E.; Bocarsly, A.B. *Inorg. Chem.* **1986**, *25*, 2910

[71] Knoll, H.; Stich, R.; Hennig, H.; Stufkens, D.J. *Inorg. Chim. Acta* **1990**, *178*, 71.

[72] Vinogradov, S.A.; Balashev, K.P.; Shagisultanova, G.A. *Koord. Khim.* **1988**, *13*, 1092.

[73] Vinogradov, S.A.; Balashev, K.P.; Shagisultanova, G.A. *Koord. Khim.* **1985**, *11*, 959.

[74] Kratochwil, N.A.; Zabel, M.; Range, K.-J.; Bednarski, P.J. *J. Med. Chem.*, **1996**, *39*, 2499.

[75] Kratochwil, N.A.; Parkinson, J.A.; Bednarski, P.J.; Sadler, P.J. *Angew. Chem. Int. Ed.* **1999**, *38*, 1460.

[76] Kratochwil, N.A.; Guo, Z.; del Socorro Murdoch, P.; Parkinson, J.A.; Bednarski, P.J.; Sadler, P.J. *J. Amer. Chem. Soc.* **1998**, *120*, 8253.

[77] Mastin, S.H.; Haake, P. *J. Chem. Soc., Chem. Commun.* **1970**, 202.

[78] Moggi, L.; Varani, G.; Sabbatini, N.; Balzani, V. *Mol. Photochem.* **1971**, *3*, 141.

[79] Barnard, C.F.J.; Vollano, J.F.; Chaloner, P.A.; Dewa, S.Z. *Inorg. Chem.* **1996**, *35*, 3280.

[80] Vogler, A.; Quett, C.; Kunkely, H. *Ber. Bunsen-Ges. Phys. Chem.* **1988**, *92*, 1486.

[81] Endicott, J.F.; Ferraudi, G. *J. Phys. Chem.* **1976**, *80*, 949.

[82] Miskowski, V.M.; Nobinger, G.L.; Hammond, G.S. *Inorg. Chem.* **1976**, *15*, 2904.

[83] Vogler, A.; Kern, A.; Hüttermann, J. *Angew. Chem., Int. Ed. Engl.* **1978**, *17*, 524.

[84] Vogler, A.; Kern, A.; Fußeder, B.; Hüttermann, J. *Z. Naturforsch.* **1978**, *33b*, 1352.

[85] Vogler, A.; Wright, R.E.; Kunkely, H. *Angew. Chem. Int. Ed. Eng.* **1980**, *19*, 717.

[86] Vogler, A.; Hlavatsch, J. *Angew. Chem. Int. Ed. Eng.* **1983**, *22*, 154.

[87] Kunkely, H.; Vogler, A. *Inorg. Chem. Commun.* **2005**, *8*, 117.

[88] Vogler, A.; Quett, C.; Paukner, A.; Kunkely, H. *J. Am. Chem. Soc.* **1986**, *108*, 8263.

[89] Ferraudi, G.; Endicott, J.F. *J. Am. Chem. Soc.* **1973**, *95*, 2371.

[90] Strähle, J. *J. Organomet. Chem.* **1995**, *488*, 15.

[91] Hennig, H.; Stich, R.; Knoll, H.; Rehorek, D. *Z. Anorg. Allg. Chem.* **1989**, *567*, 139.

[92] Weber, W.; Van Eldik, R. *Inorg. Chim. Acta.* **1986**, *111*, 129.

[93] Reed, J.L.; Gafney, H.D.; Basalo, F. *J. Am. Chem. Soc.* **1974**, *96*, 1363.

[94] Ngai, R.; Wang, Y.H.L.; Reed, J.L. *Inorg. Chem.* **1985**, *24*, 3802.

[95] Dahlgren, R.M.; Zink, J.I. *Inorg. Chem.* **1979**, *18*, 597.

[96] Ferraudi, G.; Endicott, J.F. *Inorg. Chem.* **1973**, *12*, 2389.

[97] Katz, M.; Gafney, H.D. *Inorg. Chem.* **1978**, *17*, 93.

[98] Gafney, H.D.; Reed, J.L.; Basolo, F. *J. Am. Chem. Soc.* **1973**, *95*, 7998.

[99] Reed, J.L.; Wang, F.; Basolo, F. *J. Am. Chem. Soc.* **1972**, *94*, 7173.

[100] Shukla, S.; Kamath, S.S.; Srivastava, T.S. *J. Photochem. Photobiol.* **1988**, *44A*, 143.

[101] Anbalagan, V. *J. Coord. Chem.* **2003**, *56*, 161.

[102] Balzani, V.; Carassiti, V. In *Photochemistry of Coordination Compounds*, Academic Press, New York, 1970.

[103] Poznyak, A.L.; Pavlovski, V.I. *Angew. Chem. Int. Ed.* **1988**, *27*, 789.

[104] Šima, J. *Coord. Chem. Rev.* **2006**, *online*

[105] Hennig, H.; Stich, R.; Rehorek, D.; Thomas, P. *Inorg. Chim. Acta* **1988**, *143*, 7.

[106] Knoll, H.; Stich, R.; Hennig, H.; Stufkens, D.J. *Inorg. Chim. Acta* **1990**, *178*, 71.

[107] Müller, P. PhD Thesis, University of Edinburgh, **2002**.

[108] Müller, P.; Schröder, B.; Parkinson, J.A.; Kratochwil, N.A.; Coxall, R.A.; Parkin, A.; Parsons, S.; Sadler, P.J. *Angew. Chem., Int. Ed.* **2003**, *42*, 335.

[109] Dall'Acqua, F.; Jori, G In *Principles of Medicinal Chemistry.* Foye, W.O.; Lemke, T.L.; Williams, D.A. Eds; Williams & Wilkins, Baltimore, **1995**.

[110] Wilson, S.C.; Patterson, M.S.; Flock, S.T.; Wyman, D.R. In *Photon Migration in Tissue*, Chance, B. Ed., Plenum, New York, **1990**, p. 25.

[111] Dougherty, T.J. *Advances in Photochemistry*, John Wiley and Sons, New York, **1992**.

[112] Brown, S.B.; Brown, E.A.; Walker, I. *Lancet Oncol.,* **2004**, *5,* 497.

[113] Pandey, R.K.; Herman, C.K. *Chem. Ind.,* **1998**, *18*, 739.

[114] Harris, A.L. *Nat. Rev. Cancer*, **2002**, *2*, 38.

[115] Milgrom, L.; MacRobert, S. *Chem. Br.* **1998**, *May 1998*, 45.

[116] Sharman, W.M.; Allen, C.M.; van Lier, C.E. *Drug Discov. Today,* **1999**, *4*, 507.

[117] Szaciłowski, K.; Macyk, W.; Drzewiecka-Matuszek, A.; Brindell, M.; Stochel, G. *Chem. Rev.* **2005**, *105*, 2647.

[118] Brindell, M.; Kuliś, E.; Elmroth, S.K.C.; Urbańska; Stochel, G. *J. Med. Chem.* **2005**, *48*, 7298.

[119] Menon, E.L.; Perera, R.; Navarro, M.; Kuhn, R.J.; Morrision, H. *Inorg. Chem.* **2004**, *43*, 5373.

[120] Angles-Boza, A.M.; Bradley, P.M.; Fu, P.K.L.; Shatruk, M.; Hilfiger, M.G.; Dunbar, K.R.; Turro, C. *Inorg. Chem.* **2005**, 44, 7262.

[121] Holder, A.A.; Swavey, S.; Brewer, K.J. *Inorg. Chem.* **2004**, *43*, 303.

[122] Lottner, C.; Bart, K.-C; Bernhardt, G.; Brunner, H. *J. Med. Chem.* **2002**, *45*, 2064.

[123] Loganathan, D.; Morrison, H. *Curr. Opin. Drug Disc.* **2005**, *8*, 478.

[124] Boerner, L.J.K.; Zaleski, J.M. *Curr. Opin. Chem. Biol.* **2005**, *9*, 135.

Chapter 2
Experimental Methods

2.1 Nuclear Magnetic Resonance Spectroscopy

2.1.1 Theory of Nuclear Magnetic Resonance Spectroscopy

Nuclear magnetic resonance (NMR) spectroscopy is a widely used technique which reveals information about the environment of magnetically active nuclei. In the absence of a magnetic field the possible orientations of a nucleus are of equal energy. However, when a magnetic field is applied the nucleus adopts one of a number of allowed orientations of different energy. The nucleus of the hydrogen atom (a proton), for example has just two permitted orientations, it can either align itself with, or against the field. These two energy levels are separated by an energy ΔE, which depends on the strength of interaction between the nucleus and the field. The nuclei can be flipped from the lower energy level to the higher one by applying electromagnetic radiation of frequency ν, where $\Delta E = h\nu$ (h is Planck's constant), and therefore ΔE can be measured. This is nuclear magnetic resonance spectroscopy.[1-4]

The NMR properties of some commonly studied nuclei are listed in Table 2.1. Due to the relevance to this work, the NMR spectroscopy of ^{15}N and ^{195}Pt nuclei are discussed in detail in the following sections. The heteronuclear single-quantum correlation (HSQC) NMR technique is also reviewed as it is used extensively in the following chapters.

Table 2.1 NMR properties of common nuclei.[5,6]

Nucleus	Natural abundance (%)	Sensitivity (relative to ^{1}H)	Gyromagnetic Ratio (10^7 rad T^{-1} s^{-1})	I	Frequency at 11.74 T (MHz)
^{1}H	99.984	1	26.75	½	500.00
^{2}H	0.02	1.5×10^{-6}	4.11	1	76.75
^{13}C	1.108	1.8×10^{-4}	6.73	½	36.12
^{15}N	0.366	3.9×10^{-6}	-2.71	½	50.66
^{14}N	99.634	1.0×10^{-3}	1.93	1	21.687
^{195}Pt	33.80	3.4×10^{-3}	5.77	½	64.414

I: Nuclear spin quantum number

2.1.1.1 ^{195}Pt NMR Spectroscopy[5]

^{195}Pt is a reasonably sensitive nucleus for NMR detection. It has a natural abundance of 33.8 % and nuclear spin quantum number I = ½. Its receptivity relative to ^{1}H is 3.4 x 10^{-3} but this can be improved by a factor of three by isotopic enrichment of ^{195}Pt (> 95%). The spin-lattice relaxation time (T_1) for ^{195}Pt is usually in the range of 0.3 to 1.3 s.

The ^{195}Pt chemical shift range is very large, about 15000 ppm (usually in the range from -6000 to 9000 ppm relative to $[PtCl_6]^{2-}$), and often allows easy differentiation between Pt^{II} and Pt^{IV}, which tend to have chemical shifts at the high-field and low-fields ends of the range, respectively. The ^{195}Pt chemical shift in monomeric complexes is sensitive primarily to the set of bound donor atoms. Some caution is required when searching for peaks, as the shifts of Pt^{IV} halides alone span 12000 ppm. There are also useful differences in the chemical shifts of geometrical isomers and diastereomers (chiral ligands). For ^{15}N-enriched ligands, the splitting pattern in the ^{195}Pt spectrum indicates the number of non-equivalent ^{15}N atoms coordinated. These characteristics of the ^{195}Pt chemical shift can be utilised in the detection of different intermediates formed during the reactions of Pt complexes with biomolecules. Sometimes even isotopomers are distinguishable: the ^{195}Pt isotope shift difference for ^{195}Pt-$^{35/37}$Cl is 0.17 ppm and for ^{195}Pt-$^{79/81}$Br is 0.03 ppm.[7] It is therefore in principle possible to count the number of Cl and Br ligands bonded to Pt via the isotope splitting pattern. In practice it is difficult to resolve because of line broadening, which is usually due to either relaxation mechanisms or poor temperature control of the sample. The latter is a problem because of the strong temperature dependence of ^{195}Pt NMR resonances (0.5 to 1.1 ppm / K).

The quadrupolar effects of natural abundance ^{14}N (99.6 %, I = 1) from am(m)ines which coordinate to Pt can broaden the ^{195}Pt resonances. Such quadrupolar effects of ^{14}N have the beneficial effects of shortening the ^{195}Pt relaxation times and allowing rapid pulsing without saturation effects. ^{195}Pt-^{14}N couplings in ^{195}Pt NMR spectra are usually better resolved at higher temperature, because of the decreased quadrupolar relaxation rate of ^{14}N due to the decrease in correlation time. Even in the absence of

^{14}N ligands, ^{195}Pt resonances can still be very broad owing to chemical shift anisotropy (CSA) relaxation, which can be the dominant relaxation mechanism for Pt complexes at high magnetic field strength. Similarly, ^{195}Pt satellites in ^{15}N and ^{1}H spectra of Pt^{II} complexes are often broadened beyond detection owing to CSA relaxation of ^{195}Pt. The linewidths of ^{195}Pt satellites of ^{1}H NMR resonances are dependent on the spin-lattice relaxation time of ^{195}Pt:

$$\Delta\nu_{½}(H) = [\pi T_2^*(H)]^{-1} + [2\pi T_1(Pt)]^{-1}$$

where $[\pi T_2^*(H)]^{-1}$ is the natural linewidth plus the contribution from magnetic inhomogenity broadening (measurable from the linewidth of the centre peak).[5] The contribution to ^{195}Pt T_1 relaxation from CSA is given by:

$$[\pi T_1(Pt)]^{-1}\ (CSA) = (6/7)x[\pi T_2(Pt)]^{-1}\ (CSA) = (2/15)\ x\ \gamma_{Pt}^2\ x\ B_0^2\ x\ \Delta\sigma^2\ x\ \tau_c$$

In general, ^{195}Pt satellites (and ^{195}Pt resonances) are sharper in Pt^{IV} complexes which are six coordinate and hence more symmetrical (smaller anisotropy $\Delta\sigma$); and are broader at higher fields of measurement (B_0) and in larger molecules (longer correlation time τ_c).

2.1.1.2 ^{15}N NMR Spectroscopy

^{14}N NMR spectroscopy can be useful for am(m)ine complexes, but ^{14}N is a quadrupolar nucleus, and quadrupolar relaxation is dominant when the environment of ^{14}N has a little symmetry. This can lead to very broad lines and a reduction in sensitivity. On the other hand, short relaxation times also have the advantage of allowing rapid pulsing so that a large number of transients can be acquired. Thus, it is possible to follow reactions of cisplatin in blood plasma and cell culture media at millimolar drug concentrations, and also to detect ammine release.[8]

By using ^{15}N enriched am(m)ine complexes, the broadening of ^{195}Pt signals caused by the quadrupolar effects of ^{14}N can be avoided. Both ^{15}N NMR chemical shifts and $^{1}J(^{195}Pt\text{-}^{15}N)$ coupling constants are sensitive to the nature of the *trans* ligand in Pt

am(m)ine complexes, which can provide useful information for identifying the ligands in the coordination spheres of both Pt^{II} and Pt^{IV} complexes. Typical ^{15}N and ^{1}H shift ranges for Pt-NH_3 are shown in Figure 2.1.

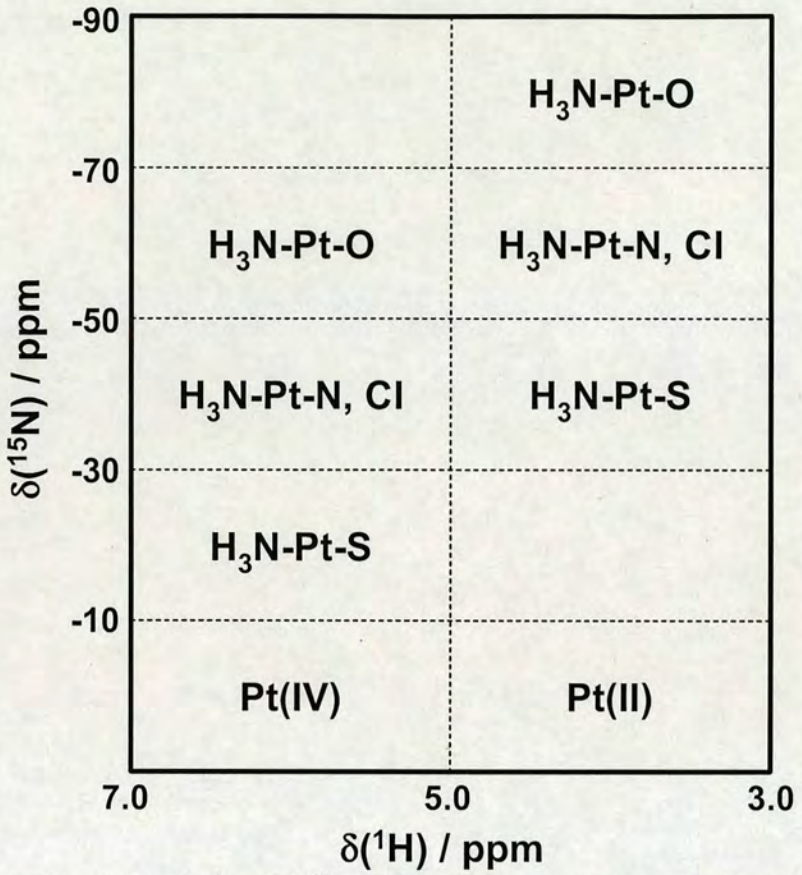

Figure 2.1 Variation in ^{1}H and ^{15}N NMR chemical shifts with the *trans* ligand in Pt-NH_3 complexes. A similar picture is obtained for amine complexes, but the shifts are offset in both dimensions, e.g. for ethylenediamine Pt complexes the ^{1}H resonances are shifted to low-field by ca. 2 ppm and the ^{15}N resonances to low-field by ca. 40 ppm.

In general, ligands with a high *trans* influence give rise to smaller ^{195}Pt-^{15}N coupling constants (S < I < Br < Cl < H_2O), and cause a low-field shift of the ^{15}N resonance. The usefulness of $^{1}J(^{195}Pt\text{-}^{15}N)$ values is limited by the difficulty in determining them for larger molecules, especially at high observation frequencies on account of the dominance of relaxation via chemical shift anisotropy (CSA). The $^{1}J(^{195}Pt\text{-}^{15}N)$ values for Pt^{IV} are smaller than Pt^{II} by a factor of about 1.5 to 1.2 and are 1.4 times larger than $^{1}J(^{195}Pt\text{-}^{14}N)$ values.

The low receptivity of ^{15}N (3.85×10^{-6} relative to ^{1}H) limits to some extent its usefulness for directly-detected ^{15}N NMR studies of Pt am(m)ine complexes. However, the sensitivity of detection can be improved by ^{15}N isotopic enrichment, combined with enhancement by polarization transfer from ^{1}H (e.g. ^{15}N-{^{1}H} DEPT and INEPT pulse sequences). The maximum enhancement in ^{15}N signal intensity achievable via polarization transfer is only 9.8 ($\gamma H/\gamma N$), which means that inverse (^{1}H-detected) ^{15}N methods are usually preferred due to the superior enhancement for ^{15}N detection. The repetition time of the pulse sequence is governed by the ^{1}H rather than the longer ^{15}N spin-lattice relaxation time (T_1), which is an additional advantage because it allows more rapid pulsing. For example, ^{15}N-{^{1}H} DEPT sequences enable the detection of rapidly changing intermediates in the reaction of ^{15}N-cisplatin with glutathione, and also ammine release following the reaction of ^{15}N-cisplatin with intracellular components in intact red blood cells at concentrations as low as 1 mM.[9]

2.1.1.3 Water Suppression

NMR spectra of biomolecules are usually run in aqueous solutions, such as D_2O (99.9 %) or H_2O / D_2O (90 % / 10 %, v/v) as this is the most biologically relevant medium. However, the Pt-NH ^{1}H NMR resonances for Pt am(m)ine complexes are not easily detected in D_2O solutions as the half-life for H-D exchange is often only a few minutes at ambient temperatures.[10,11]

Two different techniques were used to suppress the large HOD (or H_2O) signal, Presaturation and WATERGATE (WATER suppression by GrAdient Tailored Excitation).[12] Presaturation involves irradiation at the frequency of the HOD (H_2O) resonance during the relaxation delay between pulses. The disadvantage is that exchangeable NH protons can also be saturated resulting in a loss of intensity. The WATERGATE method uses selective 180° pulse field gradients to select different coherence pathways, and gives superior water suppression, however this can also results in suppression of other signals in close proximity to the water peak.

2.1.1.4 Heteronuclear Single-Quantum Coherence Experiments

The heteronuclear single-quantum coherence (HSQC) experiment is an inverse detection method used to enhance the sensitivity of ^{15}N. The sensitivity can be improved by a theoretical maximum of 306 with respect to directly detected ^{15}N, this means signals in aqueous solutions at concentration of physiological relevance (mM or even μM) can be detected.[5] ^{1}H-detected inverse methods are applicable to any system which contains a ^{15}N atom with a measurable spin-spin coupling to ^{1}H (i.e. $^{1}J(^{15}N\text{-}^{1}H)$ in ammine, primary and secondary amines, but not tertiary amines although a longer range can sometimes be utilised). In practice the best applications are for those systems with large one-bond couplings (e.g. ca 73 Hz for $^{15}NH_3$). Besides the high sensitivity, inverse detection also brings a simplification of complicated spectra because it detects only those protons directly attached to the labelled ^{15}N atoms in the sample. This is very important for investigations of ^{1}H NMR spectra of body fluids or cell culture media which contains thousands of overlapping resonances. The basic HSQC pulse sequence is shown in Figure 2.2.

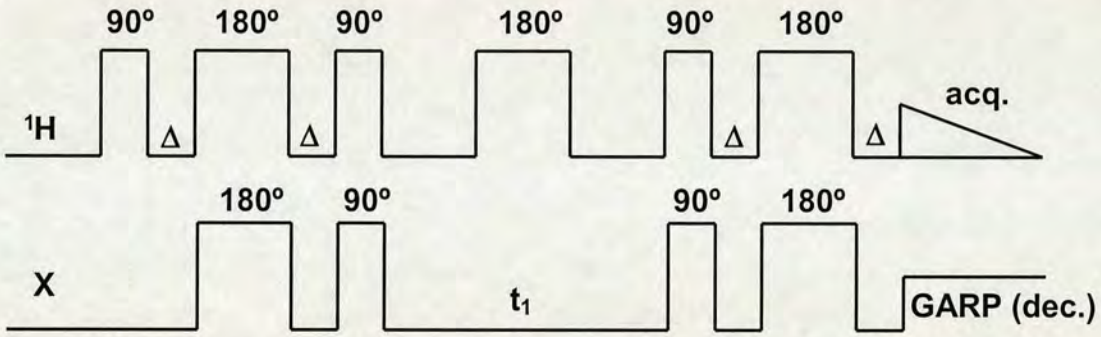

Figure 2.2 Basic HSQC pulse sequence. The delay $\Delta = ½\ J(X,H)$, where J is the one-bond HX coupling constant, and one-dimensional ^{15}N-edited spectra are obtained by setting the evolution period t_1 to zero. Spectra may be recorded with or without decoupling of ^{15}N spins (GARP) during the acquisition period.

A 1D ^{1}H spectrum containing only resonances from Pt-^{15}NH species is obtained by acquiring only the first increment in a two-dimensional experiment. If ^{15}N decoupling is employed during acquisition (e.g. the GARP method), then each distinct type of Pt-NH resonance appears as a singlet, sometimes together with the broadened ^{195}Pt satellites. In practice the water resonance is so intense that it is usually necessary to use additional solvent suppression techniques (e.g.

presaturation). The use of pulse sequences in which coherence selection is achieved by the use of pulsed field gradients allows greatly improved water suppression. By use of the HSQC sequence of Stonehouse et al.[13] (Figure 2.2), it is possible to detect NH peaks within a few Hz of the water resonance at concentrations as low as about 10 μM without the need for additional solvent suppression techniques.[5]

The combined detection of ^{1}H and ^{15}N in a 2D inverse NMR experiment is especially powerful, since both the ^{15}N NMR chemical shift, and the one-bond coupling constant $^{1}J(^{1}H\text{-}^{15}N)$ are diagnostic of the *trans* ligand (Figure 2.1). As shown in Figure 2.3, the ^{195}Pt satellites (when not broadened beyond detection by the effects of CSA relaxation) in a 2D $[^{1}H,^{15}N]$ spectrum appear as diagonal peaks which correspond to the $^{2}J(^{1}H\text{-}^{195}Pt)$ coupling constant in the $F_2(^{1}H)$ dimension and to the $^{1}J(^{15}N\text{-}^{195}Pt)$ coupling in the $F_1(^{15}N)$ dimension. Pt^{II} and Pt^{IV} am(m)ine complexes can be easily distinguished from one another by the combination of ^{1}H and ^{15}N chemical shifts (Figure 2.1).

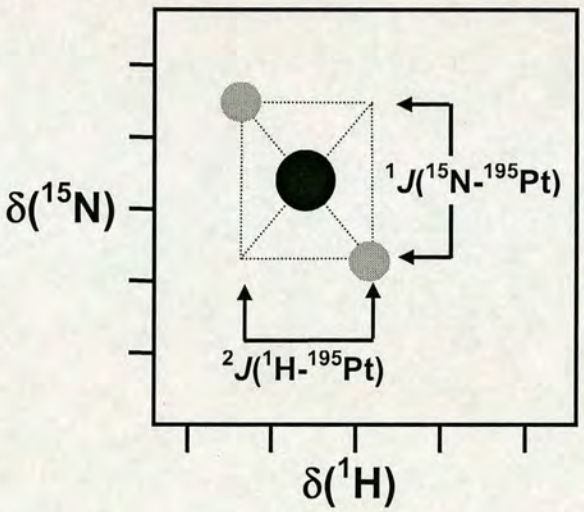

Figure 2.3 General appearance of a 2D $[^{1}H,^{15}N]$ HSQC spectrum. The ^{195}Pt satellites are usually more intense for symmetrical Pt species (Pt^{IV} rather than Pt^{II}).

2.1.2 Experimental NMR Spectroscopy

NMR spectra were recorded at 298 K on a Bruker DMX500 (^{1}H: 500.13 MHz; ^{15}N: 50.7 MHz; ^{195}Pt: 107.523 MHz) or a Bruker AVA600 (^{1}H: 599.81 MHz) NMR spectrometer, using 5 mm NMR tubes. Samples were prepared in d_6-acetone, d_6-

DMSO, or 90 % H_2O / 10 % D_2O with ^1H chemical shifts referenced internally to dioxane (δ 3.764 ppm). ^{15}N chemical shifts were referenced externally to $^{15}NH_4Cl$ (1 M) in HCl (1.5 M) (δ 0 ppm) and ^{195}Pt to $K_2[PtCl_4]$ in H_2O (δ -1623 ppm).[14] All data were processed with XWIN-NMR software (Version 3.6, Bruker, UK Ltd.). For ^1H NMR, typical acquisition conditions for 1D spectra were as follows: 45-60° pulses, 16-32 k data points, 1-3 s relaxation delay, collection of 32-128 transients, final digital resolution of 0.2-0.5 Hz/point. Water suppression was carried out by presaturation. 2D [^1H,^{15}N] HSQC NMR spectra (optimized for $^1J_{(N,H)}$ = 72 Hz) were recorded using the sequence of Stonehouse *et al.*[13] The ^{15}N-spins were decoupled by irradiation with the GARP-1 sequence during acquisition. Water suppression was achieved by presaturation. Typically, 8 scans were acquired for each of 128 increments of t_1 and the final resolution was 6 Hz / point for the F2 dimension and 8 Hz / point for the F1 dimension.

2.2 Ultraviolet and Visible Electronic Absorption Spectroscopy

Ultraviolet and visible electronic absorption spectroscopy (UV-visible spectroscopy) is based on the absorption of light by valence electrons, which are promoted from their ground state to an excited state. The energies of the orbitals involved in electronic transitions have fixed values, but the spectra produced generally contain broad peaks. This is due to the presence of vibrational and rotational energy levels which are also available to the absorbing material.[15,16]

2.2.1 Electronic Transitions

The absorption bands of metal complexes generally arise from two different types of transition: ligand field (d → d) transitions and charge-transfer transitions. Charge-transfer transitions can be further sub-divided into two categories: ligand-to-metal charge-transfer (LMCT) and metal-to-ligand charge-transfer (MLCT). Ligand-centred transitions which do not involve the metal are also possible, particularly for ligands containing π-bonds. These transitions and their selection rules are discussed in detail in Chapter 1.3.1.

2.2.2 Experimental UV-visible spectroscopy

UV-visible electronic absorption spectra were recorded on a Varian Cary 300 UV-visible spectrophotometer in 1 cm path-length cuvettes. The spectral width was 200 – 800 nm and the bandwidth was 1.0 nm. Hellma UV quartz cuvettes were used, either standard (3.5 mL) or micro (0.5 mL), supplied by Aldrich. All spectra were recorded in water and referenced to solvent alone. Data were processed with Origin 5.0.

2.3 Irradiations

Two different light sources were used to irradiate the platinum complexes. For UV irradiations a UV lamp was used, whereas for visible light irradiations an argon-krypton ion laser was used.

2.3.1 Argon-Krypton Ion Laser

Argon-krypton lasers produce reliable, high power in continuous wave (CW) operation on a multitude of lines in the visible region of the electromagnetic spectrum. As a result, CW argon-krypton lasers have found applications in fields as diverse as retinal surgery, high resolution spectroscopy, and newspaper platemaking.[17]

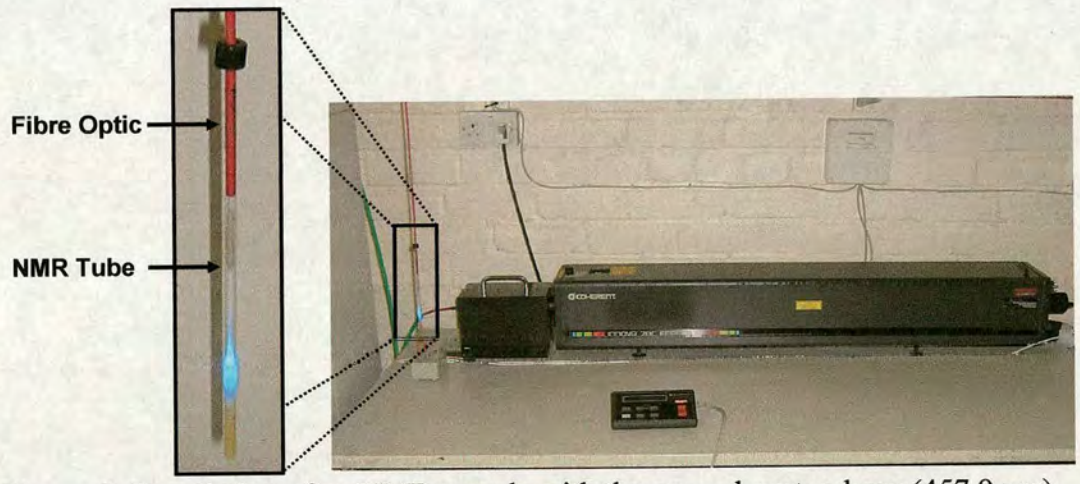

Figure 2.4 Irradiation of an NMR sample with the argon-krypton laser (457.9 nm).

The laser (Coherent Innova 70C Spectrum) used for this work was equipped with a fibre optic (FT-600-UMT, ∅ = 600 μm; Elliot Scientific) to enable delivery of light to a sample within an NMR tube (Figure 2.4). The tip of the fibre optic was always

positioned ca. 2 mm above the solution. The major lines are found at 457.9, 488, 514.5, 520.8, 530.9, 568.2 and 647.1 nm, and the laser output after the fibre optic was measured with either a Coherent 210 power meter or a Coherent Fieldmate power meter (OP2-VIS head).

2.3.2 UV Lamp

The ultraviolet light source was a UV lamp (2 x 15 W tubes, model VL-215L; Merck Eurolab, Poole, UK) which operates at 365 nm and delivers almost pure UVA light. UVB and almost all the visible light are blocked with filters (Figure 2.5).

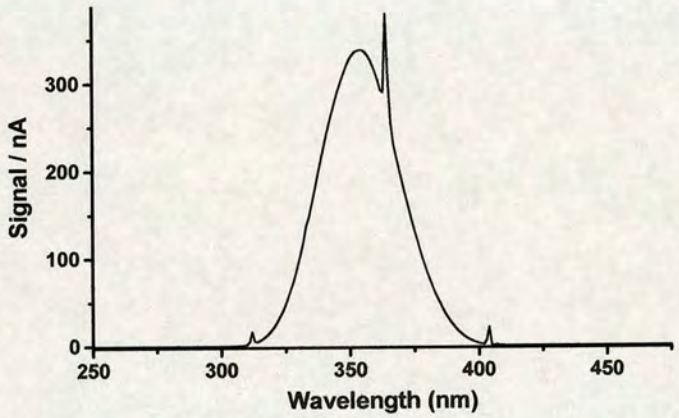

Figure 2.5 Spectral output of UV lamp

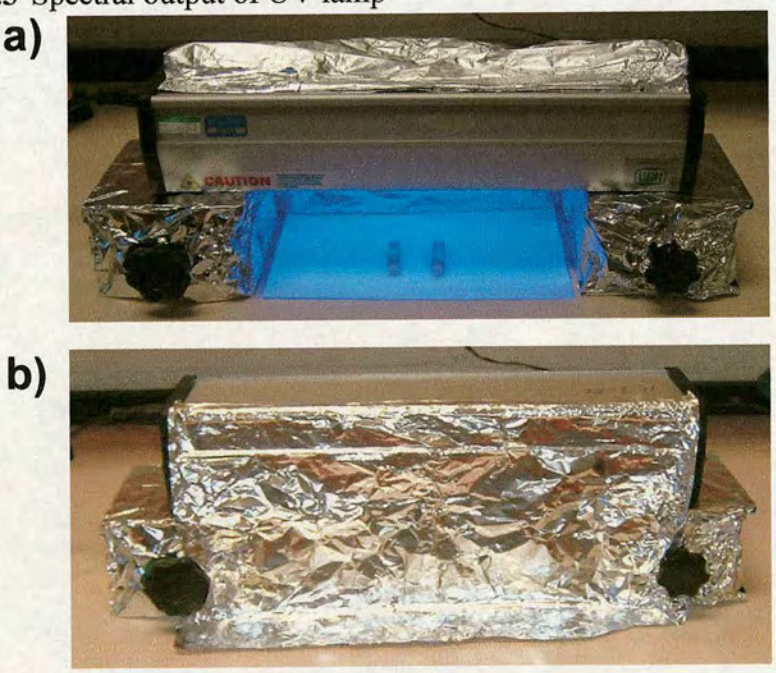

Figure 2.6 a) Irradiation of samples in quartz cuvettes with the UV lamp. b) The tin foil cover ensured any observed changes were not due to external light.

Samples were irradiated at a distance of 10 cm from the lamp where the power is ca. 1.5 mW/cm^2, this power delivers a dose of 10 J/cm^2 over 2 h. Samples were irradiated either in NMR tubes or UV quartz cuvettes (Figure 2.6). The temperature under the lamp was recorded as 298-299 K over a 30 min period.

2.4 Electrospray Ionisation Mass Spectrometry (ESI-MS)

In electrospray ionisation mass spectrometry (ESI-MS) gaseous ions are produced from a liquid solution.[18] ESI-MS is considered a "soft" technique as very little (if any) fragmentation occurs during the ionisation process. The ions are generated by creating a fine spray of charged molecules in the presence of a strong electric field. The charged molecules are sprayed from the tip of a metal nozzle at approximately 3-4 kV, and then electrostatically directed towards the mass spectrometer inlet. Either gas, heat or a combination of both are applied to the droplets to induce vaporisation prior to entering the instrument. As the solvent evaporates, the electric field density increases, hence the mutual repulsion between individual species becomes so great that it exceeds the surface tension and ions leave the droplet. The ions then continue along to the mass analyzer of the mass spectrometer. In electrospray processes the ions observed are quasimolecular ions, they are ionized by the addition of a proton to give $[M+H]^+$ (M = analyte), negative ions can be generated by the removal of a proton. In electrospray multiply charged ions such as $[M+2H]^{2+}$ are also often observed.

Positive ion electrospray mass spectrometry was performed on a Platform II Mass Spectrometer (Micromass, Manchester, UK). The samples were infused at 8 μL/min and the ions produced in an atmospheric pressure ionisation (API)/ESI ion source. The source temperature was 383 K, and the drying gas flow rate was 300 L/h. A potential of 3.5 kV was applied to the probe tip, and cone voltage gradients of 10 – 40 V over 200 – 1000 Da were used. Data acquisition was performed on a Mass Lynx (V 2.5) Windows NT PC data system. All samples were prepared in water.

2.5 Inductively Coupled Plasma Atomic Emission Spectroscopy

ICP-AES analyses were carried out on a Perkin Elmer Optimal Emission Spectrometer Optima 5300 DV. The machine was calibrated using freshly prepared dilute aqueous solutions of a 980 ppm platinum ICP standard (5 wt. % HCl) supplied by Aldrich. The emission wavelength used for platinum detection was 214.423 nm. The R.F. power was 1150 W, the nebulizer flow was 30 psi, and the pump rate was 100 rpm.

2.6 CHN Elemental Analysis

Microanalyses were carried out either at Edinburgh University in the School of Chemistry on an Exeter Analytical Elemental Analyser (CE440), or at St. Andrews University in the School of Chemistry on a Carlo Erba CHNS Analyser.

2.7 pH Measurements

pH values were measured with an Orion 710A pH meter equipped with a microcombination electrode (Aldrich) calibrated with Aldrich standard buffers (pH 4, 7 and 10), and were adjusted with $HClO_4$ (0.1 M) or NaOH (0.1 M).

2.8 References

[1] Hore, P.J. In *Nuclear Magnetic Resonance*, Oxford University Press, New York, **1995**.

[2] Abraham, R.J.; Fisher, J.; Loftus, P. In *Introduction to NMR Spectroscopy*, John Wiley and Sons, New York, **1988**.

[3] Sanders, J.K.M.; Hunter, B.K. In *Modern NMR Spectroscopy*, Oxford University Press, New York, **1997**.

[4] Friebolin, H. In *Basic One- and Two- Dimensional NMR Spectroscopy*, VCH Weinheim, Germany, **1991**.

[5] Berners-Price, S.J.; Sadler, P.J. *Coord. Chem. Rev.* **1996**, *151*, 1.

[6] Harwood, L.M.; Claridge, T.D.W. In *Introduction to Organic Spectroscopy*, Oxford University Press, New York, **1997**

[7] Ismail, I.M.; Kerrison, S.J.S.; Sadler, P.J. *J. Chem. Soc., Chem. Commun.* **1980**, *23*, 1175.

[8] Norman, R.E.; Sadler, P.J. *Inorg. Chem.* **1988**, *27*, 3583.

[9] Berners-Price, S.J.; Kuchel, P.W. *J. Inorg. Biochem.* **1990**, *38*, 327.

[10] Koubek, E.; House, D.A. *Inorg. Chim. Acta* **1992**, *191*, 103.

[11] Miller, S.K.; Marzilli, L.G. *Inorg. Chem.* **1985**, *24*, 2421.

[12] Piotto, M.; Saudek, V.; Sklenar, V. *J. Biomol. NMR* **1992**, *2*, 661.

[13] Stonehouse, J.; Shaw, G.L.; Keeler, J.; Laue, E.D. *J. Magn. Reson.* **1994**, *107*, 174.

[14] Bancroft, D.P.; Lepre, C.A.; Lippard, S.J. *J. Am. Chem. Soc.* **1990**, *112*, 6860.

[15] Shriver, D.F.; Atkins, P.W. In *Inorganic Chemistry*, Oxford University Press, Oxford, **1999**.

[16] Brisdon, A.K. In *Inorganic Spectroscopic Methods*, Oxford University Press, Oxford, **1998**.

[17] Silfvast, W.T. In *Laser Fundamentals*, 2nd Edition, Cambridge University Press, Cambridge, **2004**.

[18] Skoog, D.A.; Holler, E.J.; Nieman, T.A. In *Principles of Instrumental Analysis*, 5th Edition, Saunders College Publishing, Philadelphia, **1998**.

Chapter 3

Synthesis and Characterisation of Platinum Azide Complexes

3.1 Introduction

Platinum(IV) compounds are typically more inert than platinum(II) compounds. It is generally accepted that Pt^{IV} prodrugs exert their toxic effects by *in situ* reduction to the reactive Pt^{II} form.[1] For this reduction to occur two electrons must be donated to the platinum centre and two ligands must leave the complex; therefore the process is a reductive elimination. One of the main problems with platinum chemotherapy is its lack of selectivity which can result in some severe side-effects. The ability to generate a reactive species (e.g. a Pt^{II} complex), from a non-toxic compound (e.g. an inert Pt^{IV} complex) site specifically by photoactivation, has the potential to overcome this problem. The photoactivity of platinum complexes is well documented, and has been observed for compounds containing a variety of halogen and psuedohalogen ligands.[2-4]

Investigations into the photoactivity and DNA binding of Pt^{IV}-diiodo complexes, such as *trans, cis*-$[Pt(en)(OAc)_2I_2]$ have been carried out by Bednarski et al.[5-7] After many promising results, this compound was unfortunately found to be readily reduced to a cytotoxic Pt^{II} species by biological thiols, thus rendering Pt^{IV}-iodo complexes unsuitable as site-specific photoactivated prodrugs.

The photoactivity of Pt^{IV} complexes containing the pseudohalogen azide (N_3) is well known.[8-11] To photoreduce Pt^{IV} to Pt^{II}, two azide ligands are required. One possible mechanism is that upon irradiation the azides leave in the form of radicals ($^{\bullet}N_3$) (Figure 3.1). Azide radicals are very unstable, and decompose in water rapidly into molecular nitrogen (N_2) which prevents reoxidation of the platinum centre. This fast decomposition is believed to be the reason for the efficiency of photoredox reactions involving complexes containing azide ligands. Halogen radicals do not decompose in water, and therefore recombination to generate the starting material is an efficient process.[12]

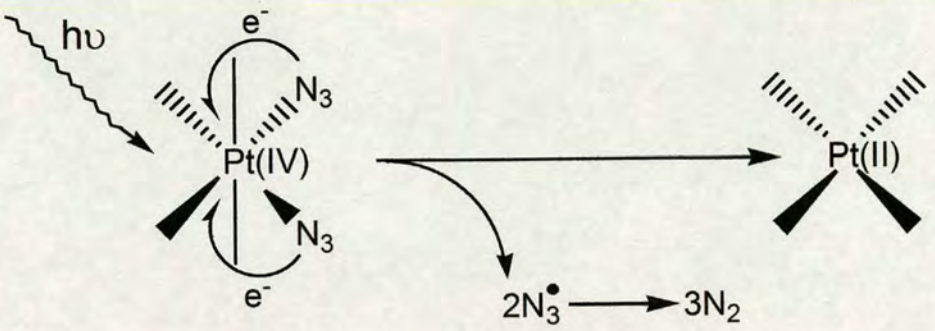

Figure 3.1 Possible mechanism for the photoreduction of a Pt^{IV}-diazido complex.

Two compounds containing azide ligands attached to a Pt^{IV} centre were designed and synthesised in our laboratory by Dr. Phil Müller, *cis, trans, cis*-$[Pt(N_3)_2(OH)_2(NH_3)_2]$ and *cis, trans*-$[Pt(en)(N_3)_2(OH)_2]$. The structures were based on cisplatin and its chelated analogue *cis*-$[Pt(en)Cl_2]$. The hydroxo ligands enhance aqueous solubility and also stabilize the Pt^{IV} oxidation state.[1,13] These complexes were found to reduce and bind to DNA upon irradiation, and importantly were stable in the presence of glutathione (the strongest reducing agent found in cells).[14,15] For structures of complexes **1** and **2** see Appendix 1.

Ideally, a photoactivated drug would absorb in the red region (ca. 650 – 710 nm) of the visible spectrum. The benefits of red light lie in the greater depth of skin penetration and the fact that it is of lower energy than blue light. However, *cis, trans, cis*-$[Pt(N_3)_2(OH)_2(NH_3)_2]$ and *cis, trans*-$[Pt(en)(N_3)_2(OH)_2]$ both absorb mainly in the UV region (< 400 nm). One of the aims of this project was to increase the wavelength of absorbance of Pt^{IV}-azide compounds by changing the amine ligands and / or the stereochemistry.

Azide compounds must be handled with care! When complexed to heavy metals they are known to be shock-sensitive detonators, and as salts are highly toxic.[16] Azides decompose and release N_2 at high temperatures. Therefore after the azide ligands are attached to platinum, the compounds should not be subjected to temperatures above 313 K. When handling Pt-azides in the solid form, certain precautions should always be taken: plastic spatulas instead of metal spatulas, and

buchner funnels with paper filters are used rather than glass sintered funnels.

The following sections describe the synthesis and characterisation of various novel Pt-azide compounds. The photoactivity, stability and DNA binding ability is discussed in subsequent chapters. The structures of all the Pt^{IV} azide complexes synthesised can be found in Appendix 1.

3.2 Experimental

3.2.1 Materials

Silver nitrate, $^{15}NH_4Cl$, methylamine (40 % solution, $MeNH_2$), ethylamine (70 % solution, $EtNH_2$), thiazole (tz), pyridine (py), 2-picoline (2-pic), 3-picoline (3-pic), 4-picoline (4-pic), ethylenediamine (en), cyclohexylamine (c-$HexNH_2$), ethanol, d_6-acetone, d_6-DMSO, D_2O and 1,4-dioxane were purchased from Aldrich. NaN_3, HCl (37 %), KI, KOH, acetone, methanol, acetic acid (> 99 %) and NaCl were from Fisher. H_2O_2 and 1,10-phenanthroline (phen) from Sigma. $HClO_4$ (60 %) and ammonia from Fisons. DMF and DMSO from Fluka. $K_2[PtCl_4]$ from Alfa Aesar, NH_4Cl from BDH and 2,2′-bipyridine (bpy) from Acros. H_2O was deionised with a USF Elga deioniser.

3.2.2 Synthesis and Characterisation

3.2.2.1 *Cis*-$[PtI_2(NH_3)_2]$

$K_2[PtCl_4]$ (1.481 g, 3.57 mmol) was dissolved in H_2O (70 mL) and KI (6.02 g, 35.67 mmol) added. After stirring for 30 min NH_4Cl (0.382 g, 7.14 mmol) was added and the pH adjusted to 10 with 2 M KOH. The pH was continually readjusted to 10 every 2-5 min until it no longer decreased. The mixture was left stirring for 30 min and then the yellow precipitate collected by filtration, washed with water, ethanol and diethyl ether and dried under vacuum.

Cis-$[PtI_2(^{15}NH_3)_2]$ was prepared as described above using $^{15}NH_4Cl$ as the source of ^{15}N.

Yield: 1.545 g (89.6 %).

CHN: Found: C, 0.00; H, 0.91; N, 5.67. Calculated for $PtH_6I_2N_2$: C, 0.00; H, 1,24; N, 5.80.

^{1}H NMR (90% H_2O/10% D_2O): δ 4.03 ppm (d, $^{15}NH_3$, $^{1}J(^{15}N\text{-}^{1}H)$ 73.0 Hz, 6H).

2D [^{1}H,^{15}N] HSQC NMR: δ (^{1}H, ^{15}N / 4.03, -52.20), $^{1}J(^{195}Pt\text{-}^{15}N)$ 268.8 Hz, $^{2}J(^{195}Pt\text{-}^{1}H)$ 58.5 Hz.

3.2.2.2 *Cis*-$[PtCl_2(NH_3)_2]$ (Cisplatin)

Cis-$[PtI_2(NH_3)_2]$ (0.698 g, 1.44 mmol) was suspended in H_2O (100 mL) and $AgNO_3$ (0.486 g, 2.87 mmol) added. After stirring at 333 K for 24 h, AgI was filtered off with an inorganic membrane filter (Whatman, Anotop 10, 0.02 μm). NaCl (0.338 g, 5.78 mmol) was added and the solvent reduced to 10 mL and stored at 277 K for 24 h. *Cis*-$[PtCl_2(NH_3)_2]$ was filtered off washed with water, ethanol and diethyl ether and dried under vacuum.

Cis-$[PtCl_2(^{15}NH_3)_2]$ was prepared from *cis*-$[PtI_2(^{15}NH_3)_2]$ by the above method.

Yield: 0.391 g (90.3 %)

CHN: Found: H, 1.93; N, 9.03; Calculated for $PtH_6Cl_2N_2$: H, 2.00; N, 9.33.

^{1}H NMR (90% H_2O/10% D_2O): δ 4.07 ppm (d, $^{15}NH_3$, $^{1}J(^{15}N\text{-}^{1}H)$ 73.0 Hz, 6H).

^{1}H NMR (d_6-DMSO): δ 3.96 ppm (br s, $^{14}NH_3$, 6H).

2D [^{1}H,^{15}N] HSQC NMR (90% H_2O/10% D_2O): δ (^{1}H, ^{15}N / 4.07, -69.32), $^{1}J(^{195}Pt\text{-}^{15}N)$ 324.6 Hz, $^{2}J(^{195}Pt\text{-}^{1}H)$ 63.0 Hz.

3.2.2.3 *Trans*-$[PtCl_2(NH_3)_2]$ (Transplatin)

Cisplatin (0.157 g, 0.524 mmol) was suspended in H_2O (15 mL) and NH_3 (35 %, 7.855 mmol, 0.434 mL) added. After refluxing for 1 h all the solvent was removed. The pure white solid was re-dissolved in HCl (1.6 M, 11 mL), and stirred in the dark at 378 K for 4 d. After cooling to room temperature the flask was placed on ice to complete precipitation. *Trans*-$[PtCl_2(NH_3)_2]$ was filtered off, washed with water, ethanol and diethyl ether and dried under vacuum, then recrystallised from hot HCl (0.1 M).

Yield: 0.114 g (72.7%)

CHN: Found: H, 1.50; N, 9.82. Calculated for $PtH_6Cl_2N_2$: H, 2.00; N, 9.33.

^{1}H NMR (d_6-DMSO): δ 4.39 ppm (br s, $^{14}NH_3$, 6H).

Trans-$[PtCl_2(^{15}NH_3)_2]$ was prepared by refluxing a suspension of *cis*-$[PtCl_2(^{15}NH_3)_2]$

(57.0 mg, 0.19 mmol) in water containing $^{15}NH_4Cl$ (1.9 mmol) at pH 11 (adjusted with 2 M KOH). After 24 h the pH was readjusted from 7 to 11 and refluxing continued for 6 h or until a clear, colorless solution was obtained. The solvent was removed and HCl (2.3 M, 2.5 mL) added. The solution was refluxed for 4 days, then cooled, placed on ice for 2 h, filtered off, washed with water, ethanol and diethyl ether and dried under vacuum.

Yield: 46.63 mg (81.8 %)

^1H NMR (90% H_2O/10% D_2O): δ 3.60 ppm (d, $^{15}NH_3$, $^1J(^{15}N\text{-}^1H)$ 72.0 Hz, 6H).

2D [^1H,^{15}N] HSQC NMR: δ (^1H, ^{15}N / 3.60, -66.95), $^1J(^{195}Pt\text{-}^{15}N)$ 277.5 Hz, $^2J(^{195}Pt\text{-}^1H)$ 52.0 Hz.

3.2.2.4 $[Pt(en)Cl_2]$

$K_2[PtCl_4]$ (1.528 g, 3.682 mmol) was dissolved in H_2O (30 mL) and ethylenediamine (en) (0.98 mol eq, 0.077 mL) added. The volume was reduced and after storing at 277 K for 1 h the yellow precipitate was filtered off, washed with water, ethanol and diethyl ether and dried under vacuum.

$[Pt(^{15}N\text{-en})Cl_2]$ was synthesized by Dr. Phil Müller as previously described.[17]

Yield: 0.884 g (73.7 %)

^1H NMR (90 % H_2O/10 % D_2O): δ 2.61 ppm (s, en CH_2).

3.2.2.5 *Cis, trans, cis*-$[Pt(N_3)_2(OH)_2(NH_3)_2]$ **(1)**

a) *Cis*-$[Pt(N_3)_2(NH_3)_2]$

Cis-$[PtI_2(NH_3)_2]$ (0.497 g, 1.029 mmol) was suspended in H_2O (100 mL) and $AgNO_3$ (1.98 mol eq, 0.346 g) added. The mixture was stirred at 333 K in the dark for 24 h. After cooling to room temperature, the AgI precipitate was removed by filtration with an inorganic membrane filter (Whatman, Anotop 10, 0.02 μm). NaN_3 (20.57 mmol, 1.34 g) was added to the solution which was stirred for 1 h in the dark at room temperature. The volume was reduced until precipitation was observed and then placed at 277 K for 24 h for further precipitation. The yellow crystals of *cis*-$[Pt(N_3)_2(NH_3)_2]$ were filtered off and washed with water, ethanol and diethyl ether then dried under vacuum.

Yield: 0.223 g (69.2 %)

^{1}H NMR (90% H_2O/10% D_2O): δ 3.84 ppm (d, $^{15}NH_3$, $^{1}J(^{15}N\text{-}H)$ 75.0 Hz, 6H).

2D [^{1}H,^{15}N] HSQC NMR: δ (^{1}H, ^{15}N / 3.84, -69.47), $^{1}J(^{195}Pt\text{-}^{15}N)$ 295.6 Hz, $^{2}J(^{195}Pt\text{-}^{1}H)$ 55.0 Hz.

b) *Cis, trans, cis*-$[Pt(N_3)_2(OH)_2(NH_3)_2]$

Cis-$[Pt(N_3)_2(NH_3)_2]$ (0.222 g, 0.709 mmol) was suspended in H_2O (100 mL) and H_2O_2 (30 %, 28.4 mmol, 2.89 mL) added. After stirring in the dark at room temperature for 1 h, the yellow solution was reduced in volume until precipitation was observed and then placed at 277 K for 24 h for further precipitation. The yellow crystals of *cis, trans, cis*-$[Pt(N_3)_2(OH)_2(NH_3)_2]$ were filtered off, washed with water, ethanol and diethyl ether and dried under vacuum.

Cis, trans, cis-$[Pt(N_3)_2(OH)_2(^{15}NH_3)_2]$ was prepared from *cis*-$[PtI_2(^{15}NH_3)_2]$.

Yield: 0.186 g (75.4 %)

^{1}H NMR (90% H_2O/10% D_2O, pH 4.82): δ 5.12 ppm (d, $^{15}NH_3$, $^{1}J(^{15}N\text{-}^{1}H)$ 73.5 Hz, 6H).

2D [^{1}H,^{15}N] HSQC NMR: δ (^{1}H, ^{15}N / 5.12, -40.27), $^{1}J(^{195}Pt\text{-}^{15}N)$ 259.8 Hz, $^{2}J(^{195}Pt\text{-}^{1}H)$ 46.0 Hz.

^{195}Pt NMR (90% H_2O/10% D_2O): 902 ppm

UV-vis: λ_{max} = 257 nm (ε = 13,721 $M^{-1}cm^{-1}$).

3.2.2.6 *Cis, trans*-$[Pt(en)(N_3)_2(OH)_2]$ **(2)**

The synthesis of *cis, trans*-$[Pt(en)(N_3)_2(OH)_2]$ was as described in section 3.2.2.5 for *cis, trans, cis*-$[Pt(N_3)_2(OH)_2(NH_3)_2]$ using $[Pt(en)Cl_2]$ as the starting material. $[Pt(^{15}N\text{-}en)Cl_2]$ was used in the preparation of *cis, trans*-$[Pt(^{15}N\text{-}en)(N_3)_2(OH)_2]$.

Cis, trans-$[Pt(en)(N_3)_2(OH)_2]$

Yield: 64.7 %

^{1}H NMR (90 % H_2O/10 % D_2O, pH 5.05): δ 6.38 ppm (d, $^{15}NH_2$, $^{1}J(^{15}N\text{-}H)$ 76.0 Hz, 4H), 2.94 ppm (s, en CH_2, 4H).

2D [^{1}H, ^{15}N] HSQC NMR: δ (^{1}H, ^{15}N / 6.38, -7.22), $^{1}J(^{195}Pt\text{-}^{15}N)$ 278.0 Hz, $^{2}J(^{195}Pt\text{-}H)$ 43.0 Hz.

UV-vis: λ_{max} = 257 nm (ε = 14,340 $M^{-1}cm^{-1}$).

3.2.2.7 *Trans, trans, trans*-$[Pt(N_3)_2(OH)_2(NH_3)_2]$ **(3)**

Trans-$[PtCl_2(NH_3)_2]$ (0.102 g, 0.341 mmol) was suspended in H_2O and $AgNO_3$ (0.664 mmol, 0.113 g) was added. The suspension was stirred in the dark at 333 K for 48 h, and then the AgCl precipitate was removed by filtration with an inorganic membrane filter (Whatman, Anotop 10, 0.02 μm). NaN_3 (1.32 mmol, 0.086 g) was added and the solution stirred in the dark for 24 h. *Trans*-$[Pt(N_3)_2(NH_3)_2]$ was collected by filtration and resuspended in H_2O (100 mL). Addition of H_2O_2 (30 %, 2.64 mmol) followed by stirring for a further 6 h resulted in a cloudy yellow solution. The insoluble AgN_3 was filtered off and the solution concentrated. Crystals appeared after storing at 277 K for 24 h. The bright yellow crystals were filtered off, washed with water, ethanol and diethyl ether and dried under vacuum. Crystals suitable for X-ray analysis were grown from H_2O at 277 K.[18]

Trans, trans, trans-$[Pt(N_3)_2(OH)_2(^{15}NH_3)_2]$ was prepared from *trans*-$[PtCl_2(^{15}NH_3)_2]$.

Yield: 66.4 mg (56.2 %)

^{1}H NMR (90% H_2O/10% D_2O, pH 4.75): δ 5.32 ppm (d, $^{15}NH_3$, $^1J(^{15}N\text{-}^1H)$ 72.0 Hz, 6H).

2D [^{1}H,^{15}N] HSQC NMR: δ (^{1}H, ^{15}N / 5.32, -41.65), $^1J(^{195}Pt\text{-}^{15}N)$ 282 Hz, $^2J(^{195}Pt\text{-}^1H)$ 47.5 Hz.

^{195}Pt NMR (90% H_2O/10% D_2O): 875 ppm

ESI-MS: $[M + Na]^+$ 370.1 m/z

UV-vis: λ_{max} = 286 nm (ε = 18,945 $M^{-1}cm^{-1}$).

3.2.2.8 *Trans, trans, trans*-$[Pt(N_3)_2(OH)_2(NH_3)(py)]$ **(4)**

a) *Trans*-$[PtCl_2(NH_3)(py)]$

Cisplatin (0.106 g, 0.352 mmol) was suspended in H_2O (3 mL) and pyridine (py) added (1.056 mmol, 84.6 μL). After stirring at 348 K for 90 min, the clear solution was cooled to room temperature and reduced to dryness to give a white solid. HCl (2 M, 2 mL) was added and the solution stirred at 343 K for 4 days. After cooling on ice, the yellow solid was filtered off, washed with water, ethanol and diethyl ether and dried under vacuum.

Trans-$[PtCl_2(^{15}NH_3)(py)]$ was prepared from *cis*-$[PtCl_2(^{15}NH_3)_2]$.

Yield: 0.100 g (78.7 %)

^{1}H NMR (d_6-acetone): δ 8.85 (d, H_o, $^1J_{o,m}$ 6.8 Hz, 2H), 7.98 (t, H_p, $^1J_{p,m}$ 7.6 Hz, 1H), 7.45 (dd, H_m, 2H), 3.86 (d, $^{15}NH_3$, $^1J(^{15}N\text{-}^1H)$ 72.0 Hz, 3H).

2D [^{1}H,^{15}N] HSQC NMR: δ (^{1}H, ^{15}N / 3.86, -70.28), $^1J(^{195}Pt\text{-}^{15}N)$ 276.7 Hz, $^2J(^{195}Pt\text{-}^1H)$ 52.0 Hz.

b) *Trans*-[$Pt(N_3)_2(NH_3)(py)$]

Trans-[$PtCl_2(NH_3)(py)$] (97.4 mg, 0.269 mmol) was suspended in H_2O (25 mL) and $AgNO_3$ (1.98 mol eq, 89.1 mg) added. After stirring at 333 K for 24 h in the dark AgCl was removed by filtration with an inorganic membrane filter (Whatman, Anotop 10, 0.02 μm). NaN_3 (0.538 mmol, 35.0 mg) was added and the suspension stirred for 6 h in the dark. The volume was reduced to 2 mL and left at 277 K for 24 h. The yellow precipitate was filtered off, washed with water, ethanol and diethyl ether and dried under vacuum.

Yield: 92.9 mg (92.1 %)

^{1}H NMR (d_6-acetone): δ 8.77 (d, H_o, $^1J_{o,m}$ 6.8 Hz, 2H), 8.08 (t, H_p, $^1J_{p,m}$ 7.5 Hz, 1H), 7.59 (dd, H_m, 2H), 3.97 (d, $^{15}NH_3$, $^1J(^{15}N\text{-}^1H)$ 72.0 Hz, 3H)

2D [^{1}H,^{15}N] HSQC NMR: δ (^{1}H, ^{15}N / 3.97, -67.39), $^1J(^{195}Pt\text{-}^{15}N)$ 322.4 Hz, $^2J(^{195}Pt\text{-}^1H)$ 53.5 Hz.

c) *Trans, trans, trans*-[$Pt(N_3)_2(OH)_2(NH_3)(py)$]

Trans-[$Pt(N_3)_2(NH_3)(py)$] (92.0 mg, 0.245 mmol) was suspended in H_2O (300 mL) and H_2O_2 (30 %, 1.470 mmol 0.150 mL) added. After stirring overnight at room temperature in the dark, the volume was reduced to 20 mL and the remaining insoluble AgN_3 was removed by filtration. All the solvent was removed and acetone was added to precipitate the product, which was collect by filtration and washed sparingly with ice cold water, ethanol and diethyl ether, then dried under vacuum. Crystals suitable for X-ray analysis were grown from H_2O at 277 K.

Yield: 75.8 mg (74.8 %)

^{1}H NMR (90 % H_2O / 10 % D_2O, pH 5.12): δ 8.72 (d, H_o, $^1J_{o,m}$ 6.0 Hz, 2H), 8.25 (t, H_p, $^1J_{p,m}$ 7.6 Hz, 1H), 7.78 (dd, H_m, 2H), 5.65 (d, $^{15}NH_3$, $^1J(^{15}N\text{-}^1H)$ 74.0 Hz, 3H)

2D [^{1}H,^{15}N] HSQC NMR: δ (^{1}H, ^{15}N / 5.65, -46.00), $^1J(^{195}Pt\text{-}^{15}N)$ 282.3 Hz, $^2J(^{195}Pt\text{-}^1H)$ 49.5 Hz.

ESI-MS: $[M + Na]^+$ 432.0 m/z

UV-vis: λ_{max} = 289 nm (ε = 18,816 $M^{-1}cm^{-1}$), 268 nm (ε = 10,800 $M^{-1}cm^{-1}$).

3.2.2.9 *Trans, trans, trans*-$[Pt(N_3)_2(OH)_2(NH_3)(MeNH_2)]$ **(5)**

a) *Trans*-$[PtCl_2(NH_3)(MeNH_2)]$

Cisplatin (0.105 g, 0.351 mmol) was suspended in H_2O (2 mL) and methylamine ($MeNH_2$, 40 % solution, 1.404 mmol, 0.121 mL) added. The mixture was stirred under nitrogen at 343 K for 2 h or until the solution was colourless. The volume was reduced to dryness and then HCl (1.7 M, 2.5 mL) was added. The reaction was stirred under nitrogen at 348 K for 24 h then cooled on ice and filtered. The filtrate was placed back under nitrogen and heated at 373 K for 6 h, then 348 K for 12 h, cooled on ice and filtered again, this was repeated once more and all three batches of solid were combined and washed with water, ethanol and diethyl ether then dried under vacuum.

Yield: 77.5 mg (70.3 %)

^1H NMR (d_6-acetone): δ 3.97 (s, NH_2, 2H), 3.37 (s, NH_3, 3H), 2.43 (t, CH_3, $^1J(CH_3$-$NH_2)$ 6.5 Hz, 3H).

b) *Trans*-$[Pt(N_3)_2(NH_3)(MeNH_2)]$

Trans-$[PtCl_2(NH_3)(MeNH_2)]$ (75.9 mg, 0.242 mmol) was suspended in H_2O (25 mL) and $AgNO_3$ (1.95 mol eq, 80.1 mg) added. The reaction was stirred in the dark at 333 K for 24 h then filtered with an inorganic membrane filter (Whatman, Anotop 10, 0.02 μm). NaN_3 (0.968 mmol, 63.0 mg) was added and the yellow solution was stirred for 4 h, then reduced to dryness. Small amounts of H_2O were added and the product filtered, washed with ethanol and diethyl ether then dried under vacuum. Crystals suitable for X-ray analysis were grown from H_2O at 277 K.

Yield: 61.3 mg (77.6 %)

^1H NMR (d_6-acetone): δ 4.20 (s, NH_2, 2H), 3.70 (s, NH_3, 3H), 2.45 (t, CH_3, $^1J(CH_3$-$NH_2)$ 6.5 Hz, 3H).

c) *Trans, trans, trans*-$[Pt(N_3)_2(OH)_2(NH_3)(MeNH_2)]$

Trans-$[Pt(N_3)_2(NH_3)(MeNH_2)]$ (59.8 mg, 0.183 mmol) was suspended in H_2O (20

mL) and H_2O_2 (0.732 mmol, 0.083 mL) added. After stirring in the dark at room temperature for 1 h the solvent was removed. Ethanol was added to precipitate the product which was filtered, washed sparingly with ice cold water, ethanol and diethyl ether then dried under vacuum.

Yield: 53.7 mg (81.3 %)

^{1}H NMR (90 % H_2O / 10 % D_2O): δ 2.36 (septet, CH_3, 3H).

ESI-MS: $[M + H]^+$ 362.1 m/z

UV-vis: λ_{max} = 286 nm (ε = 19,384 $M^{-1}cm^{-1}$).

3.2.2.10 *Trans, trans, trans*-$[Pt(N_3)_2(OH)_2(NH_3)(EtNH_2)]$ **(6)**

a) *Trans*-$[PtCl_2(NH_3)(EtNH_2)]$

Cisplatin (94.6 mg, 0.315 mmol) was suspended in H_2O (1.5 mL) and ethylamine ($EtNH_2$, 70 % solution, 2.520 mmol, 0.121 mL) added. The reaction was heated at 363 K for 2 h or until the solution was colourless, and then the solvent removed. The white solid was redissolved in HCl (2.5 M, 1.5 mL). The solution was stirred at 363 K for 48 h, cooled to room temperature and placed on ice for 2 h. The bright yellow solid was filtered, washed with water, ethanol and diethyl ether and dried under vacuum.

Yield: 76.6 mg (74.1 %)

^{1}H NMR (d_6-acetone): δ 3.98 (s, $^{14}NH_2$, 2H), 3.38 (d, $^{15}NH_3$, $^1J(^{15}N\text{-}^1H)$ 72.0 Hz, 3H), 2.75 (sextet, CH_2, 2H), 1.27 (t, CH_3, $^1J(CH_2\text{-}CH_3)$ 7.0 Hz, 3H).

2D [^{1}H,^{15}N] HSQC NMR: δ (^{1}H, ^{15}N / 3.38, -68.38), $^1J(^{195}Pt\text{-}^{15}N)$ 258.7 Hz, $^2J(^{195}Pt\text{-}^1H)$ 51.0 Hz.

b) *Trans*-$[Pt(N_3)_2(NH_3)(EtNH_2)]$

Trans-$[PtCl_2(NH_3)(EtNH_2)]$ (40.6 mg, 0.124 mmol) was suspended in H_2O (20 mL) and $AgNO_3$ (1.95 mol eq, 41.1 mg) added. The reaction was stirred in the dark at 333 K for 24 h then filtered with an inorganic membrane filter (Whatman, Anotop 10, 0.02 μm). NaN_3 (0.744 mmol, 48.3 mg) was added and the yellow solution was stirred for 24 h, then reduced to dryness. Small amounts of H_2O were added and the product filtered, washed with ethanol and diethyl ether and dried under vacuum.

Yield: 33.9 mg (80.3 %)

^{1}H NMR (d_6-acetone): δ 4.20 (s, $^{14}NH_2$, 2H), 3.70 (d, $^{15}NH_3$, $^{1}J(^{15}N\text{-}^{1}H)$ 60.0 Hz, 3H), 2.77 (sextet, CH_2, 2H), 1.32 (t, CH_3, $^{1}J(CH_2\text{-}CH_3)$ 6.0 Hz, 3H).

2D [^{1}H,^{15}N] HSQC NMR: δ (^{1}H, ^{15}N / 3.70, -43.59), $^{1}J(^{195}Pt\text{-}^{15}N)$ 247.4 Hz, $^{2}J(^{195}Pt\text{-}^{1}H)$ 41.5 Hz.

c) *Trans, trans, trans*-[$Pt(N_3)_2(OH)_2(NH_3)(EtNH_2)$]

Trans-[$Pt(N_3)_2(NH_3)(EtNH_2)$] (33.5 mg, 0.098 mmol) was suspended in H_2O (30 mL) and H_2O_2 (0.392 mmol, 0.041 mL) added. After stirring in the dark at room temperature for 1 h the solution was filtered. All the solvent was removed and then ethanol added to precipitate the product. The yellow solid was collected by filtration, washed sparingly with ice cold water, ethanol and diethyl ether and dried under vacuum.

Yield: 26.7 mg (72.7 %)

ESI-MS: $[M + H]^+$ 375.9 m/z

UV-vis: λ_{max} = 285 nm (16,516 $M^{-1}cm^{-1}$)

^{1}H NMR (90 % H_2O / 10 % D_2O, pH 4.87): 5.71 (s, NH_2, 2H), 5.29 (d, $^{15}NH_3$, $^{1}J(^{15}N\text{-}^{1}H)$ 73.3 Hz, 3H), 2.89 (sextet, CH_2, 2H), 1.33 (t, CH_3, $^{1}J(CH_2\text{-}CH_3)$ 7.3 Hz, 3H).

2D [^{1}H,^{15}N] HSQC NMR: δ (^{1}H, ^{15}N / 5.29, -41.35), $^{1}J(^{195}Pt\text{-}^{15}N)$ 265.2 Hz, $^{2}J(^{195}Pt\text{-}^{1}H)$ 46.7 Hz.

3.2.2.11 *Trans, trans, trans*-[$Pt(N_3)_2(OH)_2(NH_3)(tz)$] **(7)**

a) *Trans*-[$PtCl_2(NH_3)(tz)$]

Cisplatin (81.8 mg, 0.273 mmol) was suspended in H_2O (2 mL) and thiazole (tz, 0.819 mmol, 0.058 mL) added. The reaction was stirred at 343 K for 2 h, brought to reflux, then cooled. HCl (3.276 mmol, 0.273 mL) was added and the solution stirred at 378 K for 6 h. After cooling to room temperature the product was further precipitated by cooling on ice, then filtered, washed with water, ethanol and diethyl ether and dried under vacuum.

Yield: 77.7 mg (77.3 %)

^{1}H NMR (d_6-acetone): δ 9.53 (dd, H-2, $^{2}J_{2,4}$ 0.9 Hz, $^{2}J_{2,5}$ 2.4 Hz, 1H), 8.29 (dd, H-4, $^{1}J_{4,5}$ 3.7 Hz, 1H), 7.81 (dd, H-5, 1H), 3.81 (s, NH_3, 3H).

b) *Trans*-$[Pt(N_3)_2(NH_3)(tz)]$

Trans-$[PtCl_2(NH_3)(tz)]$ (40.3 mg, 0.110 mmol) was suspended in H_2O (20 mL) and $AgNO_3$ (1.98 mol eq, 36.9 mg) added. The reaction was stirred in the dark at 333 K for 24 h, then filtered with an inorganic membrane filter (Whatman, Anotop 10, 0.02 μm). NaN_3 (0.440 mmol, 28.6 mg) was added and the solution stirred in the dark at room temperature for 24 h. The volume was reduced to 2 mL and the yellow product collected by filtration, washed with water, ethanol and diethyl ether and dried under vacuum.

Yield: 32.3 mg (77.4 %)

^{1}H NMR (d_6-acetone): δ 9.42 (dd, H-2, $^2J_{2,4}$ 0.9 Hz, $^2J_{2,5}$ 2.4 Hz, 1H), 8.12 (dd, H-4, $^1J_{4,5}$ 3.7 Hz, 1H), 7.95 (dd, H-5, 1H), 4.07 (s, NH_3, 3H).

c) *Trans, trans, trans*-$[Pt(N_3)_2(OH)_2(NH_3)(tz)]$

Trans-$[Pt(N_3)_2(NH_3)(tz)]$ (31.7 mg, 0.083 mmol) was suspended in H_2O (500 mL) and H_2O_2 (30 %, 0.332 mmol, 0.034 mL) added. After stirring in the dark at room temperature for 24 h, the volume was reduced to 15 mL and filtered. All solvent was then removed and acetone added to precipitate product. The yellow solid was filtered off and washed sparingly with ice-cold water, ethanol and diethyl ether, and dried under vacuum.

Yield: 24.8 mg (71.2 %)

ESI-MS: $[M + H]^+$ 415.9 m/z

UV-vis: λ_{max} = 289 nm (15,234 $M^{-1}cm^{-1}$), 236 nm (8,630 $M^{-1}cm^{-1}$).

^{1}H NMR (90 % H_2O / 10 % D_2O): δ 9.51 (dd, H-2, $^2J_{2,4}$ 1.0 Hz, $^2J_{2,5}$ 2.4 Hz, 1H), 8.24 (dd, H-4, $^1J_{4,5}$ 3.6 Hz, 1H), 8.04 (dd, H-5, 1H).

3.2.2.12 *Trans, trans, trans*-$[Pt(N_3)_2(OH)_2(NH_3)(2\text{-pic})]$ **(8)**

a) *Trans*-$[PtCl_2(NH_3)(2\text{-pic})]$

Cisplatin (0.103 g, 0.343 mmol) was suspended in H_2O (1 mL) and 2-picoline (1.372 mmol, 0.1277 g) added. The reaction was stirred at 348 K for 2.5 h and then refluxed for 30 min. The solvent was removed and HCl (2.7 M, 1.5 mL) added. The solution was stirred at 378 K for 5 h then cooled to 277 K for 24 h and filtered. The filtrate was returned to heat at 378 K for a further 6 h and then cooled to 277 K and filtered

again. The two batches of yellow solid were combined and washed with water, ethanol and diethyl ether and dried under vacuum.

Trans-[$PtCl_2(^{15}NH_3)$(2-picoline)] was synthesized from ^{15}N-cisplatin.

Yield: 88.3 mg (68.5 %)

^{1}H NMR (d_6-acetone): δ 8.80 (d, H-6, ^1J 5.7 Hz, 1H), 7.78 (td, H-4, ^1J 7.7 Hz, ^2J 1.5 Hz, 1H), 7.43 (d, H-3, ^1J 7.7 Hz, 1H), 7.27 (t, H-5, 1H), 3.68 (s, NH_3, $^1J(^{15}N\text{-}^1H)$ 72.0 Hz, 1H), 3.13(s, CH_3, 3H).

2D [^{1}H,^{15}N] HSQC NMR: δ (^{1}H, ^{15}N / 3.68, -69.67), $^1J(^{195}Pt\text{-}^{15}N)$ 267.0 Hz, $^2J(^{195}Pt\text{-}^1H)$ 53.0 Hz.

b) *Trans*-[$Pt(N_3)_2(NH_3)$(2-pic)]

Trans-[$PtCl_2(NH_3)$(2-pic)] (87.3 mg, 0.232 mmol) was suspended in H_2O (50 mL) and DMF (0.5 mL). $AgNO_3$ (1.95 mol eq, 76.9 mg) was added and the reaction stirred in the dark at 333 K for 24 h. All the solvent was removed and the solid redissolved in H_2O (50 mL). NaN_3 (0.928 mmol, 60.3 mg) was added and the solution stirred for 4 h, the volume was then reduced to 3 mL and the bright yellow solid filtered, washed with water, ethanol and diethyl ether and dried under vacuum.

Yield: 81.2 mg (90.0 %)

^{1}H NMR (d_6-acetone): δ 8.95 (d, H-6, ^1J 5.9 Hz, 1H), 7.89 (td, H-4, ^1J 7.7 Hz, ^2J 1.7 Hz, 1H), 7.59 (d, H-3, 1H) 7.42 (t, H-5, 1H), 3.74 (s, NH_3, $^1J(^{15}N\text{-}^1H)$ 72.0 Hz, 3H), 3.20(s, CH_3, 3H).

2D [^{1}H,^{15}N] HSQC NMR: δ (^{1}H, ^{15}N / 3.74, -65.78), $^1J(^{195}Pt\text{-}^{15}N)$ 334.0 Hz, $^2J(^{195}Pt\text{-}^1H)$ 55.2 Hz.

c) *Trans, trans, trans*-[$Pt(N_3)_2(OH)_2(NH_3)$(2-pic)]

Trans-[$Pt(N_3)_2(NH_3)$(2-pic)] (80.0 mg, 0.206 mmol) was suspended in H_2O (500 mL) and H_2O_2 (30 %, 0.824 mmol, 0.085 mL) added. The reaction was stirred in the dark at room temperature for 24 h and then the volume was reduced to 50 mL. The yellow solution was filtered to remove any remaining AgN_3 and then reduced to dryness. Small amounts of H_2O were added and the solid recovered by filtration and washed with water, ethanol and diethyl ether then dried under vacuum. Crystals suitable for X-ray analysis were grown from H_2O at 277 K.

Yield: 64.9 mg (73.4 %)

ESI-MS: $[M + Na]^+$ 446.6 m/z

UV-vis: λ_{max} = 292 nm (17,888 $M^{-1}cm^{-1}$), 276 nm (sh, 14,500 $M^{-1}cm^{-1}$)

^{1}H NMR (90 % H_2O / 10 % D_2O, pH 5.04): δ 8.66 (d, H-6, ^1J 6.4 Hz, 1H), 8.04 (td, H-4, ^1J 7.7 Hz, 1H), 7.54 (d, H-3, 1H) 7.51 (t, H-5, 1H), 5.67 (d, $^{15}NH_3$, $^1J(^{15}N\text{-}^1H)$ 74.2 Hz, 3H), 3.06 (d, CH_3, 3H).

2D [^{1}H,^{15}N] HSQC NMR: δ (^{1}H, ^{15}N / 5.67, -44.65), $^1J(^{195}Pt\text{-}^{15}N)$ 300.6 Hz, $^2J(^{195}Pt\text{-}^1H)$ 50.4 Hz.

3.2.2.13 *Trans, trans, trans*-$[Pt(N_3)_2(OH)_2(NH_3)(3\text{-pic})]$ **(9)**

a) *Trans*-$[PtCl_2(NH_3)(3\text{-pic})]$

Cisplatin (50.3 mg, 0.168 mmol) was suspended in H_2O (4 mL) and 3-picoline (0.504 mmol, 46.9 mg) added. The reaction was stirred at 378 K for 1 h or until colourless, then HCl (2.02 mmol, 0.168 mL) added. The solution was stirred at 363 K for 12 h then cooled and placed on ice to precipitate the product, which was collected by filtration. The filtrate was returned to heat at 363 K for a further 12 h and then cooled and filtered again. The two batches of yellow solid were combined and washed with water, ethanol and diethyl ether and dried under vacuum.

Yield: 31.1 mg (49.3 %)

^{1}H NMR (d_6-acetone): δ 8.66 (s, H-2, 1H), 8.64 (d, H-6, $^1J_{5,6}$ 5.9 Hz, 1H), 7.78 (d, H-4, $^1J_{4,5}$ 7.9 Hz, 1H), 7.32 (dd, H-5, 1H), 3.74 (s, NH_3, 3H), 2.37 (s, CH_3, 3H).

b) *Trans*-$[Pt(N_3)_2(NH_3)(3\text{-pic})]$

Trans-$[PtCl_2(NH_3)(3\text{-pic})]$ (9.5 mg, 0.025 mmol) was suspended in H_2O (10 mL) and DMF (200 μL). $AgNO_3$ (2 mol eq, 8.5 mg) was added and the reaction stirred in the dark at 333 K for 24 h. NaN_3 (0.100 mmol, 6.6 mg) was added and the solution stirred for 24 h, then all the solvent was removed. H_2O (2 mL) was added and the yellow solid collected by filtration and washed with water, ethanol and diethyl ether and dried under vacuum.

Yield: 7.2 mg (73.2 %)

^{1}H NMR (d_6-acetone): δ 8.59 (s, H-2, 1H), 8.57 (d, H-6, $^1J_{5,6}$ 5.9 Hz, 1H), 7.88 (d, H-4, $^1J_{4,5}$ 7.9 Hz, 1H), 7.46 (dd, H-5, 1H), 3.95 (s, NH_3, 3H), 2.42 (s, CH_3, 3H).

c) *Trans, trans, trans*-[$Pt(N_3)_2(OH)_2(NH_3)$(3-pic)]

Trans-[$Pt(N_3)_2(NH_3)$(3-pic)] (6.9 mg, 0.018 mmol) was suspended in H_2O (20 mL) and H_2O_2 (30 %, 0.071 mmol, 7 μL) added. The reaction was stirred in the dark at room temperature for 24 h and then the volume reduced to 3 mL. The yellow solution was filtered to remove any remaining AgN_3 and then reduced to dryness. Small amounts of H_2O were added and the solid recovered by filtration and washed with water, ethanol and diethyl ether then dried under vacuum.

Yield: 6.2 mg (81.4 %)

ESI-MS: $[M + Na]^+$ 424.0 m/z

UV-vis: λ_{max} = 289 nm (13,575 $M^{-1}cm^{-1}$)

^1H NMR (90 % H_2O / 10 % D_2O): δ 8.53 (s, H-2, 1H), 8.51 (d, H-6, 1H), 8.07 (d, H-4, $^1J_{4,5}$ 7.9 Hz, 1H), 7.65 (dd, H-5, 1H), 2.50 (s, CH_3, 3H).

3.2.2.14 *Trans, trans, trans*-[$Pt(N_3)_2(OH)_2(NH_3)$(4-pic)] **(10)**

a) *Trans*-[$PtCl_2(NH_3)$(4-pic)]

Cisplatin (0.148 g, 0.494 mmol) was suspended in H_2O (4 mL) and 4-picoline (1.483 mmol, 0.1381 g) added. The reaction was stirred at 378 K for 1 h or until colourless, then HCl (5.93 mmol, 0.495 mL) added. The solution was stirred at 363 K for 12 h then cooled and placed on ice to precipitate the product, which was collected by filtration. The filtrate was returned to heat at 363 K for a further 12 h and then cooled and filtered again. The two batches of yellow solid were combined and washed with water, ethanol and diethyl ether and dried under vacuum.

Yield: 0.126 g (67.9 %)

^1H NMR (d_6-acetone): δ 8.66 (d, H-2, H-6, $^1J_{(2,6\text{-}3,5)}$ 6.6 Hz, 2H), 7.26 (d, H-3, H-5, 2H), 3.71 (s, NH_3, 3H), 2.41 (s, CH_3, 3H).

b) *Trans*-[$Pt(N_3)_2(NH_3)$(4-pic)]

Trans-[$PtCl_2(NH_3)$(4-pic)] (45.9 mg, 0.122 mmol) was suspended in H_2O (40 mL) and DMF (200 μL). $AgNO_3$ (2 mol eq, 41.3 mg) was added and the reaction stirred in the dark at 333 K for 24 h. NaN_3 (1.22 mmol, 79.4 mg) was added and the solution stirred for 24 h, then all the solvent was removed. H_2O (2 mL) was added and the yellow solid collected by filtration and washed with water, ethanol and diethyl ether

and dried under vacuum.

Yield: 40.0 mg (84.2 %)

^{1}H NMR (d_6-acetone): δ 8.57 (d, H-2, H-6, $^1J_{(2,6\text{-}3,5)}$ 6.6 Hz, 2H), 7.41 (d, H-3, H-5, 2H), 3.94 (s, NH_3, 3H), 2.46 (s, CH_3, 3H).

c) *Trans, trans, trans*-[$Pt(N_3)_2(OH)_2(NH_3)$(4-pic)]

Trans-[$Pt(N_3)_2(NH_3)$(4-pic)] (19.4 mg, 0.050 mmol) was suspended in H_2O (200 mL) and H_2O_2 (30 %, 0.20 mmol, 0.020 mL) added. The reaction was stirred in the dark at room temperature for 24 h and then the volume was reduced to ~ 20 mL. The yellow solution was filtered to remove any remaining AgN_3 and then reduced to dryness. Small amounts of H_2O were added and the solid recovered by filtration and washed with water, ethanol and diethyl ether then dried under vacuum.

Yield: 14.4 mg (68.2 %)

ESI-MS: $[M + Na]^+$ 424.0 m/z

UV-vis: λ_{max} = 289 nm (14,318 M^{-1} cm^{-1})

^{1}H NMR (90 % H_2O / 10 % D_2O): δ 8.51 (d, H-2, H-6, $^1J_{(2,6\text{-}3,5)}$ 6.8 Hz, 2H), 7.60 (d, H-3, H-5, 2H), 2.58 (s, CH_3, 3H).

3.2.2.15 *Trans, trans, trans*-[$Pt(N_3)_2(OH)_2(NH_3)$(c-HexNH_2)] **(11)**

a) *Trans*-[$PtCl_2(NH_3)$(c-HexNH_2)]

Cisplatin (0.127 g, 0.422 mmol) was suspended in H_2O (2 mL) and cyclohexylamine (c-HexNH_2, 1.265 mmol, 0.144 mL) added. After stirring at 343 K for 4 h, HCl (5.06 mmol, 0.422 mL) was added to the clear solution and heating and stirring was continued for a further 6 h. The flask was cooled to 277 K for 12 h then the yellow precipitate was collected by filtration, washed with water, ethanol and diethyl ether and dried under vacuum.

Yield: 84.5 mg (52.4 %)

^{1}H NMR (d_6-acetone): δ 3.89 (s, NH_2), 3.39 (s, NH_3), 2.36 (m, H-1, 1H), 1.74 (m, H-2a,5a, 2H), 1.58 (d, H-3a,5a, 2H), 1.29 (t, H4a, 1H), 1.16 (m, H-2b,3b,5b,6b, 4H), 0.88 (m, H-4b, 1H). a are equatorial, b are axial hydrogens.

b) *Trans*-[$Pt(N_3)_2(NH_3)$(c-HexNH_2)]

Trans-[$PtCl_2(NH_3)$(c-HexNH_2)] (7.97 mg, 0.021 mmol) was dissolved in DMF (2 mL), NaN_3 (0.044 mmol, 2.87 mg) was dissolved in methanol (0.5 mL) and then the two solutions added together and stirred at 298 K for 2 days. The volume was reduced and crystals suitable for structure determination were grown at 298 K.

^{1}H NMR (d_6-acetone): δ 4.18 (s, NH_2), 3.75 (s, NH_3), 2.35 (m, H-1, 1H), 1.76 (m, H-2a,5a, 2H), 1.61 (d, H-3a,5a, 2H), 1.33 (t, H4a, 1H), 1.16 (m, H-2b,3b,5b,6b, 4H), 0.88 (m, H-4b, 1H).

c) *Trans, trans, trans*-[$Pt(N_3)_2(OH)_2(NH_3)$(c-HexNH_2)]

Trans-[$Pt(N_3)_2(NH_3)$(c-HexNH_2)] (5.0 mg, 0.013 mmol) was suspended in H_2O (2 mL) and H_2O_2 (0.500 mmol, 51 μL) was added. After stirring at 298 K for 12 h the volume was reduced and the solution stored at 277 K. This produced crystals suitable for structure determination.

ESI-MS: $[M + Na]^+$ 452.1 m/z

^{1}H NMR (90 % H_2O / 10 % D_2O): 2.94 (m, H-1, 1H), 2.14 (m, H-2a,5a, 2H), 1.76 (d, H-3a,5a, 2H), 1.63 (t, H4a, 1H), 1.35 (m, H-2b,3b,5b,6b, 4H), 1.18 (m, H-4b, 1H).

3.2.2.16 *Cis, trans, cis*-[$Pt(N_3)_2Cl_2(NH_3)_2$] **(12)**

Cis, trans, cis-[$Pt(N_3)_2(OH)_2(NH_3)_2$] (31.2 mg, 0.090 mmol) was dissolved in H_2O (10 mL) and HCl (0.359 mmol, 0.030 mL) added. The solution was stirred in the dark at room temperature for 24 h, then concentrated and stored at 277 K until crystals appeared. These crystals were suitable for X-ray analysis.

Cis, trans, cis-[$Pt(N_3)_2(OH)_2(^{15}NH_3)_2$] was used in the preparation of *cis, trans, cis*-[$Pt(N_3)_2Cl_2(^{15}NH_3)_2$]. However 2D [^{1}H,^{15}N] HSQC NMR analysis of the solution after stirring for 24 h with 4 mol eq of HCl revealed the presence of several species. The solution was concentrated and crystals grown at 277 K. **During filtration this solid exploded and all work on this compound was stopped.** Presumably the explosive complex is a side product from the reaction.

^{1}H NMR (90 % H_2O / 10 % D_2O): δ 5.49 (septet, NH_3, $^1J(^1H\text{-}^{14}N)$ 105 Hz, $^2J(^1H\text{-}^{195}Pt)$ 51.0 Hz, 6H).

2D [^{1}H,^{15}N] HSQC NMR (natural abundance): δ (^{1}H, ^{15}N / 5.49, -41.27), $^{1}J(^{195}Pt\text{-}^{15}N)$ 242.7 Hz, $^{2}J(^{195}Pt\text{-}^{1}H)$ 46.5 Hz.

ESI-MS: $[M + H]^{+}$ 385 m/z

UV-vis: λ_{max} = 264 nm

3.2.2.17 *Cis, trans*-[Pt(bpy)$(N_3)_2(OH)_2$] **(13)**

a) [Pt(bpy)Cl_2]

$K_2[PtCl_4]$ (0.151 g, 0.363 mmol) was dissolved in H_2O (8 mL) and 2,2′-bipyridine (bpy) (1.05 mol eq, 59.4 mg) in acetone (2.36 mL) was added. Stirring at 338 K for 12 h produced a yellow solid which was collected by filtration and washed with water, ethanol and diethyl ether, then dried under vacuum.

Yield: 136.8 mg (89.3 %)

^{1}H NMR (d_6-DMSO): δ 9.51 (d, $H_{6,6'}$, $^{1}J_{5,6}$ 5.9 Hz, 2H), 8.59 (d, $H_{3,3'}$, $^{1}J_{3,4}$ 8.0 Hz, 2H), 8.42 (t, $H_{4,4'}$, $^{1}J_{4,5}$ 7.7 Hz, 2H), 7.85 (t, $H_{5,5'}$, 2H).

b) [Pt(bpy)$(N_3)_2$]

[Pt(bpy)Cl_2] (98.5 mg, 0.233 mmol) was suspended in DMF (15 mL) and NaN_3 (0.152 g, 2.14 mmol) added. The solution was stirred for 3 days, and the colour changed from bright yellow to orange. The volume was reduced to 1-2 mL and H_2O added to precipitate the product. [Pt(bpy)$(N_3)_2$] was filtered off and washed with water, ethanol and diethyl ether then dried under vacuum. Crystals suitable for X-ray structure determination were grown from DMF at 277 K.

Yield: 93.1 mg (91.7 %)

^{1}H NMR (d_6-DMSO): δ 8.91 (d, $H_{6,6'}$, $^{1}J_{5,6}$ 5.7 Hz, 2H), 8.57 (d, $H_{3,3'}$, $^{1}J_{3,4}$ 8.0 Hz, 2H), 8.40 (t, $H_{4,4'}$, $^{1}J_{4,5}$ 7.7 Hz, 2H), 7.82 (t, $H_{5,5'}$, 2H).

c) *Cis, trans*-[Pt(bpy)$(N_3)_2(OH)_2$]

[Pt(bpy)$(N_3)_2$] (7.8 mg, 0.018 mmol) was suspended in H_2O (1.5 mL) and acetone (0.5 mL). H_2O_2 (0.036 mmol, 3.7 μL) was added and the mixture stirred at 298 K for 24 h. After being left to evaporate to dryness in the back of a fume hood, H_2O (7 mL) was added. There was no dissolution therefore oxidation had not occurred. H_2O_2 (0.720 mmol, 73 μL) was added and the solution stirred for 24 h and again left to

evaporate in the back of a fume hood. Crystals appeared after several weeks and were submitted for X-ray structure determination. All attempts to repeat this synthesis were unsuccessful.

ESI-MS: $[M + H]^+$ 470.1 m/z, $[M + Na]^+$ 492.0 m/z.

^{1}H NMR (d_6-DMSO): δ 9.03 (d, $H_{6,6'}$, $^1J_{5,6}$ 5.8 Hz, 2H), 8.82 (d, $H_{3,3'}$, $^1J_{3,4}$ 7.7 Hz, 2H), 8.48 (t, $H_{4,4'}$, $^1J_{4,5}$ 7.7 Hz, 2H), 8.03 (t, $H_{5,5'}$, 2H).

3.2.2.18 *Trans, cis*-$[Pt(bpy)(OAc)_2(N_3)_2]$ **(14)**

Acetic acid (> 99 %, 0.82 mL) was added to a small amount of $[Pt(bpy)(N_3)_2]$ (17.8 mg, 0.041 mmol), then H_2O_2 (30 %, 0.410 mmol, 42 μL) was added and the suspension stirred for 24 h.

Caution! Mixing H_2O_2 and acetic acid can result in the formation of explosive compounds.[19] No such reactions were reported in references which used a similar oxidation procedure to that described here. [20,21] However, care was taken and the reaction was carried out on a small scale behind a blast screen.

The bright orange solution produced was left to evaporate at the back of the fume hood. After 24 h, 100 mL H_2O was added to the dry vessel, after stirring and sonicating briefly any undissolved solid was removed by filtration. The volume was reduced to 3 mL. A precipitate appeared, the solution was then refiltered and stored at 277 K for crystallization. Crystals suitable for X-ray structure determination were obtained.

^{1}H NMR (90 % H_2O / 10 % D_2O): δ 9.27 (d, $H_{6,6'}$, $^1J_{5,6}$ 5.8 Hz, 2H), 8.56 (d, $H_{3,3'}$, $^1J_{3,4}$ 8.1 Hz, 2H), 8.43 (t, $H_{4,4'}$, $^1J_{4,5}$ 7.9 Hz, 2H), 7.98 (t, $H_{5,5'}$, 2H), 1.84 (s, CH_3, 6H).

ESI-MS: $[M + H]^+$ 554.1 m/z; $[M + Na]^+$ 576.0 m/z

UV-vis: 250 nm (ε = 19,102 $M^{-1}cm^{-1}$), 304 nm (ε = 11,402 $M^{-1}cm^{-1}$), 315 nm (ε = 9,756 $M^{-1}cm^{-1}$).

3.2.2.19 *Trans, cis*-$[Pt(phen)(OAc)_2(N_3)_2]$ **(15)**

a) $[Pt(phen)Cl_2]$

Synthesised by the same method as $[Pt(bpy)Cl_2]$.

Yield: 82.3 %

^{1}H NMR (d_6-DMSO): δ 9.71 (d, $H_{2,9}$, ^1J 5.3 Hz, 2H), 9.05 (d, $H_{4,7}$, ^1J 8.3 Hz, 2H), 8.30 (s, $H_{5,6}$, 2H), 8.18 (d, $H_{3,8}$, 2H).

b) [Pt(phen)$(N_3)_2$]

Synthesised by the same method as [Pt(bpy)$(N_3)_2$]. Crystals suitable for structure determination were grown from DMF at 277 K.

Yield: 82.8 %

^{1}H NMR (d_6-DMSO): δ 9.20 (d, $H_{2,9}$, ^1J 5.3 Hz, 2H), 9.02 (d, $H_{4,7}$, ^1J 8.3 Hz, 2H), 8.28 (s, $H_{5,6}$, 2H), 8.14 (d, $H_{3,8}$, 2H).

c) *Trans, cis*-[Pt(phen)$(OAc)_2(N_3)_2$]

Synthesised by the same method as *trans, cis*-[Pt(bpy)$(OAc)_2(N_3)_2$]. Crystals suitable for structure determination were grown from water at 277 K.

^{1}H NMR (90 % H_2O / 10 % D_2O): δ 9.52 (d, $H_{2,9}$, ^1J 5.3 Hz, 2H), 8.95 (d, $H_{4,7}$, ^1J 8.3 Hz, 2H), 8.30 (s, $H_{5,6}$, 2H), 8.27 (d, $H_{3,8}$, 2H), 1.74 (s, CH_3, 3H).

UV-vis: 204 nm, 224 nm (sh), 271 nm, 304 nm (sh).

3.2.2.20 *Trans*-[Pt$(N_3)_2(py)_2$] (16)

a) *Trans*-[Pt$Cl_2(py)_2$]

K_2[$PtCl_4$] (0.136 g, 0.327 mmol) was dissolved in H_2O (3.3 mL) and pyridine (8.18 mmol, 0.66 mL) in H_2O (6.6 mL) was added. After stirring at 358 K for 1 h, a clear solution was obtained, removal of all the solvent left a white solid. This solid was redissolved in HCl (1 M, 3.5 mL). After stirring at 348 K for 24 h, then cooling to 277 K for 2 h the yellow solid was collected by filtration, washed with water, ethanol and diethyl ether, then dried under vacuum.

Yield: 49.3 g (35.5 %)

^{1}H NMR (d_6-acetone): δ 8.90 (dd, H_o, $^1J_{o,m}$ = 6.6 Hz, $^2J_{o,p}$ = 1.7 Hz, 4H), 8.03 (tt, H_p, $^1J_{p,m}$ = 7.7 Hz, 2H), 7.53 (dd, H_m, 4H).

b) *Trans*-[Pt$(N_3)_2(py)_2$]

Trans-[Pt$Cl_2(py)_2$] (48.6 mg, 0.115 mmol) was suspended in DMF (200 μL) and H_2O

(10 mL) and $AgNO_3$ (1.98 mol eq, 38.6 mg) added. After stirring at 333 K overnight the AgCl precipitate was filtered off with an inorganic membrane filter (Whatman, Anotop 10, 0.02 μm). NaN_3 (0.4584 mmol, 29.8 mg) was added and the solution stirred for 4 h. All solvent was removed and acetone added, the undissolved AgN_3 and excess NaN_3 were collected leaving a yellow solution. All solvent was removed again, small amounts of H_2O added and the yellow solid of *trans*-$[Pt(N_3)_2(py)_2]$ filtered off, washed with water, ethanol and diethyl ether, then dried under vacuum.
Yield: 34.0 mg (67.9 %)
^{1}H NMR (d_6-acetone): δ 8.86 (dd, H_o, $^1J_{o,m}$ = 6.6 Hz, $^2J_{o,p}$ = 1.7 Hz, 4H), 8.12 (tt, H_p, $^1J_{p,m}$ = 7.7 Hz, 2H), 7.67 (dd, H_m, 4H).

3.3 Results and Discussion

Caution! Heavy metal azides (e.g. $Pb(N_3)_2$ and $Hg(N_3)_2$) are known to be shock sensitive detonators, therefore it is essential that any platinum azide compound be handled with extreme care. It is important to avoid the application of any pressure to these materials in the crystalline form.

The structures of all the Pt^{IV} azide complexes synthesised can be found in Appendix 1.

3.3.1 *Cis*-$[PtI_2(NH_3)_2]$

Cis-$[PtI_2(NH_3)_2]$ was synthesized according to the Dhara method.[22] The chloride ligands of $K_2[PtCl_4]$ were replaced by iodide before the addition of NH_4^+. The stronger *trans*-directing effect of iodide[23] ensures that only the *cis* diammine isomer is produced. The pH was adjusted to 10 to increase the concentration of ammonia. The purity of the product was checked by CHN, or by NMR spectroscopy when ^{15}N-labelled.

3.3.2 *Cis*-$[PtCl_2(NH_3)_2]$ (Cisplatin)

Cisplatin was synthesized from *cis*-$[PtI_2(NH_3)_2]$ by removal of the iodide ligands with silver nitrate ($AgNO_3$) which readily forms the insoluble silver salt AgI. The reaction was accelerated by heating to 333 K, and carried out in the dark due to the

photoactivity of silver. Slightly less than 2 molar equivalents of $AgNO_3$ were used to avoid any excess silver in the product. Inorganic membrane filters had previously been found to be the best filtration method for removal of AgI.[24] The complex now contains aqua ligands in place of the iodide ligands and is therefore more reactive towards the entering chlorides. *Cis*-$[PtCl_2(NH_3)_2]$ is much less soluble than *cis*-$[Pt(OH_2)_2(NH_3)_2](NO_3)_2$ and so precipitated when the volume was reduced.

The yellow solid was characterized by CHN and 1D [^{1}H] NMR spectroscopy in d_6-DMSO, or by 1D [^{1}H] and 2D [^{1}H,^{15}N] NMR spectroscopy in 90 % H_2O / 10 % D_2O when ^{15}N-labelled. After preparing the NMR sample in d_6-DMSO, it was essential to record the spectrum immediately as platinum compounds are reactive to DMSO which can bind as a ligand. Indeed this reaction was followed by NMR to ensure the original peak observed was due to cisplatin and not a DMSO-adduct. The chemical shifts of the peak in the 2D spectrum agreed well with literature values.[25]

3.3.3 *Trans*-$[PtCl_2(NH_3)_2]$ (Transplatin)

Transplatin was prepared by the published method.[26] Excess ammonia was added to cisplatin which resulted in the displacement of the two chloride ligands to form the tetra-ammine complex $[Pt(NH_3)_4]Cl_2$. Removal of the solvent was necessary to get rid of the excess ammonia, and if the reaction was complete a pure white solid was produced. Addition of HCl resulted in two chloride ligands binding to platinum *trans* to each other due to the greater *trans*-directing effect of chloride compared to ammonia.[4] The first ammonia is labilized at low pH and subsequently substituted by chloride. This, in turn, directs the second chloride ligand into the *trans* position.

Transplatin was characterized in the same way as cisplatin. It is more reactive than cisplatin and even if the NMR spectra were recorded immediately after preparation in either d_6-DMSO or 90 % H_2O / 10 % D_2O, peaks corresponding to a DMSO-adduct or the mono-aqua species *trans*-$[PtCl(OH_2)(NH_3)_2]$ were seen. However, aquation in the aqueous sample was avoided by the addition of excess NaCl. The NMR spectra were recorded in d_6-DMSO to check for cisplatin impurities in ^{14}N-transplatin, the Pt-NH ^{1}H NMR resonances for Pt am(m)ine complexes are not easily

detected in D_2O solutions as the half-life for H-D exchange is only a few minutes at ambient temperatures.[29] Even though the peaks are broad, the chemical shifts of transplatin and cisplatin are far enough apart (4.39 ppm and 3.96 ppm, respectively) to enable the detection of impurities.

The preparation of ^{15}N-transplatin first involved the synthesis of the tetra-ammine from ^{15}N-cisplatin using excess $^{15}NH_4Cl$. The pH was increased to provide a high enough concentration of NH_3 to bind to platinum, as described for the synthesis of *cis*-$[PtI_2(NH_3)_2]$. After this, the method was continued as for ^{14}N-transplatin. Characterization was by 2D [^{1}H,^{15}N] HSQC NMR spectroscopy and the peaks agreed well with literature values.[25]

3.3.4 [Pt(en)Cl$_2$]

$[Pt(en)Cl_2]$ was synthesized from an aqueous solution of $K_2[PtCl_4]$ by adding ethylenediamine, which had been purified by distillation and stored under argon. Upon addition of en, the product immediately began to precipitate. The labelled compound $[Pt(^{15}N\text{-}en)Cl_2]$ had been previously synthesized by Dr. Phil Müller from ^{15}N-en.2HCl by the literature method.[27] The chemical shifts in the 1D [^{1}H] and 2D [^{1}H,^{15}N] NMR spectroscopy agreed well with the literature values.[25]

3.3.5 *Cis, trans, cis*-[Pt(N$_3$)$_2$(OH)$_2$(NH$_3$)$_2$] (1)

Cis, trans, cis-$[Pt(N_3)_2(OH)_2(NH_3)]$ was synthesized using the method described by Dr. Phil Müller.[24] The azides are inserted after first removing the chloride ligands from cisplatin with $AgNO_3$ to produce *cis*-$[Pt(NH_3)_2(OH_2)_2](NO_3)_2$, and then adding excess NaN_3. A 20-fold molar excess of NaN_3 was used to accelerate the reaction, upon addition the solution immediately turns from colourless to bright yellow. This colour change is caused by azide binding to platinum, which leads to a ligand-to-metal charge-transfer band (LMCT) in the visible region of the spectrum.[10] The product *cis*-$[Pt(N_3)_2(NH_3)_2]$ is much less soluble in water than NaN_3 and so the excess azide salt stays in the solution.

Oxidation from Pt^{II} to Pt^{IV} was carried out with H_2O_2 (30 % vol/vol) which was also

added in a large excess (40 mol eq). In the syntheses described later these reagents (NaN_3 and H_2O_2) were not used in such large amounts as it was found to be unnecessary.

The UV-visible spectrum of **1** contains one main absorption band at 256 nm (ε_{max} 13,700 $M^{-1}cm^{-1}$) which is assigned as a LMCT band from the azide ligand to Pt^{IV}.[9] This band has a tail which extends out into the visible region. The extinction coefficients at the various excitation wavelengths used for photoactivation are listed in Table 3.1.

The 1D [^{1}H] and 2D [^{1}H,^{15}N] HSQC NMR spectroscopy results agreed well with the published values.[17,24] The ^{195}Pt NMR spectrum was also recorded and a peak at + 902 ppm was observed. This is in the expected region and compares well with the ^{195}Pt chemical shift of *cis, trans, cis*-$[PtCl_2(OH)_2(NH_3)_2]$ of + 860 ppm.[28]

The aqueous solubility of **1** is ca. 13 mM. It is one of the least soluble compounds synthesized in this work. Solubility properties and electronic absorption spectra are discussed and compared in more detail in section 3.3.7.

3.3.6 *Cis, trans*-$[Pt(en)(N_3)_2(OH)_2]$ (2)

Cis, trans-$[Pt(en)(N_3)_2(OH)_2]$ was also synthesized using the method of Dr. Phil Müller.[17,24] The LMCT absorption band is centred at 258 nm with an extinction coefficient of 14,300 $M^{-1}cm^{-1}$ which is higher than that of **1**. However, the aqueous solubility of **2** was lower (ca. 9 mM) when compared with **1**.

3.3.7 *Trans, trans, trans*-$[Pt(N_3)_2(OH)_2(NH_3)_2]$ (3)

The synthesis of *trans*-$[Pt(N_3)_2(NH_3)_2]$ was carried out in a similar way to that of cisplatin. The chlorides were removed from *trans*-$[PtCl_2(NH_3)_2]$ with $AgNO_3$, which resulted in the formation of the insoluble AgCl This reaction did not go to completion. The first chloride is easily lost, but it is very difficult to remove the second. After the AgCl has been filtered off, excess NaN_3 was added and a yellow colour immediately appeared, however, a cloudy precipitate was also formed. A

yellow colour was produced by the formation of platinum-azide bonds which have a LMCT band in the visible region.[10] The cloudy precipitate was AgN_3 which, like the silver halides is also insoluble in water. At this point there was probably still some platinum-bound chloride, and so to remove this, the mixture was stirred for at least 24 h. During this time any residual bound chloride was replaced by azide. The yellow solid *trans*-$[Pt(N_3)_2(NH_3)_2]$ was recovered by filtration but AgN_3 was also still present. The product was resuspended in water and 8 molar equivalents of H_2O_2 (30 % vol/vol) added. The progress of the reaction was easily followed by observing the dissolution of the yellow solid. This left a cloudy yellow solution, from which the AgN_3 impurity was removed by filtration. It was found unnecessary to add 40 molar equivalents of hydrogen peroxide to oxidize Pt^{II} to Pt^{IV}, (as for previous syntheses),[17,24] the reaction was found to occur almost as fast with only 8 equivalents. Smaller volumes of H_2O_2 are safer and easier to handle, especially when the solutions are concentrated for crystallisation of the product.

The ^{15}N chemical shift of an am(m)ine is dependent on the ligand *trans* to it.[29] The 2D [^1H,^{15}N] HSQC NMR chemical shifts of *trans, trans, trans*-$[Pt(N_3)_2(OH)_2(NH_3)_2]$ (^1H, ^{15}N / 5.32, -41.65) are in the expected region for a Pt^{IV}-NH_3 unit with a nitrogen ligand in the *trans* position.[29] The $^1J(^{195}Pt\text{-}^{15}N)$ value of 282 Hz is also in the range expected for an amine *trans* to ammonia.[29] The purity of the product was confirmed by the presence of only one cross-peak.

A ^{195}Pt NMR peak at 875 ppm was observed. This peak is shifted to a higher field compared to that of complex **1** (902 ppm), which agrees with published data for Pt^{IV} *cis* / *trans* isomers.[30,31] This could possibly be explained by the *trans* influence, which is discussed in Chapter 1. By comparing the Pt-N bond lengths of the azide ligands for the two isomers it can be seen that the *trans* isomer (**3**) contains longer Pt-azide bonds (2.045 Å cf. 2.034 Å). This longer bond would result in more electron density on the platinum centre and consequently more shielding and a shift to higher field.

The positive electrospray mass spectrum exhibited a peak with the typical platinum

isotope pattern at 370.1 m/z which can be assigned as the sodium adduct ($[M + Na]^+$ = 347.0 + 23).

The purpose of synthesising the *trans* isomer (**3**) was to investigate whether Pt^{IV} diazido compounds retained their photoactivity and DNA binding ability when the azides were *trans* to one another. Not only was *trans, trans, trans*-$[Pt(N_3)_2(OH)_2(NH_3)_2]$ found to be as (if not more) photoactive than the *cis* isomers, several other properties were also enhanced. These include the solubility, the λ_{max} and the extinction coefficient. The solubility of **3** is ca. 19 mM, whereas the solubility of **1** is only ca. 13 mM.

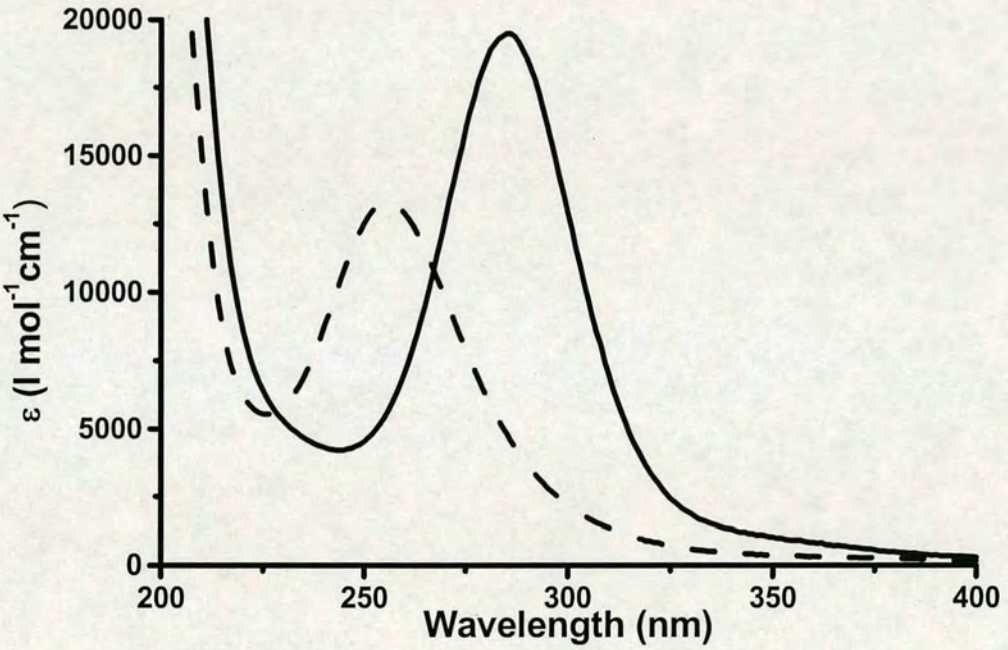

Figure 3.2 Electronic absorption spectra of *cis, trans, cis*-$[Pt(N_3)_2(OH)_2(NH_3)_2]$ (**1**) (dashed line) and *trans, trans, trans*-$[Pt(N_3)_2(OH)_2(NH_3)_2]$ (**3**) (solid line).

The LMCT band of the *trans* isomer is shifted towards the visible region with a maximum at 285 nm, compared to 256 nm for the *cis* isomer (Figure 3.2). This is quite a significant wavelength increase and means the "tail" of the absorbance will extend further into the visible region (Table 3.1). The magnitude of the extinction

coefficient was also increased (19,500 $M^{-1}cm^{-1}$ cf. 13,305 $M^{-1}cm^{-1}$) . The increase in λ_{max} can be accounted for in a similar way to the ^{195}Pt chemical shift change. In *cis, trans, cis*-$[Pt(N_3)_2(OH)_2(NH_3)_2]$ the azides are more tightly bound and so Δ_o will be greater and hence the LMCT band energy increases. So by simply changing the geometry, several important properties have been improved.

3.3.8 *Trans, trans, trans*-$[Pt(N_3)_2(OH)_2(NH_3)(py)]$ (4)

The synthesis of *trans*-$[PtCl_2(NH_3)(py)]$ was carried out in a similar way to the published method,[32] but with some conditions changed slightly to improve the yield. The first step in the synthesis involved replacing the chlorides of cisplatin with pyridine. Only a slight excess (3 molar equivalents) of pyridine was required for this step. Incorporation of chloride ligands in a *trans* position was accomplished by the addition of HCl, as in the synthesis of transplatin. Increasing the temperature can increase the rate of the reaction, however this can also lead to decomposition and the formation of black Pt^0. The yield was slightly improved by cooling and filtering the reaction after 2 days, and then continuing to heat the filtrate as before for a further 2 days.

The synthesis of *trans*-$[Pt(N_3)_2(NH_3)(py)]$ was carried out as for the preparation of *trans*-$[Pt(N_3)_2(NH_3)_2]$. Occasionally a small amount of chloride was found (by NMR spectroscopy), to be still bound to platinum. This can be rectified by resuspending the product in plenty (ca. 50 mL for 10 mg sample) of water and stirring with 10-20 molar equivalents of NaN_3 for a further 24 h.

Oxidation of *trans*-$[Pt(N_3)_2(NH_3)(py)]$ was relatively difficult compared to most of the other compounds synthesised. This is believed to be due to its insolubility. A large volume of water was required in order to solubilise sufficient complex for the oxidation step, however only a small amount of H_2O_2 ($\leq$ 6 mol eq) could be used because the product *trans, trans, trans*-$[Pt(N_3)_2(OH)_2(NH_3)(py)]$ was extremely water soluble. All of the solvent had to be removed to recover the product and any significant amount of excess H_2O_2 could have made this unsafe. Hydrogen peroxide has a significantly higher boiling point than water (414 K), and so there is the

potential for the production of a concentrated solution of H_2O_2.

The NMR chemical shifts of *trans, trans, trans*-$[Pt(N_3)_2(OH)_2(^{15}NH_3)(py)]$ (^1H, ^{15}N / 5.65, -46.00) are similar to those of *trans, trans, trans*-$[Pt(N_3)_2(OH)_2(^{15}NH_3)_2]$ (^1H, ^{15}N / 5.32, -41.65), and the coupling constants also compare well (Table 3.2).

Trans, trans, trans-$[Pt(N_3)_2(OH)_2(NH_3)(py)]$ was designed with *trans* geometry, in the hope that it would retain some of the beneficial properties of *trans, trans, trans*-$[Pt(N_3)_2(OH)_2(NH_3)_2]$. The pyridine ring was incorporated in place of one of the ammonia ligands because it was thought that the presence of an aromatic group might improve the photoactivity. The LMCT absorption band shifted only slightly (λ_{max} 289 nm), and the extinction coefficient was lower than that of *trans, trans, trans*-$[Pt(N_3)_2(OH)_2(NH_3)_2]$ (18,880 cf. 19,500 $M^{-1}cm^{-1}$), but an extra band appeared as a shoulder at 268 nm due to the pyridine ring. Free pyridine in water was found to absorb at 256 nm, and a red shift on metal complexation is expected.[33] *Trans, trans, trans*-$[Pt(N_3)_2(OH)_2(NH_3)(py)]$ was, however, very soluble in water giving concentrations of > 50 mM.

3.3.9 *Trans, trans, trans*-$[Pt(N_3)_2(OH)_2(NH_3)(MeNH_2)]$ (5)

The synthesis of *trans*-$[PtCl_2(NH_3)(MeNH_2)]$ was carried out under nitrogen, as extremely low yields were obtained for this reaction in air. The ^1H NMR spectra of the reaction mixture indicated the presence of Pt^{IV} species and so it was concluded that oxidation was taking place. Oxidation from Pt^{II} to Pt^{IV} in aqueous solution has been observed for similar compounds.[34] It was important not to place the flask containing cisplatin and methylamine into a hot oil bath because of the volatility of methylamine. Cooling, filtering and then reheating the filtrate several times was found to improve the yield. *Trans*-$[Pt(N_3)_2(NH_3)(MeNH_2)]$ was prepared in a similar way to *trans*-$[Pt(N_3)_2(NH_3)_2]$ and *trans*-$[Pt(N_3)_2(NH_3)(py)]$, and was then easily oxidised using only 4 equivalents of hydrogen peroxide.

The absorption spectrum of *trans, trans, trans*-$[Pt(N_3)_2(OH)_2(NH_3)(MeNH_2)]$ closely resembles that of *trans, trans, trans*-$[Pt(N_3)_2(OH)_2(NH_3)_2]$ (Table 3.1), which is not

surprising as their structures are very similar. *Trans, trans, trans*-$[Pt(N_3)_2(OH)_2(NH_3)(MeNH_2)]$ is the more soluble compound though and the aqueous solubility is > 20 mM.

3.3.10 *Trans, trans, trans*-$[Pt(N_3)_2(OH)_2(NH_3)(EtNH_2)]$ (6)

Trans, trans, trans-$[Pt(N_3)_2(OH)_2(NH_3)(EtNH_2)]$ was synthesised in the same way as *trans, trans, trans*-$[Pt(N_3)_2(OH)_2(NH_3)(MeNH_2)]$ except that it was not necessary to prepare *trans*-$[PtCl_2(NH_3)(EtNH_2)]$ under nitrogen as no oxidation in air was observed.

The absorption spectrum contains a band in exactly the same position as *trans, trans, trans*-$[Pt(N_3)_2(OH)_2(NH_3)_2]$ and the extinction coefficient is 16,516 $M^{-1}cm^{-1}$. The NMR chemical shifts (^1H, ^{15}N / 5.29, -41.35) are also very close to those of *trans, trans, trans*-$[Pt(N_3)_2(OH)_2(^{15}NH_3)_2]$ (^1H, ^{15}N / 5.32, -41.65).

3.3.11 *Trans, trans, trans*-$[Pt(N_3)_2(OH)_2(NH_3)(tz)]$ (7)

The synthesis of *trans*-$[PtCl_2(NH_3)(tz)]$ has been described previously,[35] however this method led to relatively low yields (ca. 50 %) and recrystallisation was necessary to obtain a pure product. It was found that high yields of pure *trans*-$[PtCl_2(NH_3)(tz)]$ could be obtained by a similar method to that of *trans*-$[PtCl_2(NH_3)(py)]$. The preparation of *trans*-$[Pt(N_3)_2(NH_3)(tz)]$ and subsequent oxidation were also carried out in the same way as for *trans*-$[Pt(N_3)(NH_3)(py)]$ and *trans, trans, trans*-$[Pt(N_3)_2(OH)_2(NH_3)(py)]$. This is because of the similarities between the respective compounds, i.e. the insolubility of the diazido-Pt^{II} species and the solubility of the Pt^{IV} product. The $N_3 \rightarrow Pt$ LMCT band is centred at 289 nm and has an extinction coefficient of 15,234 $M^{-1}cm^{-1}$. There is also a peak at 236 nm due to absorption by the thiazole ring. Free thiazole in water absorbs at 233 nm.

The X-ray crystal structures of *trans*-$[PtCl_2(tz)_2]$ and *trans*$[PtCl_2(NH_3)(tz)]$ have been determined by the Farrell group.[35,36] In both cases platinum is bound to the nitrogen atom of thiazole. Although Pt^{II} is a soft metal centre and is known to have a large affinity for sulphur donors, calculations on the electronic structure of thiazole

have shown that the net charge of the thioether-type sulphur is positive.[36] The negative charge resides on the nitrogen and it is therefore a much better donor to platinum. For this reason it is assumed that *trans, trans, trans*-$[Pt(N_3)_2(OH)_2(NH_3)(tz)]$ also has thiazole bound through the nitrogen.

3.3.12 *Trans, trans, trans*-$[Pt(N_3)_2(OH)_2(NH_3)(2\text{-pic})]$ (8)

Cis-$[PtCl_2(NH_3)(2\text{-pic})]$ is currently in Phase I / II clinical anticancer trials,[37] and is discussed in more detail in Chapter 1. The steric hindrance caused by the methyl group is believed to destabilize the trigonal bipyramidal transition state formed during deactivating substitution reactions, thereby leading to enhanced cytotoxicity.

The promising phototoxicity of *trans, trans, trans*-$[Pt(N_3)_2(OH)_2(NH_3)(py)]$ against several different cell lines (Appendix 2), led to the design of complexes containing substituted ring systems in an attempt to gain some insight into the structure-activity relationships of these Pt^{IV}-azide compounds.

Trans-$[PtCl_2(NH_3)(2\text{-pic})]$ was prepared in the same way as *trans*-$[PtCl_2(NH_3)(py)]$. An alternative preparation with slightly higher yields (~ 80 % cf. ~ 70 %) uses *cis*-$[PtCl_2(2\text{-pic})_2]$ as the starting material instead of cisplatin,[38] but due to the extra steps and only a slight improvement in the yield this method was not used.

For the silver nitrate reaction, it was decided to add a small amount of DMF (0.5 mL) to help solubilise the Pt^{II} starting material and hopefully allow the reaction to go further towards completion. However, upon addition of NaN_3 a precipitate was still produced. This precipitate may be the silver salt AgN_3 which is one of the more shock sensitive metal azides. Care should be taken and the formation of this compound in large amounts avoided. *Trans*-$[Pt(N_3)_2(NH_3)(2\text{-pic})]$ was very insoluble in water and so the oxidation step was always carried out in a large volume of water, as for the pyridine- and thiazole- containing complexes.

The NMR chemical shifts compare well with those of *trans, trans, trans*-$[Pt(N_3)_2(OH)_2(NH_3)(py)]$ (Table 3.2). The LMCT ($N_3 \rightarrow Pt$) band in the electronic

absorbance spectrum is at 292 nm (Table 3.1). This is at a longer wavelength than any of the other Pt^{IV} azide compounds synthesised. There is also an absorbance at 276 nm from the 2-picoline ring. Although *trans, trans, trans*-$[Pt(N_3)_2(OH)_2(NH_3)(2\text{-pic})]$ does not retain the high aqueous solubility seen for *trans, trans, trans*-$[Pt(N_3)_2(OH)_2(NH_3)(py)]$, it is still reasonably soluble (ca. 20 mM).

3.3.13 *Trans, trans, trans*-$[Pt(N_3)_2(OH)_2(NH_3)(3\text{-pic})]$ (9)

Problems with spontaneous oxidation to Pt^{IV} occurred during the synthesis of *trans, trans, trans*-$[Pt(N_3)_2(OH)_2(NH_3)(3\text{-pic})]$. This was not surprising as oxidation in aqueous solutions of Pt^{II} 3-picoline compounds has been previously observed.[39] Methyl substituents in positions 2 and 4 on the ring have an electron-donating effect and so increase electron density on the platinum centre. This means that nucleophilic attack is less favourable. The opposite is true of 3-picoline as it is electron withdrawing and so promotes nucleophilic attack, resulting in a Pt^{IV} product.

3.3.14 *Trans, trans, trans*-$[Pt(N_3)_2(OH)_2(NH_3)(4\text{-pic})]$ (10)

Trans, trans, trans-$[Pt(N_3)_2(OH)_2(NH_3)(4\text{-pic})]$ was prepared in a very similar way to *trans, trans, trans*-$[Pt(N_3)_2(OH)_2(NH_3)(2\text{-pic})]$. The LMCT ($N_3 \rightarrow Pt$) band was at 289 nm with the absorbance from the ring at 274 nm.

3.3.15 *Trans, trans, trans*-$[Pt(N_3)_2(OH)_2(NH_3)(c\text{-}HexNH_2)]$ (11)

A Pt^{IV} compound containing a cyclohexylamine ring is currently in Phase II clinical trials.[40] Satraplatin, also known as JM216 (*trans, cis, cis*-$[Pt(OCOCH_3)_2Cl_2(NH_3)(c\text{-}HexNH_2)]$ is discussed in more detail in Chapter 1. Problems were encountered during the synthesis of **11** and often the Pt^{II} species oxidized to Pt^{IV} in water. Pt^{IV} N-H NMR peaks were seen in the ^1H spectra carried out in d_6-acetone. This may be the reason for the relatively low yield of *trans*-$[PtCl_2(NH_3)(c\text{-}HexNH_2)]$ (~ 50 %), and is why the chlorides were converted to azides in DMF / methanol rather than by the usual silver nitrate method in water. Unfortunately this reaction was only successful once, every other attempt gave a mixture of products, thought to be DMF adducts. However, crystals of both the Pt^{II} and Pt^{IV} diazido-compounds were successfully grown and the structures of the complexes determined (Chapter 4).

It would be interesting to investigate the phototoxicity of *trans, trans, trans*-$[Pt(N_3)_2(OH)_2(NH_3)(c\text{-}HexNH_2)]$ due to its structural similarities to JM216, however the synthesis would have to be optimized to produce sufficient amounts for these studies.

3.3.16 *Cis, trans, cis*-$[Pt(N_3)_2Cl_2(NH_3)_2]$ (12)

Cis, trans, cis-$[Pt(N_3)_2Cl_2(NH_3)_2]$ was synthesized to determine whether replacing the hydroxide ligands with chloride had an appreciable effect on the photoactivity. The chloride concentration outside cells is ca. 0.1 M and it has previously been shown that *cis, trans, cis*-$[Pt(N_3)_2(OH)_2(NH_3)_2]$ can react with NaCl (0.1 M) to produce *cis, trans, cis*-$[Pt(N_3)_2Cl_2(NH_3)_2]$.[24]

There are two possible synthetic routes to *cis, trans, cis*-$[Pt(N_3)_2Cl_2(NH_3)_2]$. The hydroxide ligands of *cis, trans, cis*-$[Pt(N_3)_2(OH)_2(NH_3)_2]$ can be replaced with chloride using HCl, or the chlorides can be added by oxidation of *cis*-$[Pt(N_3)_2(NH_3)_2]$ with PCl_5 or chlorine gas. Previous work which involved the synthesis of the carboplatin analogue *trans, cis*-$[Pt(cbdca)Cl_2(NH_3)_2]$ found that replacement of the hydroxide ligands using HCl is the best method.[24]

The presence of chloride in the product was confirmed by the isotope splitting pattern in the mass spectrum (Figure 3.3). Crystals were submitted for X-ray structure determination and it was confirmed that the hydroxides had been replaced by chlorides.

The synthesis was repeated using *cis, trans, cis*-$[Pt(N_3)_2(OH)_2(^{15}NH_3)_2]$ as the starting material so that the photoactivity of the products could be followed by 2D $[^1H,^{15}N]$ HSQC NMR spectroscopy. After 24 h, 200 μL of the solution was removed for NMR spectroscopic analysis. Several peaks could be seen, but the main peak corresponded to *cis, trans, cis*-$[Pt(N_3)_2Cl_2(NH_3)_2]$. The solution was concentrated and crystals grown at 277 K. These crystals were filtered and dried but while weighing them out with a polystyrene spatula a ***small explosion*** occurred within the glass vial. A black solid coated the inside of the vial but it did not break. It was

thought perhaps the crystals had accidently been put under pressure between the glass and the spatula. More crystals had grown in the filtrate and so these were filtered. Upon dropping the second drop of crystals and supernatant onto the filter paper, again there was a ***small explosion***. The second explosion is less likely to have been caused by the crystals being put under pressure, but could have been due to two crystals knocking together and then detonating.

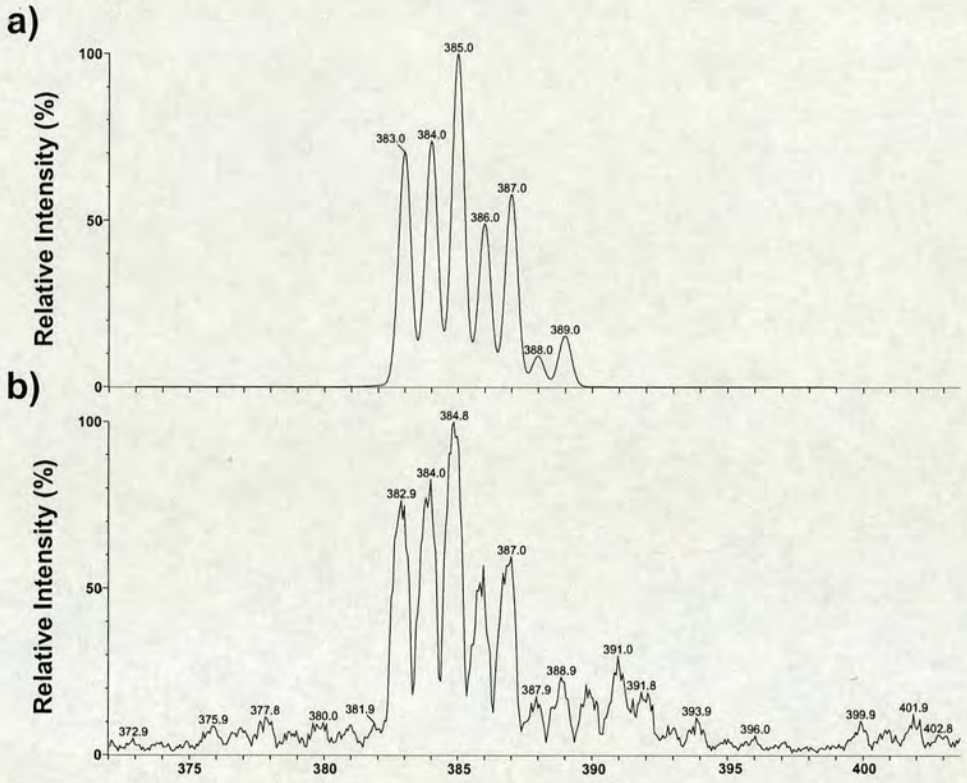

Figure 3.3 Positive ion electrospray ionisation mass spectroscopy of *cis, trans, cis*-$[Pt(N_3)_2Cl_2(NH_3)_2]$. a) Simulated spectrum for $PtN_8H_6Cl_2$, b) Observed spectrum of *cis, trans, cis*-$[Pt(N_3)_2Cl_2(NH_3)_2]$ in water.

3.3.17 *Cis, trans*-$[Pt(bpy)(N_3)_2(OH)_2]$ (13)

One of the methods employed to extend the wavelength of absorption into the visible region was to incorporate chelating aromatic ligands. Platinum(II) complexes such as $[Pt(N\text{-}N)X_2]$ (where N-N = bpy or phen, and X = Cl or N_3) absorb relatively strongly at wavelengths > 350 nm.[41] Although it has been stated that LF excitation does not lead to photoactivation,[10] evidence of reduction upon irradiation at wavelengths where only ligand-field transitions are present has been reported.[42,43] These

photoreductions are believed to be due to internal conversion or intersystem crossing. The wavelength of absorption can be further increased by careful choice and positioning of substituents on the aromatic rings.[44-46]

Platinum(II) α-diimine complexes are capable of photosensitizing the production of singlet oxygen ($^1O_2$).[47-49] The efficiency of photogeneration of $^1O_2$ has been investigated for the compounds [Pt(Me-bpy)X_2] (where X = N_3^-, Cl^-, I^-, NO_2^-,) and [Pt(N-N)X_2] (where N-N = phen or bpy and X = N_3^-, Cl^-, I^-, Br^-, SCN^- or CN^-).[57,58] In all cases the most efficient photosensitizers were the azide-containing complexes. [Pt(Me-bpy)$(N_3)_2$] was found to be 34.6 % as efficient as hematoporphyrin-IX (a precursor of PDT porphyrin drugs).

Several groups have investigated the cytotoxicity of Pt^{II}-bipyridine compounds. Complexes containing chelating amino acids have shown growth inhibition against P-388 lymphocytic leukemic cells,[50,51] and work has now turned to dinuclear compounds.[52,53] Another active compound found to have an IC_{50} value comparable to that of cisplatin is the carboplatin analogue [Pt(bpy)(cbdca)].[54] However, no examples of cytotoxicity testing on Pt^{IV}-bipyridine compounds could be found.

[Pt(bpy)Cl_2] and [Pt(bpy)$(N_3)_2$] were synthesised by known procedures, where the chloride ligands were substituted for azides in DMF by stirring at 298 K for several days.[41,55] The silver nitrate method was not used to remove the chlorides because this reaction has been reported to produce an oxygen-bridged dimer which can only be cleaved under harsh conditions (e.g. boiling in acid).[56] Upon complexation of the bipyridine to Pt^{II}, a low-field shift of the ligand protons is observed in the ^1H NMR spectrum. Subsititution of the chloride ligands of [Pt(bpy)Cl_2] for azide ligands leads to a high field shift of the bipyridine protons, due to the stronger bonding of azide ions to the platinum centre and the larger degree of back bonding from platinum to bipyridine.[41]

The photoactivity of [Pt(bpy)$(N_3)_2$] has been investigated,[57,58] but no examples of a Pt^{IV}-bpy-azide complex could be found in the literature. The attempted oxidation of

$[Pt(bpy)(N_3)_2]$ with H_2O_2 repeatedly failed. This is believed to be due to the stability of the Pt^{II} complex. The π-bonding of ligands such as bipyridine and phenanthroline imparts some aromatic character to the chelate ring. They are π-acceptors and so help to stabilise compounds.[59]

In $[Pt(bpy)(N_3)_2]$, the highest occupied molecular orbital (HOMO) is the metal-based $d_{x^2-y^2}$ orbital, and the lowest unoccupied molecular orbital (LUMO) is the π^* orbital situated on the bipyridine.[33,41,58] The transition between the HOMO and LUMO leads to a metal-to-ligand charge-transfer (MLCT) band corresponding to the lowest energy absorption in the UV-visible spectrum. The analogous palladium compound $[Pd(bpy)(N_3)_2]$ is harder to oxidise as the energy of the $d_{x^2-y^2}$ orbital is lower and thus the MLCT band is at a higher energy.[33] By the same reasoning, changing the energy of the LUMO also leads to compounds which are easier to oxidise and have absorption at longer wavelengths.[41] Electron-withdrawing groups lower the LUMO; bipyridine is more electron withdrawing than phenanthroline and consequently is easier to oxidise and has its MLCT band at a slightly longer wavelength. The decrease of electron density by electron-withdrawing groups on the metal centre also promotes nucleophilic attack.[61]

Most oxidations of $[Pt(bpy)X_2]$ compounds found in the literature were carried out under conditions which could not be used in the presence of azide ligands (eg. high temperatures, photocatalysis).[60-62] Eventually a preparation which had been left to sit for several weeks was found to contain yellow crystals of *cis, trans*-$[Pt(bpy)(N_3)_2(OH)_2]$.

3.3.18 *Trans, cis*-$[Pt(bpy)(OAc)_2(N_3)_2]$ (14)

The exchange of hydroxide ligands for acetate ligands on Pt^{IV} diazido complexes has previously been carried out by Dr. Phil Müller, who synthesised *trans, cis, cis*-$[Pt(OCOCH_3)_2(N_3)_2(NH_3)_2]$ from *cis, trans, cis*-$[Pt(N_3)_2(OH)_2(NH_3)_2]$ in dichloromethane and acetic anhydride. The acetate complex was found to be photoactive upon irradiation with blue light, but no further studies (e.g. DNA binding) were carried out.[24]

The oxidation of a Pt^{II}-bpy complex in acetic acid has been reported.[20] Hydrogen peroxide is the oxidising agent and the reaction is carried out at room temperature. This method was found to be successful for the oxidation of $[Pt(bpy)(N_3)_2]$ to produce *trans, cis*-$[Pt(bpy)(OCOCH_3)_2(N_3)_2]$.

Initially a mixture of products was obtained, as well as *trans, cis*-$[Pt(bpy)(OCOCH_3)_2(N_3)_2]$, several other compounds including *cis, trans*-$[Pt(bpy)(N_3)_2(OH)_2]$ and *trans, cis*-$[Pt(bpy)(OCOCH_3)(N_3)_2(OH)]$ were also present. Purification was carried out by recrystallisation from water. Further recrystallisation of the filtrate produced crystals of *trans, cis*-$[Pt(bpy)(OCOCH_3)(N_3)_2(OH)]$ as confirmed by ^1H NMR and ESI-MS. From the ^1H NMR spectrum of the unpurified solution the main species was identified as the mono-acetate compound *cis, trans*-$[Pt(bpy)(N_3)_2(OH)(OAc)]$. A theory to explain the difficulty of substituting the second hydroxide by acetate has been proposed, and involves pK_a values.[63] The first step in the substitution is believed to be protonation of the hydroxide ligand by the acid to form an aqua ligand. Acetate is a much stronger nucleophile than water and so a nucleophilic substitution takes place. The pK_a of the second hydroxide has been estimated to be lower than ca. 4.7 and so protonation does not occur so readily.[63]

The ^1H NMR chemical shifts of the bipyridine ligands in *trans, cis*-$[Pt(bpy)(OCOCH_3)_2(N_3)_2]$ (**14**) and *cis, trans*-$[Pt(bpy)(N_3)_2(OH)_2]$ (**13**) are far enough apart to allow them to be distinguished. The UV-visible spectrum of **14** contains 3 main peaks at 250, 304, 317 nm (Figure 3.4). By comparison with previous assignments of Pt^{II}-bipyridine compounds, the peaks at 304 and 317 nm are due to π–π^* transitions of the bipyridine rings.[33,44] In Pt^{II} complexes the high energy band is usually assigned as a MLCT absorption. However this seems unlikely for a Pt^{IV} complex and so the absorbance at 250 nm is probably at least partly due to a LMCT from N_3 to Pt. The UV-visible spectrum and assignments are further discussed in Chapter 5. The extinction coefficient at 647 nm is 38 $M^{-1}cm^{-1}$ (Table 3.1) which is the highest of any of the compounds synthesised.

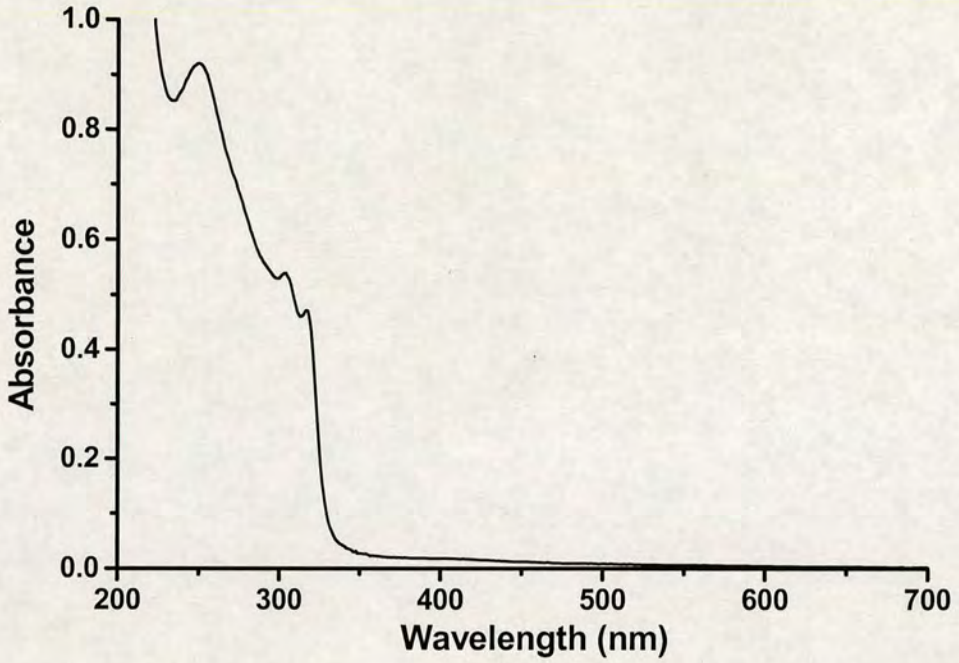

Figure 3.4 Electronic absorption spectrum of *cis, trans*-[Pt(bpy)$(N_3)_2(OAc)_2$] (**14**) in water (0.048 mM).

3.3.19 *Trans, cis*-[Pt(phen)$(OAc)_2(N_3)_2$] (15)

Trans, cis-[Pt(phen)$(OAc)_2(N_3)_2$] was synthesised and crystallised in the same way as *trans, cis*-[Pt(bpy)$(OAc)_2(N_3)_2$]. [Pt(phen)$(N_3)_2$] is reported to be more difficult to oxidise than [Pt(bpy)$(N_3)_2$] as discussed in Section 3.3.18.[33]

3.3.20 *Trans*-[Pt$(N_3)_2$(py)$_2$] (16)

Trans-[Pt$(N_3)_2(py)_2$] was synthesised directly from $K_2[PtCl_4]$ by a slight variation of the literature method.[64] The chlorides were replaced by pyridine to give a colourless solution of $[Pt(py)_4]Cl_2$ which was then converted to *trans*-$[PtCl_2(py)_2]$ by heating with excess HCl. The chlorides were then removed with silver nitrate and upon addition of NaN_3, *trans*-[Pt$(N_3)_2(py)_2$] precipitated.

Oxidation of *trans*-[Pt$(N_3)_2(py)_2$] proved very difficult. This could be due to electronic effects similar to those of the Pt^{II}-bipyridine complexes, or it could simply be due to insolubility in water. Oxidation of *trans*-[Pt$(N_3)_2(NH_3)$(py)] was carried out

with only 4 molar equivalents of H_2O_2, but required large volumes of water to achieve sufficient solubilisation of the Pt^{II} starting material (section 3.2.2.8). Unfortunately the use of large volumes of water or addition of small amounts of acetone or DMF to the oxidation reaction of *trans*-$[Pt(N_3)_2(py)_2]$ did not give rise to product.

Table 3.1 Electronic spectral data for Pt^{IV}-diazide complexes. The λ_{max} (nm) and ε ($M^{-1}cm^{-1}$) values at the absorption maximum and at various wavelengths of irradiation used for photoactivation are tabulated.

Complex	λ_{max} (nm)	ε_{max} ($M^{-1}cm^{-1}$)	ε_{365} ($M^{-1}cm^{-1}$)	ε_{458} ($M^{-1}cm^{-1}$)	ε_{647} ($M^{-1}cm^{-1}$)
1	257	13,721	274	18	6
2	257	14,340	298	8	< 1
3	286	18,945	547	44	8
4	289	18,816	535	42	3
5	286	19,384	567	39	1
6	285	16,516	545	25	< 1
7	288	15,234	510	32	< 1
8	292	17,888	603	58	8
9	289	13,575	441	21	< 1
10	289	14,318	536	40	< 1
14	250	19,102	738	199	38

Table 3.2 ^{1}H and ^{15}N NMR chemical shifts and coupling constants (J / Hz) for Pt^{IV}-diazide complexes.

Complex	δ (^{1}H) (ppm)	δ (^{15}N) (ppm)	^{1}J (^{15}N-^{1}H)	^{1}J (^{195}Pt-^{15}N)	^{2}J (^{195}Pt-^{1}H)
1	5.12	-40.27	73.5	259.8	46.0
2	6.38	-7.22	76.0	278.0	43.0
3	5.32	-41.65	72.0	282	47.5
4	5.65	-46.00	74.0	282.3	49.5
6	5.29	-41.35	73.3	265.2	46.7
8	5.67	-44.65	74.2	300.6	50.4
12	5.49	-41.27	-	242.7	46.5

3.4 Conclusions

Thirteen novel Pt^{IV} diazido complexes were successfully synthesised and characterised. By incorporation of the azides in a *trans* position, the LMCT (N_3 → Pt) absorption band was shifted towards the visible region, and the extinction coefficient increased. Several compounds with high aqueous solubility (> 20 mM) were also prepared. This work shows that there is a vast number of potential compounds which could be produced by varying the am(m)ine ligands alone, and therefore the scope for further improving the properties of these Pt^{IV} diazido complexes is great.

3.5 References

[1] Hall, M.D.; Hambley, T.W. *Coord. Chem. Rev.* **2002**, *232*, 49.

[2] Horvath, O.; Stevenson, K.L. In *Charge Transfer Photochemistry of Coordination Compounds* VCH, Weinheim, Germany, **1993**.

[3] Ferraudi, G.J. In *Elements of Inorganic Photochemistry*, Wiley-Interscience, NY, **1988**.

[4] Roundhill, D.M. In *Photochemistry and Photophysics of Metal Complexes*. Plenum Press, NY, **1994**.

[5] Kratochwil, N.A.; Zabel, M.; Range, K.-J.; Bednarski, P.J. *J. Med. Chem.* **1996**, *39*, 2499.

[6] Kratochwil, N.A.; Bednarski, P.J.; Mrozek, H.; Vogler, A.; Nagle, J.K. *Anti-Cancer Drug Des.* **1996**, *11*, 155.

[7] Kratochwil, N.A.; Parkinson, J.A.; Bednarski, P.J.; Sadler, P.J. *Angew. Chem.* **1999**, *111*, 1566.

[8] Vogler, A.; Hlavatsch, J. *Angew. Chem., Int. Ed. Eng.* **1983**, *22*, 154.

[9] Vogler, A.; Kern, A.; Hüttermann, J. *Angew. Chem., Int. Ed. Engl.* **1978**, *17*, 524.

[10] Vogler, A.; Quett, C.; Kunkely, H. *Ber. Bunsen-Ges. Phys. Chem.* **1988**, *92*, 1486.

[11] Weber, W.; Van Eldik, R. *Inorg. Chim. Acta.* **1986**, *111*, 129.

[12] Vogler, A.; Kern, A.; Rußeder, B. *Z. Naturforsch.* **1978**, *33b*, 1352.

[13] Lemma, K.; Berglund, J.; Farrell, N.; Elding, L.I. *J. Biol. Inorg. Chem.* **2000**, *5*, 300.

[14] Neumann, C.; Boubakari; Grüner, R.; Bednarski, P.J. *Anal. Biochem.* **2003**, *320*, 170.

[15] Eastman, A. *Biochem. Pharmacol.* **1987**, *36*, 4177.

[16] Hagenbuch, J.P. *Chimia* **2003**, *57*, 773.

[17] Müller, P.; Schröder, B.; Parkinson, J.A.; Kratochwil, N.A.; Coxall, R.A.; Parkin, A.; Parsons, S.; Sadler, P.J. *Angew. Chem., Int. Ed.* **2003**, *42*, 335.

[18] Mackay, F.S.; Woods, J.A.; Moseley, H.; Ferguson, J.; Dawson, A.; Parsons, S.; Sadler, P.J. *Chem. Eur. J.* **2006**, *12*, 3155.

[19] L. Bretherick Ed. Hazards in the Chemical Laboratory. 3rd Edition, RSC,

London **1981**.

[20] Lee, Y.-A.; Yoo, K.H.; Jung, O.-S. *Bull. Chem. Soc. Jpn.* **2003**, *76*, 107.

[21] Ren, S.; Cai, L.; Segal, B.M. *J. Chem. Soc., Dalton Trans.* **1999**, 1413.

[22] Dhara, S.C. *Indian J. Chem.* **1970**, *8*, 193.

[23] Shriver, D.F.; Atkins, P.W.; Langford, C.H. In *Inorganic Chemistry*, 2nd Edition, Oxford University Press, Oxford, **1996**.

[24] Müller, P. PhD Thesis, University of Edinburgh **2002**.

[25] Berners-Price S.J., Frey, U.; Ranford, J.D.; Sadler, P.J. *J. Amer. Chem. Soc.* **1993**, *115*, 8649.

[26] Kauffman, G.B.; Cowan, D.O. *Inorg. Syn.* **1963**, *7*, 239.

[27] Zang, E.; Sadler, P.J. *Synthesis-Stuttgart* **1997**, 410.

[28] Kuroda, R.; Neidle, S.; Ismail, I.M.; Sadler, P.J. *Inorg. Chem.* **1983**, *22*, 3620.

[29] Berners-Price, S.J.; Sadler, P.J. *Coord. Chem. Rev.* **1996**, *151*, 1.

[30] Kerrison, S.J.S.; Sadler, P.J. *J. Chem. Soc., Dalton Trans.* **1982**, 2363.

[31] Pregosin, P.S. *Ann. R. NMR S.* **1986**, *17*, 285.

[32] Kelland, L.R.; Barnard, C.F.J.; Evans, I.G.; Murrer, B.A.; Theobald, B.R.C.; Wyer, S.B.; Goddard, P.M.; Jones, M.; Valenti, M.; Bryant, A.; Rogers, P.M.; Harrap, K.R. *J. Med. Chem.* **1995**, *38*, 3016.

[33] Gidney, P.M.; Gillard, R.D.; Heaton, B.T. *J. Chem. Soc., Dalton Trans* **1973**, 132.

[34] Pizarro, A.M.; Munk, V.P.; Navarro-Ranninger, C.; Sadler, P.J. *Angew. Chem. Int. Ed.* **2003**, *42*, 5339.

[35] Bierbach, U.; Qu, Y.; Hambley, T.W.; Peroutka, J.; Nguyen, H.L.; Doedee, M.; Farrell, N. *Inorg. Chem.* **1999**, *38*, 3535.

[36] Beusichem, M.V.; Farrell, N. *Inorg. Chem.* **1992**, *31*, 634.

[37] *www.neorx.com*

[38] Tessier, C.; Rochon, F.D. *Inorg. Chim. Acta* **1999**, *295*, 25.

[39] McGowan, G. PhD Thesis, University of Edinburgh, **2005**.

[40] McKeage, M.J.; Boxall, F.E.; Jones, M.; Harrap, K.R. *Cancer Res.* **1994**, *54*, 629.

[41] Kamath, S.S.; Uma, V.; Srivastava, T.S. *Inorg. Chim. Acta* **1989**, *161*, 49.

[42] Cameron, R.E.; Bocarsly, A.B. *Inorg. Chem.* **1986**, *25*, 2910.

[43] Knoll, H.; Stich, R.; Hennig, H.; Stufkens, D.J. *Inorg. Chim. Acta* **1990**, *178*, 71.

[44] McInnes, E.J.L.; Farley, R.D.; Rowlands, C.C.; Welch, A.J.; Rovatti, L.; Yellowlees, L.J. *J. Chem. Soc., Dalton Trans.* **1999**, 4203.

[45] Geary, E.A.M.; Hirata, N.; Clifford, J.; Durrant, J.R.; Parsons, S.; Dawson, A.; Yellowlees, L.J.; Robertson, N. *J. Chem. Soc., Dalton Trans.* **2003**, 3757.

[46] Geary, E.A.M.; Yellowlees, L.J.; Jack, L.A.; Oswald, I.D.H.; Parsons, S.; Hirata, N.; Durrant, J.R.; Robertson, N. *Inorg. Chem.* **2005**, *44*, 242.

[47] Anbalagan, V.; Srivastava, T.S. *J. Photochem. Photobiol.* **1992**, *66A*, 345.

[48] Anbalagan, V.; Srivastava, T.S. *J. Photochem. Photobiol.* **1994**, *77A*, 141.

[49] Anbalagan, V.; Srivastava, T.S. *J. Photochem. Photobiol.* **1995**, *89A*, 113.

[50] Jain, N.; Mittal, R.; Sen Ray, K.; Srivastava, T.S.; Bhattacharya, R.K. *J. Inorg. Biochem.* **1987**, *31*, 57.

[51] Kumar, L.; Kandasamy, N.R.; Srivastava, T.S.; Amonkar, A.J.; Adwankar, M.K.; Chitnis, M.P. *J. Inorg. Biochem.* **1985**, *23*, 1.

[52] Jain, N.; Mittal, R.; Srivastava, T.S.; Satyamoorthy, K.; Chitnis, M.P. *J. Inorg. Biochem.* **1994**, *53*, 79.

[53] Mansuri-Torshizi, H.; Srivastava, T.S.; Parekh, H.K.; Chitnis, M.P. *J. Inorg. Biochem.* **1992**, *45*, 135.

[54] Mansuri-Torshizi, H.; Ghadimy, S.; Akbarzadeh, N. *Chem. Pharm. Bull.* **2001**, *49*, 1517.

[55] Newkome, G.R.; Theriot, K.J.; Fronczek, F.R.; Villar, B. *Organometallics*, **1989**, *8*, 2513.

[56] Wimmer, S.; Castan, P. *Inorg. Chim. Acta* **1988**, *142*, 13.

[57] Shukla, S.; Kamath, S.S.; Srivastava, T.S. *J. Photochem. Photobiol.* **1988**, *44A*, 143.

[58] Anbalagan, V. *J. Coord. Chem.* **2003**, *56*, 161.

[59] Lindoy, L.F.; Livingstone, S.E. *Coord. Chem. Rev.* **1967**, *2*, 173.

[60] Vogler, A.; Kunkely, H. *Angew. Chem., Int. Ed.* **1982**, *21*, 209.

[61] Peloso, A. *J. Chem. Soc., Dalton Trans.* **1976**, 985.

[62] Hodges, K.D.; Rund, J.V. *Inorg. Chem.* **1975**, *14*, 525.

[63] Song, R.; Kim, K.M.; Sohn, Y.S. *Inorg. Chim. Acta* **2002**, *338*, 89.

[64] Kauffman, G.B. *Inorg. Synth.* **1963**, *7*, 249.

Chapter 4
Crystal Structures of Platinum Azide Complexes

4.1 Introduction

The azide ion (N_3^-) is linear and symmetric, possessing equal N-N distances of ca. 1.154 Å.[1] However, when bound through one of the terminal nitrogens (Figure 4.1a), azide becomes asymmetric with bond lengths which compare well with those of diimide (1.23 Å), and nitrogen (1.10 Å).[2] The bound structure is best described as a resonance hybrid (Figure 4.1b).

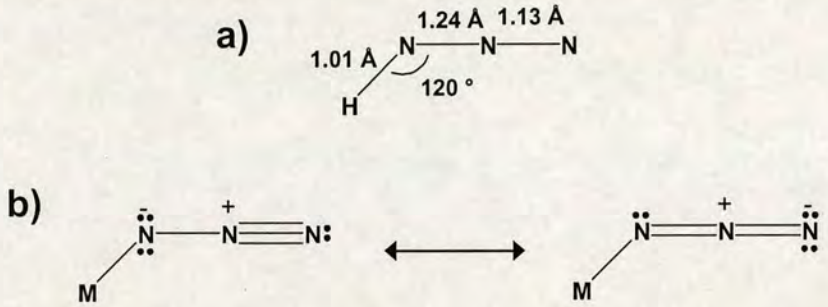

Figure 4.1 Structure of azide. a) Bond lengths and angles when bound to hydrogen (hydrazoic acid HN_3), b) resonance structures of azide ligand bound to a metal (M).

Seven crystal structures of Pt^{IV} azide compounds have been published with a crystallographic R-factor of < 0.05: *trans*-$[Pt(N_3)_4(SCN)_2](PPh_4)_2$, *trans*-$[Pt(N_3)_4(SeCN)_2](PPh_4)_2$,[3] *trans*-$[Pt(N_3)_4Cl_2](PPh_4)_2$,[4] $[Pt(N_3)Cl_5](AsPh_4)_2$, $[Pt(N_3)_6](AsPh_4)_2$,[5] $[Pt(N_3)_6](PPh_4)_2$, and $[Pt(N_3)_{5.28}Cl_{0.72}](AsPh_4)_2$.[6] All of these complexes crystallise in a triclinic crystal system with the space group P-1.

The crystal structures of *cis, trans, cis*-$[Pt(N_3)_2(OH)_2(NH_3)_2]$ (**1**) and *cis, trans*-$[Pt(en)(N_3)_2(OH)_2]$ (**2**) have previously been reported by Dr. Phil Müller.[7,13] These compounds have the azide ligands in a *cis* configuration. Complex **1** crystallised in a triclinic crystal system with the space group P-1, while complex **2** crystallised in a monoclinic crystal system with the space group $P2_1/c$. The bond lengths and angles generally agreed well with the seven other published Pt^{IV} azide structures.[3-6] However, the Pt-N_α bond lengths for **1** and **2** are amongst the shortest reported, this can be explained by the stronger *trans* influence of azide and chloride ligands compared to ammonia. Overall, **1** and **2** have close to octahedral geometry, and the azide ligands are almost linear (∠ N-N-N 173.2 ° – 175.7 °).

This chapter describes the X-ray crystal structures of platinum azide complexes obtained during this work. The complexes are discussed with focus on the azide ligands, and compared to similar structures where possible. There are five sections, divided according to the structures of the complexes; *trans*-Pt^{IV}, *trans*-Pt^{II}, *cis*-Pt^{II}, Pt^{IV} with chelating aromatic ligands and Pt^{II} with chelating aromatic ligands (*cis* or *trans* refers to the geometry of the azide ligands).

4.2 Experimental

X-ray crystal structure data were collected and solved by Dr Simon Parsons and colleagues. Diffraction data were collected with $Mo_{K\alpha}$ radiation on a Bruker Smart Apex CCD diffractometer equipped with an Oxford Cryosystems low-temperature device operating at 150 K. Data were corrected for absorption using the SADABS procedure,[8] and the structures solved by either direct (SHELXS)[9] or Patterson (DIRDIF)[10] methods. The structures were refined by full-matrix least-squares against F^2 (SHELXL).[11]

4.3 X-ray Crystal Structures

The crystallographic data for complexes **1**, **2** and **3** can be obtained from the Cambridge Crystallographic Data Centre. The depository numbers are CSD-412674 (**1**), CCDC-190265 (**2**) and CCDC-288954 (**3**). Data for all the X-ray structures described here can be found on the enclosed CD.

4.3.1 *Trans*-Pt^{IV} Diazido Complexes

The X-ray crystal structures of four *trans*-Pt^{IV}-diazido complexes have been determined, *trans, trans, trans*-$[Pt(N_3)_2(OH)_2(NH_3)_2]$ (**3**), *trans, trans, trans*-$[Pt(N_3)_2(OH)_2(NH_3)(py)]$ (**4**), *trans, trans, trans*-$[Pt(N_3)_2(OH)_2(NH_3)(2\text{-pic})]$ (**8**), and *trans, trans, trans*-$[Pt(N_3)_2(OH)_2(NH_3)(c\text{-}HexNH_2)]$ (**11**). The crystallographic data are listed in Table 4.1, and the bond lengths and angles of the azide ligands of each compound are in Table 4.2. To facilitate comparison of the azide ligands in Table 4.2, the nitrogens are labelled according to the generic structure shown in Figure 4.2.

Table 4.1 Crystal structure data for the *trans* Pt^{IV} diazido complexes *trans, trans, trans*-$[Pt(N_3)_2(OH)_2(NH_3)_2]$ (**3**), *trans, trans, trans*-$[Pt(N_3)_2(OH)_2(NH_3)(py)]$ (**4**), *trans, trans, trans*-$[Pt(N_3)_2(OH)_2(NH_3)(2\text{-pic})]$ (**8**) and *trans, trans, trans*-$[Pt(N_3)_2(OH)_2(NH_3)(c\text{-}HexNH_2)]$ (**11**).

Property	**3**	**4**	**8**	**11**
Empirical formula	$H_{16}N_8O_6Pt$	$C_5H_{10}N_8O_2Pt$	$C_6H_{12}N_8O_2Pt$	$C_6H_{18}N_8O_2Pt$
Formula weight	419.30	409.30	423.33	429.35
Crystal description	yellow block	yellow block	Pale yellow lath	yellow block
Crystal size (mm)	0.52x0.30x0.29	0.27x0.16x0.13	0.52x0.28x0.12	0.24x0.14x0.12
Crystal system	Triclinic	Orthorhombic	Monoclinic	Triclinic
Space group	*P*-1	*P*bca	*I*2/a	*P*-1
Unit cell dimensions (Å)	$a = 5.4038(5)$ $b = 5.8538(5)$ $c = 9.0518(8)$ $\alpha = 87.813(1)°$ $\beta = 78.790(1)°$ $\gamma = 72.456(1)°$	$a = 7.9640(7)$ $b = 11.585(1)$ $c = 24.150(2)$ $\alpha = 90°$ $\beta = 90°$ $\gamma = 90°$	$a = 12.9666(2)$ $b = 7.8790(1)$ $c = 21.5367(4)$ $\alpha = 90°$ $\beta = 92.898(1)°$ $\gamma = 90°$	$a = 5.5050(2)$ $b = 13.3500(4)$ $c = 17.8930(6)$ $\alpha = 75.307(2)°$ $\beta = 82.238(2)°$ $\gamma = 81.007(2)°$
Z	1	8	8	4
Density (calc.) (mg/m^3)	2.600	2.440	2.559	2.281
Absorption coeff. (mm^{-1})	13.133	12.597	12.778	11.232
F(000)	198	1520	1584	816
θ range for data collection (°)	2.29 to 28.64	1.69 to 30.44	2.75 to 29.98	1.590 to 30.494
Reflections collected	2337	15616	15237	7070
Independent reflections	1226	3310	3171	7070
Volume ($Å^3$)	267.74(4)	2228.2(3)	2197.46(6)	1250.07(7)
Temperature (K)	150(2)	150(2)	150(2)	150(2)
Wavelength (Å)	0.71073	0.71073	0.71073	0.71073
Conventional *R*	0.0157	0.0270	0.0191	0.0355
wR_2	0.0384	0.0646	0.0467	0.0817

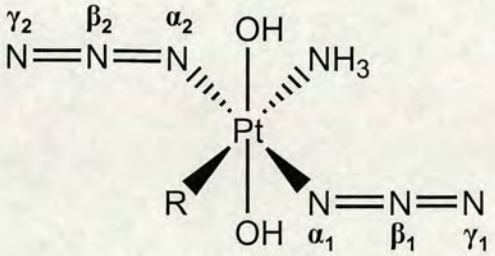

Figure 4.2 Labelling of azide ligands in *trans*-Pt^{IV} diazido complexes. R is NH_3 for complex **3**, pyridine for **4**, 2-picoline for **8** and cyclohexylamine for **11**.

Table 4.2 Bond lengths (Å) and angles (°) of azide ligands in *trans, trans, trans*-$[Pt(N_3)_2(OH)_2(NH_3)_2]$ (**3**), *trans, trans, trans*-$[Pt(N_3)_2(OH)_2(NH_3)(py)]$ (**4**), *trans, trans, trans*-$[Pt(N_3)_2(OH)_2(NH_3)(2\text{-pic})]$ (**8**) and *trans, trans, trans*-$[Pt(N_3)_2(OH)_2(NH_3)(c\text{-}HexNH_2)]$ (**11**, **11′**).

Bond / Angle	**3**	**4**	**8**	**11**	**11′**
Pt-N(α_1)	2.046(3)	2.044(3)	2.054(2)	2.041(7)	2.028(7)
Pt-N(α_2)	-	2.046(3)	2.051(2)	2.032(7)	2.053(7)
N(α_1)-N(β_1)	1.210(4)	1.203(5)	1.212(4)	1.224(10)	1.190(10)
N(β_1)-N(γ_1)	1.143(5)	1.139(6)	1.158(4)	1.139(11)	1.149(11)
N(α_2)-N(β_2)	-	1.216(5)	1.222(4)	1.194(11)	1.213(10)
N(β_2)-N(γ_2)	-	1.138(5)	1.141(4)	1.148(11)	1.142(10)
Pt-N(α_1)-N(β_1)	117.2(2)	119.0(3)	115.7(2)	114.9(5)	123.5(6)
N(α_1)-N(β_1)-N(γ_1)	174.5(3)	174.4(5)	175.3(3)	175.6(9)	174.0(9)
Pt-N(α_2)-N(β_2)	-	114.5(3)	115.3(2)	119.0(6)	116.5(6)
N(α_2)-N(β_2)-N(γ_2)	-	175.9(5)	175.0(3)	174.0(9)	174.5(9)
N(α_1)-Pt-N(α_2)-N(β_2)	0	-154.1	-114.5	-119.4	104.2
N(α_2)-Pt-N(α_1)-N(β_1)	0	-124.5	164.4	-91.2	127.0

4.3.1.1 *Trans, trans, trans*-$[Pt(N_3)_2(OH)_2(NH_3)_2]$ (**3**)

X-ray crystallography of *trans, trans, trans*-$[Pt(N_3)_2(OH)_2(NH_3)_2].4H_2O$ confirmed the octahedral stereochemistry and the presence of an inversion centre (Figure 4.3).[12] The azide ligands are almost linear (∠ N(α_1)-N(β_1)-N(γ_1) 174.5 °) and the Pt-N(α)-N(β) angle is 117.2° (Table 4.2). The azide N-N bond closest to platinum (N(α)-N(β) 1.210 Å) is ca. 0.07 Å longer than the terminal azide N-N bond (N(β)-N(γ) 1.143 Å), which is typical for azide ligands and can be explained by the resonance structure (Figure 4.1).[2] The bond lengths and angles of **3**.$4H_2O$ are comparable to those of the *cis* isomer **1**,[13] and are in good agreement with literature values for related Pt^{IV} azide complexes.[3-6]

The crystal structure of **3**.$4H_2O$ consists of layers of molecules formed through OH···N_3 and NH···OH hydrogen bonds which connect molecules in pairs across inversion centres (Figure 4.4). The layers are interleaved with water molecules which H-bond to the NH_3 groups. Details of the H-bonds are listed in Table 4.3.

Table 4.3 Hydrogen bonding distances (Å) and angles (°) in the crystal structure of *trans, trans, trans*-$[Pt(N_3)_2(OH)_2(NH_3)_2].4H_2O$.

D-H	d(D-H)	d(H..A)	<DHA	d(D..A)	A
O1-H1	0.845	2.175	156.45	2.969	N1a[a]
N1-H1a	0.910	1.978	164.97	2.867	O1[b]
N1-H1b	0.910	2.074	161.04	2.950	O1W
O1W-H1W1	0.839	2.003	175.44	2.840	O2W[c]
O1W-H2W1	0.835	2.197	163.05	3.006	O2W[d]
O2W-H1W2	0.832	1.926	168.92	2.748	O1
O2W-H2W2	0.826	2.343	129.72	2.941	O1W[e]
O1W-H1W1	0.826	2.628	144.87	3.338	O1W

Symmetry operations : [a] [x, y+1, z] [b] [x-1, y, z] [c] [x, y-1, z] [d] [-x+1, -y, -z-1] [e] [-x, -y, -z-1]

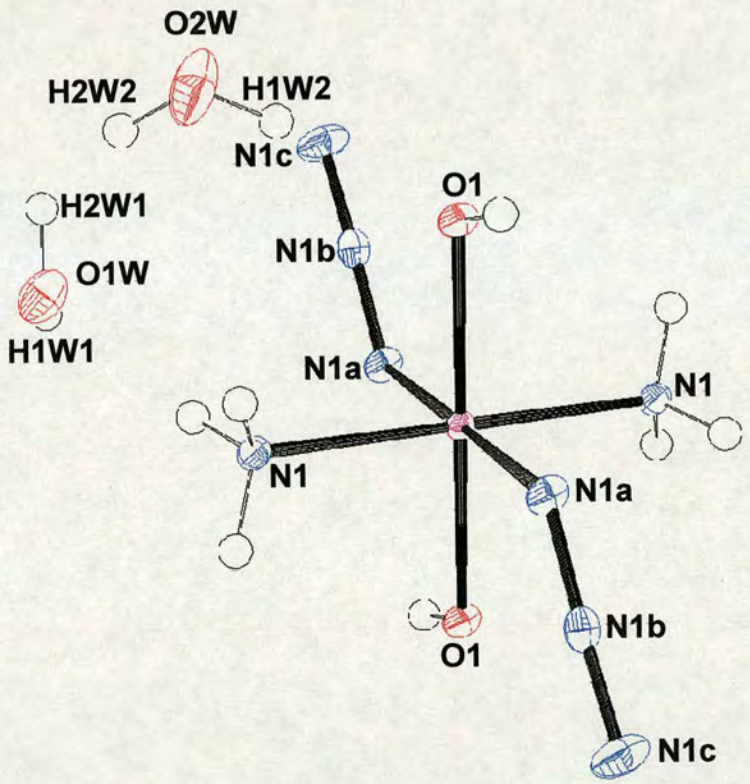

Figure 4.3 X-ray crystal structure of *trans, trans, trans*-$[Pt(N_3)_2(OH)_2(NH_3)_2].4H_2O$ (**3**). Thermal ellipsoids at 50 % probability level. Two water molecules have been omitted, they are related by symmetry to the two molecules of H_2O shown.

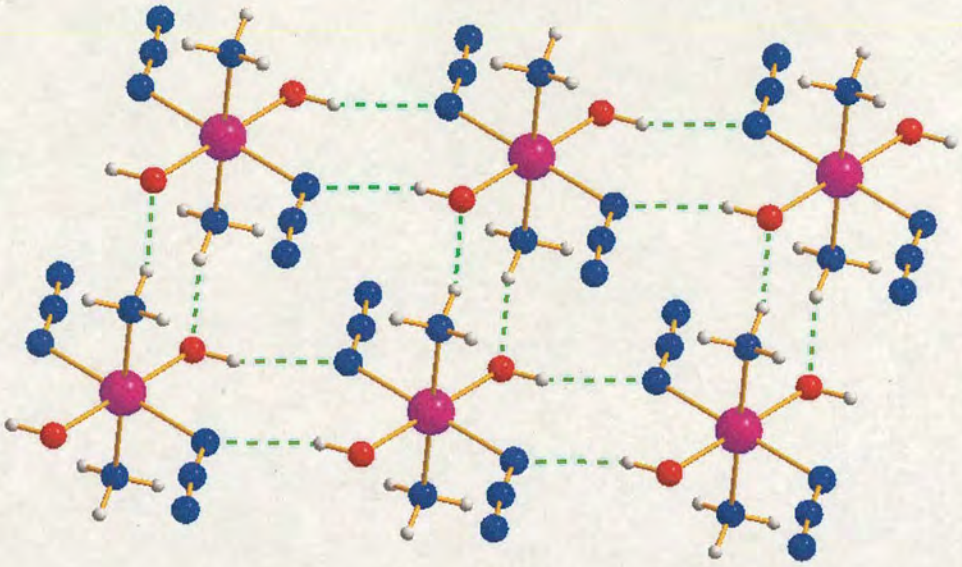

Figure 4.4 Hydrogen bonding involved in the layering of molecules of *trans, trans, trans*-$[Pt(N_3)_2(OH)_2(NH_3)_2].4H_2O$. Water molecules are not shown.

The crystal structure of the dichloro analogue of complex **3** has been determined.[14] *Trans, trans, trans*-$[PtCl_2(OH)_2(NH_3)_2]$ also contains an inversion centre and has an extensive hydrogen bonding network. The Pt-NH_3 and Pt-OH bond lengths are very similar to those of **3**.$4H_2O$, but the Pt-Cl bonds are significantly longer than the Pt-N_3 bonds (Table 4.4). This was expected as nitrogen is a stronger donor ligand than chloride towards platinum. The geometry of *trans, trans, trans*-$[PtCl_2(OH)_2(NH_3)_2]$ is closer to octahedral than **3**.$4H_2O$, this is probably due to steric hindrance caused by the bulky azide groups.

Table 4.4 Bond lengths (Å) in the crystal structures of **3**.$4H_2O$ and *trans, trans, trans*-$[PtCl_2(OH)_2(NH_3)_2]$.[14]

Bonds	**3**.$4H_2O$	*t,t,t*-$[PtCl_2(OH)_2(NH_3)_2]$
Pt-NH_3	2.036(3)	2.038(4)
Pt-OH	2.006(2)	2.000(5)
O-H	0.845(19)	0.89(7)
Pt-N_3	2.046 (3)	-
Pt-Cl	-	2.303(1)

4.3.1.2 *Trans, trans, trans*-$[Pt(N_3)_2(OH)_2(NH_3)(py)]$ (**4**)

Trans, trans, trans-$[Pt(N_3)_2(OH)_2(NH_3)(py)]$ (Figure 4.5) crystallised in an orthorhombic crystal system with the space group *P*bca (Table 4.1). This is the only known Pt^{IV} azide compound with this space group, and one of only two which exist in an orthorhombic crystal system, the other being *trans, cis*-$[Pt(bpy)(OAc)_2(N_3)_2]$ (Section 4.3.4.2). The azide bond lengths of complex **4** are all within experimental error of those of *trans, trans, trans*-$[Pt(N_3)_2(OH)_2(NH_3)_2]$ (**3**) (Table 4.2). Complex **4** deviates from an octahedral geometry by a few degrees more than complex **3**, most likely due to steric hindrance between the azides and pyridine. The Pt - NH_3 / pyridine bond lengths agree well with related structures.[15-17]

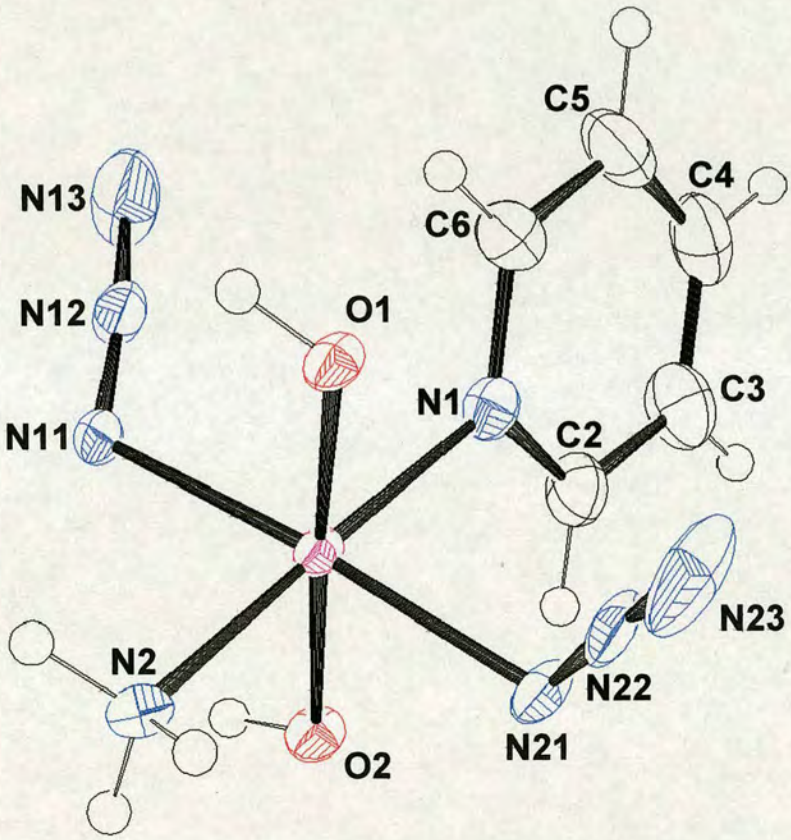

Figure 4.5 X-ray crystal structure of *trans, trans, trans*-$[Pt(N_3)_2(OH)_2(NH_3)(py)]$ (**4**). Thermal ellipsoids at 50 % probability level.

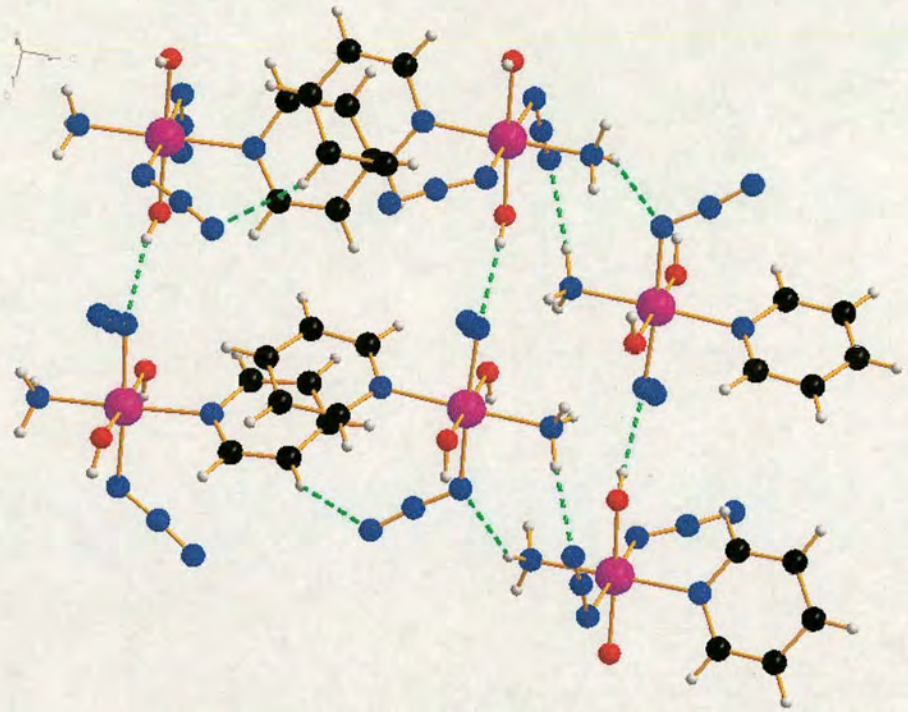

Figure 4.6 X-ray crystal structure of *trans, trans, trans*-$[Pt(N_3)_2(OH)_2(NH_3)(py)]$ with intermolecular hydrogen bonds indicated by the dashed green lines. Some weak $\pi - \pi$ stacking between the pyridine ligands also exists.

There are intermolecular hydrogen bonds present (Figure 4.6), though they are generally weaker than those of complex **3** (Table 4.5). The pyridine ring only forms one H-bond, which is to a terminal azide nitrogen. Both the terminal and platinum-bound nitrogens of azide are involved in H-bonding. The $\pi - \pi$ stacking between the pyridine ligands, with centroid spacing is 4.372 Å and a dihedral angle of 8.7 ° is very weak.

Table 4.5 Hydrogen bonding distances (Å) and angles (°) in the crystal structure of *trans, trans, trans*-$[Pt(N_3)_2(OH)_2(NH_3)(py)]$ (**4**).

D-H	d(D-H)	d(H..A)	<DHA	d(D..A)	A
N2-H	0.911	2.238	168.80	3.136	N23[a]
O1-H	0.841	2.178	161.22	2.987	N21[b]
N2-H	0.910	2.295	142.21	3.065	N11[a]
C5-H5	0.949	2.489	155.38	3.376	N13[c]

Symm. operations: [a] [x+½, -y+½, -z] [b] [-x+½, y+½, z] [c] [x-½, y, -z+½]

4.3.1.3 *Trans, trans, trans*-$[Pt(N_3)_2(OH)_2(NH_3)(2\text{-pic})]$ (**8**)

Trans, trans, trans-$[Pt(N_3)_2(OH)_2(NH_3)(2\text{-pic})]$ (Figure 4.7) crystallised in an monoclinic crystal system with the space group *I*2/a (Table 4.1). The azide bond lengths and angles are very similar to the other Pt^{IV} azide compounds (Table 4.2). The Pt-N(2-pic) bond length is significantly longer (2.092(5) Å) than that of Pt-N(py) in compound **4** (2.059(4) Å), which is presumably due to steric hindrance caused by the methyl group of 2-picoline. In the crystal structure of *trans*-$[Pt^{II}Cl_2(NH_3)(2\text{-pic})]$ the methyl group lies over the square-plane above the platinum atom.[18,19]

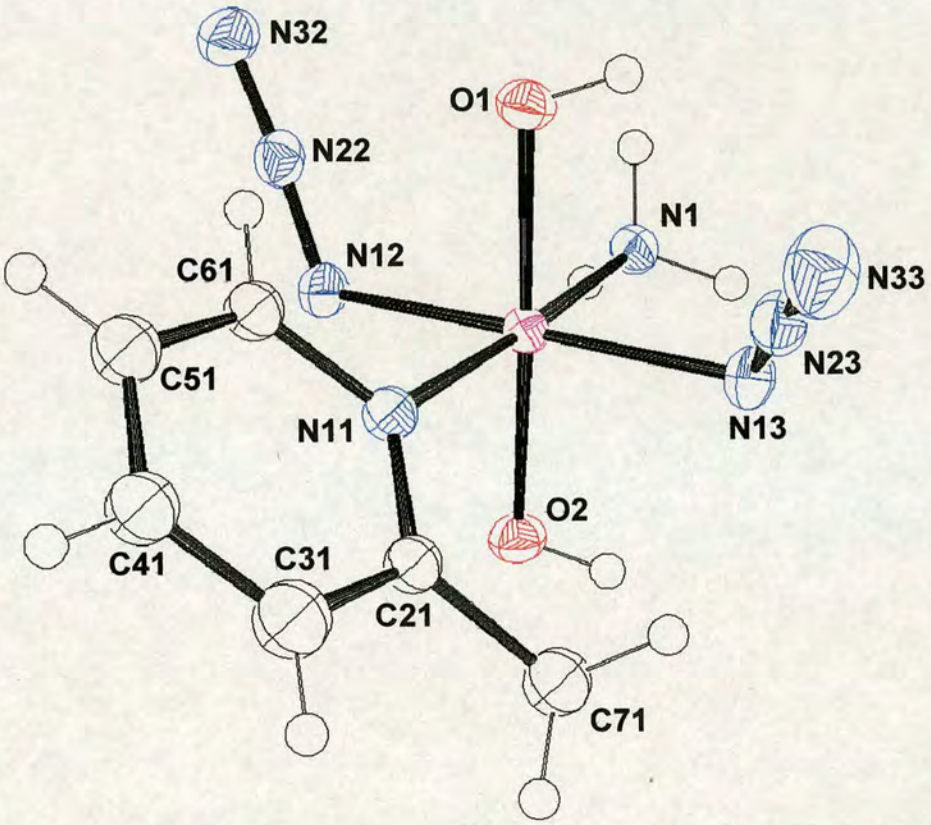

Figure 4.7 X-ray crystal structure of *trans, trans, trans*-$[Pt(N_3)_2(OH)_2(NH_3)(2\text{-pic})]$ (**8**). Thermal ellipsoids at 50 % probability level.

The 2-picoline ligand is disordered by a 180 ° rotation about the Pt-N bond. The system is hydrogen-bonded to produce "slabs" of molecules bound either side of the hydrophobic picolines (Figure 4.8). The centroid-centroid separation of the $\pi - \pi$ stacked picoline rings is 3.355 Å with a dihedral angle of 0.00(27) °.

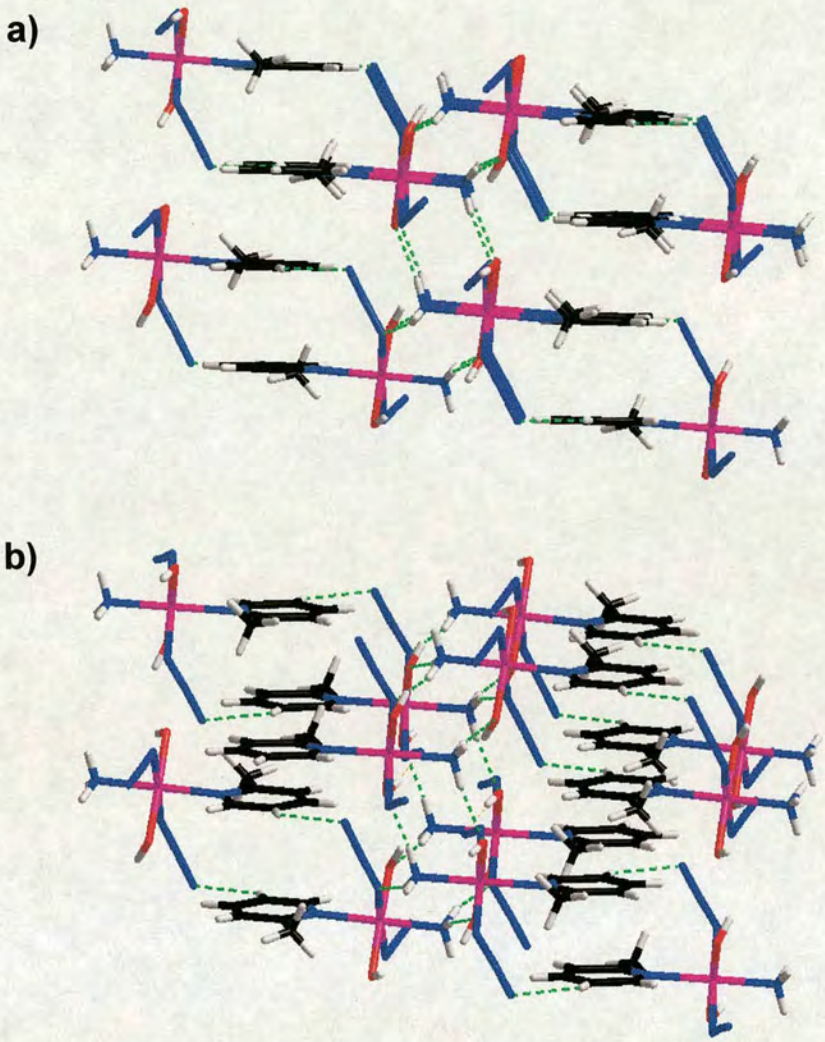

Figure 4.8 X-ray crystal structure of *trans, trans, trans*-$[Pt(N_3)_2(OH)_2(NH_3)(2\text{-pic})]$ from two different projections illustrating a) the layers of molecules and b) intermolecular hydrogen bonding (green dashed lines).

4.3.1.4 *Trans, trans, trans*-$[Pt(N_3)_2(OH)_2(NH_3)(c\text{-}HexNH_2)]$ (**11**)

Trans, trans, trans-$[Pt(N_3)_2(OH)_2(NH_3)(c\text{-}HexNH_2)]$ (Figure 4.9) crystallised in a triclinic crystal system with the space group *P*-1, as did complex **3** (Table 4.1). The azide bond lengths and angles are very similar to the other Pt^{IV} azide compounds (Table 4.2). The X-ray structure of *trans, cis, cis*-$[Pt(OAc)_2Cl_2(NH_3)(c\text{-}HexNH_2)]$ (JM216, Chapter 1) has been determined; it crystallised in a monoclinic crystal system with space group $P2_1/a$.[20] The

cyclohexylamine bond lengths and angles of complex **11** compare well with those of JM216, as do the Pt – am(m)ine bond lengths. The geometry of **11** is nearly octahedral with the cyclohexylamine ring adopting a chair conformation.

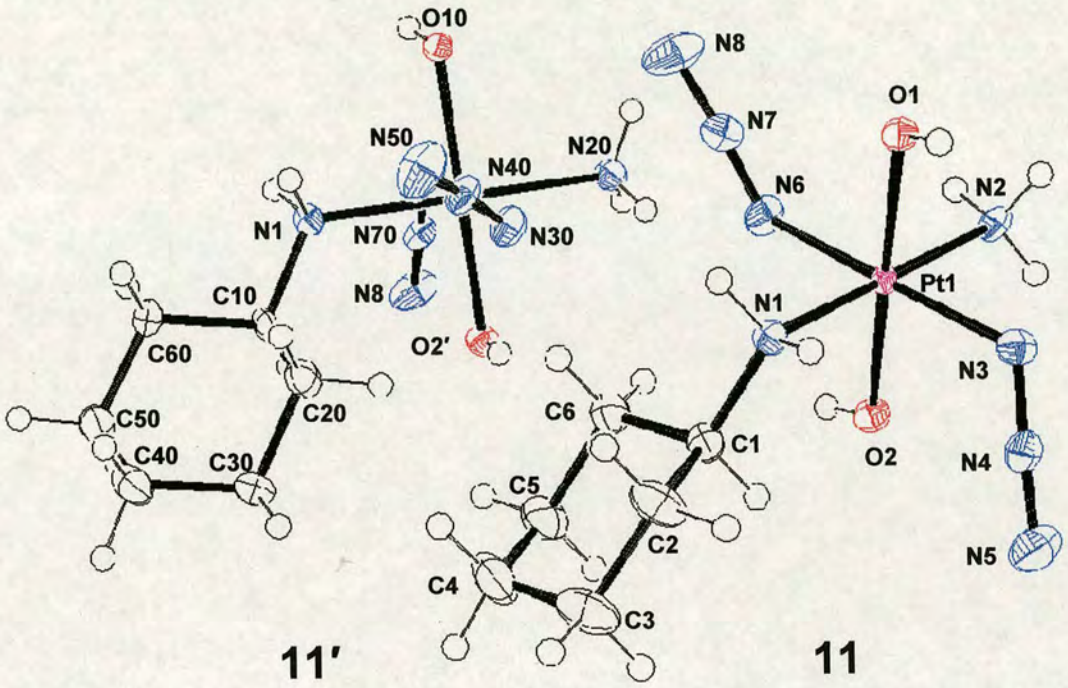

Figure 4.9 X-ray crystal structure of *trans, trans, trans*-[$Pt(N_3)_2(OH)_2(NH_3)$(c-$HexNH_2$)] (**11**). Thermal ellipsoids at 50 % probability level.

Complex **11** crystallised with four molecules in the unit cell, two of which were different. Intermolecular hydrogen bonding between the ammonia, hydroxide and azide ligands is present (Figure 4.10), as for complexes **3**, **4** and **8**. An NH_2 hydrogen and the equatorial ring hydrogen attached to C2 are also involved in intramolecular hydrogen bonding to the azide ligands.

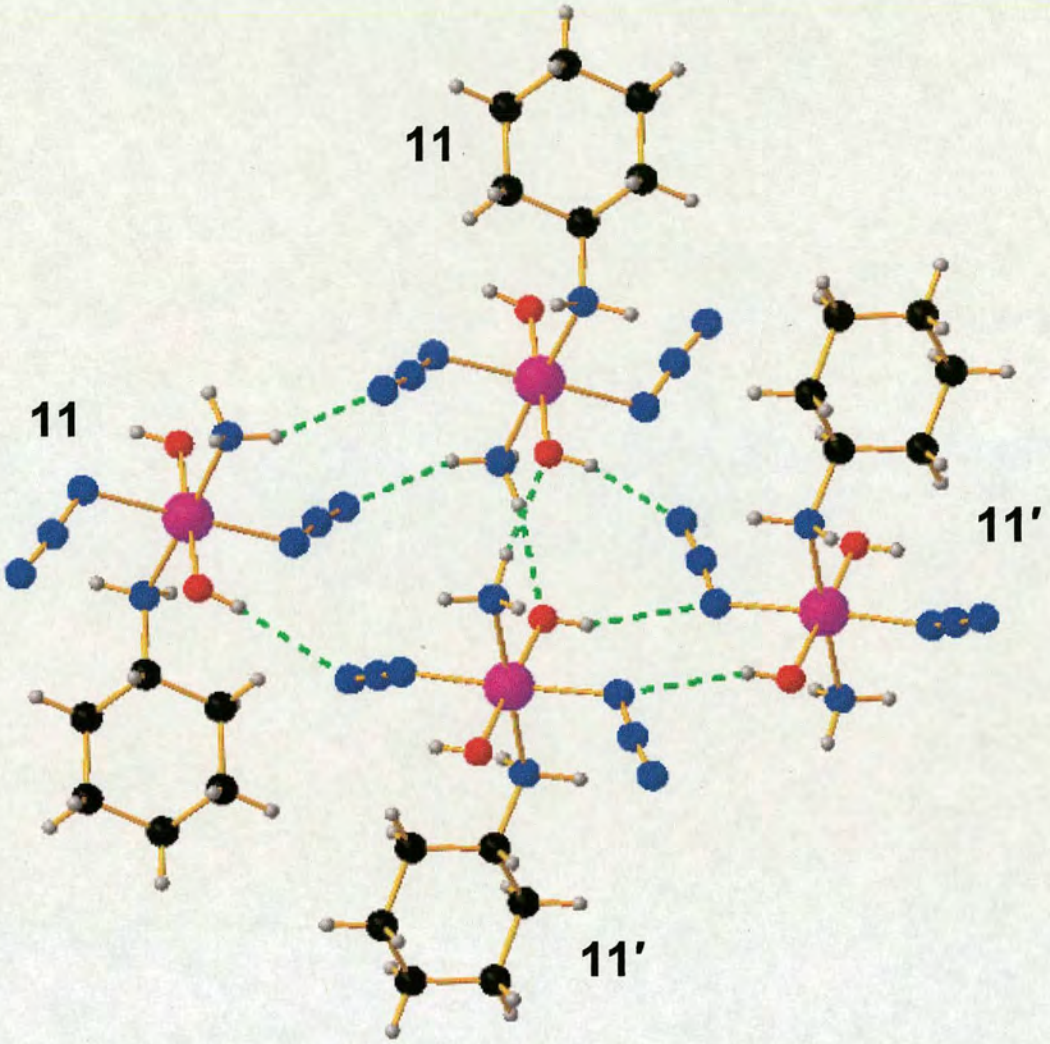

Figure 4.10 X-ray crystal structure of *trans, trans, trans*-$[Pt(N_3)_2(OH)_2(NH_3)(c\text{-}HexNH_2)]$ (**11** and **11′**) with intermolecular hydrogen bonds indicated by the dashed green lines.

4.3.2 *Trans*-Pt^{II} Diazido Complexes

The X-ray crystal structures of two *trans*-Pt^{II}-diazido complexes were determined, *trans*-$[Pt(N_3)_2(NH_3)_2(MeNH_2)]$ (**5a**) and *trans*-$[Pt(N_3)_2(NH_3)(c\text{-}HexNH_2)]$ (**11a**). The crystallographic data are listed in Table 4.6, and the bond lengths and angles of the azide ligands are in Table 4.7. As for the Pt^{IV} compounds, the azide ligands have been given generic labels (Figure 4.11).

Table 4.6 Crystal structure data for the *trans* Pt^{II} diazido complexes *trans*-$[Pt(N_3)_2(NH_3)(MeNH_2)]$ (**5a**) and *trans*-$[Pt(N_3)_2(NH_3)(c\text{-}HexNH_2)]$ (**11a**).

Property	**5a**	**11a**
Empirical formula	CH_8N_8Pt	$C_6H_{16}N_8Pt$
Formula weight	327.24	395.36
Crystal description	yellow block	yellow block
Crystal size (mm)	0.28 x 0.16 x 0.10	0.39 x 0.37 x 0.22
Crystal system	Monoclinic	Monoclinic
Space group	$P2_1/c$	$P2_1/n$
Unit cell dimensions (Å)	a = 13.4380(2) b = 7.65630(10) c = 6.99530(10) α = 90° β = 96.7290(10) ° γ = 90°	a = 6.12230(10) b = 21.9394(5) c = 8.1404(2) α = 90° β = 98.8660(10)° γ = 90°
Z	4	4
Density (calc.) (mg/m^3)	3.041	2.431
Absorption coefficient (mm^{-1})	19.572	12.972
$F(000)$	592	744
θ range for data collection (°)	3.05 to 30.35	1.86 to 43.18
Reflections collected	13043	18880
Independent reflections	2117	6296
Volume ($Å^3$)	714.756(17)	1080.35(4
Temperature (K)	150(2)	150(2)
Wavelength (Å)	0.71073	0.71073
Conventional R	0.0197	0.0329
wR_2	0.0503	0.0710

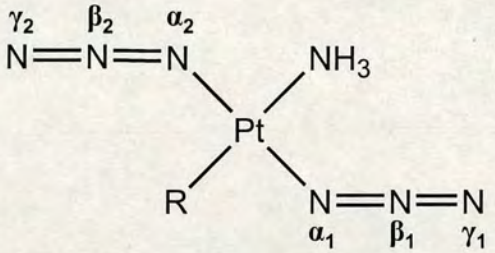

Figure 4.11 Labelling of azide ligands in *trans*-Pt^{II} diazido complexes. R is $MeNH_2$ for complex **5a** and cyclohexylamine for **11**.

Table 4.7 Bond lengths (Å) and angles (°) in azide ligands in *trans*-$[Pt(N_3)_2(NH_3)(MeNH_2)]$ (**5a**) and *trans*-$[Pt(N_3)_2(NH_3)(c\text{-}HexNH_2)]$ (**11a**).

Bond / Angle	**5a**	**11a**
Pt-N(α_1)	2.030(2)	2.039(3)
Pt-N(α_2)	2.027(2)	2.041(3)
N(α_1)-N(β_1)	1.204(3)	1.197(4)
N(β_1)-N(γ_1)	1.152(3)	1.150(4)
N(α_2)-N(β_2)	1.202(3)	1.203(4)
N(β_2)-N(γ_2)	1.155(3)	1.146(5)
Pt-N(α_1)-N(β_1)	124.48(19)	121.1(2)
N(α_1)-N(β_1)-N(γ_1)	173.8(3)	175.7(3)
Pt-N(α_2)-N(β_2)	122.48(19)	121.0(2)
N(α_2)-N(β_2)-N(γ_2)	174.5(3)	174.7(3)
N(α_1)-Pt-N(α_2)-N(β_2)	-44.2	175.4
N(α_2)-Pt-N(α_1)-N(β_1)	-149.1	-2.97

4.3.2.1 *Trans*-$[Pt(N_3)_2(NH_3)(MeNH_2)]$ (**5a**)

Trans-$[Pt(N_3)_2(NH_3)(MeNH_2)]$ crystallised in a monoclinic crystal system with the space group $P2_1/c$ (Figure 4.12). The azide bond lengths compare very well with other platinum azide compounds (Pt^{II} and Pt^{IV}) (Table 4.2 and Table 4.7). The Pt-N(α)-N(β) angles agreed well with the other Pt^{II} complexes, but were found to be significantly larger than those of the Pt^{IV} compounds (**3**, **4**, **8** and **11**). This same difference is seen for the *cis*-diazido Pt^{II} and Pt^{IV} structures.[7,13] The smaller Pt-N(α)-N(β) angle for Pt^{IV} complexes could be a result of intramolecular hydrogen bonding between the axial hydroxide hydrogen and the azide ligand.

The X-ray structure of *trans*-$[PtCl_2(MeNH_2)_2]$ has been published,[21] the bond lengths did not differ significantly from those of transplatin.[22] These am(m)ine bond lengths are also very similar to those of complex **5a**. The geometry of **5a** is square planar and the angles are all very close to 90 °.

There is intermolecular hydrogen bonding between the NH_2 hydrogens and both the terminal and platinum-bound nitrogens of azide, and also between an ammonia hydrogen and a platinum-bound azide nitrogen.

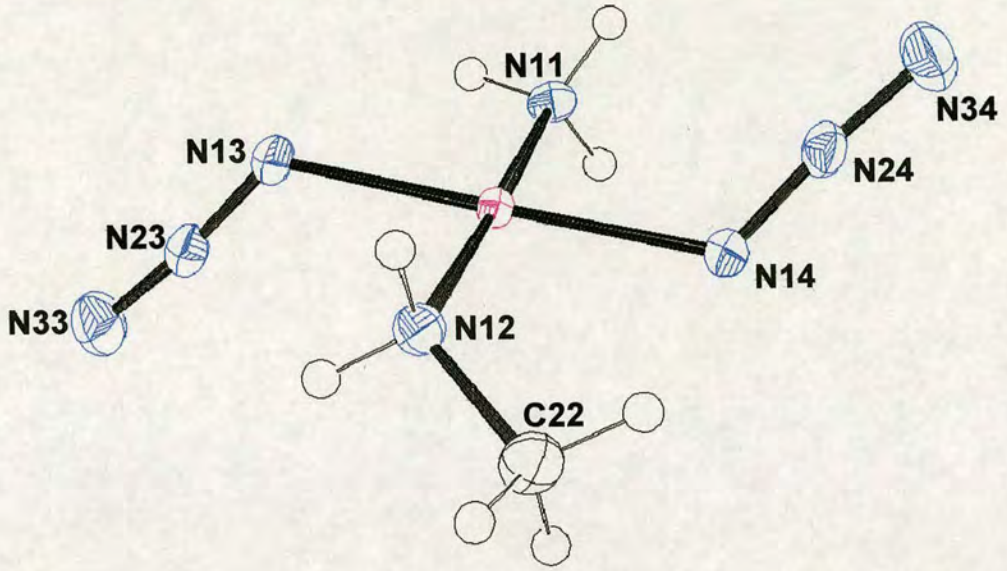

Figure 4.12 X-ray crystal structure of *trans*-[$Pt(N_3)_2(NH_3)(MeNH_2)$] (**5a**). Thermal ellipsoids at 50 % probability level.

4.3.2.2 *Trans*-[$Pt(N_3)_2(NH_3)$(c-$HexNH_2$)] (**11a**)

Trans-[$Pt(N_3)_2(NH_3)$(c-$HexNH_2$)] crystallised in a monoclinic crystal system with the space group $P2_1/n$ (Figure 4.13). The azide bond lengths and angles compare well with the other platinum azide structures (Table 4.2 and Table 4.7). The geometry is distorted from square planar (Figure 4.14), the angle between the cyclohexylamine ring and the azide ligand which is orientated towards it (N(12)-N(22)-N(32)) is ca. 95 ° (Table 4.8). This distortion is not seen for *trans*-[$PtCl_2(NH_3)$(c-$HexNH_2$)] where the angles are all 90 ± 1 °.[23] The complex is still relatively planar around the platinum centre with angles very close to 180 ° (Table 4.8) *Trans*-[$PtCl_2(NH_3)$(c-$HexNH_2$)] also crystallised in a monoclinic crystal system, but with the space group $P2_1/c$.

The molecules form hydrogen-bonded chains as shown in Figure 4.15, the bond distances are given in Table 4.9. Similar hydrogen bonds are found in the analogous chloride compound *trans*-[$PtCl_2(NH_3)$(c-$HexNH_2$)].[23]

Table 4.8 Bond angles around the platinum centre of *trans*-[$Pt(N_3)_2(NH_3)$(c-$HexNH_2$)] (**11a**).

Bond	Angle (°)
N(11)-Pt-N(12)	95.69(10)
N(12)-Pt-N(1)	84.99(11)
N(1)-Pt-N(13)	94.52(11)
N(13)-Pt-(11)	84.80(11)
N(12)-Pt-N(13)	179.49(11)
N(11)-Pt-N(1)	178.42(10)

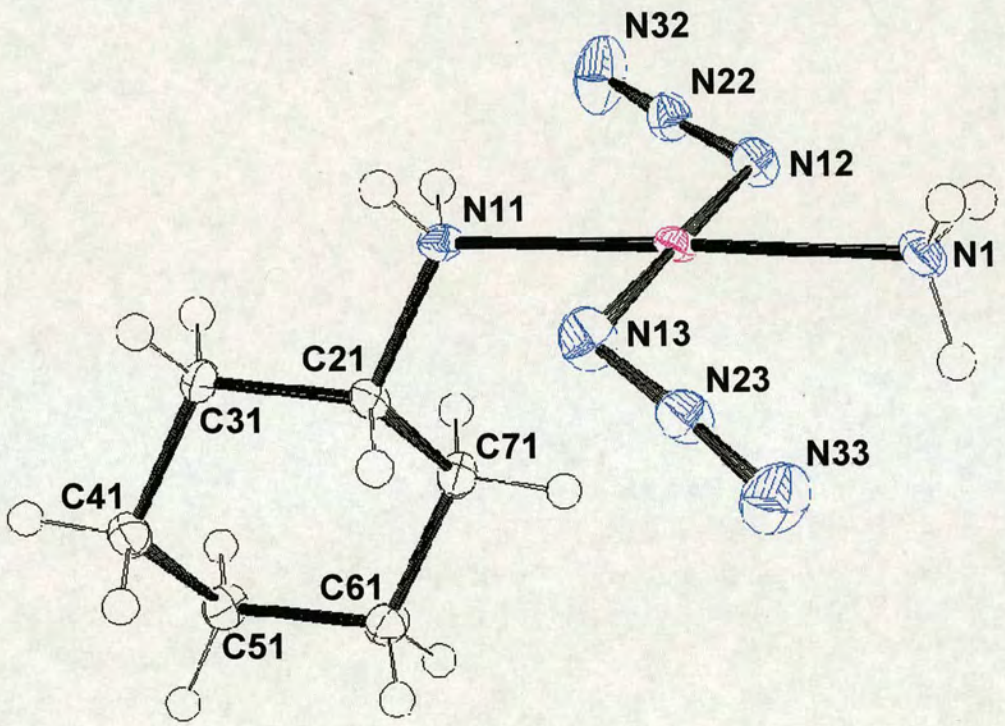

Figure 4.13 X-ray crystal structure of *trans*-[$Pt(N_3)_2(NH_3)$(c-$HexNH_2$)] (**11a**). Thermal ellipsoids at 50 % probability level.

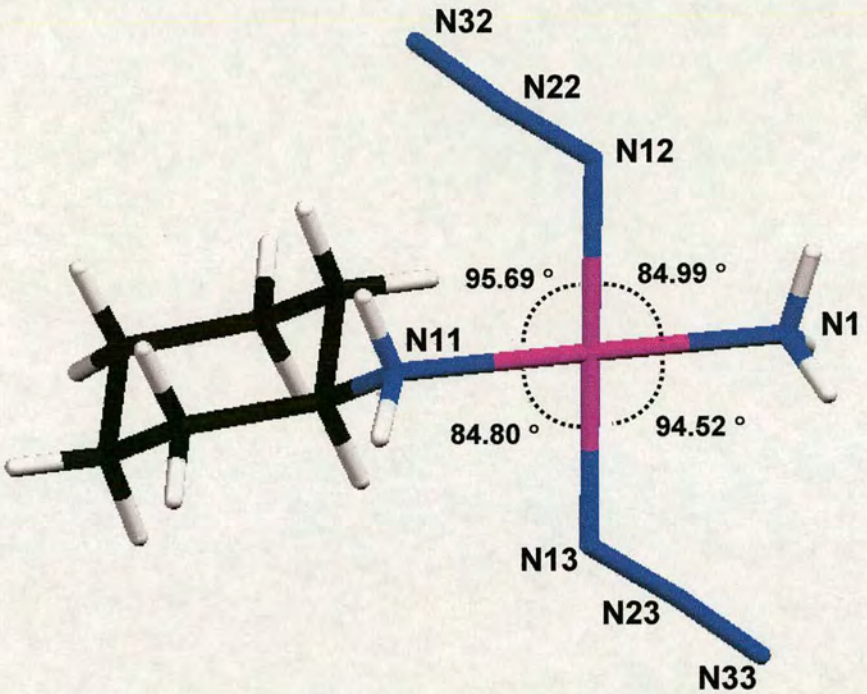

Figure 4.14 X-ray crystal structure of *trans*-[$Pt(N_3)_2(NH_3)$(c-HexNH_2)] (**11a**) showing the angles between the ligands attached to platinum to illustrate the distortion from square-planar geometry.

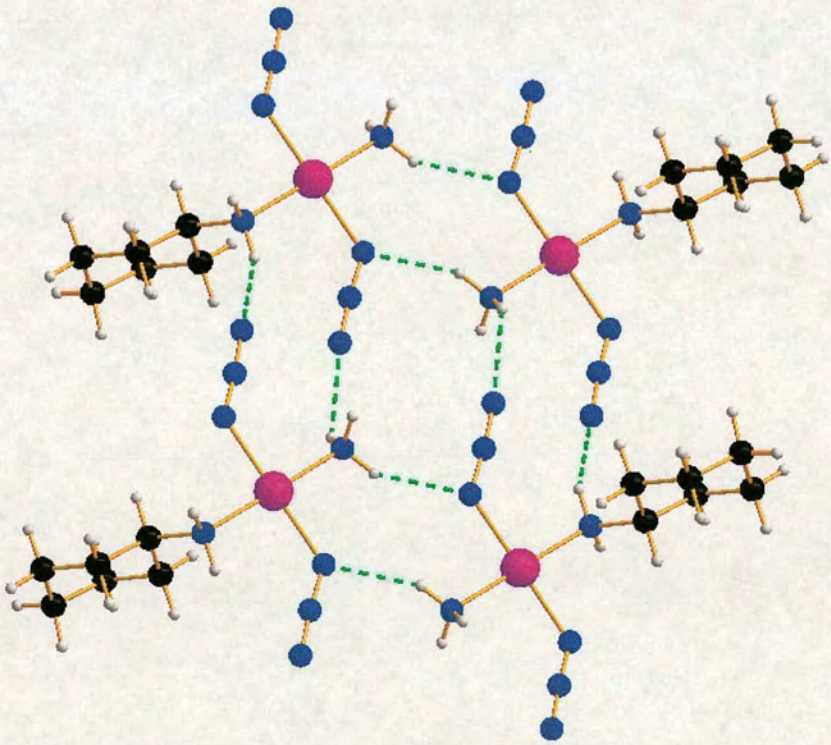

Figure 4.15 X-ray crystal structure of *trans*-[$Pt(N_3)_2(NH_3)$(c-HexNH_2)] (**11a**) with intermolecular hydrogen bonds indicated by the dashed green lines.

Table 4.9 H-bonding distances (Å) and angles (°) of complex **11a**.

D-H	d(D-H)	d(H..A)	<DHA	d(D..A)	A
N1-H	0.910	2.289	150.44	3.113	N12[a]
N1-H	0.910	2.542	133.98	3.241	N32[b]
N1-H	0.910	2.200	162.45	3.079	N33[c]
N11-H	0.920	2.598	156.11	3.459	N12[d]
N11-H	0.920	2.419	141.81	3.193	N33[e]

Symmetry operations : [a] [-x+1, -y, -z+1] [b] [x, y, z-1] [c] [-x, -y, -z] [d] [x-1, y, z] [e] [x, y, z+1]

4.3.3 *Cis*-Pt^{IV} Diazido Complexes

Although the main focus of this work was on compounds with *trans* geometry, the X-ray crystal structure of one *cis*-Pt^{IV}-diazido complex was determined.

4.3.3.1 *Cis, trans, cis*-$[Pt(N_3)_2Cl_2(NH_3)_2]$ (**12**)

The crystallographic data, and bond lengths and angles of the azide ligands of *cis, trans, cis*-$[Pt(N_3)_2Cl_2(NH_3)_2]$ are listed in Table 4.10 and Table 4.11, respectively.

Table 4.10 Crystal structure data for *cis, trans, cis*-$[Pt(N_3)_2Cl_2(NH_3)_2]$ (**12**).

Property	**12**
Empirical formula	$H_4Cl_2N_6O_2Pt$
Formula weight	386.08
Crystal description	yellow block
Crystal size (mm)	0.35 x 0.31 x 0.25
Crystal system	Monoclinic twinned on 2[100]
Space group	$P2_1$
Unit cell dimensions (Å)	$a = 5.1954(4)$ $\alpha = 90$ ° $b = 10.6764(9)$ $\beta = 90.585(5)$ ° $c = 7.3518(6)$ $\gamma = 90$ °
Z	2
Density (calc.) (mg/m^3)	3.144
Absorption coefficient (mm^{-1})	17.824
$F(000)$	348
θ range for data collection (°)	1.91 to 30.49
Reflections collected	3043
Independent reflections	1681
Volume ($Å^3$)	407.77(6)
Wavelength (Å)	0.71073
Conventional R	0.0867
wR_2	0.2271

Table 4.11 Bond lengths (Å) and angles (°) of azide ligands in *cis, trans, cis*-$[Pt(N_3)_2Cl_2(NH_3)_2]$ (**12**).

Bond / Angle	**12**
Pt-N(12)	2.07(3)
Pt-N(11)	2.12(3)
N(12)-N(22)	1.19(5)
N(22)-N(32)	1.13(5)
N(11)-N(21)	1.22(4)
N(21)-N(31)	1.13(5)
Pt-N(12)-N(22)	119(2)
N(12)-N(22)-N(32)	174(4)
Pt-N(11)-N(21)	115(2)
N(11)-N(21)-N(31)	170(4)
N(12)-Pt-N(11)-N(21)	79.6
N(11)-Pt-N(12)-N(22)	-86.2

The crystals of *cis, trans, cis*-$[Pt(N_3)_2Cl_2(NH_3)_2]$ (**12**) had a "crazed" appearance, and the crystal analysed was twinned. This is believed to be the reason for inadequate absorption correction. No attempt was made to place the hydrogens. From the cell dimensions, the system was assumed to be orthorhombic, but subsequent analysis showed that it was a monoclinic twin.

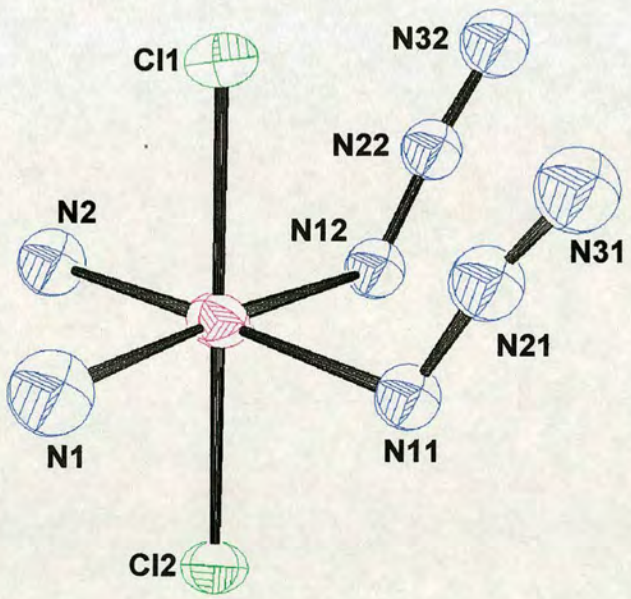

Figure 4.16 X-ray crystal structure of *cis, trans, cis*-$[Pt(N_3)_2Cl_2(NH_3)_2]$ (**12**). Thermal ellipsoids at 50 % probability level.

4.3.4 Pt^{IV} Diazido Complexes with Chelating Ligands

The X-ray crystal structures of three Pt^{IV}-diazido complexes with chelating ligands were determined, *cis, trans*-[Pt(bpy)$(N_3)_2(OH)_2$].2[$Me_2C(OOH)_2$] (**13**), *trans, cis*-[Pt(bpy)$(OAc)_2(N_3)_2$] (**14**) and *trans, cis*-[Pt(phen)$(OAc)_2(N_3)_2$] (**15**). The crystallographic data are listed in Table 4.12, and the bond lengths and angles of the azide ligands can be found in Table 4.13. The azide labelling scheme is shown in Figure 4.17.

Table 4.12 Crystal structure data for *cis, trans*-[Pt(bpy)$(N_3)_2(OH)_2$].2[$Me_2C(OOH)_2$] (**13**), *trans, cis*-[Pt(bpy)$(OAc)_2(N_3)_2$] (**14**) and *trans, cis*-[Pt(phen)$(OAc)_2(N_3)_2$] (**15**).

Property	**13**	**14**	**15**
Empirical formula	$C_{16}H_{26}N_8O_{10}Pt$	$C_{14}H_{14}N_8O_4Pt$	$C_{16}H_{14}N_8O_4Pt$
Formula weight	685.54	553.42	577.43
Crystal description	yellow block	Yellow plate developed in (001)	yellow block
Crystal size (mm)	0.26 x 0.25 x 0.20	0.84 x 0.55 x 0.04	0.35 x 0.20 x 0.15
Crystal system	Monoclinic	Orthorhombic	Monoclinic
Space group	$P2_1/c$	*P*bcn	*P*2/n
Unit cell dimensions (Å)	a = 11.7262(4) b = 20.1996(7)) c = 10.3283(4) α = 90 ° β = 100.572(2) ° γ = 90°	a = 8.0488(4) b = 14.1103(7) c = 15.3280(7) α = 90 ° β = 90 ° γ = 90°	a = 7.03030(10) b = 11.7849(2) c = 11.3271(2) α = 90°. β = 101.2360(10)° γ = 90°
Z	4	4	2
Density (calc.) (mg/m^3)	1.893	2.112	2.083
Absorption coefficient (mm^{-1})	5.902	8.101	7.665
F(000)	1344	1056	552
θ range for data collection (°)	1.77 to 38.67	2.66 to 29.61	1.728 to 29.544
Reflections collected	55188	21880	14648
Independent reflections	9271	2307	2454
Volume ($Å^3$)	2404.88(15)	1740.82(15)	920.48(3)
Temperature (K)	150(2)	150(2)	150(2)
Wavelength (Å)	0.71073	0.71073	0.71073
Conventional R	0.0248	0.0243	0.0305
wR_2	0.0562	0.0582	0.0690

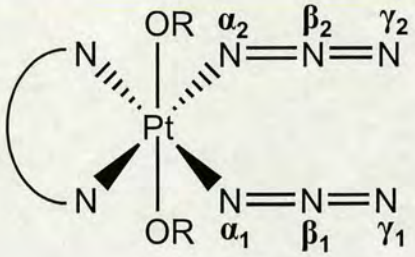

Figure 4.17 Labelling of azide ligands in chelated Pt^{IV} diazido complexes.

Table 4.13 Bond lengths (Å) and angles (°) of azide ligands in *cis, trans*-$[Pt(bpy)(N_3)_2(OH)_2].2[Me_2C(OOH)_2]$ (**13**), *trans, cis*-$[Pt(bpy)(OAc)_2(N_3)_2]$ (**14**) and *trans, cis*-$[Pt(phen)(OAc)_2(N_3)_2]$ (**15**).

Bond / Angle	**13**	**14**	**15**
Pt-N(α_1)	2.0196(16)	2.022(3)	2.001(3)
Pt-N(α_2)	2.0561(17)	-	-
N(α_1)-N(β_1)	1.229(2)	1.225(5)	1.175(6)
N(β_1)-N(γ_1)	1.138(2)	1.147(5)	1.154(6)
N(α_2)-N(β_2	1.193(3)	-	-
N(β_2)-N(γ_2)	1.147(3)	-	-
Pt-N(α_1)-N(β_1)	115.90(14)	115.0(3)	118.5(4)
N(α_1)-N(β_1)-N(γ_1)	174.0(2)	175.2(5)	173.1(5)
Pt-N(α_2)-N(β_2)	114.03(15)	-	-
N(α_2)-N(β_2)-N(γ_2)	175.9(3)	-	-
N(α_1)-Pt-N(α_2)-N(β_2)	-49.8	-45.2	35.33
N(α_2)-Pt-N(α_1)-N(β_1)	-56.5	-45.2	35.33

4.3.4.1 *Cis, trans*-$[Pt(bpy)(N_3)_2(OH)_2].2[Me_2C(OOH)_2]$ (**13**)

Cis, trans-$[Pt(bpy)(N_3)_3(OH)_2]$ (**13**) co-crystallised with two molecules of the explosive compound peroxyacetone ($C_3H_8O_4$).[24] This is believed to have been formed by oxidation of residual acetone with hydrogen peroxide. The synthesis is described in Section 3.2.2.17 in Chapter 3. Peroxyacetone is an unusual molecule to find as a co-crystallite and only one other entry was found in the CCDC,[25] a crystal structure which consisted of the 1:2 adduct (bis(diphenylphosphinoyl)ethane).2(2,2-dihydroperoxypropane)($dppeO_2$).2$[Me_2C(OOH)_2]$, and was synthesised from a solution containing acetone and H_2O_2. The peroxyacetone moiety was reported to be stabilised by hydrogen bonds formed between its OH groups and the oxygens of $dppeO_2$. Similar hydrogen bonds are found in the structure of **13**.$Me_2C(OOH)_2$, the

OH hydrogen of peroxyacetone bonds to both the oxygens attached to platinum (O1 and O2) and also to one of the middle azide nitrogens (N22).

Table 4.14 Hydrogen bonding distances (Å) and angles (°) in the crystal structure of *cis, trans*-$[Pt(bpy)(N_3)_3(OH)_2].2[Me_2C(OOH)_2]$.

D-H	d(D-H)	d(H..A)	<DHA	d(D..A)	A
O54-H	0.840	1.940	155.38	2.726	O1[a]
O74-H	0.840	1.963	160.42	2.769	O1[a]
O55-H	0.840	2.034	152.35	2.805	O2[b]
O55-H	0.840	2.685	133.33	3.318	N22[b]
O75-H	0.840	1.902	158.62	2.702	O2[b]

Symmetry operations: [a] [x, -y+1/2, z+1/2], [b] [x+1, y, z]

Complex **13**.$Me_2C(OOH)_2$ crystallised in an monoclinic crystal system with the space group $P2_1/c$. The bond lengths and angles of the bipyridine ligand compare well with the related structure $[Pt(bpy)Cl_4]$.[26] The Pt-N bond lengths of **13**.$Me_2C(OOH)_2$ are slightly different than those of the Pt^{II} analogue $[Pt^{II}(bpy)(N_3)_2]$ (**13a**, Section 4.3.5.1), the Pt-N(bpy) bonds are ca. 0.02 Å longer in the Pt^{IV} complex. This difference is also seen for $[Pt^{IV}(bpy)Cl_4]$[26] and $[Pt^{II}(bpy)Cl_2]$[27] where the Pt-N(bpy) bonds of Pt^{IV} were reported to be ca. 0.04 Å longer. The azide bond lengths are very similar to other Pt azide complexes (Table 4.2 and Table 4.13).

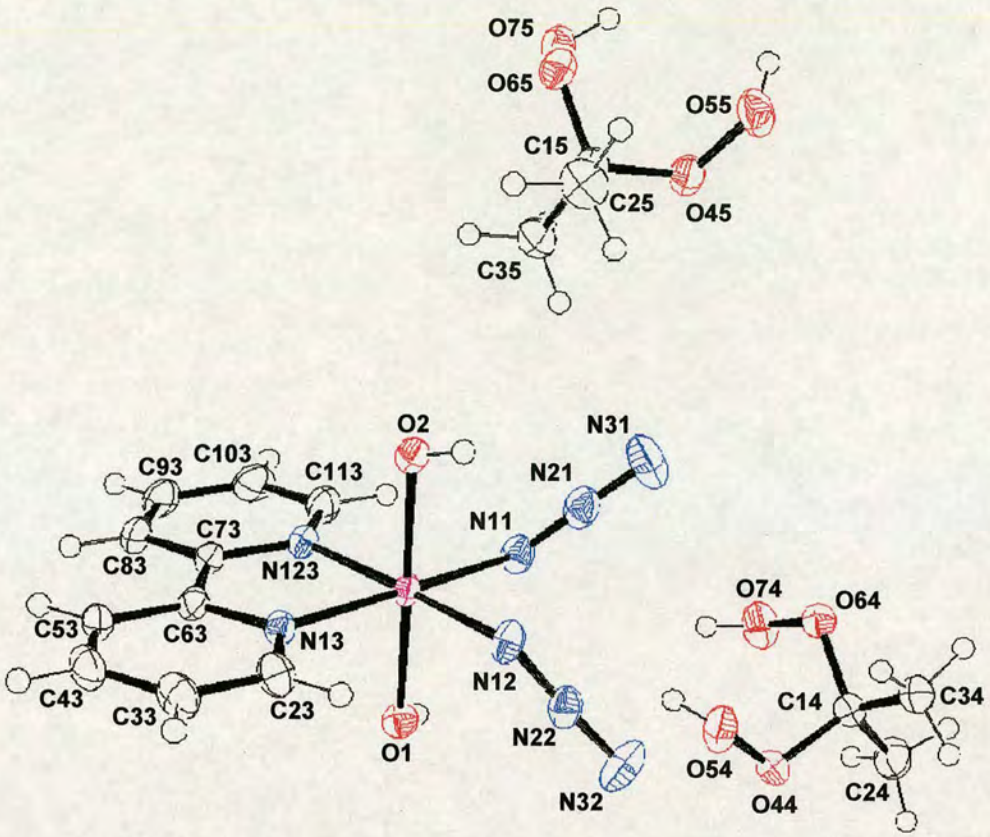

Figure 4.18 X-ray crystal structure of *trans, cis*-[Pt(bpy)$(N_3)_2(OH)_2$].2[MeC$(OOH)_2$] (**13**). Thermal ellipsoids at 50 % probability level.

4.3.4.2 *Trans, cis*-[Pt(bpy)$(OAc)_2(N_3)_2$] (**14**)

Trans, cis[Pt(bpy)$(OAc)_2(N_3)_2$] (**14**) crystallised in an orthorhombic crystal system with space group *P*bcn. The only other known orthorhombic Pt^{IV} azide compound was complex **4** (Section 4.3.1.2), and no other platinum azides have been crystallised in space group *P*bcn. The platinum sits on a 2-fold axis and so there is only one set of azide bond lengths and angles in Table 4.13.

The azide bond lengths of complex **14** compare well with other platinum azide compounds (Figure 4.2 and Table 4.13), and the bipyridine ligand bond lengths and angles are very similar to related structures, complexes **13** and **13a**. The Pt-N(bpy) bond lengths are very similar to those of complex **13** and consequently are larger than those of complex **13a,** as described in Section 4.3.4.1.

There is extensive hydrogen bonding in this structure, both intra- and intermolecular.

The intermolecular bonds are shown in Figure 4.20; intramolecular bonds exist between the platinum bound azide nitrogens and the hydrogens on C22 of bipyridine.

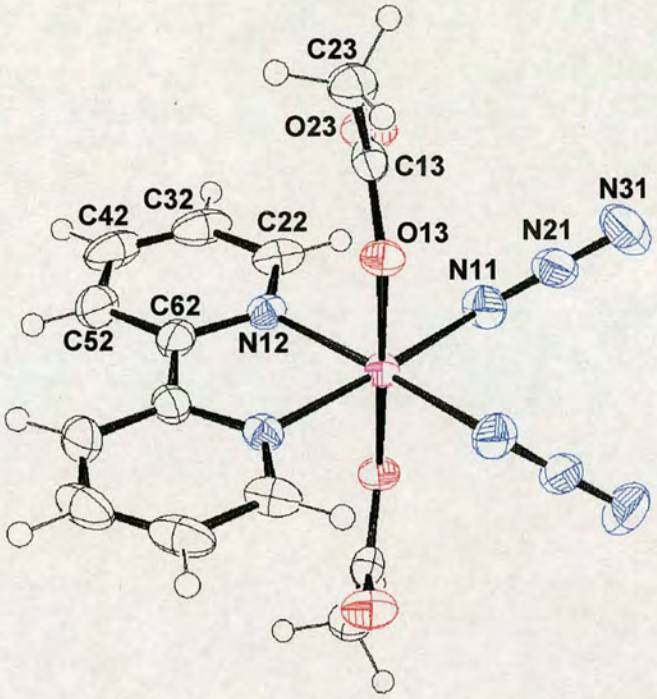

Figure 4.19 X-ray crystal structure of *trans, cis*-[Pt(bpy)$(OAc)_2(N_3)_2$] (**14**). Thermal ellipsoids at 50 % probability level.

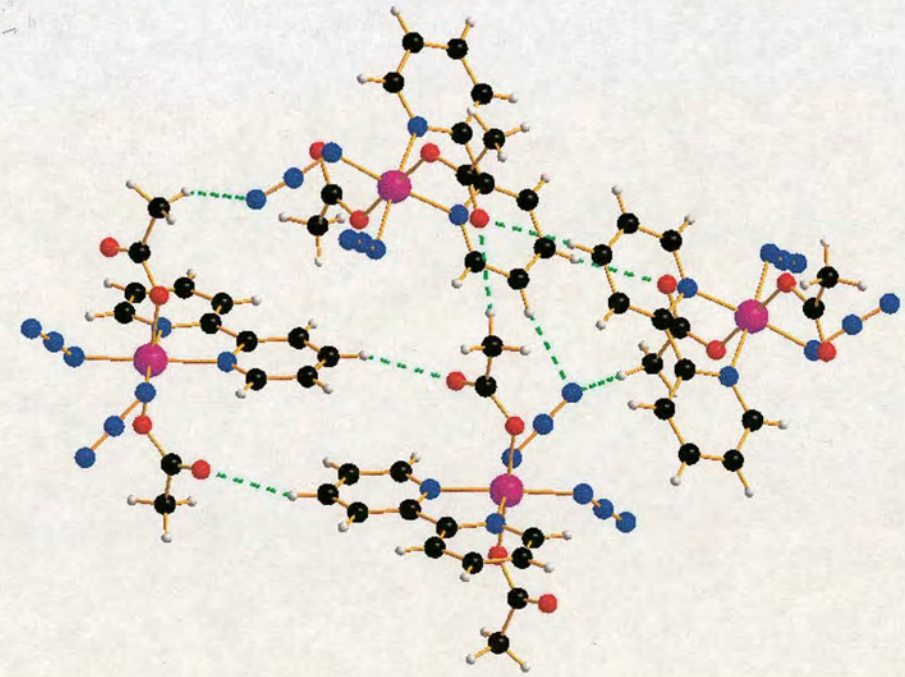

Figure 4.20 X-ray crystal structure of *trans, cis*-[Pt(bpy)$(OAc)_2(N_3)_2$] (**14**) with intermolecular hydrogen bonds indicated by the dashed green lines.

4.3.4.3 *Trans, cis*-[Pt(phen)$(OAc)_2(N_3)_2$] (**15**)

Trans, cis-[Pt(phen)$(OAc)_2(N_3)_2$] crystallised in a monoclinic crystal system with the space group *P*2/n (Figure 4.21). The azide bond lengths and angles compare well with the other platinum azide structures (Table 4.2 and Table 4.13). The phenanthroline and acetate bond lengths and angles are also within the expected range. Like the bipyridne structure (**14**), the platinum in complex **15** sits on a 2-fold axis.

The Pt-N(phen) bond lengths of complex **15** are significantly longer than those of the analogous Pt^{II} compound [Pt(phen)$(N_3)_2$] (**15a**, Section 4.3.5.2). This was also observed for the bipyridine complexes and has been reported in the literature.[26] The intermolecular hydrogen bonding of complex **15** is similar to that of complex **14** which is expected due to the similarity of these structures. However, some weak π-π stacking also exists between molecules of the phenanthroline complex. The centroid-centroid distance is 3.996 Å, with a dihedral angle of 2.530(146) °.

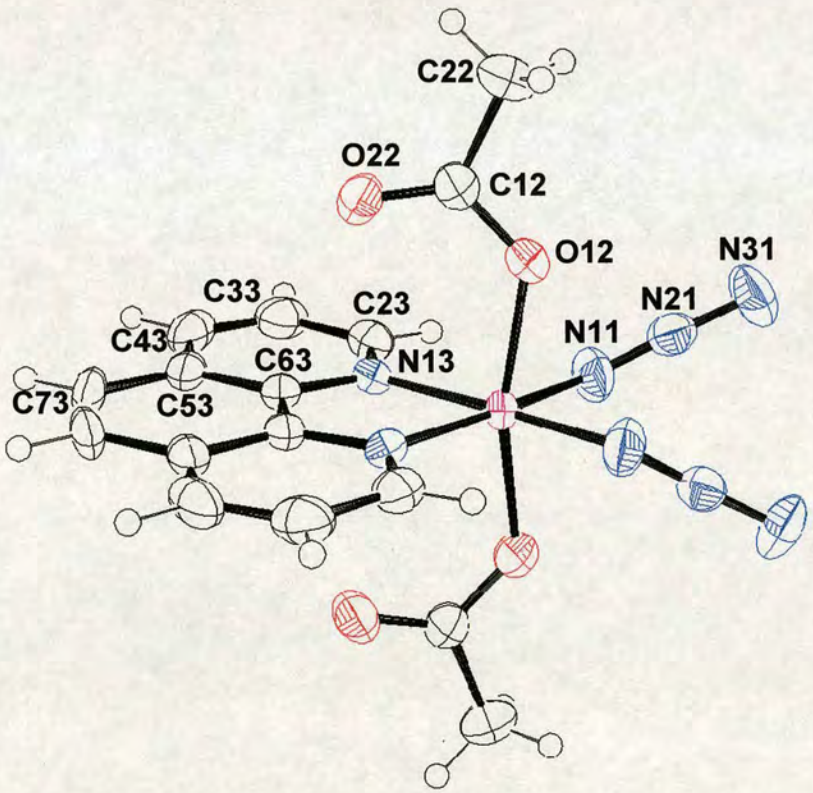

Figure 4.21 X-ray crystal structure of *trans, cis*-[Pt(phen)$(OAc)_2(N_3)_2$] (**15**). Thermal ellipsoids at 50 % probability level.

4.3.5 Pt^{II} Diazido Complexes with Chelating Ligands

The X-ray crystal structures of two Pt^{II}-diazido complexes with chelating ligands were determined, $[Pt(bpy)(N_3)_2]$ (**13a**) and $[Pt(phen)(N_3)_2]$ (**15a**). The crystallographic data are listed in Table 4.15, and the bond lengths and angles of the azide ligands are in Figure 4.16. The azide labelling scheme is shown in Figure 4.22.

Table 4.15 Crystal structure data for $[Pt(bpy)(N_3)_2]$ (**13a**) and $[Pt(phen)(N_3)_2]$ (**15a**).

Property	**13a**	**15a**
Empirical formula	$C_{10}H_8N_8Pt$	$C_{12}H_8N_8Pt$
Formula weight	435.32	459.34
Crystal description	orange needle	yellow block
Crystal size (mm)	0.82 x 0.10 x 0.10	0.26 x 0.12 x 0.10
Crystal system	Monoclinic	Monoclinic
Space group	*C*2/c	*C*2/c
Unit cell dimensions (Å)	$a = 10.9346(5)$ $b = 15.3328(8)$ $c = 7.0453(4)$ $\alpha = 90°$ $\beta = 94.717(3)°$ $\gamma = 90°$	$a = 19.3584(7)$ $b = 10.1802(4)$ $c = 13.8692(4)$ $\alpha = 90°$ $\beta = 113.816(2)°$ $\gamma = 90°$
Z	4	8
Density (calc.) (mg/m^3)	2.456	2.440
Absorption coefficient (mm^{-1})	11.919	11.230
F(000)	808	1712
θ range for data collection (deg)	2.293 to 28.731	2.300 to 28.824
Reflections collected	6926	9019
Independent reflections	1453	3057
Volume ($Å^3$)	1177.20(11)	2500.49(16)
Temperature (K)	150	150
Wavelength (Å)	0.71073	0.71073
Conventional *R*	0.0192	0.0326
*wR*2	0.0478	0.0825

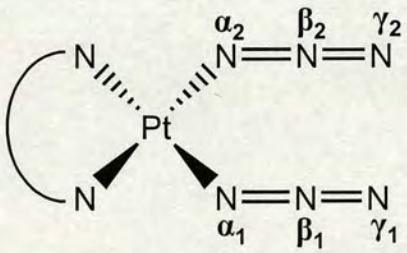

Figure 4.22 Labelling of azide ligands in chelated Pt^{II} diazido complexes.

Table 4.16 Bond lengths (Å) and angles (°) in azide ligands in [Pt(bpy)$(N_3)_2$] (**13a**) and [Pt(phen)$(N_3)_2$] (**15a**).

Bond / Angle	**13a**	**15a**
Pt-N(α_1)	2.034(3)	2.022(6)
Pt-N(α_2)	-	2.037(5)
N(α_1)-N(β_1)	1.190(4)	1.179(8)
N(β_1)-N(γ_1)	1.150(5)	1.167(8)
N(α_2)-N(β_2)	-	1.182(7)
N(β_2)-N(γ_2)	-	1.164(8)
Pt-N(α_1)-N(β_1)	119.3(2)	125.1(4)
N(α_1)-N(β_1)-N(γ_1)	175.2(4)	174.2(7)
Pt-N(α_2)-N(β_2)	-	121.8(4)
N(α_2)-N(β_2)-N(γ_1)	-	174.5(6)
N(α_1)-Pt-N(α_2)-N(β_2)	40.3	29.8
N(α_2)-Pt-N(α_1)-N(β_1)	40.3	29.5

4.3.5.1 [Pt(bpy)$(N_3)_2$] (**13a**)

[Pt(bpy)$(N_3)_2$] (**13a**) crystallised in a monoclinic crystal system with the space group *C*2/c (Figure 4.23). The azide bond lengths and angles compare well with the other platinum azide structures (Table 4.7 and Table 4.16). The molecule sits on a 2-fold axis, as do complexes **14** and **15**.

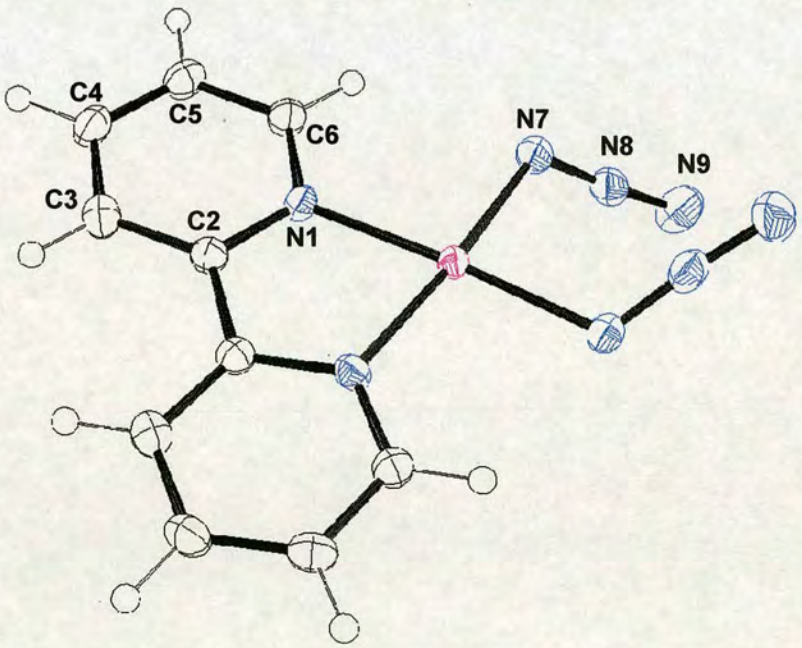

Figure 4.23 X-ray crystal structure of [Pt(bpy)$(N_3)_2$] (**13a**). Thermal ellipsoids at 50 % probability level.

The two rings within a single molecule are skewed with respect to each other at an angle of 5.12 °. This is also seen for the Pt^{IV} bipyridine complexes, although it is less pronounced; the angle of complex **13** is 3.71 ° and for complex **14** is 3.41 °. Some weak intermolecular hydrogen bonding exists between the azide ligands and the ring hydrogens. The centroid-centroid distance (4.036 Å) and angle (6.117 °) indicate that π-π stacking does not play a large role in the structure of complex **13a**.

4.3.5.2 $[Pt(phen)(N_3)_2]$ (**15a**)

$[Pt(phen)(N_3)_2]$ (**15a**) crystallised in a monoclinic crystal system with the space group *C*2/c (Figure 4.24). Interestingly this is the same crystal system and space group as complex **13a**, but $[Pt(phen)(N_3)_2]$ does not contain a 2-fold axis of symmetry.

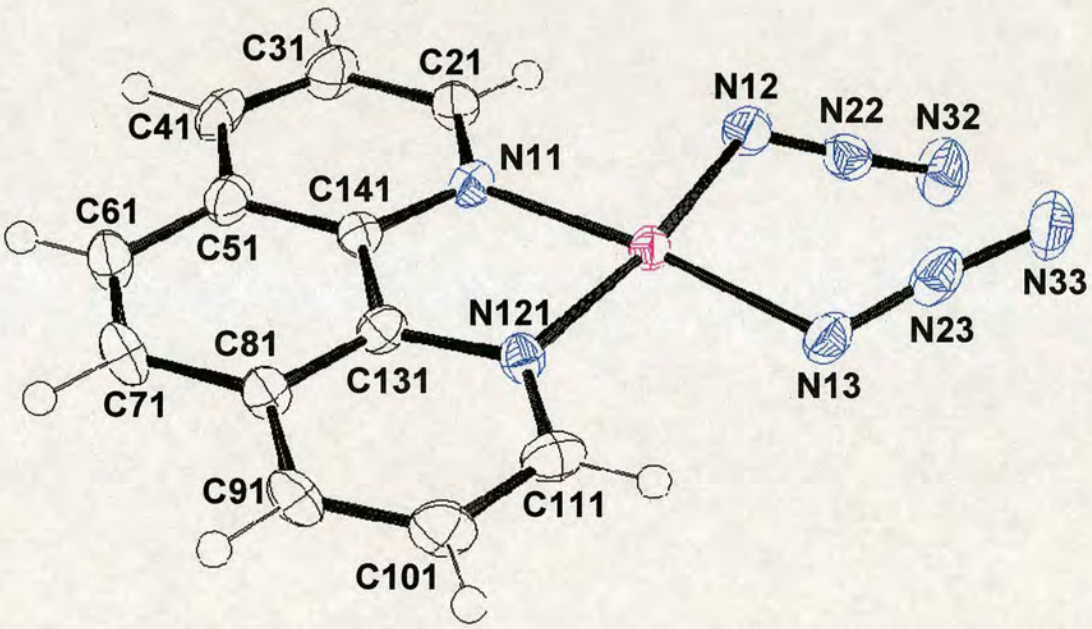

Figure 4.24 X-ray crystal structure of $[Pt(phen)(N_3)_2]$ (**15a**). Thermal ellipsoids at 50 % probability level.

There is some intermolecular hydrogen bonding between ring hydrogens and terminal azide nitrogens. The structure consists of dimers which are connected by a short platinum-platinum bond (Figure 4.25). It is not unusual to find Pt-Pt bonds in square-planar Pt^{II} complexes, often linear chains are formed bonded through the

platinum centres.[28] Such bonds are found in Pt^{II}-bipyridine complexes where the Pt-Pt bond is generally around 3.4 Å, however there were no platinum-platinum bonds present in the crystal structure of complex **13a** $[Pt(bpy)(N_3)_2]$ (Section 4.3.5.1). The $[Pt(phen)(N_3)_2]$ dimers are also π-π stacked at a distance of 3.631 Å and a dihedral angle of 5.334(204) °

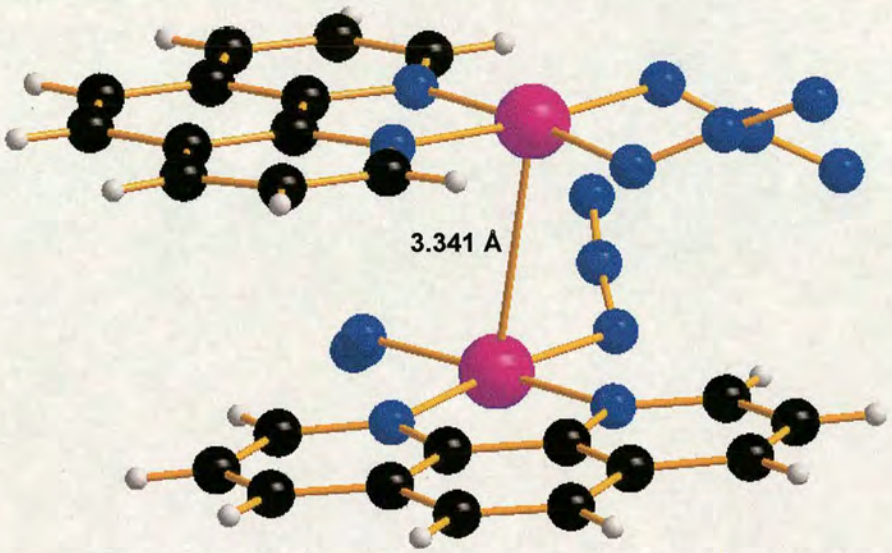

Figure 4.25 X-ray crystal structure of $[Pt(phen)(N_3)_2]$ (**15**) showing the short Pt – Pt contact between molecules.

4.4 Conclusions

The X-ray crystal structures of twelve novel platinum azide complexes have been determined. These structures include Pt^{II} and Pt^{IV} complexes, and compounds with *cis* and *trans* geometry with respect to the azide ligands. Several Pt^{IV} complexes containing the chelating aromatic ligands 2,2′-bipyridine and 1,10-phenanthroline were crystallised and their structures solved. The difficulty in oxidising Pt^{II} bipyridine and phenanathroline complexes has been reported and was experienced during this work (Chapter 3);[29] these problems are exacerbated by the presence of the azide ligands which are not stable under harsh conditions (e.g. high temperatures). Therefore it was particularly important to have determined the structures of the three Pt^{IV} complexes containing bipyridine and phenanthroline ligands to confirm their identities.

4.5 References

[1] Dori, Z.; Ziolo, R.F. *Chem. Rev.* **1973**, *73*, 247.

[2] Sharpe, A.G. In *Inorganic Chemistry*, Longman, Harlow, **1981**.

[3] Schröder, S.; Preetz, W. *Z. Anorg. Allg. Chem.* **2000**, *626*, 1915.

[4] Schröder, S.; Preetz, W. *Z. Anorg. Allg. Chem.* **2000**, *626*, 1757.

[5] Schröder, S.; Preetz, W. *Z. Anorg. Allg. Chem.* **2001**, *627*, 390.

[6] Neumüller, B.; Schmock, F.; Schlecht, S.; Dehnicke, K. *Z. Anorg. Allg. Chem.* **2000**, *626*, 1792.

[7] Müller, P. PhD Thesis, University of Edinburgh **2002**.

[8] Sheldrick, G.M. SADABS, University of Göttingen, Göttingen (Germany), **2004**.

[9] Sheldrick, G.M. SHELXS, University of Göttingen, Göttingen (Germany), **1997**.

[10] Beurskens, P.T.; Beurkskens, G.; Bosman, W.P.; de Gelder, R.; Garcia-Granda, S.; Gould, R.O.; Israel, R.; Smits, J.M.M. Crystallography Laboratory, University of Nijmegen, The Netherlands, **1996.**

[11] Sheldrick, G.M. SHELXL, University of Göttingen, Göttingen (Germany), **1997**.

[12] Mackay, F.S.; Woods, J.A.; Moseley, H.; Ferguson, J.; Dawson, A.; Parsons, S.; Sadler, P.J. *Chem. Eur. J.* **2006**, *12*, 3155.

[13] Müller, P.; Schröder, B.; Parkinson, J.A.; Kratochwil, N.A.; Coxall, R.A.; Parkin, A.; Parsons, S.; Sadler, P.J. *Angew. Chem., Int. Ed.* **2003**, *42*, 335.

[14] Kuroda, R.; Neidle, S.; Ismail, I.M.; Sadler, P.J. *Inorg. Chem.* **1983**, *22*, 3620.

[15] Colamarino, P.; Oriolli, P.L. *J. Chem. Soc., Dalton Trans.* **1975**, 1656.

[16] Junicke, H.; Schenzel, K.; Heinemann, F.W.; Pelz, K.; Bögel, H.; Steinborn, D. *Z. Anorg. Allg. Chem.* **1997**, *623*, 603.

[17] Bierbach, U.; Qu, Y.; Hambley, T.W.; Peroutka, J.; Nguyen, H.L.; Doedee, M.; Farrell, N. *Inorg. Chem.* **1999**, *38*, 3535.

[18] McGowan, G. PhD Thesis, University of Edinburgh **2005**.

[19] McGowan, G.; Parsons, S.; Sadler, P.J. *Inorg. Chem.* **2005**, *44*, 7459.

[20] Neidle, S.; Snook, C.F. *Acta Cryst.* **1995**, *C51*, 822.

[21] Arpalahti, J.; Lippert, B.; Schöllhorn, H.; Thewaltm, U. *Inorg. Chim. Acta.* **1988**, *153*, 45.

[22] Milburn, G.H.W.; Truter, M.R. *J. Chem. Soc., A*, **1966**, 1609.

[23] Talman, E.G.; Brüning, W.; Reedijk, J.; Spek, A.L.; Veldman, N. *Inorg. Chem.* **1997**, *36*, 854.

[24] Milas, N.A.; Golubović, A. *J. Am. Chem. Soc.* **1959**, *81*, 6461.

[25] Pettinari, C.; Marchetti, F.; Cingolani, A.; Drozdov, A.; Troyanov, S. *J. Chem. Soc., Chem. Commun.* **2000**, 1901.

[26] Hambley, T.W. *Acta Cryst.* **1986**, *C42*, 49.

[27] Osborn, R.S.; Rogers, D. *J. Chem. Soc., Dalton Trans.* **1974**, 1002.

[28] Miskowski, V.M.; Houlding, V.H. *Inorg. Chem.* **1989**, *28*, 1529.

[29] Hodges, K.D.; Rund, J.V. *Inorg. Chem.* **1975**, *14*, 525.

Chapter 5
Stability and Photoreactions

5.1 Introduction

The stability of photoactive complexes under physiological conditions is an important factor to consider for potential photochemotherapeutic drugs. A previous class of photoactive Pt^{IV} di-iodo complexes was found to be too easily reduced by thiols to cytotoxic Pt^{II} species.[1-3] Pt^{IV} diazido complexes **1** and **2** have previously been found to be relatively stable.[4,5] This chapter further investigates the stability of complex **1** and also includes stability studies on the *trans* complexes **3**, **4**, **5**, and **8**.

Metal azides have been found to undergo a variety of different photoreactions which include (i) photosubstitution of the azide ligand,[6,7] (ii) photoreduction of an oxidising metal,[8-18] (iii) the generation of metal-nitrenes,[19-25] and (iv) production of singlet oxygen.[26,27] Determining the mechanism of photoactivation of Pt^{IV} azide compounds is therefore not a simple task. The photoreactivity of the Pt^{IV}-azide complexes was studied by both ^{1}H and 2D [^{1}H,^{15}N] HSQC NMR spectroscopy as well as UV-visible spectroscopy in an attempt to understand the photoactivation pathway.

5.2 Experimental

5.2.1 Materials

Complexes **1-14**, ^{15}N-cisplatin, ^{15}N-transplatin and [$Pt(^{15}NH_3)(py)Cl_2$] were synthesised as previously described (Chapter 3). Silver nitrate, D_2O and 1,4-dioxane were purchased from Aldrich; NaCl and NaOH from Fisher; 5′-GMP and reduced glutathione from Acros; EBSS and H_2O_2 from Sigma, and $HClO_4$ from Fisons.

5.2.2 Syntheses

5.2.2.1 *Cis*-[$Pt^{IV}(^{15}NH_3)_2(OH/OH_2)_4$]

^{15}N-cisplatin (7.5 mg, 0.025 mmol) was suspended in H_2O (5 mL) and $AgNO_3$ (8.4 mg, 0.05 mmol) added. After stirring for 24 h at 333 K, the insoluble AgCl was filtered off. An NMR sample was prepared using 0.54 mL of the above solution and 60 μL of D_2O, and the pH adjusted to 5 ± 0.2. The ^{1}H and 2D [^{1}H,^{15}N] HSQC NMR spectra were acquired, and then 4 mol equiv H_2O_2 (30 % v/v, 1.1 μL) added to the tube. The solution was stirred in the NMR tube overnight, the pH was readjusted to 5

± 0.2 and the NMR spectra acquired again.

5.2.2.2 *Trans*-[$Pt^{IV}(^{15}NH_3)_2(OH)_4$]

^{15}N-transplatin (4.6 mg, 0.015 mmol) was suspended in H_2O (3.1 mL) and $AgNO_3$ (5.1 mg, 0.030 mmol) added. The reaction was continued as described for *cis*-[$Pt^{IV}(^{15}NH_3)_2(OH/OH_2)_4$] (section 5.2.2.1). The Pt^{IV} NMR sample was then analysed by ESI-MS.

5.2.2.3 *Trans*-[$Pt^{IV}(^{15}NH_3)(py)(OH)_4$]

[$Pt^{II}(^{15}NH_3)(py)Cl_2$] (3.4 mg, 0.009 mmol) was suspended in H_2O (3 mL) and $AgNO_3$ (3.2 mg, 0.018 mmol) added. The reaction was continued as described for *cis*-[$Pt^{IV}(^{15}NH_3)_2(OH/OH_2)_4$] (section 5.2.2.1). The Pt^{IV} NMR sample was then analysed by ESI-MS.

5.2.3 Stability Studies

The stability of several Pt^{IV} azide compounds was monitored by 1D ^{1}H and 2D [^{1}H,^{15}N] HSQC NMR spectroscopy. The samples were all prepared in 90 % H_2O / 10 % D_2O with 1,4-dioxane (1 %, 2 μL) added as the internal ^{1}H reference, the only exceptions were those set-up to determine the stability in cell culture media. These samples were prepared in 90 % Earle's Balanced Salt Solution (EBSS) / 10 % D_2O.

All samples were kept in the dark at 294 K in between measurements, except for the sample used to determine stability at physiological temperatures; this sample was incubated at 310 K also in the dark. NMR spectra were acquired on a DMX500 NMR spectrometer as previously described (Chapter 2.1.2).

5.2.4 Photoreactions

Details of the acquisition of NMR spectra, ESI-MS and pH adjustments are described in Chapter 2.1.2.

UV irradiation (365 nm) was carried out with a UV lamp, the experimental set-up is described in detail in Chapter 2.3.

5.3 Results

5.3.1 Stability Studies

Reactions of Pt^{IV} diazido-dihydroxy complexes can be followed by ^1H NMR studies of the am(m)ine protons if the reactions are carried out in H_2O. However, at neutral pH, no ^1H am(m)ine peaks are detected due to fast exchange of the NH protons with the solvent. With decreasing pH the signals appear, and so the pH is usually adjusted to 5 in order to observe the Pt^{IV} am(m)ine protons by NMR.

For each sample the spectrum reported as recorded at '0 h' was the first one acquired after preparation. For samples where the pH was not adjusted this will be less than 5 min. Adjusting the pH generally takes approximately 5 min, so samples where the pH is changed were acquired ca. 10 min after preparation.

The NMR spectra for all experiments are shown in Appendix 3, for peak assignments and coupling constants see Chapter 3. A single peak for dioxane is present at 3.764 ppm in all ^1H NMR spectra.

5.3.1.1 Aqueous Stability

a) *Trans, trans, trans*-$[Pt(N_3)_2(OH)_2(^{15}NH_3)_2]$ (**3**)

A 3 mM solution of complex **3** was prepared and the pH adjusted from 6.4 to 4.8. 1D ^1H and 2D [^1H,^{15}N] HSQC NMR spectra were acquired after 0 h, 24 h, 6 d, 12 d, 93 and 154 d. After 154 d no new peaks appeared in either the 1D or 2D spectra and only a peak for complex **3** was present, therefore no hydrolysis had occurred (Appendix 3, Figure A3.1).

b) *Trans, trans, trans*-$[Pt(N_3)_2(OH)_2(NH_3)(py)]$ (**4**)

A 3 mM solution of complex **4** was prepared. The pH was measured as 6.3, but as the complex was not ^{15}N-labelled no pH adjustment was necessary. ^1H NMR spectra were recorded after 0 h, 24 h, 6 d, 47 d, 93 d and 154 d. This compound was found to be very stable, after 154 d only peaks for complex **4** were present (Appendix 3, Figure A3.2).

c) *Trans, trans, trans*-[$Pt(N_3)_2(OH)_2(NH_3)(MeNH_2)$] (**5**)

This sample was prepared and spectra obtained as described above for complex **4**. The pH was measured as 6.4. This compound was also found to be very stable, after 154 d only peaks for complex **5** were present (Appendix 3, Figure A3.3). Therefore no hydrolysis had occurred.

d) *Trans, trans, trans*-[$Pt(N_3)_2(OH)_2(NH_3)$(2-pic)] (**8**)

This sample was prepared and spectra obtained as described above for complex **4**. The pH was measured as 6.4. This compound was also found to be very stable, after 154 d only peaks for complex **8** were present (Appendix 3, Figure A3.4). Therefore no hydrolysis had occurred.

5.3.1.2 Stability towards Chloride

The stability towards chloride was investigated by adding NaCl (100 mM) to 3 mM solutions of *cis, trans, cis*-[$Pt(N_3)_2(OH)_2(^{15}NH_3)_2$] (**1**) and *trans, trans, trans*-[$Pt(N_3)_2(OH)_2(^{15}NH_3)_2$] (**3**). The pH of both samples was adjusted to 5 before recording the 0 h spectra. 1D ^1H and 2D [^1H,^{15}N] HSQC NMR spectra were acquired after 0 h, 2h, 5 h, 24 h, 6 d, 12 d, 47 d, 93 d and 154 d for complex **1** and 0 h, 24 h, 6 d, 47 d, 79 d and 140 d for complex **3**. The $^{15}NH_3$ peaks were observed to decrease in intensity in both the 1D ^1H and 2D [^1H,^{15}N] HSQC NMR spectra over the course of the stability study (Appendix 3, Figure A3.5 and A3.6), however no new peaks appeared. The pH of both samples had risen significantly by the end of the experiment (complex **1** pH 6.19; complex **3** pH 6.93). This pH rise along with the decrease of the $^{15}NH_3$ peaks suggests chloride is replacing the ammonia ligands. If this happened on a short time scale (e.g < 48 h) it could be a problem, however after 12 d for **1** and 6 d for **3** the majority of the $^{15}NH_3$ is still bound to platinum (Appendix 3, Figure A3.5 and A3.6).

5.3.1.3 Stability towards Nucleotides

Trans, trans, trans-[$Pt(N_3)_2(OH)_2(^{15}NH_3)_2$] (**3**)

Two molar equivalents of 5′-GMP were added to a 3 mM solution of complex **3** and the pH adjusted from 8.0 to 4.8. 1D ^1H and 2D [^1H,^{15}N] HSQC NMR spectra were

recorded after 0 h, 24 h, 9 d, 21 d and 47 d. There were no new peaks visible after 47 days (Appendix 3, Figure A3.7).

5.3.1.4 Stability in Cell Culture Media

These samples were prepared in 90 % Earle's Balanced Salt Solution (EBSS) / 10 % D_2O. The pH of EBSS was 7.5 before the addition of any platinum complex. An extra 4 μL of dioxane was added as the signal was masked by those of EBSS.

a) *Trans, trans, trans*-$[Pt(N_3)_2(OH)_2(NH_3)(py)]$ (**4**)

A 3 mM sample of complex **4** was prepared and the pH measured as 8.4. ^1H NMR spectra were acquired after 0 h, 1.5 h, 5 h, 24 h, 6 d, 47 d, 93 d and 154 d. After 154 d only peaks corresponding to complex **4** and EBSS were present, no new peaks appeared (Appendix 3, Figure A3.8).

b) *Trans, trans, trans*-$[Pt(N_3)_2(OH)_2(NH_3)(MeNH_2)]$ (**5**)

This reaction was carried out as described above for complex **4**. After 154 d only peaks corresponding to complex **5** and EBSS were present, no new peaks appeared (Appendix 3, Figure A3.9).

5.3.1.5 Stability towards Glutathione

The stability towards glutathione (GSH) was investigated by adding 2 mol equiv of reduced GSH to a 3.3 mM solution of complex **3**. The pH was measured as 3.7, therefore adjustment to < 7 was not necessary. 1D ^1H and 2D [^1H,^{15}N] HSQC NMR spectra were recorded after 0 h, 24 h, 9 d and 21 d. There was no change in the spectra after 24 h. After 9 d, two new Pt^{II} peaks had appeared at δ(^1H,^{15}N) 3.87, -61.24 ppm (**18**) and 3.55, -64.92 ppm (**19**) in the HSQC spectrum. These peaks had increased slightly in intensity by 21 d, and accounted for 2.6 % (**18**) and 1.5 % (**19**) of all Pt-NH_3 present (Appendix 3, Figure A3.10). These new peaks are in the region for Pt^{II}-$^{15}NH_3$ *trans* to N or Cl.[30] By comparison with literature chemical shifts,[28] it seems likely that these Pt^{II} products are [{*trans*-$Pt(SG)(NH_3)_2$}$_2$-μ-SG] (**18**) and *trans*-$[Pt(NH_3)_2(GS)_2]$ (**19**). There are small peaks in the ^1H spectrum which could correspond to platinum bound glutathione. Also visible in the ^1H spectrum are peaks

for oxidised glutathione (GSSG), however after 21 d only 15 % had been converted to the oxidised form. The spectra of oxidised (GSSG) and reduced (GSH) glutathione are shown in Appendix 3, Figure A3.11. Oxidation may be caused by either air and/or complex **3**, the majority of **3** was still in the Pt^{IV} state after 21 d, so autooxidation of glutathione by air might have occurred.

These results demonstrate the remarkable stability of complex **3**, less than 5 % had been reduced after 21 d in the presence of 6.6 mM glutathione.

5.3.1.6 Stability at 310 K

A 3 mM sample of complex **3** was prepared, and the pH adjusted from 6.2 to 4.9. The 1D ^{1}H and 2D [^{1}H,^{15}N] HSQC NMR spectra were recorded, and then the sample was incubated at 310 K. Spectra were rerecorded after 24 h, 9 d and 21 d. The spectrum after 21 d only contained peaks for complex **3** (Appendix 3, Figure A3.12).

5.3.2 Photoreactions

To observe the ^{1}H am(m)ine peaks of Pt^{IV} diazido dihydroxy complexes it was necessary to adjust the pH to 5 as explained in section 5.3.1. However, when these complexes were irradiated with UVA light, even for a very short amount of time (e.g. 1 min), the pH was found to increase. Therefore to follow the course of the Pt^{IV} species during the photoreactions, the pH was readjusted to 5 after each irradiation, but before acquiring the NMR spectra.

The change in pH with increasing irradiation time can be seen in Figure 5.1 for complexes **1**, **3** and **4**. The pH of solutions of the *cis* compound (**1**) increased much more than either of the *trans* compounds (**3** and **4**) upon irradiation. Adjustment of the pH to 5 throughout the photoreactions was carried out for the majority of experiments described in this chapter, however occasionally the pH was only changed to 5 at the start (i.e. before irradiation).

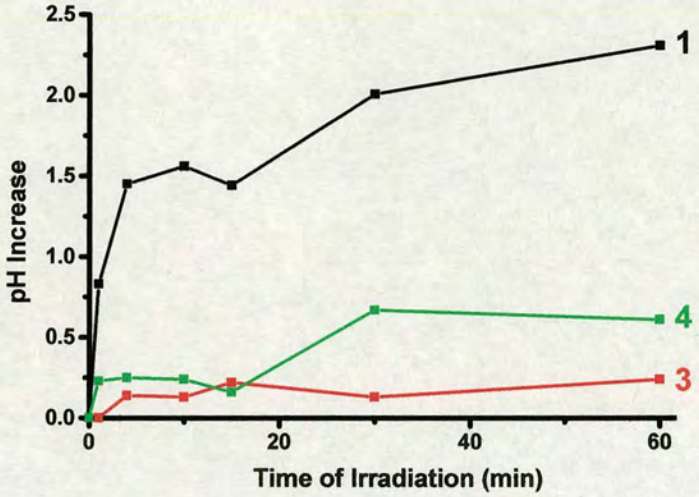

Figure 5.1 The increase in pH (from 5 ± 0.2) after each irradiation for *cis, trans, cis*-$[Pt(N_3)_2(OH)_2(^{15}NH_3)_2]$ (**1**), *trans, trans, trans*-$[Pt(N_3)_2(OH)_2(^{15}NH_3)_2]$ (**3**) and *trans, trans, trans*-$[Pt(N_3)_2(OH)_2(^{15}NH_3)(py)]$ (**4**).

5.3.2.1 NMR Spectroscopy

a) *Cis, trans, cis*-$[Pt(N_3)_2(OH)_2(^{15}NH_3)_2]$ (**1**)

A 3 mM sample of *cis, trans, cis*-$[Pt(N_3)_2(OH)_2(^{15}NH_3)_2]$ was prepared, and the pH adjusted to 5. The sample was irradiated in an NMR tube with the UV lamp, and the 1D ^1H and 2D [^1H,^{15}N] HSQC spectra recorded after 0, 1, 3, 6, 11, 16, 26, 36, 46, 66, 96, 126 and 246 min. During irradiation the pH increased, after 246 min it was 8.9 and, therefore no Pt^{IV}-$^{15}NH_3$ [^1H,^{15}N] peaks were visible (Figure 5.2a). Upon readjusting the pH to 5 with $HClO_4$, several new peaks appeared (Figure 5.2b). Overall there was a large loss in signal intensity by the end of irradiation, which is most likely due to the formation of an insoluble precipitate.

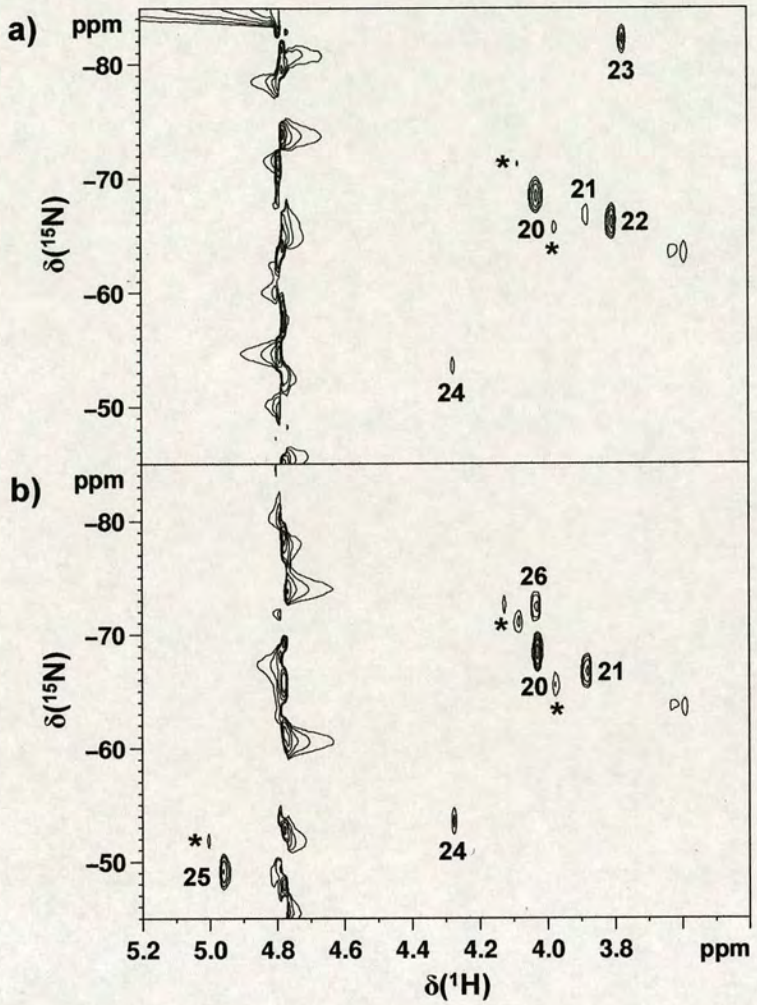

Figure 5.2 2D [^{1}H,^{15}N] HSQC NMR spectra of *cis, trans, cis*-[$Pt(N_3)_2(OH)_2(^{15}NH_3)_2$] (3 mM) after irradiation with UVA light for 246 min at a) pH 8.9, and b) pH 5.0. * ^{195}Pt satellites.

Peak **25** is the only peak visible in the region for Pt^{IV} compounds, in the spectrum recorded after 246 min irradiation with the pH adjusted to 5 (Figure 5.2b). As the pH had previously been high (~ 9) for this sample, peak **25** could be due to a stable Pt^{IV} hydroxy-bridged dimer, which was not cleaved into monomers upon lowering the pH. Hydroxy-bridged dimers have been observed for Pt^{II} compounds at pH values lower than 5.[29]

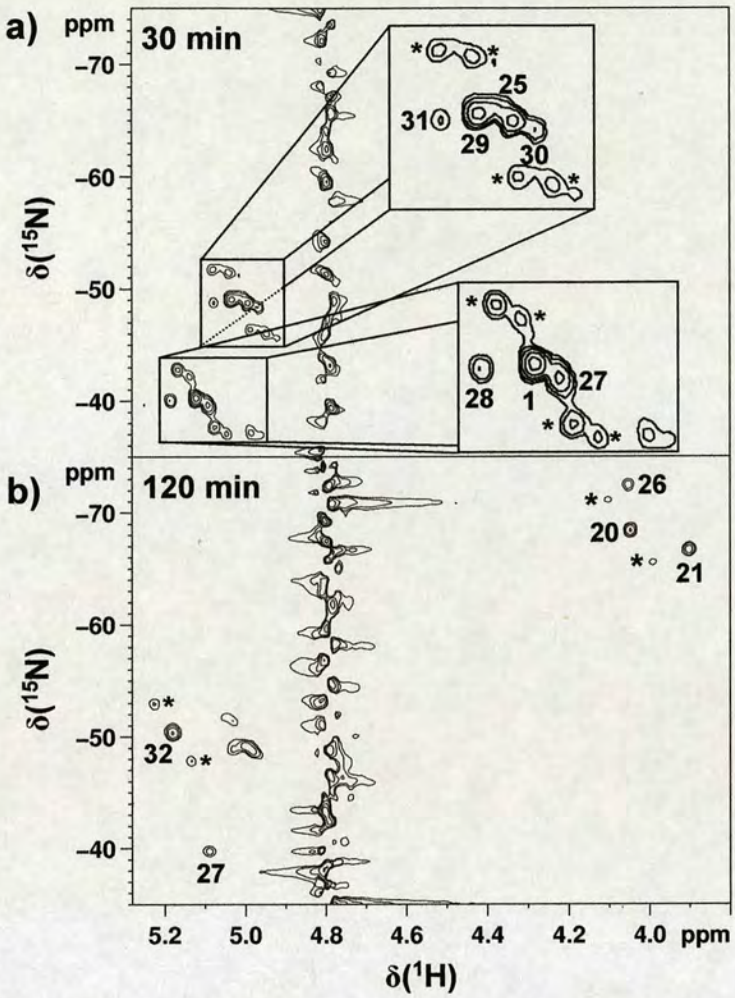

Figure 5.3 2D [^{1}H,^{15}N] HSQC NMR spectra of *cis, trans, cis*-[Pt$(N_3)_2(OH)_2(^{15}NH_3)_2$] (3 mM) after irradiation with UVA light for a) 30 min and b) 120 min. * ^{195}Pt satellites.

Peak **23** is most likely assignable to *cis*-[Pt$(^{15}NH_3)_2(OH)_2$]; it is in the region for Pt^{II}-$^{15}NH_3$ *trans* to O and as the pH is high, the water ligands will be deprotonated (*cis*-$[Pt^{II}(NH_3)_2(OH)(OH_2)]^+$ pK_a 7.21),[54] this assignment is consistent with the fact that peak **23** disappears when the pH was lowered to 5; the chemical shifts also agree well with published values.[52,54] Peaks **20** and **21** became more intense when the pH was lowered, but did not change position. Peak **22** disappeared completely and peak **26** appeared. These peaks could be due to bridged dimers or even trimers which would explain the pH effects.

The reaction was repeated, with the pH readjusted to 5 after each irradiation. Spectra were acquired after 0, 1, 5, 15, 30, 60 and 120 min of irradiation. Three main Pt^{II} peaks (**20**, **21**, **26**) were seen after 120 min, several Pt^{IV} peaks were also still present (Figure 5.3).

Table 5.1 ^{1}H and ^{15}N NMR chemical shifts (ppm), coupling constants (Hz) and assignments to Pt^{II} and Pt^{IV} compounds.

Peaks[a]	$\delta(^{1}H)$	$\delta(^{15}N)$	^{1}J ^{195}Pt-^{15}N	^{2}J ^{195}Pt-^{1}H	Assignments
1	5.12	-40.27	260	46	*c,t,c*-$[Pt(N_3)_2(OH)_2(^{15}NH_3)_2]$
20	4.04	-68.48	281	55	Pt^{II} photoproduct
21	3.90	-66.86	286	55	Pt^{II} photoproduct
22	3.82	-66.23	-	-	Pt^{II} photoproduct
23	3.79	-82.26	-	-	*c*-$[Pt(^{15}NH_3)_2(OH)_2]$
24	4.27	-54.80	-	-	Pt^{II} photoproduct
25	4.95	-49.25	276	50	Pt^{IV} photoproduct
26	4.03	-72.47	-	-	Pt^{II} photoproduct
27	5.09	-40.04	259	45	*c*-$[Pt(^{15}NH_3)_2(N_3)(OH)_2(OH/OH_2)]$ $^{15}NH_3$ *trans* to N_3
28	5.19	-40.22	261	50	Pt^{IV} photoproduct
29	5.03	-49.11	274	45	*c*-$[Pt(^{15}NH_3)_2(N_3)(OH)_2(OH/OH_2)]$ $^{15}NH_3$ *trans* to O
30	4.97	-48.39	-	-	Pt^{IV} photoproduct
31	5.08	-48.78	269	45	Pt^{IV} photoproduct
32	5.19	-50.38	269	45	*c*-$[Pt^{IV}(^{15}NH_3)_2(OH/OH_2)_4]$

a) See Figure 5.2 and Figure 5.3 for peak labels.

Peaks **27** and **29** are tentatively assigned as the mono-azide species with an oxygen donor (OH or OH_2) replacing the other azide ligand. Both **27** and **29** appear at the same time and increase at roughly the same rate; it was not possible to measure accurate integrals due to overlapping peaks. They also both begin to disappear between 30 and 60 min of irradiation, and are very small after 120 min; this is

consistent with the second azide subsequently being lost. These two peaks were not visible in the first reaction when the pH was lowered (Figure 5.2b), but this sample had undergone irradiation for 246 min (nearly twice as long), and so it is unlikely that any azide would still be bound to platinum. The most intense peak for Pt^{IV}-$^{15}NH_3$ species after 120 min irradiation is peak **32** which is in the region for Pt^{IV}-$^{15}NH_3$ *trans* to O,[30] and has been assigned as Pt^{IV} with 2 ammonia and 4 oxygen-donor ligands (either OH or OH_2). The synthesis of *cis*-[Pt($^{15}NH_3$)$_2$(OH/OH_2)$_4$] was carried out by oxidising *cis*-[Pt($^{15}NH_3$)$_2$(OH_2)$_2$] with H_2O_2; the pH was adjusted to 5 and the 1D [^{1}H] and 2D [^{1}H,^{15}N] HSQC NMR spectra recorded. The chemical shifts of the main product (5.20, -49.71) and the coupling constants (^2J (^{195}Pt-^{1}H) 47.4 Hz, ^1J (^{195}Pt-^{15}N) 276 Hz) agree well with those of **32** (Table 5.1). None of the Pt^{II} peaks seen upon irradiation of **1** were due to *cis*-[Pt($^{15}NH_3$)$_2$(OH_2)$_2$] which has chemical shifts of δ(^{1}H,^{15}N), 4.44, -87.03 ppm at pH 5.

b) *Cis, trans*-[Pt(^{15}N-en)(N_3)$_2$(OH)$_2$] (**2**)

A 3 mM sample of *cis, trans*-[Pt(^{15}N-en)(N_3)$_2$(OH)$_2$] (**2**) was prepared and the pH adjusted to 5. The solution was irradiated in an NMR tube with the UV lamp, and 2D [^{1}H,^{15}N] HSQC spectra recorded after 0, 1, 3, 6, 11, 16, 26, 36, 46, 66, 96 and 126 min. Irradiation led to two new sets of peaks in the 2D [^{1}H,^{15}N] HSQC NMR spectra. The pattern of peaks in box **33** (Figure 5.4a) is characteristic of inequivalent $^{15}NH_2$ protons,[51] and is in the region for Pt^{IV}-$^{15}NH_2$ *trans* to O.[30] The main product is a Pt^{II} compound (**34**, 5.11, -33.43) which was first detected after 11 min. Overall there was a large loss in signal intensity, this is at least partly due to the formation of an insoluble yellow precipitate (as seen during irradiation of compound **1**), but could also be caused by the pH. The pH of this reaction was adjusted to 5 at the start, but by the end of the reaction it had risen to > 7. Above pH 7 the Pt^{IV} peaks are no longer visible due to fast exchange of the ^{15}NH protons. Compound **34** is not the diaqua species [Pt(^{15}N-en)(OH_2)$_2$] which has been reported at δ(^{15}N) -45.9 ppm,[31] however it could be the hydroxide complex, which given the higher pH would be more likely. Another possibility is an oxygen-bridged dimer, such complexes have previously been reported at high pH and studied by ^{195}Pt NMR spectroscopy.[32]

The photoreaction of complex **2** on its own appears to be a much more straightforward reaction than those of the other Pt^{IV}-azide complexes (**1** or **3**). Only two new compounds appear in the 2D [^{1}H,^{15}N] HSQC NMR spectra (**33** and **34**), however due to the rising pH, it is possible that other new Pt^{IV} peaks are not visible.

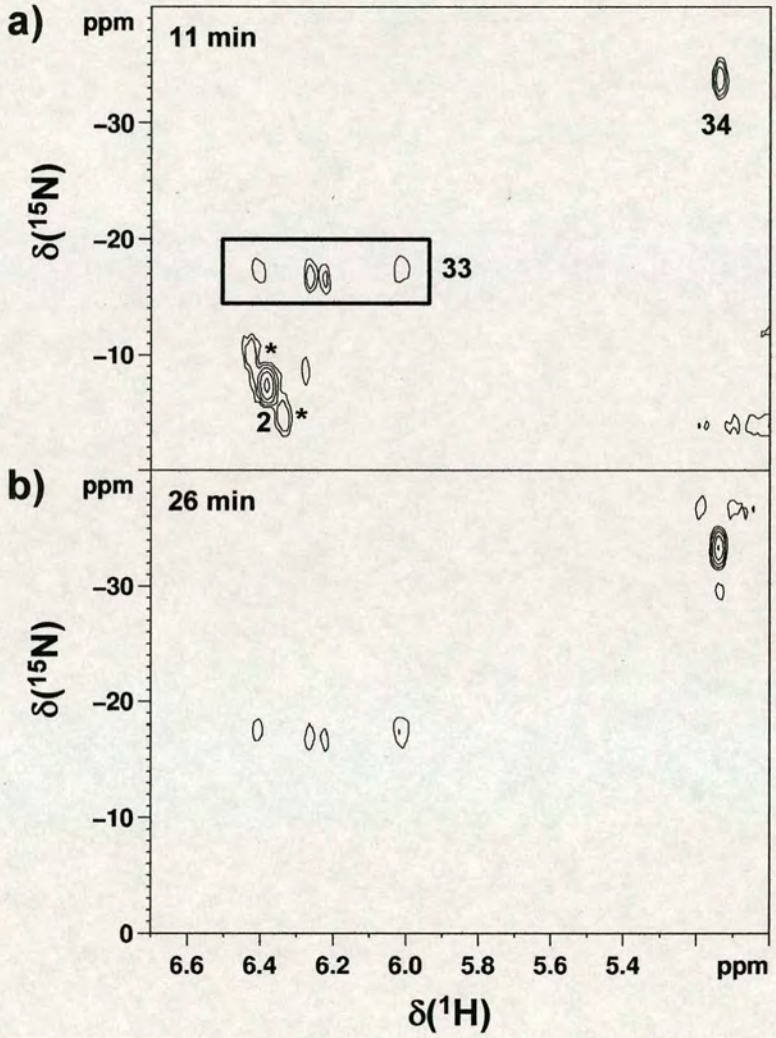

Figure 5.4 2D [^{1}H,^{15}N] HSQC NMR spectra of *cis, trans*-[Pt(^{15}N-en)$(N_3)_2(OH)_2$] (3 mM) after irradiation with UVA light for a) 11 and b) 26 min. The pH was adjusted to 5 before irradiation. * ^{195}Pt satellites.

c) *Trans, trans, trans*-$[Pt(N_3)_2(OH)_2(NH_3)_2]$ (**3**)

A 3 mM solution of *trans, trans, trans*-$[Pt(N_3)_2(OH)_2(^{15}NH_3)_2]$ was prepared and the pH adjusted to 5. The sample was irradiated with UVA light in an NMR tube and 1D ^{1}H and 2D [^{1}H,^{15}N] HSQC NMR spectra were acquired after 0, 1, 5, 15, 30, 60 and 120 min of irradiation with the pH was readjusted to 5 each time.

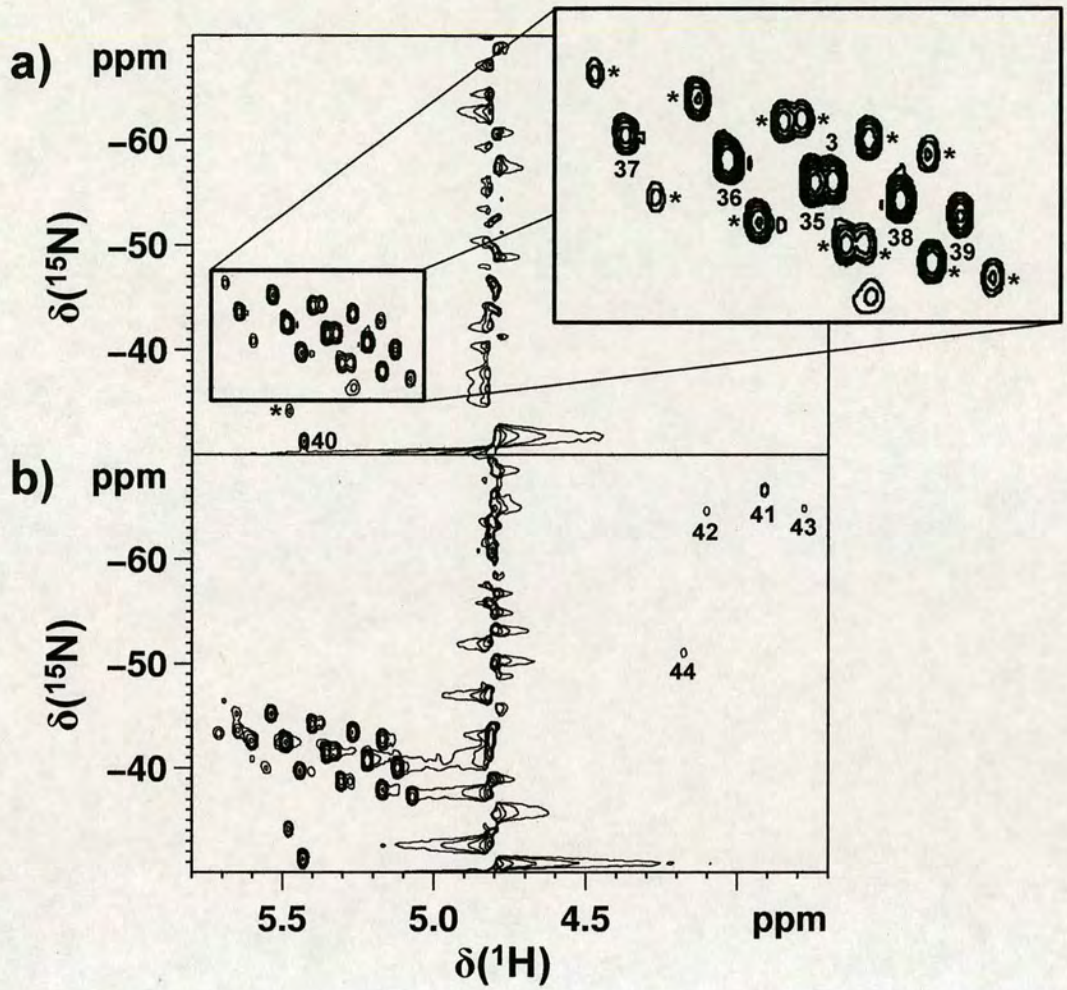

Figure 5.5 2D [^{1}H,^{15}N] HSQC NMR spectra of *trans, trans, trans*-[$Pt(N_3)_2(OH)_2(^{15}NH_3)_2$] (**3**) after irradiation with UVA light for a) 30 min and b) 120 min. * ^{195}Pt satellites.

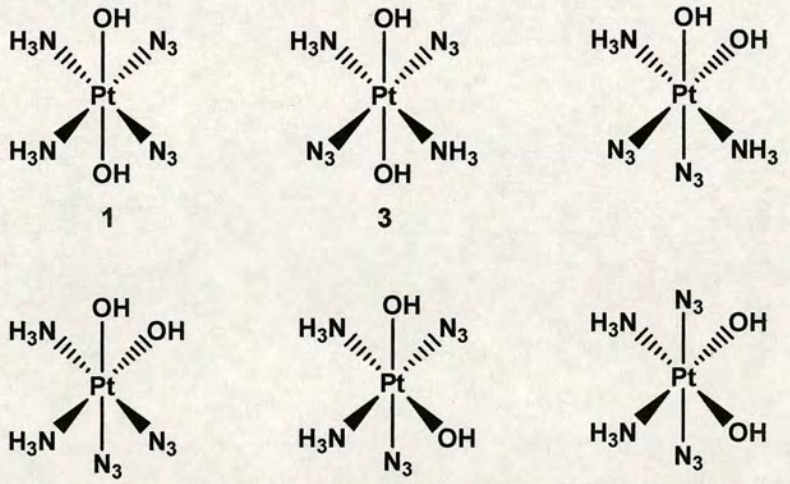

Figure 5.6 Structures of the six geometric isomers of [$Pt(N_3)_2(OH)_2(NH_3)_2$].

Table 5.2 ^{1}H and ^{15}N NMR chemical shifts (ppm), coupling constants (Hz) and assignments to Pt^{II} and Pt^{IV} diammine compounds.

Peaks[a]	$\delta(^{1}H)$	$\delta(^{15}N)$	^{1}J ^{15}N-^{1}H	^{2}J ^{195}Pt-^{1}H	Assignments
1	5.12	-40.27	259.8	46.0	*c,t,c*-$[Pt(N_3)_2(OH)_2(^{15}NH_3)_2]$
3	5.32	-41.65	282	47.5	*t,t,t*-$[Pt(N_3)_2(OH)_2(^{15}NH_3)_2]$
35	5.34	-41.56	278	50	Pt^{IV} photoproduct
36	5.48	-42.56	278	45	Pt^{IV} photoproduct
37	5.63	-43.68	280	45	Pt^{IV} photoproduct
38	5.21	-40.78	280	50	*trans*-$[Pt(N_3)(OH)_3(^{15}NH_3)_2]$
39	5.12	-40.07	279	50	*trans*-$[Pt(OH)_4)(^{15}NH_3)_2]$
40	5.42	-31.35	291	50	Pt^{IV} photoproduct
41	3.91	-66.56	-	-	Pt^{II} photoproduct
42	4.10	-64.61	-	-	Pt^{II} photoproduct
43	3.78	-64.86	-	-	Pt^{II} photoproduct
44	4.17	-51.13	-	-	Pt^{II} photoproduct
45	3.94	-64.02	-	-	*trans*-$[Pt(^{15}NH_3)_2(OH_2)_2]^{2+}$
46	3.82	-65.64	-	-	*trans*-$[Pt(^{15}NH_3)_2Cl(OH_2)]^{+}$
47	5.14	-40.05	285	49	*trans*-$[Pt(^{15}NH_3)_2(OH)_4]$
48	5.25	-40.20	276	50	*trans*-$[Pt(^{15}NH_3)_2(OH)_3Cl]$

a) See Figure 5.5 and Figure 5.8 for peak labels.

After 30 min irradiation of complex **3** six new Pt^{IV} peaks were present (**35-40**), initially these peaks were believed to be due to isomers. Photoisomerisation of Pt^{IV} compounds has previously been reported and utilised in synthesis.[33,34] There are six possible geometric isomers of *trans, trans, trans*-$[Pt(N_3)_2(OH)_2(^{15}NH_3)_2]$ (Figure 5.6). Peak **39** has very similar chemical shifts to those of complex **1** (*cis, trans, cis*-$[Pt(N_3)_2(OH)_2(NH_3)_2]$), but the coupling constants do not compare well.(Table 5.2)

Mass spectra of an irradiated solution of **3** contained peaks at 320.1, 345.2 and 370.3 m/z (Figure 5.7). Table 5.3 lists compounds which these peaks could correspond to.

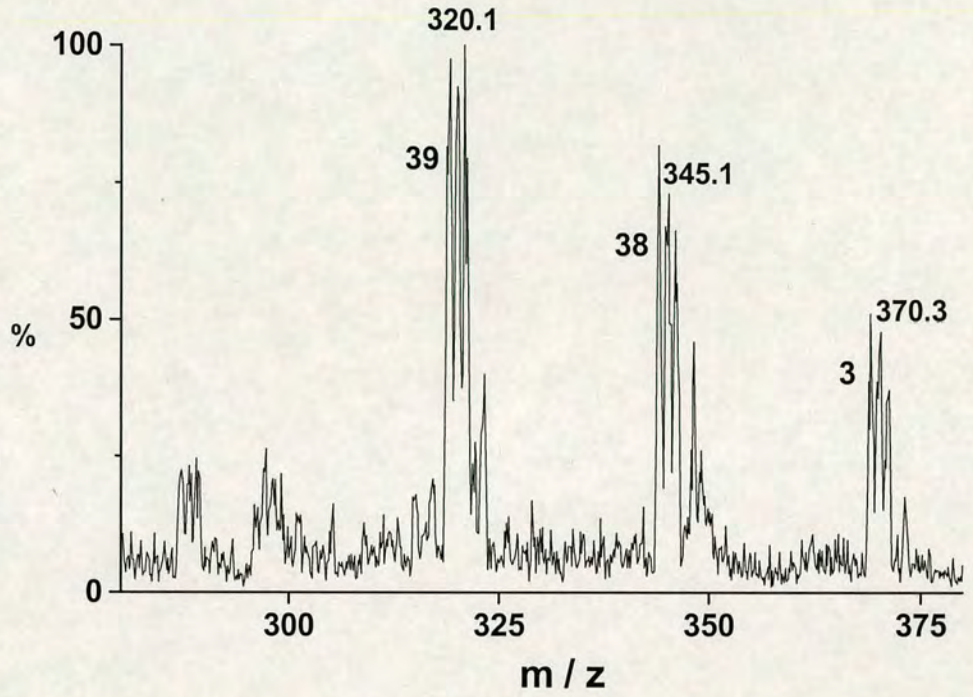

Figure 5.7 Positive ion electrospray ionisation mass spectrum of a solution of complex **3** which had been irradiated for 60 min with UVA light.

Table 5.3 Table of calculated and detected m/z values for an irradiated solution of complex **3**.

Species	Calculated m/z	Detected m/z
trans, trans, trans-$[Pt(N_3)_2(OH)_2(NH_3)_2]$ (**3**) + Na^+	370.2	370.3
trans-$[Pt(N_3)(OH)_3(NH_3)_2]$ (**38**) + Na^+	345.1	345.2
trans-$[Pt(OH)_4(NH_3)_2]$ (**39**) + Na^+	320.1	320.1

To determine whether *trans*-$[Pt(NH_3)_2(OH)_4]$ was indeed a photoproduct, it was synthesised from ^{15}N-labelled transplatin and then analysed by 2D [^1H,^{15}N] HSQC NMR spectroscopy and ESI-MS. The chlorides were removed from transplatin with silver nitrate to yield the diaqua adduct *trans*-$[Pt(NH_3)_2(OH_2)_2]^{2+}$. The pH was adjusted to 5 with NaOH (0.1 M) and the NMR spectrum acquired (Figure 5.8a), the two peaks were assigned from literature values[51] as *trans*-$[Pt(^{15}NH_3)_2(OH_2)_2]^{2+}$ (**45**; 3.94, -64.02) and *trans*-$[Pt(^{15}NH_3)_2(OH_2)Cl]^+$ (**46**; 3.82, -65.64). Oxidation was

carried out with H_2O_2, the pH was readjusted to 5, and then the solution was analysed by NMR spectroscopy and ESI-MS. Two new Pt^{IV} species were visible in the NMR spectrum **47** (5.14, -40.05) and **48** (5.25, -40.20) (Figure 5.8b). These peaks were calculated to be of the same ratio to each other as **45** and **46** (Table 5.2). In the mass spectrum the major peaks were due to *trans*-$[Pt(^{15}NH_3)_2(OH)_4] + H^+$ (m/z 300.0) and its sodium adduct *trans*-$[Pt(^{15}NH_3)_2(OH)_4] + Na^+$ (m/z 322.0). Peaks for the monochloro compound *trans*-$[Pt(^{15}NH_3)_2(OH)_3Cl]$ were also present at m/z 318 (Figure 5.9). Therefore, compounds **47** and **48** can be assigned as *trans*-$[Pt(^{15}NH_3)_2(OH)_4]$ and *trans*-$[Pt(^{15}NH_3)_2(OH)_3Cl]$, respectively.

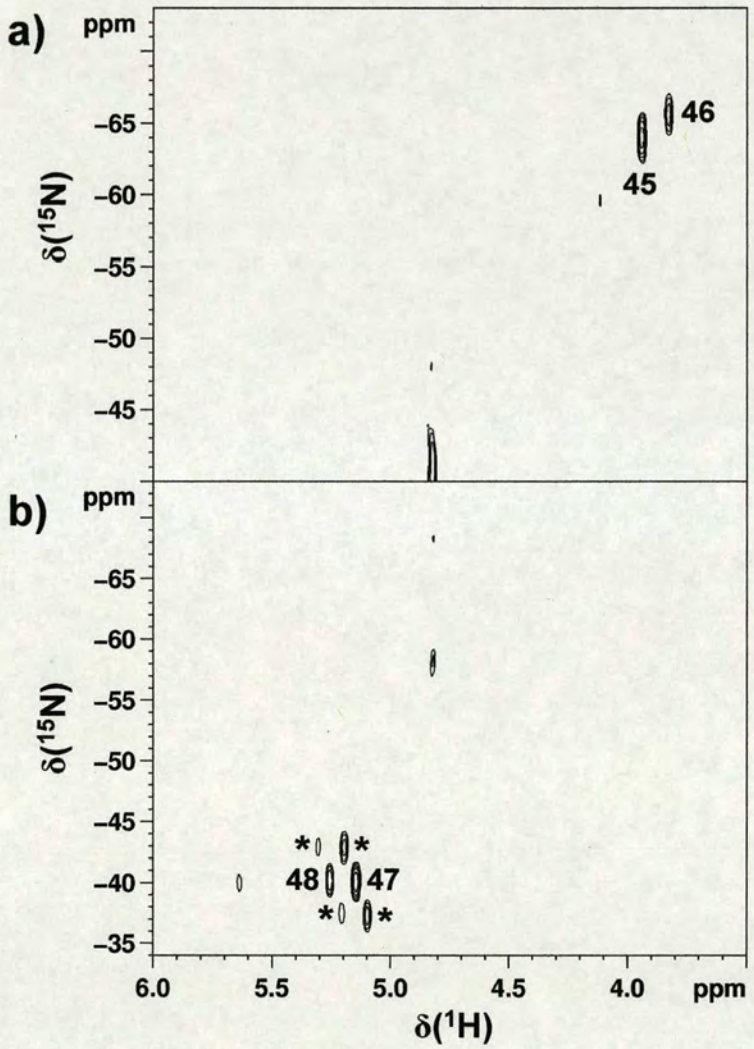

Figure 5.8 2D [^1H,^{15}N] HSQC NMR spectra of a) *trans*-$[Pt^{II}(^{15}NH_3)_2(OH_2)_2]^{2+}$ (**45**) and *trans*-$[Pt^{II}(^{15}NH_3)_2Cl(OH_2)]^+$ (**46**) and b) *trans*-$[Pt^{IV}(^{15}NH_3)_2(OH)_4]$ (**47**) and *trans*-$[Pt^{IV}(^{15}NH_3)_2Cl(OH)_3]$ (**48**) at pH 5. * ^{195}Pt.

The chemical shifts and coupling constants of peaks **39** and **47** are almost identical (Table 5.2) and so photoproduct **39** can be assigned as the tetrahydroxy compound *trans*-[Pt($^{15}NH_3$)$_2$(OH)$_4$]. These results also help assign peak **38**. The chemical shifts of the diazide, dihydroxy (**3**) and the tetrahydroxy (**47**) compounds are known, and it seems likely that the monoazide, trihydroxy complex *trans*-[Pt(N_3)(OH)$_3$($^{15}NH_3$)$_2$] would appear somewhere between these two peaks, therefore compound **38** must be *trans*-[Pt(N_3)(OH)$_3$($^{15}NH_3$)$_2$]. This complex is also clearly visible in the mass spectrum of the irradiated solution of complex **3** (Figure 5.7). The position of peaks **3**, **38** and **39** relative to each other is the same as that produced by oxidised transplatin (*t,t,t*-[PtCl$_2$(OH)$_2$($^{15}NH_3$)$_2$], 5.48, -41.14 ppm), **47** and **48**. This result was expected due to the similar electronic properties of chloride and azide ligands.

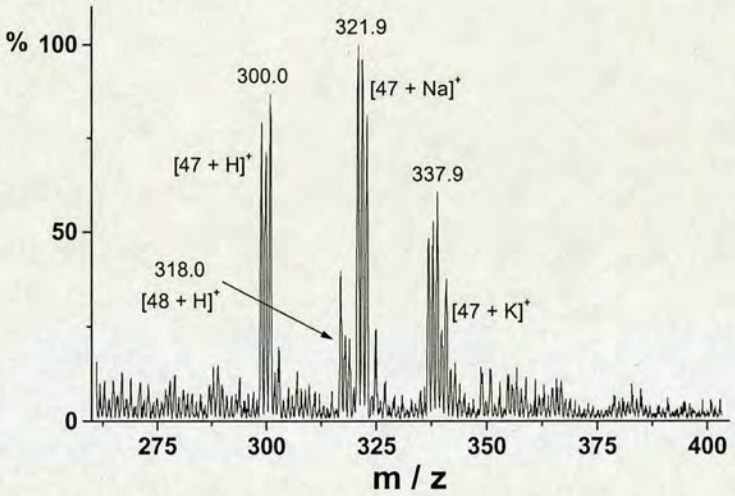

Figure 5.9 Positive ion electrospray ionisation mass spectrum of *trans*-[Pt^{IV}($^{15}NH_3$)$_2$(OH)$_4$] (**47**) and *trans*-[Pt^{IV}($^{15}NH_3$)$_2$(OH)$_3$Cl] (**48**).

The ^{195}Pt NMR spectra of **1** and **3** contained peaks at +902 and +875 ppm, respectively (Figure 5.10 a and b). After irradiation of **3** for 1 h with UVA light, three new peaks were seen (+862, +1331 and +428 ppm) in the range analysed (+2130 to -310 ppm) (Figure 5.10 c, d and e). The largest of these new peaks (+1331 ppm) could be either compound **38** or **39** by comparison with the chemical shifts of similar compounds (Table 5.4). There was no pH control during this experiment, so to ensure the products were the same as those produced at pH 5 (Figure 5.5) a natural abundance 2D [^{1}H,^{15}N] HSQC NMR spectrum was acquired. Peaks **3** and **35** to **40** were all clearly visible.

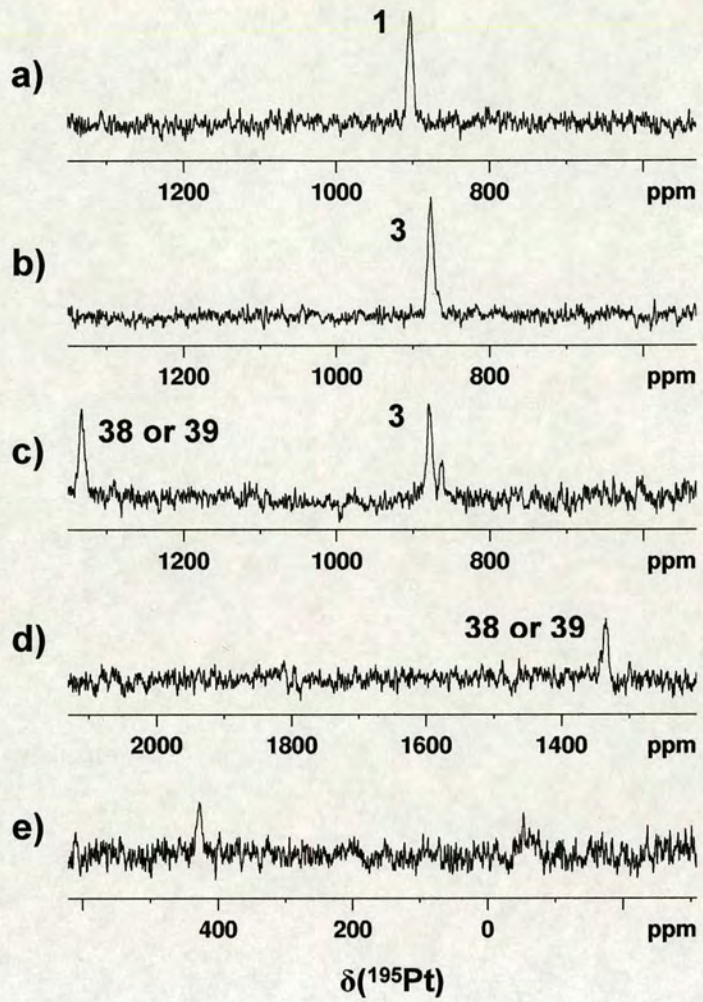

Figure 5.10 ^{195}Pt NMR spectra of a) *cis, trans, cis*-$[Pt(N_3)_2(OH)_2(NH_3)_2]$ (**1**), b) *trans, trans, trans*-$[Pt(N_3)_2(OH)_2(NH_3)_2]$ (**3**), and c), d) and e) different regions for complex **3** after 1 h irradiation.

Table 5.4 ^{195}Pt chemical shifts of Pt^{IV}-hydroxy complexes

Pt^{IV} Complexes	**δ(^{195}Pt) ppm**	**Reference**
c,t,c-$[PtCl_2(OH)_2(NH_3)_2]$	+860	35
t-$[Pt(OH)_4(NH_3)_2]$	+1735	36
c,t,c-$[PtCl_2(OH)_2(propylamine)_2]$	+881	35
t-$[Pt(OH)_4(propylamine)_2]$	+1521	35
t,t,t-$[Pt(N_3)_2(OH)_2(NH_3)_2]$ (**3**)	+875	This work
t-$[Pt(N_3)(OH)_3(NH_3)_2]$ (**38**) or *t*-$[Pt(OH)_4(NH_3)_2]$ (**39**)	+1331	This work

Very little reduction to Pt^{II} is seen upon irradiation of **3**. After 120 min there are four weak Pt^{II} peaks (**41**-**44**) present (Figure 5.5, Table 5.2). These peaks do not increase significantly upon further irradiation (up to 240 min), indicating that the Pt^{IV} photoproducts must be relatively stable. All the new Pt^{II} peaks are in the region for $H_3{}^{15}N$-Pt^{II} *trans* to N or Cl, and since there is no chloride present in the solution all the compounds must contain ammonia *trans* to another nitrogen (probably $^{15}NH_3$). Peak **42** has similar chemical shifts to *trans*-$[Pt(^{15}NH_3)_2(OH_2)_2]$ (**45**), and the chemical shifts of peak **41** are the same as those of a Pt^{II} product (**21**), visible after irradiation of *cis, trans, cis*-$[Pt(N_3)_2(OH)_2(^{15}NH_3)_2]$ (**1**) (Figure 5.3).

There was only a very small amount of precipitation during this photoreaction in comparison to the amount generated upon irradiation of complexes **1** and **2**. Perhaps this can be explained by the position of the ammonia ligands, the *trans* geometry may obstruct oxygen bridging and therefore could hinder the formation of insoluble multinuclear species.

d) *Trans, trans, trans*-$[Pt(N_3)_2(OH)_2(NH_3)(py)]$ (**4**)

A 3 mM solution of *trans, trans, trans*-$[Pt(N_3)_2(OH)_2(^{15}NH_3)(py)]$ (**4**) was prepared and the pH adjusted to 5. The sample was irradiated with UVA light in an NMR tube and 1D [^{1}H] and 2D [^{1}H,^{15}N] HSQC NMR spectra were acquired after 0, 1, 5, 15, 30, 60 and 120 min of irradiation with the pH readjusted to 5 each time.

Interestingly, the same pattern of Pt^{IV} peaks was seen in the 2D [^{1}H,^{15}N] HSQC spectrum after 15 min irradiation of complex **4** (Figure 5.11a), as that produced upon irradiation of complex **3** (Figure 5.5). Unlike complex **3** the Pt^{IV} peaks began to disappear after 60 min irradiation, and by 120 min only three relatively weak Pt^{IV} peaks remained, however the Pt^{II} peaks did not increase in intensity. A Pt^{II} peak first appeared after 15 min irradiation. After 60 min, there were two Pt^{II} peaks with chemical shifts of $\delta(^1H,^{15}N)$ 3.97, -66.80 ppm (**55**) and 4.34, -64.35 ppm (**56**) both in the region of $H_3{}^{15}N$-Pt *trans* to N (Table 5.5).[30] Some precipitation occurred but less compared to that produced upon irradiation of complex **1**.

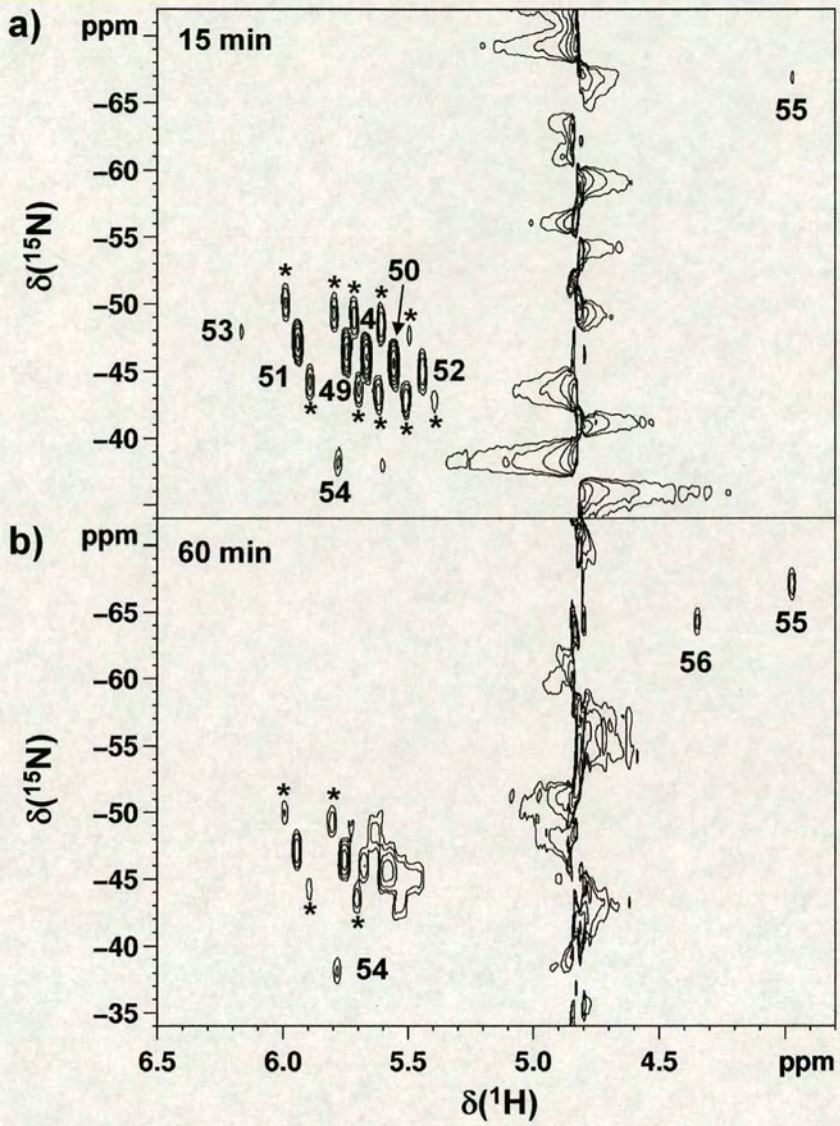

Figure 5.11 2D [^{1}H,^{15}N] HSQC NMR spectra of *trans, trans, trans*-[$Pt(N_3)_2(OH)_2(^{15}NH_3)(py)$] (**4**) after a) 15 min and b) 60 min irradiation. * ^{195}Pt satellites.

Table 5.5 ^{1}H and ^{15}N NMR chemical shifts (ppm), coupling constants (Hz) and assignments of Pt^{IV} and Pt^{II} pyridine complexes.

Peaks[a]	$\delta(^{1}H)$	$\delta(^{15}N)$	^{2}J ^{195}Pt-^{1}H	^{1}J ^{15}N-^{1}H	Assignments
4	5.65	-46.00	282.3	49.5	*t,t,t*-$[Pt^{IV}(N_3)_2(OH)_2(^{15}NH_3)(py)]$
49	5.74	-45.44	283	49	
50	5.56	-45.62	298	50	*t*-$[Pt^{IV}(^{15}NH_3)(py)(OH)_3(N_3)]$
51	5.94	-47.10	290	48	
52	5.45	-45.03	269	51	*t*-$[Pt^{IV}(^{15}NH_3)(py)(OH)_4]$
53	6.16	-47.95	-	-	
54	5.78	-38.29	-	-	
55	3.97	-66.80	-	-	
56	4.34	-64.35	-	-	
57	4.13	-66.90	-	-	*t*-$[Pt^{II}(^{15}NH_3)(py)(OH_2)(OH)]$
58	4.00	-68.55	-	-	*t*-$[Pt^{II}(^{15}NH_3)(py)Cl(OH_2)]$
59	5.45	-45.08	288	50	*t*-$[Pt^{IV}(^{15}NH_3)(py)(OH)_4]$
60	5.60	-45.47	278	50	*t*-$[Pt^{IV}(^{15}NH_3)(py)(OH)_3Cl]$

a) See Figure 5.11 and Figure 5.12 for peak labels.

By comparison with the photoproducts of complex **3** it was thought that peak **52** was most likely due to *trans*-$[Pt(^{15}NH_3)(py)(OH)_4]$, to confirm this the tetrahydroxy complex was synthesised. The first step in the synthesis of *trans*-$[Pt(^{15}NH_3)(py)(OH)_4]$ involved removing the chlorides from *trans*-$[Pt(^{15}NH_3)(py)Cl_2]$ with silver nitrate. The pH was adjusted to 5 with NaOH (0.1 M) and the NMR spectra acquired (Figure 5.12a). The NMR sample was analysed by mass spectrometry and the peaks assigned as *trans*-$[Pt^{II}(^{15}NH_3)(py)(OH)(OH_2)]^+$ (**57**; 4.13, -66.90; 327.1 m/z) and *trans*-$[Pt(^{15}NH_3)(py)Cl(OH_2)]^+$ (**58**; 4.00, -68.55; 345.0 m/z). Oxidation was carried out by addition of 4 mol eq H_2O_2 (30 % solution), the pH was adjusted to 5 and the solution analysed by NMR spectroscopy (Figure 5.12b) and mass spectrometry. Two new peaks were visible in the NMR spectrum **59** (5.45, -45.08) and **60** (5.60, -45.47). These peaks were of the same ratio to each other as **57** and **58** (Table 5.5). In the mass spectrum of this NMR sample, the major peaks were

due to *trans*-[Pt($^{15}NH_3$)(py)$(OH)_4$] + H^+ (361.1 m/z) and its sodium adduct (383.1 m/z), a small peak for the monochloro compound *trans*-[Pt($^{15}NH_3$)(py)Cl$(OH)_3$] + H^+ (379.5 m/z) was also present. Compounds corresponding to peaks **59** and **60** can therefore be assigned as *trans*-[Pt($^{15}NH_3$)(py)$(OH)_4$] and *trans*-[Pt($^{15}NH_3$)(py)$(OH)_3$Cl], respectively. The chemical shifts and coupling constants of peaks **52** and **59** are almost identical (Table 5.5) and photoproduct **52** can therefore be assigned as the tetrahydroxy compound *trans*-[Pt($^{15}NH_3$)(py)$(OH)_4$]. By applying the same reasoning as for complex **3** peak **50** must be the monoazide compound *trans*-[Pt($^{15}NH_3$)(py)$(OH)_3(N_3)$] (see section 5.3.2.1d).

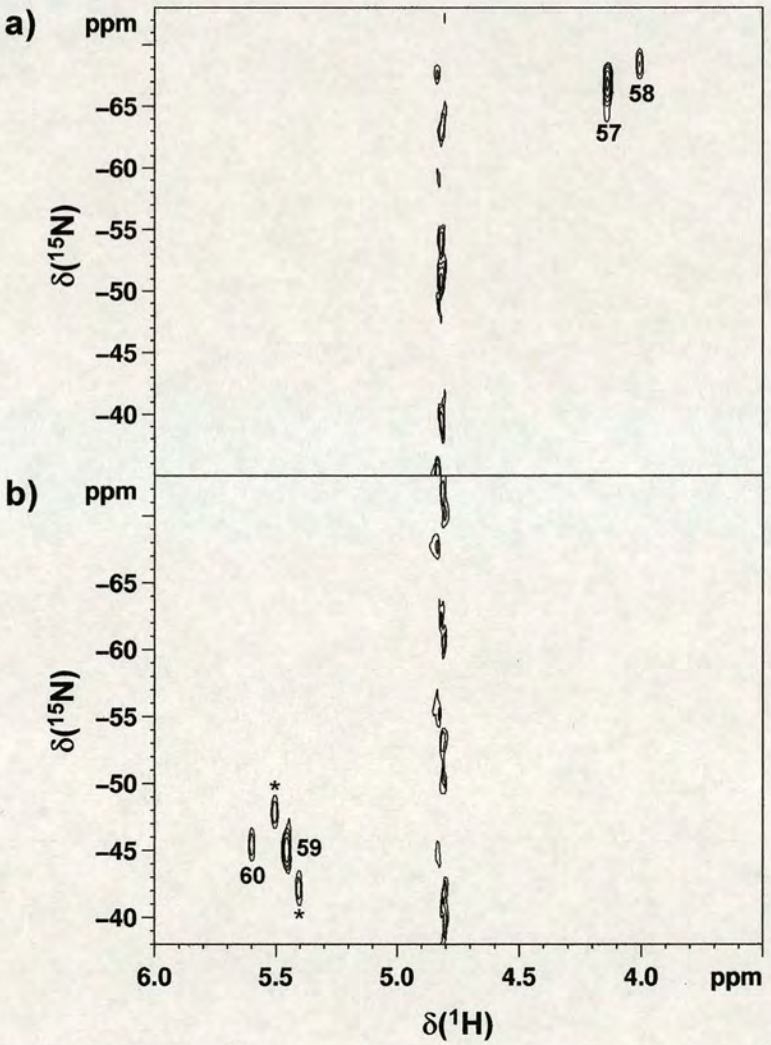

Figure 5.12 2D [^1H,^{15}N] HSQC NMR spectra of a) *trans*-[Pt^{II}(py)($^{15}NH_3$)(OH)(OH_2)]$^+$ (**57**) and *trans*-[Pt^{II}(py)($^{15}NH_3$)Cl(OH_2)]$^+$ (**58**) and b) *trans*-[Pt^{IV}(py)($^{15}NH_3$)$(OH)_4$] (**59**) and *trans*-[Pt^{IV}(py)($^{15}NH_3$)$(N_3)(OH)_3$] (**60**), all at pH 5. * ^{195}Pt satellites.

During irradiation of **4** new peaks emerge in the ^{1}H NMR spectra at ~8 and ~7.55 ppm. These are probably due to the Pt^{II} species which are observed in the 2D [^{1}H,^{15}N] NMR spectra. No new peaks are visible at ~8.55 ppm indicating that pyridine is not released from the platinum centre (Table 5.6). Another photoreaction was carried out without pH adjustment, and so after 120 min irradiation the pH was > 8. This reaction was followed by 1D [^{1}H] and 2D [^{1}H,^{1}H] COSY NMR spectroscopy in an attempt to separate out the pyridine proton signals. In the 1D ^{1}H spectra the peaks were much more well-defined than at pH 5. Two new pyridine ring systems could be seen in the COSY spectrum after 120 min irradiation, but they were not shifted far enough to high-field to be due to free pyridine. These results help to confirm that pyridine is not being released from the platinum centre upon irradiation.

Table 5.6 ^{1}H NMR chemical shifts of free pyridine and Pt-pyridine complexes.

Compound	pH	δ(^{1}H) / ppm		
		H_o	H_p	H_m
Pyridine	5	8.55	7.98	7.54
Pyridine	8.8	8.49	7.83	7.42
4	5	8.72	8.25	7.78
57	5	8.67	8.02	7.56
59	5	8.67	8.22	7.74

A solution of pyridine in 90 % H_2O / 10 % D_2O was prepared. The 1D [^{1}H] and 2D [^{1}H,^{1}H] COSY NMR spectra were recorded before and after 2 h irradiation with the UV lamp. This was too ensure UVA light was not modifying the pyridine ligand in complex **4**. No changes were observed after 2 h irradiation.

5.3.2.2 UV-Visible Spectroscopy

The photoreactions of Pt^{IV} azide complexes can also be followed by UV-visible spectroscopy. Aqueous solutions containing 50 μM to 80 μM Pt were used for these experiments as the extinction coefficients are all between 13,000 and 20,000 $M^{-1}cm^{-1}$ (Chapter 3, Section 3.2.2). Irradiations were carried out with the UV lamp on 3 mL samples in UV quartz cuvettes. Compounds **1** - **12** have intense N_3 → Pt ligand-to-metal charge-transfer (LMCT) bands between 250 – 300 nm.[10,12] Upon irradiation

this band decreases indicating loss of the azide ligands.[37]

There were clear differences in the behaviour of the *cis* and *trans* compounds upon UVA irradiation. After 1 min irradiation the absorbance between 250 – 300 nm for *cis, trans*-$[Pt(en)(N_3)_2(OH)_2]$ (**2**) and *cis, trans, cis*-$[Pt(N_3)_2Cl_2(NH_3)_2]$ (**12**) increased, and for *cis, trans, cis*-$[Pt(N_3)_2(OH)_2(NH_3)_2]$ (**1**) there was no change (Figure 5.14 and Figure 5.15). Continued irradiation resulted in a decrease of the LMCT band. The evolution of a gas, presumed to be nitrogen formed from the azide ligands, was clearly visible during these photoreactions (Figure 5.13).

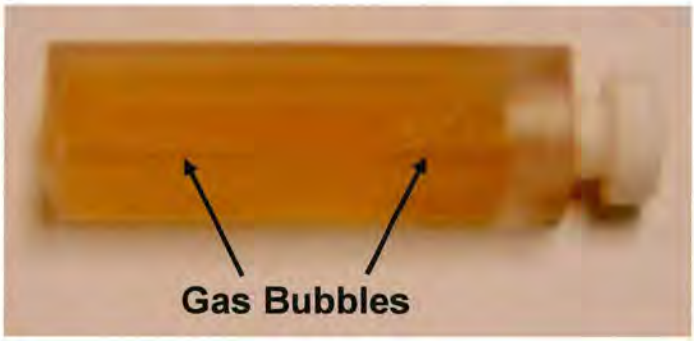

Figure 5.13 *Cis, trans*-$[Pt(en)(N_3)_2(OH)_2]$ (**2**) after 60 min UV irradiation. Gas bubbles are clearly visible.

When *trans, trans, trans*-$[Pt(N_3)_2(OH)_2(^{15}NH_3)_2]$ (**3**) was irradiated a new absorbance was seen after 5 min (Figure 5.14). This new peak was shifted to a higher energy (253 nm) than the LMCT of complex **3**, and is believed to be due to the monoazide species *trans, trans, trans*-$[Pt(N_3)(OH)_3(^{15}NH_3)_2]$ (**38**). This assignment is based on the decrease of the new peak upon further irradiation – suggesting that further decomposition is occurring. There was also evidence for complex **38** found by NMR spectroscopy (Section 5.3.2.1c). The spectrum of *trans*-$[Pt(NH_3)_2(OH)_4]$ was also recorded but it does not contain any bands between 225 and 300 nm.

The appearance and subsequent decrease (upon further irradiation) of a new band at higher energy was also seen for the other complexes with *trans* geometry (Figure 5.14 and Figure 5.15). For the pyridine (**4**) and picoline (**8** - **10**) complexes the new monoazide peak may be masked by intraligand absorbances of the aromatic systems.

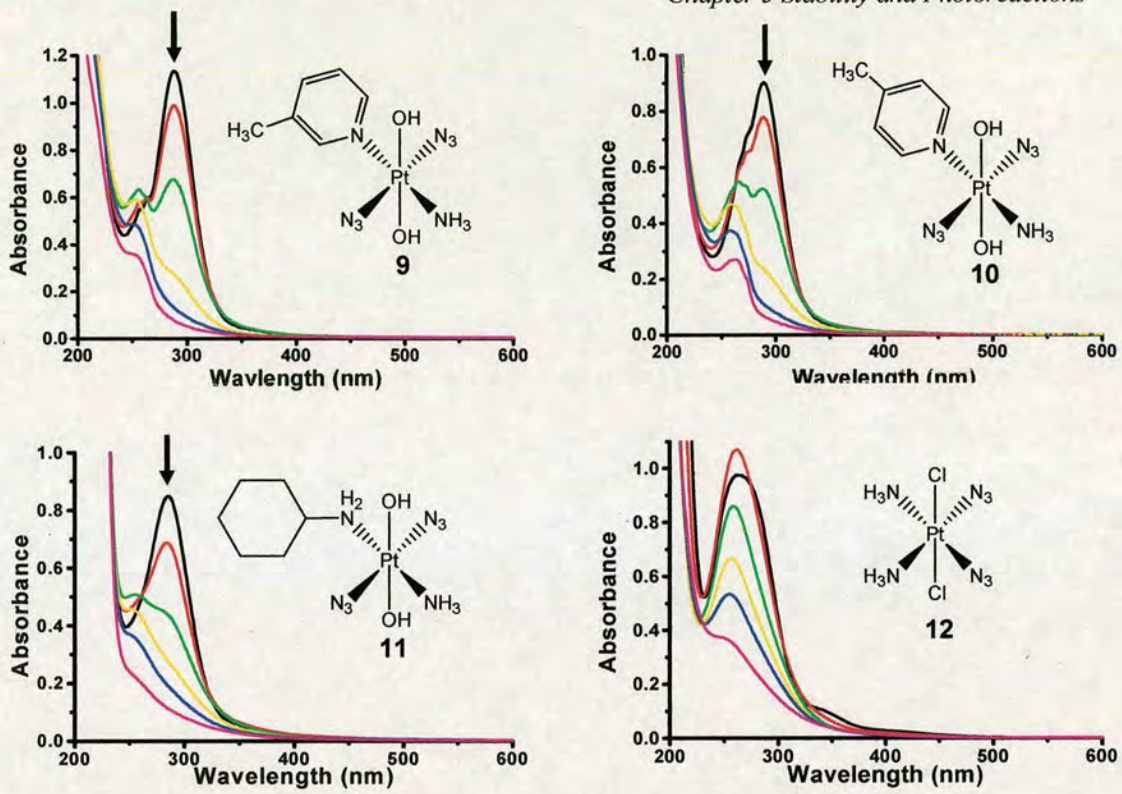

Figure 5.15 UV-visible spectra of Pt^{IV} azide complexes **9** - **12** after UVA irradiation for 0 (—), 1 (—), 5 (—), 15 (—), 30 (—) and 60 (—) min.

The electronic absorption spectrum of *trans, cis*-[Pt(bpy)$(OAc)_2(N_3)_2$] (**14**) was complicated by the presence of the bipyridine ring. The assignment of the bands in the spectrum has been discussed previously (Chapter 3, Section 3.3.18). Briefly the peaks at 304 and 317 nm are due to π-π* transitions of the bipyridine ring, and the absorbance at 250 nm is believed to be at least partly due to N_3 → Pt LMCT.[38,39] Upon UVA irradiation, the main band (250 nm) decreased up to 15 min, but after 30 min irradiation it began to increase (Figure 5.16). The absorbance now consisted of a peak (248 nm) and a shoulder (ca. 267 nm). The intraligand peaks (304 and 317 nm) also decreased in intensity up to 15 min and then increased after 30 min irradiation, although the effect was less pronounced. An interesting feature was the emergence of a peak at 370 nm with increasing irradiation time. By comparison with Pt^{II} bipyridine complexes in the literature, it seems likely that this band is due to metal-to-ligand charge-transfer (MLCT),[39,40] which suggests that reduction has occurred and Pt^{II} species are now present. MLCT would be less likely to occur for Pt^{IV} due to the lack of electron density on the metal.

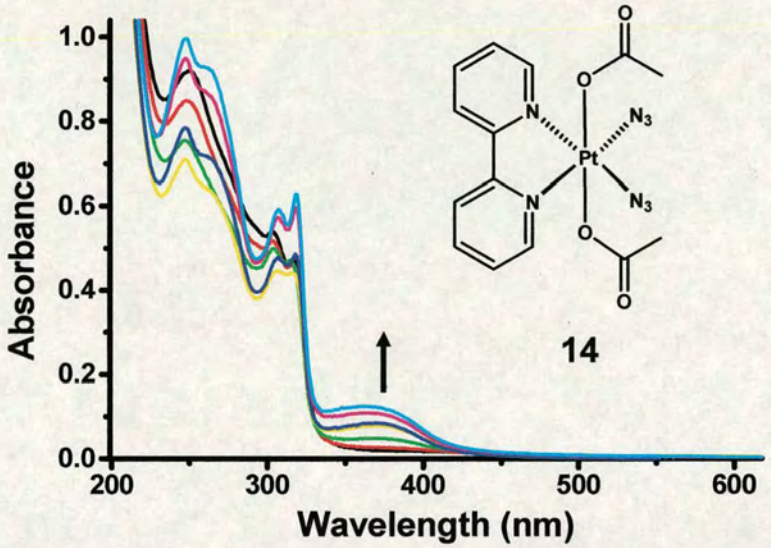

Figure 5.16 UV-visible spectra of *trans, cis*-[Pt(bpy)(OAc)$_2$(N$_3$)$_2$] (**14**) after UV irradiation for 0 (—), 1 (—), 5 (—), 15 (—), 30 (—), 60 (—) and 120 (—) min. The arrow denotes the increase of the absorption at 370 nm with increasing irradiation time.

The spectrum of complex **14** after 120 min of irradiation, and the published spectra of [Pt(bpy)(OH)$_2$] and [{Pt(bpy)(μ-OH)}$_2$] are similar (Figure 5.17).[41] The irradiated solution was analysed by ESI-MS and the two main peaks corresponded to [Pt(bpy)(OH)$_2$] (M + H$^+$ 386.2 m/z) and [{Pt(bpy)(μ-OH)}$_2$] (M^{2+} 368.2 m/z) (Figure 5.18).

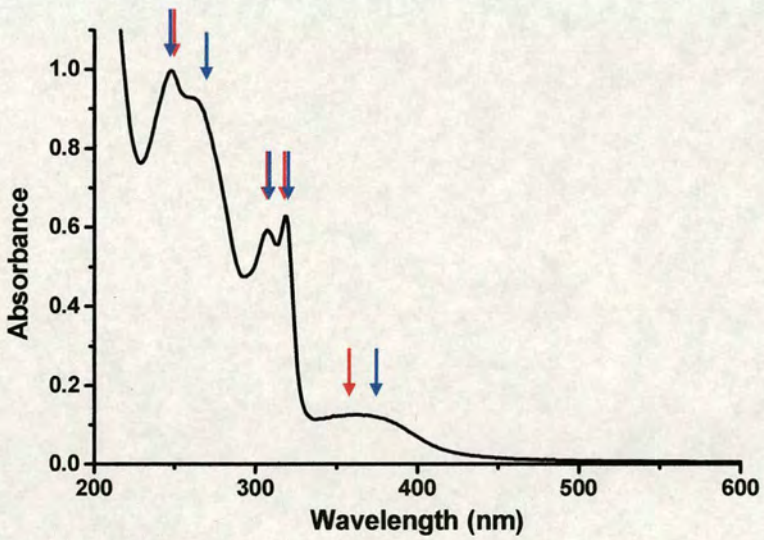

Figure 5.17 UV-visible spectrum of *trans, cis*-[Pt(bpy)(OAc)$_2$(N$_3$)$_2$] after 120 min UVA irradiation. Blue arrows indicate the peak positions of [Pt(bpy)(OH)$_2$], and the red arrows indicate the peak positions of [{Pt(bpy)(μ-OH)}$_2$].[41]

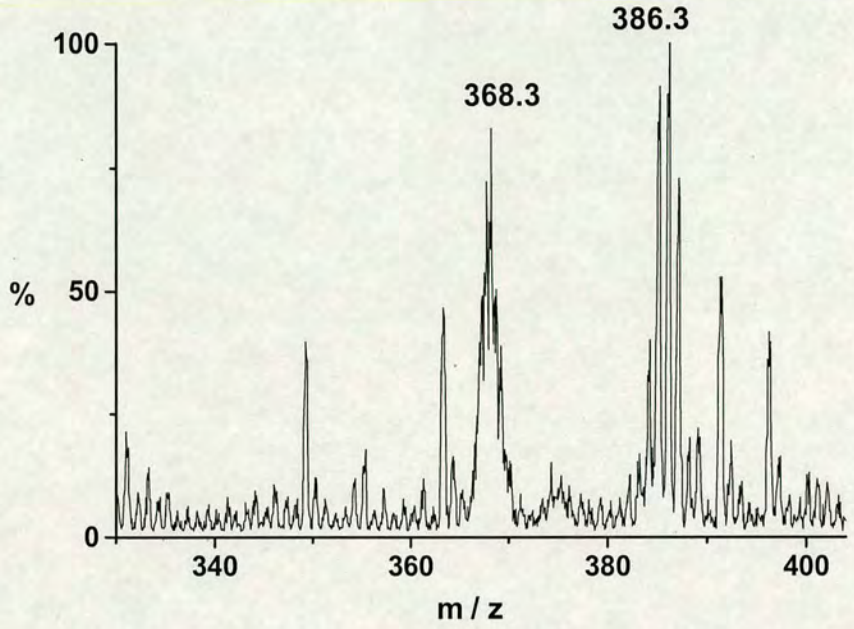

Figure 5.18 Positive ion electrospray mass spectrum of *trans, cis*-$[Pt(bpy)(OAc)_2(N_3)_2]$ after 120 min UV irradiation.

5.4 Discussion

5.4.1 Stability Studies

The stability of potential photochemotherapeutic drugs under physiological conditions is an important factor to consider. It is essential that a prodrug remains in an inactive state until selectively activated, to ensure it exerts its effects site-specifically, and can therefore reduce side-effects. The stability of the azide ligands is of particular importance, as their decomposition would mean loss of photoactivity.

Glutathione (GSH) is the most abundant reducing agent found in cells with concentrations up to 10 mM;[42] therefore it is preferable that photoactive Pt^{IV} compounds are not readily reduced by it. Also of concern is whether the diazido complexes are stable in solution towards potential targets such as the guanine bases of DNA in the dark.

5.4.1.1 Aqueous Stability

Previous studies have shown that *cis, trans, cis*-$[Pt(N_3)_2(OH)_2(^{15}NH_3)_2]$ (**1**) is stable in aqueous solution for over 90 d at 298 K.[5] *Trans, trans, trans*-$[Pt(N_3)_2(OH)_2(^{15}NH_3)_2]$ (**3**) was also found to be stable over 154 d at 294 K, the 1D ^1H and 2D [^1H,^{15}N] NMR spectra did not change over this time period.

The stability of complexes **4**, **5** and **8** in water was studied by 1D [^1H] NMR spectroscopy. After 154 d, there were no new peaks in any of the spectra. There was also no significant decrease in intensity of any of the signals.

These results demonstrate the remarkable stability of four platinum(IV) azide complexes (**3**, **4**, **5** and **8**) in water over long time periods (> 5 months).

5.4.1.2 Stability towards Chloride

The chloride concentration outside cells in blood plasma is ca. 104 mM;[43] it is therefore important to determine whether chloride is capable of replacing the azide ligands, as such a substitution would mean loss of the photoactivity.

The stability of complexes **1** and **3** towards chloride in the dark was investigated by incubation of each platinum compound (3 mM) with NaCl (100 mM) at 294 K for 154 and 140 d, respectively. As both samples were ^{15}N-labelled, adjustment of the pH to 5 (before addition of the NaCl) was necessary to observe the ammine protons. No new peaks were seen in either spectra after 140 and 154 d, however there was a decrease in intensity of the $^{15}NH_3$ peaks with increasing time. There was also an increase in pH and by the end of the experiment the pH had risen to 6.19 for complex **1** and 6.93 for complex **3**. This suggests chloride is replacing the ammonia ligands which would account for both the loss of intensity and increase in pH. However, this substitution takes place relatively slowly as no significant decrease in intensity can be seen after 12 d for complex **1** and 6 d for complex **3** (Appendix 3, Figures A3.5 and A3.6). It is not possible to measure the rate of substitution by comparing the integrals because of the proximity of the $^{15}NH_3$ peaks to the water signal. Water suppression also results in some suppression of neighbouring peaks.

A previous more in-depth study of the stability of complex **1** towards chloride has been carried out,[5] the results were somewhat ambiguous, but it was concluded that chloride was not replacing the azide ligands. The results shown here for complexes **1** and **3** support this conclusion, but chlorides do appear to be capable of replacing ammonia ligands. However, the reaction was carried out at the maximum concentration of chloride found in the body (ca. 100 mM); and the rate of substitution was very slow, so it is not expected that chloride substuituion would cause problems in a physiological environment.

5.4.1.3 Stability towards Nucleotides

DNA is generally accepted to be the main target of cisplatin.[44] Once inside the cell cisplatin hydrolyses to the monoaqua or diaqua species, which form lethal cross-links on DNA. The N7 position of two adjacent guanine bases is the preferred binding site of cisplatin.[45] The stability of *trans, trans, trans*-$[Pt(N_3)_2(OH)_2(^{15}NH_3)_2]$ (**3**) towards 5′-GMP in the dark was investigated. Complex **3** was found to be totally unreactive in the presence of the mononucleotide; these results compliment previous studies which have found *cis, trans, cis*-$[Pt(N_3)_2(OH)_2(^{15}NH_3)_2]$ (**1**) and *cis, trans*-$[Pt(^{15}N\text{-}en)(N_3)_2(OH)_2]$ (**2**) to be inert to 5′-GMP in the dark.[5] The stability of Pt^{IV} azide complexes to 5′-GMP is an important result, as it has been shown that 5′-GMP can reduce and activate Pt^{IV} compounds such as $[Pt^{IV}(dach)Cl_4]$ (dach is diaminocyclohexane).[46]

5.4.1.4 Stability in Cell Culture Media

Earle's balanced salt solution (EBSS) (Table 5.7) was the cell culture media used during phototoxicity testing. EBSS is buffered at between pH 7.2 – 7.6 so it is not possible to reduce the pH to 5 to observe the Pt^{IV}-^{15}NH signals. Therefore the stability of complexes **4** and **5** was investigated as they both contain CH protons and the reaction could be followed by ^1H NMR spectroscopy. Despite the presence of many salts both complexes were found to be totally stable. This is encouraging as it means the compounds are likely to remain intact on cell culture plates.

Table 5.7 Formulation of Earle's balanced salt solution used for phototoxicity testing and stability experiments.

Components	**g / L**	**mM**
$CaCl_2.2H_2O$	0.265	1.8
$MgSO_4$ (anhydrous)	0.09767	0.8
KCl	0.4	5.4
$NaHCO_3$	2.2	26.2
NaCl	6.8	116.2
NaH_2PO_4 (anhydrous)	0.122	1.0
D-glucose	1.0	5.6

5.4.1.5 Stability towards Glutathione

Glutathione (GSH, γ-L-Glu-L-Cys-Gly) is the most abundant reducing agent found in cells, and can be present at concentrations up to 10 mM.[42,47] Reduction of Pt^{IV} compounds by GSH and other biomolecules is believed to be necessary for anticancer activity.[48] However it is essential that a photoactive platinum(IV) prodrug is not readily reduced by cellular thiols, and remains intact until selectively activated by light.

Complex **1** has previously been shown to be inert towards GSH,[5] no Pt^{II}-$^{15}NH_3$ peaks were seen in the 2D [^{1}H,^{15}N] HSQC NMR spectrum after 38 d. Complex **3** was also found to be relatively stable, only two small Pt^{II} peaks are present after 21 d, the only other peak is due to complex **3**.

5.4.1.6 Stability at 310 K

Azides decompose at high temperatures, and during synthesis care is taken to ensure that the platinum azide complexes are never subjected to temperatures above 313 K (Chapter 3). The stability at 310 K was investigated as this is the physiological temperature and also the temperature the cells are kept at during phototoxicity experiments. Complex **3** was found to be stable at 310 K over a period of 21 d which means the azides are not lost or disintegrating at the temperatures used during cell tests.

Overall, the platinum(IV) azide compounds have proved to be very stable under the various conditions tested. This is encouraging as previous work carried out by Kratochwil *et al.*, on photoactive Pt^{IV}-diiodo complexes was abandoned due to instability towards reducing agents.[3] Halides are good leaving groups and are therefore prone to attack, whereas azide ligands are more strongly bound.

5.4.2 Photoreactions

5.4.2.1 NMR Spectroscopy

a) *Cis, trans, cis*-$[Pt(N_3)_2(OH)_2(^{15}NH_3)_2]$ (**1**)

The irradiation of *cis, trans, cis*-$[Pt(N_3)_2(OH)_2(^{15}NH_3)_2]$ (**1**) was carried out with and without pH adjustment. During irradiation of Pt^{IV} diazido complexes the pH rises, Pt^{IV}-^{15}NH peaks can usually only be observed at pH values below 7; this is due to fast exchange of the am(m)ine protons as discussed earlier (Section 5.3.2). Therefore to observe the Pt^{IV} photoproducts the pH was adjusted to 5 after each irradiation.

Interestingly when the pH was only changed to 5 at 0 h and then after 246 min irradiation, the main Pt^{II} products were the same as those produced after 120 min irradiation with the pH adjusted to 5 at each time point (0, 1, 5, 15, 30, 60 and 120 min) (Figure 5.2b and Figure 5.3b). The Pt^{IV} photoproducts were different, but they were all in the region for $H_3{}^{15}N$-Pt *trans* to oxygen-donor ligands, which are believed to be either hydroxide or water. The formation of Pt^{IV} bridged dimers should also be considered.[49,50] Pt^{II} oxygen-bridged dimers have been observed at pH values as low as 2.5.[29]

During irradiation of an aqueous solution of complex **1** the overall signal intensity decreased significantly; this is due to the formation of a dark orange insoluble precipitate. This solid is insoluble in all common solvents and has not been further characterised. It is thought to be a multinuclear platinum species, formed from the interaction of highly reactive photoproducts.

The assignment of peaks **27** and **29** as the monoazide complex *cis, trans, cis*-$[Pt(N_3)(OH)_3(^{15}NH_3)_2]$, suggests that the azide ligands do not leave the platinum

centre in a concerted manner. Results from the photoreactions of complexes **3** and **4** also support the theory that the two azides within a molecule leave separately.

The photoreaction of complex **1** had previously been carried out with blue light (488 nm, 10 mW).[5] After 20 h irradiation, no Pt^{II} peaks were present but 6 new Pt^{IV} peaks were visible. Five of these peaks are the same as those produced upon UV irradiation (**25**, **27-30**) (Table 5.1). This suggests that the absorbance was so low at 488 nm that the reaction was much slower, but occured by the same pathway as seen upon UVA irradiation.

There was no evidence to suggest the sample continued reacting after irradiation was stopped (i.e during pH adjustment and NMR acquisition). The 2D [^{1}H,^{15}N] NMR peaks were generally well-defined, peaks which are "streaky" are characteristic of an ongoing reaction. Several samples were also left in the dark at 294 K overnight after irradiation for various lengths of time. The spectra and pH of each of these samples had not changed when re-measured after ca. 12 h.

b) *Cis, trans*-[Pt(^{15}N-en)$(N_3)_2(OH)_2$] (**2**)

Compound **32** (δ ^{1}H,^{15}N; 5.11, -33.43 ppm) was the main photoproduct from irradiation of *cis, trans*-[Pt(en)$(N_3)_2(OH)_2$]. It is a Pt^{II} complex but is not the diaqua species [Pt(^{15}N-en)$(OH_2)_2$], which has an ^{15}N shift of ~ -45 ppm.[31] Complex **32** may be the dihydroxide complex [Pt(^{15}N-en)$(OH)_2$] or the oxygen bridged dimer [Pt_2(^{15}N-en)$_2(\mu\text{-}OH)_2]^{2+}$ which has been reported to form at pH values as low as 5.[32] By comparison with the ^{15}N NMR chemical shifts of *cis*-diammonia hydroxy/aqua compounds it can be seen that upon deprotonation, the signal is shifted to low field by between 5 – 15 ppm (Table 5.8), discrepancies between the values are due to different pH values, however the general trend remains the same. If the *trans* hydroxide is bridging the ^{15}N shift remains remarkably similar to the aqua species, therefore this indicates that compound **32** is most likely due to [Pt(^{15}N-en)$(OH)_2$].

Table 5.8 ^{15}N NMR chemical shifts of *cis*-Pt^{II}-diammonia hydroxy/aqua compounds. Peaks are all referenced to $^{15}NH_4Cl$.

***Cis*-Pt^{II}-Diammonia Complexes**	**$\delta(^{15}N)$ / ppm**
cis-$[Pt(^{15}NH_3)_2(OH_2)_2]^{2+}$	-87.2[a]; -91.4[b]; -92.53[c]
cis-$[Pt(^{15}NH_3)_2(OH)_2]^{2+}$	-83.6[b]; -79.9[d];
$[\{cis\text{-}Pt(^{15}NH_3)_2(OH_2)\}_2(\mu\text{-}OH)]^{3+}$	-89.8 (*trans* to OH_2)[c] -88.53 (*trans* to μ-OH)[c]
$[\{cis\text{-}Pt(^{15}NH_3)_2(OH)\}_2(\mu\text{-}OH)]^{3+}$	-80.68 (*trans* to OH)[c] -88.85 (*trans* to μ-OH)[c]
$[Pt(^{15}NH_3)_2(OH)]_2^{2+}$	-88.3[b]

a) Reference 51, b) reference 52, c) reference 53, d) reference 54.

The peaks in box **33** of Figure 5.4 are in the region for Pt^{IV}-$^{15}NH_2$ *trans* to O.[30] This product could arise from isomerisation, but is more likely to be due to replacement of the azide ligands by water or hydroxide. The inequivalence of the ^{15}NH's could perhaps be explained by the presence of one aqua and one hydroxide ligand.

A similar reaction has previously been carried out with blue light (457.9 nm),[5] but the results were very different when compared to those produced upon UVA irradiation. Many new peaks were observed but none were close to peak **32**. Four new peaks with chemical shifts close to those of complex **2**, which is the region for Pt^{IV}-NH_2 *trans* to N were present; and two new peaks were seen in the Pt^{IV}-NH_2 *trans* to O region, however these did not match the signals for compound **33**. Three new peaks were also seen at ~ -45 ppm which were assigned to Pt^{II}-NH_2 *trans* to OH_2. This difference in the photoproducts produced between irradiation with blue or UVA light could be due to pH effects. The pH was adjusted to 5 before the start of both reactions but was not changed again. The reaction is much faster with UV light and consequently the pH rise will be more rapid. The species seen upon blue light irradiation could be intermediates, and perhaps they are only visible because the pH is still relatively low.

c) *Trans, trans, trans*-$[Pt(N_3)_2(OH)_2(^{15}NH_3)_2]$ (**3**)

The behaviour of *trans, trans, trans*-$[Pt(N_3)_2(OH)_2(^{15}NH_3)_2]$ (**3**) upon irradiation was

very different to that of the *cis* isomer (**1**). Very little precipitate was observed and after 120 min UVA irradiation the majority of platinum remained in the +4 oxidation state. The new Pt^{IV} peaks were originally thought to be isomers, but two of the Pt^{IV} photoproducts were identified as the monoazide species *trans*-$[Pt(N_3)(OH)_3(^{15}NH_3)_2]$ (**37**) and the tetrahydroxy compound *trans*-$[Pt(OH)_4(^{15}NH_3)_2]$ (**38**). The identification of the monoazide complex by 2D HSQC NMR spectroscopy and ESI-MS, confirms that the azides do not leave the platinum centre together.

The lack of Pt^{II} photoproducts means reduction is not occurring readily. The azides are therefore not leaving as azide radicals after each donating an electron to Pt^{IV} but more likely as free azide (N_3^-). The azide anion (N_3^-) is also photoactive and can form N_2 upon irradiation.[55] Perhaps some of the azide ligands break down while still attached to platinum, the formation of nitrene species upon irradiation of metal azide complexes has been previously reported.[19-25] Nitrenes are highly reactive and would go on to react further until stable, this could help explain the unidentified Pt^{IV} NMR peaks (**34-36, 39**). However, it seems unlikely that azide would react in two completely different ways during the same experiment. Another possibility is the formation of dimers; loss of the azides to form tri- and tetra-hydroxy species means that there are now several oxygen ligands free to bridge the platinum centres. Platinum(II) oxygen bridged dimers are well known,[29,56] and Pt^{IV} dimers have also been reported.[49,50] The formation of dimers is believed to be the most likely explanation for the extra NMR peaks.

Initially the reluctance of the *trans* isomer to reduce to Pt^{II} upon irradiation was unexpected. However, the behaviour of complex **3** in the presence of nucleobases was found to be totally different (Chapter 6).

d) *Trans, trans, trans*-$[Pt(N_3)_2(OH)_2(NH_3)(py)]$ (**4**)

The pattern of peaks observed in the 2D [^1H,^{15}N] HSQC NMR spectra after irradiation of *trans, trans, trans*-$[Pt(N_3)_2(OH)_2(^{15}NH_3)(py)]$ (**4**) for 15 min (Figure 5.11a) is remarkably similar to that produced upon irradiation of complex **3** (Figure 5.5a). This suggests that the photoproducts are the same, except with pyridine in

place of an $^{15}NH_3$ ligand. As there is only one ^{15}N-labelled ammonia in ^{15}N-**4** this result gives further evidence against the new Pt^{IV} peaks being due to photoisomerisation. Peaks **66** and **68** (Figure 5.11 and Table 5.5) were identified as the monoazide (*trans*-[$Pt(N_3)(OH)_3(^{15}NH_3)(py)$]) and tetrahydroxy (*trans*-[$Pt(OH)_4(^{15}NH_3)(py)$]) species, respectively. This was carried out in the same way as for complex **3**. The two small Pt^{II} peaks clearly visible after 60 min irradiation (Figure 5.11b) are in the region for $H_3{}^{15}N$-Pt^{II} *trans* to N.[30]

Unlike experiments with complex **3,** continued irradiation of solutions of complex **4** led to further changes in the Pt^{IV} peaks. After 120 min, peaks **65**, **66** and **68** were the only Pt^{IV} peaks present. An insoluble precipitate was produced which presumably accounts for the overall loss in signal intensity. There was much more precipitate than for complex **3**, but not as much as for complexes **1** and **2**.

By 1D [^{1}H] and 2D [^{1}H,^{1}H] COSY NMR spectroscopy, it has been confirmed that pyridine is not released from platinum upon irradiation. The stability studies also showed that pyridine does not leave the Pt^{IV} centre in water or cell culture media over long periods of time.

5.4.2.2 UV-Visible Spectroscopy

Compounds **1** – **12** and **14** were irradiated with UVA light, and the reactions followed by UV-visible spectroscopy. All the compounds were photoactive, and the overall trend was a decrease in the N_3 → Pt LMCT band. However, after only 1 min irradiation, the absorbance bands of the *cis* compounds (**1**, **2** and **12**) did not decrease. For complexes **2** and **12** the peak intensity increased slightly (Figure 5.14 and Figure 5.15), but continued irradiation for 5 min and beyond then led to the expected decrease of the LMCT band. It is not clear why the absorbance initially increased upon irradiation only for compounds with *cis* geometry, but NMR studies have shown the photoreactions of *cis* (**1**) and *trans* (**3**) complexes produce very different photoproducts (Sections 5.3.2.1 a and c).

Complex **12** contains chloride ligands which when bound to Pt^{IV} also give LMCT

bands in the UV-visible spectrum.[57] These bands appear in roughly the same region as those of azide due to the similar placement of the two ligands in the spectrochemical series $N_3^- \sim Cl^-$.[58] This helps explain the broad shape of the LMCT peak at 264 nm (Figure 5.15).

The complexes with *trans* geometry (**3** – **11**) generally showed a relatively large decrease in the LMCT band after only 1 min irradiation. For the *trans* complexes which do not contain pyridine or picoline rings (**3**, **5** – **7**, **11**) a new peak appeared at slightly higher energy (ca. 250 nm) after 5 min irradiation. This new peak is probably present for complexes **4** and **8** – **10** as well, but is masked by the aromatic ring absorbances. This new peak can be assigned to Pt^{IV} monoazide species, in which one of the azide ligands has been replaced with a hydroxide group (e.g. *trans, trans, trans*-$[Pt(N_3)(OH)_3(NH_3)_2]$). The Pt^{IV} monoazide compound is likely to be photoactive too, and indeed this new peak decreases upon further irradiation. *Trans, trans, trans*-$[Pt(N_3)(OH)_3(NH_3)_2]$ (**38**) has also been identified as a photoproduct of complex **3** by NMR spectroscopy as has *trans, trans, trans*-$[Pt(N_3)(OH)_3(NH_3)(py)]$ (**50**) from complex **4**.

The electronic absorption spectrum of *trans, cis*-$[Pt(bpy)(OAc)_2(N_3)_2]$ (**14**) during irradiation was complicated by absorbance bands from the bipyridine ring. The reaction could not be followed by the disappearance of the N_3 → Pt LMCT band. Instead, after an initial decrease of the peak assigned as the LMCT band (250 nm), another band with a similar λ_{max} began to increase. Presumably the decrease is due to loss of the azide ligands and consequently the N_3 → Pt LMCT band, but the photoproduct(s) formed must also absorb strongly in this region.

The photoproducts were identified as $[Pt(bpy)(OH)_2]$ and $[\{Pt(bpy)(\mu\text{-}OH)\}_2]$ with extinction coefficients at ca. 250 nm of 14,400 and 16,000, respectively.[41] The electronic spectrum of an irradiated solution of **14** (Figure 5.18) was remarkably similar to those of $[Pt(bpy)(OH)_2]$ and $[\{Pt(bpy)(\mu\text{-}OH)\}_2]$, and these compounds are also the main species seen by ESI-MS.

An interesting feature of the photoreaction of *trans, cis*-$[Pt(bpy)(OAc)_2(N_3)_2]$ was the appearance of a broad peak at 370 nm, which increased with increasing irradiation time (Figure 5.16). The photochemical oxidative addition of chloride to $[Pt^{II}(bpy)Cl_2]$ to produce $[Pt^{IV}(bpy)Cl_4]$ has been reported,[59] this reaction was also followed by UV-visible spectroscopy and a decrease of a broad absorbance at ca. 400 nm was observed. This band can be assigned as a metal-to-ligand charge-transfer (MLCT) from the HOMO, which is the metal based $d_{x^2-y^2}$ orbital, to the LUMO which is the π^* anti-bonding orbital on bipyridine.[39,40] This MLCT band would be expected to appear upon reduction of Pt^{IV} to Pt^{II} as observed upon irradiation of *trans, cis*-$[Pt(bpy)(OAc)_2(N_3)_2]$.

Two photoproducts from the irradiation of *trans, cis*-$[Pt(bpy)(OAc)_2(N_3)_2]$ have been identified, but it is surprising that neither of them contained acetate. Perhaps further study of the photoreaction of complex **14** could help the overall understanding of the mechanism of photoactivation of Pt^{IV} azide complexes.

5.5 Conclusions

All the Pt^{IV} azide complexes synthesised (**1** – **14**) were found to be photoactive, as determined by observing the changes in the UV-visible spectra. These Pt^{IV} diazide complexes also proved to be very stable in the absence of light under the various conditions tested. *Trans, trans, trans*-$[Pt(N_3)_2(OH)_2(NH_3)_2]$ (**3**) was even found to be stable to reduction by glutathione.

1D ^1H and 2D [^1H,^{15}N] HSQC NMR spectroscopic studies of the photoreactions of *cis, trans, cis*-$[Pt(N_3)_2(OH)_2(^{15}NH_3)_2]$ (**1**), *cis, trans*-$[Pt(^{15}N\text{-en})(N_3)_2(OH)_2]$ (**2**), *trans, trans, trans*-$[Pt(N_3)_2(OH)_2(^{15}NH_3)_2]$ (**3**) and *trans, trans, trans*-$[Pt(N_3)_2(OH)_2(^{15}NH_3)(py)]$ (**4**) have demonstrated the different behaviour of the *cis* (**1**, **2**) and *trans* (**3**, **4**) complexes upon irradiation (Figure 5.19). Pt^{IV} photoproducts with hydroxides substituted for the azide ligands were identified for complexes **3** and **4**. This means that the mechanism of photoactivation (at least for **3** and **4**) does not involve the transfer of an electron from each azide ligand to reduce the platinum centre to Pt^{II}. Perhaps the different behaviour of the *cis* and *trans* complexes upon

irradiation can help to explain the increased cytotoxicity of the *trans* complexes (Appendix 2).

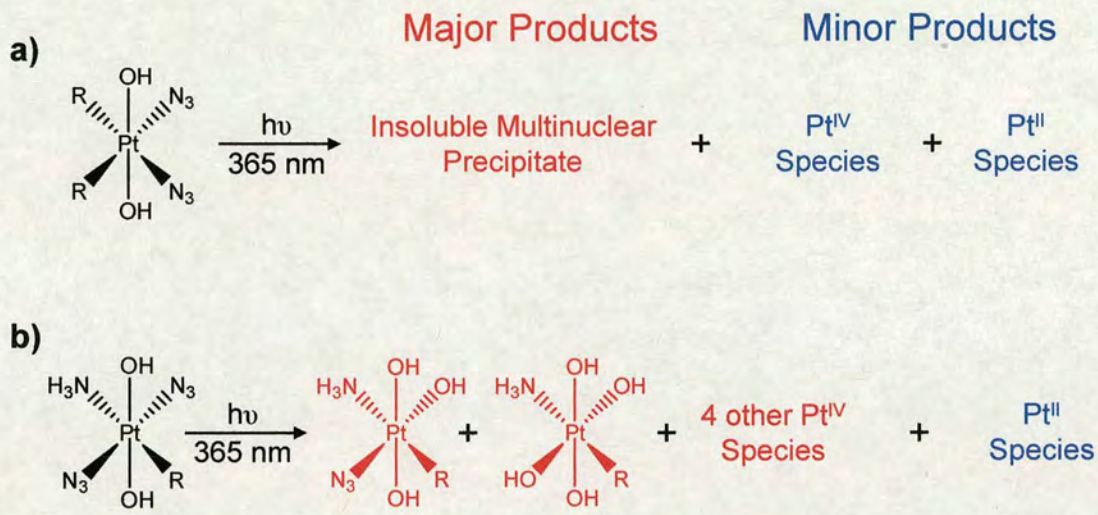

Figure 5.19 Summary of the photoreactions of a) the *cis* complexes **1** and **2**, and b) the *trans* complexes **3** and **4** in aqueous solution.

Two of the major photoproducts from irradiation of *trans, cis*-$[Pt(bpy)(OAc)_2(N_3)_2]$ (**14**) were also identified, both of which were Pt^{II} complexes (Figure 5.20). This indicates the major photoreaction of complex **14** is reduction.

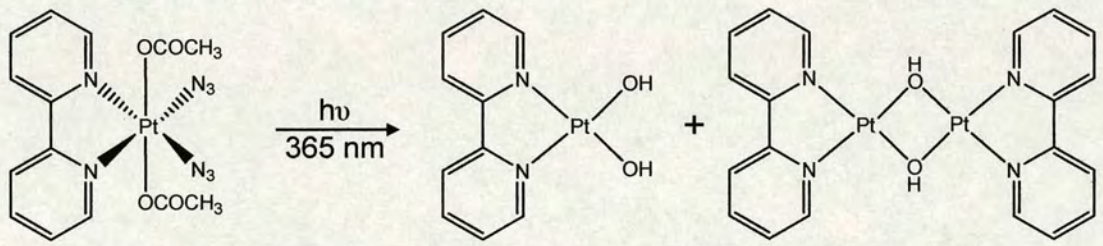

Figure 5.20 Photoproducts produced upon irradiation of *trans, cis*-$[Pt(bpy)(OAc)_2(N_3)_2]$ (**14**) with UV light (365 nm).

5.6 References

[1] Kratochwil, N.A.; Zabel, M.; Range, K.-J.; Bednarski, P.J. *J. Med. Chem.* **1996**, *39*, 2499.

[2] Kratochwil, N.A.; Parkinson, J.A.; Bednarski, P.J.; Sadler, P.J. *Angew. Chem., Int. Ed.* **1999**, *111*, 1566.

[3] Kratochwil, N.A.; Guo, Z.; del Socorro Murdoch, P.; Parkinson, J.A.; Bednarski, P.J.; Sadler, P.J. *J. Amer. Chem. Soc.* **1998**, *120*, 8253.

[4] Müller, P.; Schöder, B.; Parkinson, J.A.; Kratochwil, N.A.; Coxall, R.A.; Parkin, A.; Parsons, S.; Sadler, P.J. *Angew. Chem., Int. Ed.* **2003**, *42*, 335.

[5] Müller, P. PhD Thesis, University of Edinburgh **2002**.

[6] Endicott, J.F.; Ferraudi, G. *J. Phys. Chem.* **1976**, *80*, 949.

[7] Miskowski, V.M.; Nobinger, G.L.; Hammond, G.S. *Inorg. Chem.* **1976**, *15*, 2904.

[8] Vogler, A.; Quett, C.; Kunkely, H. *Ber. Bunsen-Ges. Phys. Chem.* **1988**, *92*, 1486.

[9] Vogler, A.; Kern, A.; Fußder, B.; Hüttermann J. *Z. Naturforsch.* **1978**, *33b*, 1352.

[10] Vogler, A.; Kern, A.; Hüttermann, J. *Angew. Chem., Int. Ed. Engl.* **1978**, *17*, 524.

[11] Vogler, A.; Wright, R.E.; Kunkely, H. *Angew. Chem., Int. Ed. Eng.* **1980**, *19*, 717.

[12] Vogler, A.; Hlavatsch, J. *Angew. Chem., Int. Ed. Eng.* **1983**, *22*, 154.

[13] Kunkely, H.; Vogler, A. *Inorg. Chem. Commun.* **2005**, *8*, 117.

[14] Vogler, A.; Quett, C.; Paukner, A.; Kunkely, H. *J. Am. Chem. Soc.* **1986**, *108*, 8263.

[15] Ferraudi, G.; Endicott, J.F. *J. Am. Chem. Soc.* **1973**, *95*, 2371.

[16] Strähle, J. *J. Organomet. Chem.* **1995**, *488*, 15.

[17] Hennig, H.; Stich, R.; Knoll, H.; Rehorek, D. *Z. Anorg. Allg. Chem.* **1989**, *567*, 139.

[18] Weber, W.; Van Eldik, R. *Inorg. Chim. Acta.* **1986**, *111*, 129.

[19] Reed, J.L.; Gafney, H.D.; Basalo, F. *J. Am. Chem. Soc.* **1974**, *96*, 1363.

[20] Ngai, R.; Wang, Y.H.L.; Reed, J.L. *Inorg. Chem.* **1985**, *24*, 3802.

[21] Dahlgren, R.M.; Zink, J.I. *Inorg. Chem.* **1979**, *18*, 597.

[22] Ferraudi, G.; Endicott, J.F. *Inorg. Chem.* **1973**, *12*, 2389.

[23] Katz, M.; Gafney, H.D. *Inorg. Chem.* **1978**, *17*, 93.

[24] Gafney, H.D.; Reed, J.L.; Basolo, F. *J. Am. Chem. Soc.* **1973**, *95*, 7998.

[25] Reed, J.L.; Wang, F.; Basolo, F. *J. Am. Chem. Soc.* **1972**, *94*, 7173.

[26] Shukla, S.; Kamath, S.S.; Srivastava, T.S. *J. Photochem. Photobiol.* **1988**, *44A*, 143.

[27] Anbalagan, V. *J. Coord. Chem.* **2003**, *56*, 161.

[28] Oehlsen, M.E.; Qu, Y.; Farrell, N. *Inorg. Chem.* **2003**, *42*, 5798.

[29] Appleton, T.G.; Berry, R.D.; Davis, C.A.; Hall, J.R.; Kimlin, H.A. *Inorg. Chem.* **1984**, *23*, 3514.

[30] Berners-Price, S.J.; Sadler, P.J. *Coord. Chem. Rev.* **1996**, *151*, 1.

[31] Alei, M.; Vergamini, P.J.; Wageman, W.E. *J. Am. Chem. Soc.* **1979**, *101*, 5415.

[32] Hollis, L.S.; Stern, E.W.; Amundsen, A.R.; Miller, A.V.; Doran, S.L. *J. Am. Chem. Soc.* **1987**, *109*, 3596.

[33] Kuroda, R.; Neidle, S.; Ismail, I.M.; Sadler, P.J. *Inorg. Chem.* **1983**, *22*, 3620.

[34] Barnard, C.F.J.; Vollano, J.F.; Chaloner, P.A.; Dewa, S.Z. *Inorg. Chem.* **1996**, *35*, 3280.

[35] Pregosin, P.S. *Ann. Rep. NMR Spectr.* **1986**, *17*, 285.

[36] Appleton, T.G.; Hall, J.R.; Ralph, S.F. *Inorg. Chem.* **1985**, *24*, 4685.

[37] Knoll, H.; Stich, R.; Hennig, H.; Stufkens, D.J. *Inorg. Chim. Acta* **1990**, *178*, 71.

[38] McInnes, E.J.L.; Farley, R.D.; Rowlands, C.C.; Welch, A.J.; Rovatti, L.; Yellowlees, L.J. *J. Chem. Soc., Dalton Trans.* **1999**, 4203.

[39] Gidney, P.M.; Gillard, R.D.; Heaton, B.T. *J. Chem. Soc., Dalton Trans* **1973**, 132.

[40] Kamath, S.S.; Uma, V.; Srivastava, T.S. *Inorg. Chim. Acta* **1989**, *161*, 49.

[41] Wimmer, S.; Castan, P.; Wimmer, F.L.; Johnson, N.P. *J. Chem. Soc., Dalton Trans.* **1989**, 403.

[42] Neumann, C.; Boubakari; Grünert, R.; Bednarksi, P.J. *Anal. Biochem.* **2003**, *320*, 170.

[43] Rosenberg, B. *Met. Ions Biol. Syst.*, **1980**, *11*, 127.

[44] Bloemink, M.J.; Reedijk, J. *Metal Ions in Biological Systems* **1996**, *32*, 641.

[45] Fichtinger-Schepman, A.M.J.; Van der Veer, J.L.; Den Hartog, J.H.J.; Lohman, P.H.M.; Reedijk, J. *Biochemistry* **1985**, *24*, 707.

[46] Choi, S.; Mahalingaiah, S.; Delaney, S.; Neale, N.R.; Masood, S. *Inorg. Chem.* **1999**, *38*, 1800.

[47] Eastman, A. *Biochem. Pharmacol.* **1987**, *36*, 4177.

[48] Hall, M.D.; Hambley, T.W. *Coord. Chem. Rev.* **2002**, *232*, 49.

[49] Al-Baker, S.; Dabrowiak, J.C. *Inorg. Chem.* **1987**, *26*, 613.

[50] Al-Baker, S.; Vollano, J.F.; Dabrowiak, J.C. *J. Am. Chem. Soc.* **1986**, *108*, 5643.

[51] Berners-Price, S.J.; Frey, U.; Ranford, J.D.; Sadler, P.J. *J. Am. Chem. Soc.* **1993**, *115*, 8649.

[52] Boreham, C.J.; Broomhead, J.A.; Fairlie, D.P. *Aust. J. Chem.* **1981**, *34*, 659.

[53] Berners-Price, S.J.; Ranford, J.D.; Sadler, P.J. *Inorg. Chem.* **1994**, *33*, 5842.

[54] Berners-Price, S.J.; Frenkiel, T.A.; Frey, U.; Ranford, J.D.; Sadler, P.J. *J. Chem. Soc., Chem. Commun.* **1992**, 789.

[55] Šima, J. *Coord. Chem. Rev.* **2006**, *Online.*

[56] Bignozzi, C.A.; Bartocci, C.; Maldotti, A.; Carassiti, V. *Inorg. Chim. Acta* **1982**, *62*, 187.

[57] Swihart, D.L.; Mason, W.R. *Inorg. Chem.* **1970**, *9*, 1749.

[58] Schmidtke, H.H.; Garthoff, D. *J. Am. Chem. Soc.* **1967**, *89*, 1317.

[59] Vogler, A.; Kunkely, H. *Angew. Chem., Int. Engl.* **1982**, *21*, 209.

Chapter 6
DNA and Nucleotide Binding

6.1 Introduction

The reactions of platinum(IV) azide complexes upon irradiation have been investigated by several techniques (Chapter 5). The interaction of these complexes with nucleobases and DNA is also of interest as DNA is generally accepted to be the main target of cisplatin.[1] Once inside the cell, cisplatin hydrolyses to the mono- and di-aqua species, *cis*-$[Pt(NH_3)_2Cl(OH_2)]^+$ and *cis*-$[Pt(NH_3)_2(OH_2)_2]^{2+}$, which form lethal cross-links on DNA. The N7 positions of two adjacent guanine bases are the preferred binding sites of cisplatin.[2] Besides GG intrastrand cross-links (70 %), the other major DNA adducts are intrastrand AG (but not GA) cross-links (15 %). Minor adducts include 1,3-intrastrand and interstrand cross-links involving two non-neighbouring guanines.[2]

The photoreactions of several Pt^{IV} azide complexes in the presence of the nucleotides 5′-GMP and d(GpG), and 9-ethylguanine have been followed by 1D ^1H and 2D [^1H,^{15}N] HSQC NMR spectroscopy. The preferential platination site for *cis, trans*-$[Pt(en)(N_3)_2(OH)_2]$ has been determined by a transcription mapping study on plasmid DNA, and HPLC analysis of a platinated DNA duplex.

6.2 Experimental

6.2.1 Materials

Complexes **1-4**, and $[PtCl_2(^{15}NH_3)(py)]$ were synthesised as previously described (Chapter 3). Silver nitrate, D_2O and 1,4-dioxane were purchased from Aldrich, 5′-GMP and reduced glutathione from Acros, $HClO_4$ from Fisons, 9-ethylguanine (9-EtG), H_2O_2 and the sodium salt of d(GpG) from Sigma.

6.2.2 Synthesis of *trans*-$[Pt(^{15}NH_3)(py)(5'\text{-GMP})_2]^{2+}$

$[Pt^{II}Cl_2(^{15}NH_3)(py)]$ (3.4 mg, 0.009 mmol) was suspended in H_2O (3 mL) and $AgNO_3$ (3.2 mg, 0.018 mmol) added. After stirring for 24 h at 333 K, the insoluble AgCl was filtered off. An NMR sample was prepared using 0.54 mL of the above solution and 60 μL of D_2O, 5′-GMP (4 mol equiv, 2.8 mg) was added and the pH adjusted to 5 ± 0.2. The 1D ^1H and 2D [^1H,^{15}N] HSQC NMR spectra were acquired after 24 h (pH measured as 5.09), and then the sample was analysed by ESI-MS.

6.2.3 Photoreactions in the Presence of 5′-GMP, 9-Ethylguanine and d(GpG)

Samples were prepared by dissolving the 5′-GMP or 9-ethylguanine in 90 % H_2O / 10 % D_2O (0.6 mL) plus 2 μL dioxane (1 %), and then adding this solution to 0.5 mol equiv of the Pt^{IV} azide complex. The sample was transferred to an NMR tube and the pH adjusted to 5 with $HClO_4$ (0.1 M) and NaOH (0.1 M). Samples with d(GpG) were made up in the same way, except a 3:2 molar ratio of Pt^{IV} azide complex to dinucleotide was used.

Details of the acquisition of NMR spectra, ESI-MS and pH adjustments are described in Chapter 2. UV irradiation (365 nm) was carried out with a UV lamp, while an argon:krypton laser was used for photoreactions at visible wavelengths (457.9 and 647.1 nm); these light sources and the experimental set-up used for irradiations are described in detail in Chapter 2.3.

6.2.4 Transcription Mapping of DNA Adducts

A stock solution of cisplatin (5×10^{-4} M in 10 mM $NaClO_4$) was prepared at 298 K and used immediately. Plasmid pSP73KB [2455 base pairs (bp)] was isolated according to standard procedures and banded twice in CsCl/ethidium bromide equilibrium density gradients. Riboprobe Gemini System II for transcription mapping containing T7 RNA polymerase was purchased from Promega.

Plasmid DNA was incubated with cisplatin in 10 mM $NaClO_4$ at 310 K in the dark for 24 h, or treated with a 0.5 molar equivalent of *cis, trans*-$[Pt(en)(N_3)_2(OH)_2]$ (**2**) in 10 mM $NaClO_4$ and irradiated (λ = 457.9 nm, 10 mW) for 3 h, while an identical sample was kept in the dark. These samples were then precipitated by ethanol and redissolved in the medium required for subsequent analysis. An aliquot of each sample was used to determine the value of r_b (r_b is defined as the number of molecules of the platinum compound bound per nucleotide residue) by flameless atomic absorption spectrophotometry (FAAS).

Transcription of the (*Nde*I / *Hpa*I) restriction fragment of pSP73KB DNA with DNA-dependent T7 RNA polymerase and electrophoretic analysis of transcripts

were performed according to the protocols recommended by Promega (Promega Protocols and Applications, 43-46 (1989/90) and previously described in detail).[3,4]

The incubations and irradiations were carried out by the author at the University of Edinburgh. Transcription mapping was conducted by Dr. Jana Kašpárková and Prof. Viktor Brabec at the Academy of Sciences of the Czech Republic, Brno.

6.2.5 HPLC Analysis of DNA Adducts

The oligodeoxyribonucleotide duplex containing 40 bp,
5'-CCCGGATTATACGGCTTAAACCAAATTGCTTAAATTGGCC/
5'-GGCCAATTTAAGCAATTTGGTTTAAGCCGTATAATCCGGG
was from East Port (Prague, Czech Republic); the single-stranded oligonucleotides constituting this duplex were purified by strong anion exchange chromatography (Pharmacia MonoQ column) on a Pharmacia FPLC system with 10 mM NaOH, 0.2 – 0.8 M NaCl gradient. The duplex was formed by heating a mixture of the complementary single-stranded oligonucleotides at equal concentrations (related to the mononucleotide content) at 263 K for 5 min followed by incubation at 298 K for 4 h. DNase I from bovine pancreas, nuclease P1 from *Penicillium citrinum* and alkaline phosphatase from calf intestine were also from Sigma-Aldrich. Acrylamide, (bis)acrylamide and urea were from Merck KgaA (Darmstadt, Germany).

The oligonucleotide duplex was treated with 1.5 molar equivalents of *cis, trans*-$[Pt(en)(N_3)_2(OH)_2]$ in 100 mM $NaClO_4$ and irradiated (λ = 457.9 nm, 30 mW) for 6 h, while an identical sample was kept in the dark. These samples were then exhaustively dialyzed against 100 mM $NaClO_4$ in the dark. Aliquots were used to determine the value of r_b by FAAS.

These analyses were performed using a Hitachi Series 4 liquid chromatograph equipped with a LCI-100 computing integrator and a Waters μBondapack C18 column. The products were separated by reverse phase (RP) HPLC (isocratic elution with 0.1 M ammonium acetate, pH 5.0 in 4 % CH_3CN at 1 ml/min flow rate). The following enzymatic digestion protocol was used in order to characterize the

platinated deoxyribooligonucleotides. The samples (50 μg of the oligonucleotide) were incubated with 72 units of DNase I at 310 K. After 4 h nuclease P1 (40 μg) was added, and the reaction was allowed to continue at 310 K for 18 h. Finally, alkaline phosphatase (39 units) was added and the incubation continued for an additional 4 h at 310 K. The digested samples containing constituent nucleosides were then heated for 2 min at 80 °C, centrifuged and the supernatant analyzed by RP-HPLC. Each analysis was performed four times and the data varied on average ± 1 % from their mean.

The incubations and irradiations were carried out by the author at the University of Edinburgh. HPLC analysis was conducted by Dr. Jana Kašpárková and Prof. Viktor Brabec at the Academy of Sciences of the Czech Republic, Brno.

6.3 Results

The binding of 5′-GMP and d(GpG) to *cis, trans, cis*-$[Pt(N_3)_2(OH)_2(^{15}NH_3)_2]$ (**1**) and *cis, trans*-$[Pt(^{15}N\text{-en})(N_3)_2(OH)_2]$ (**2**) upon irradiation with blue light (457.9 nm) has been shown previously.[5,12] These reactions were repeated with UV light (365 nm) to determine whether the photoproducts were the same. It was thought that the higher energy light would perhaps cause some fragmentation of the reactants or products. UV light (365 nm) has been used to activate the Pt^{IV} azide compounds in the cell cytotoxicity experiments (Appendix 2), therefore their chemical behaviour upon irradiation at 365 nm is important.

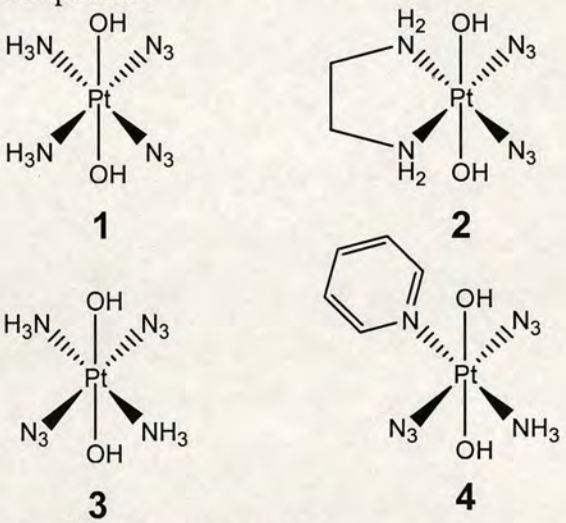

Figure 6.1 Structures of Pt^{IV} azide compounds.

Reactions of Pt^{IV} diazido-dihydroxy complexes can be followed by ^1H NMR studies of the am(m)ine protons if the reactions are carried out in H_2O. However at neutral pH no ^1H am(m)ine peaks are detected due to fast exchange of the NH protons with the solvent. With decreasing pH the signals appear, and so the pH is usually adjusted to 5.

As explained above in order to observe the ^1H am(m)ine peaks of Pt^{IV} diazido dihydroxy complexes it is necessary to adjust the pH to 5. However, when these complexes were irradiated on their own in solution the pH was found to increase (Section 5.3.2). The increase in pH with longer irradiation times was more pronounced for complex **1** than for **3** or **4** (Chapter 5, Figure 5.1). When these reactions are carried out in the presence of 5′-GMP, the pH increase followed a similar trend for complexes **3** and **4**, compared to the complexes alone. However the pH increase for complex **1** was significantly less than for irradiation of **1** on its own (Figure 6.2). This is perhaps due to buffering effects caused by the phosphate group of 5′-GMP (pK_a 6.25).[9] Adjustment of the pH to 5 after irradiation, but before acquiring NMR spectra was carried out for all experiments unless otherwise stated.

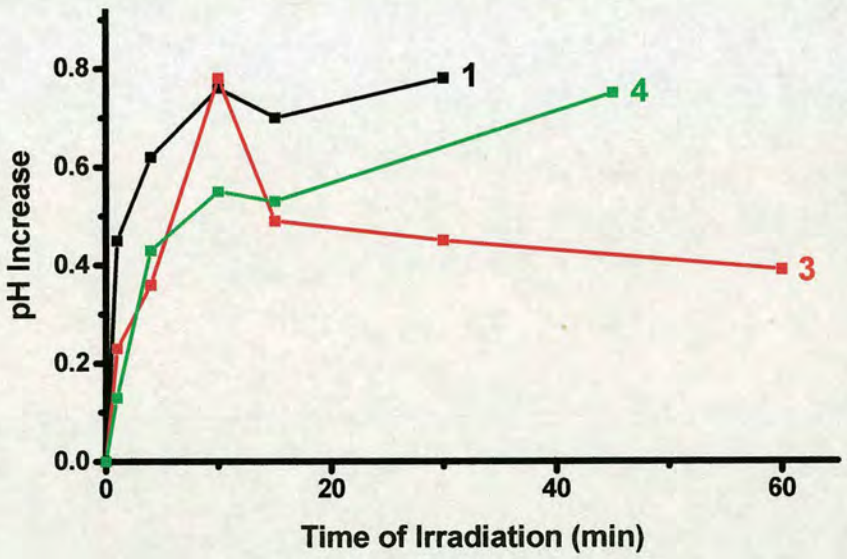

Figure 6.2 The increase in pH (from 5 ± 0.2) after each irradiation determined for *cis, trans, cis*-$[Pt(N_3)_2(OH)_2(^{15}NH_3)_2]$ (**1**), *trans, trans, trans*-$[Pt(N_3)_2(OH)_2(^{15}NH_3)_2]$ (**3**) and *trans, trans, trans*-$[Pt(N_3)_2(OH)_2(^{15}NH_3)(py)]$ (**4**) in the presence of 2 mol equiv 5′-GMP.

6.3.1 Photoreactions of Pt^{IV} Azide Complexes with 5′-GMP and 9-Ethylguanine

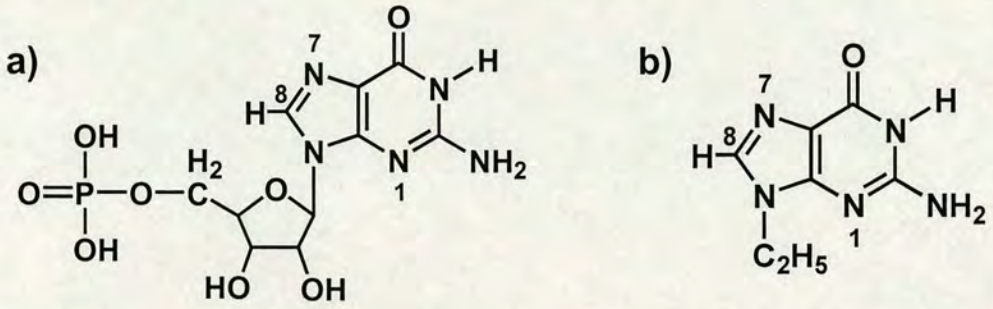

Figure 6.3 Structures and atom numbering schemes for a) 5′-GMP and b) 9-ethylguanine.

6.3.1.1 *Cis, trans, cis*-$[Pt(N_3)_2(OH)_2(^{15}NH_3)_2]$ (**1**)

A 3 mM sample of *cis, trans, cis*-$[Pt(N_3)_2(OH)_2(^{15}NH_3)_2]$ (**1**) was irradiated with UVA light in the presence of 2 molar equivalents of 5′-GMP. 1D [^{1}H] and 2D [^{1}H,^{15}N] HSQC NMR spectra were acquired after 0, 1, 5, 15, 30 and 60 min of irradiation with the pH readjusted to 5 each time.

After 1 min, four new [^{1}H,^{15}N] NMR cross-peaks assignable to Pt^{II} species were visible (**70**-**73**), including one which corresponded to *cis*-$[Pt(^{15}NH_3)_2$(5′-GMP-*N7*)$_2]^{2+}$ (**70**) (Table 6.1).[6] After 5 min another new peak for a Pt^{II} complex (**74**) appeared (Table 6.1), which has been assigned as *trans*-$[Pt(^{15}NH_3)_2$(5′-GMP-*N7*)$_2]^{2+}$ (Figure 6.4). The chemical shifts of **74** agree well with the literature values,[36] and are almost identical to those of the major product formed on photoreaction of *trans, trans, trans*-$[Pt(N_3)_2(OH)_2(^{15}NH_3)_2]$ with 5′-GMP. This product was confirmed as *trans*-$[Pt(^{15}NH_3)_2$(5′-GMP-*N7*)$_2]^{2+}$ (Section 6.3.1.2).

The three other peaks (**71**-**73**) are as yet unassigned. However, peaks **71** and **72** grew in intensity at the same rate and so are likely to be due to inequivalent $^{15}NH_3$'s within the same molecule. Perhaps one of the bound 5′-GMP components has undergone a modification caused by the light, however no reaction was seen when a 6 mM sample of 5′-GMP in 90 % H_2O / 10 % D_2O was irradiated at 365 nm for 4 h. The reaction was monitored by ^{1}H NMR spectroscopy and the spectrum was identical before and after irradiation.

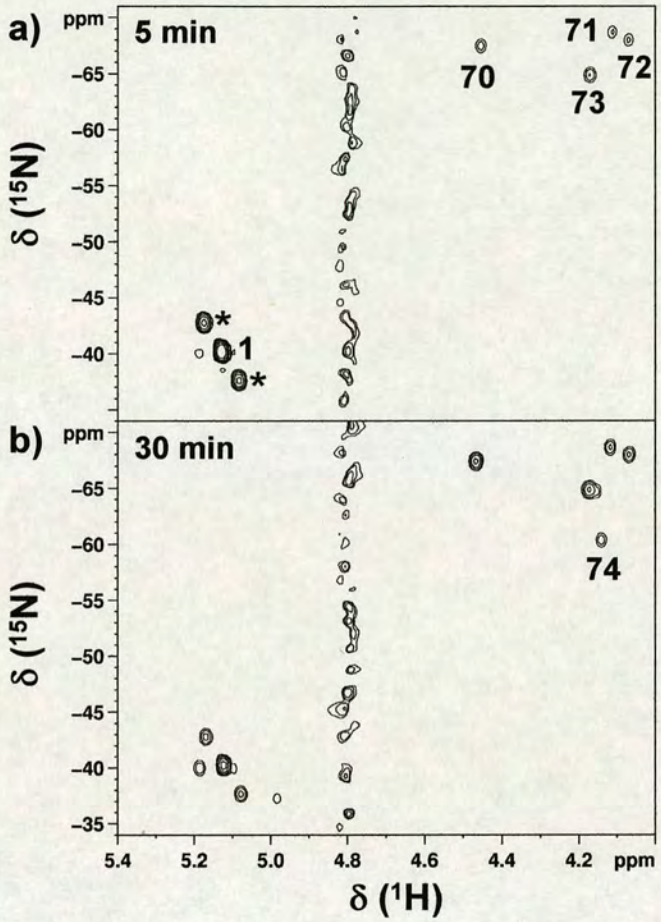

Figure 6.4 2D [^{1}H,^{15}N] HSQC NMR spectra of *cis, trans, cis*-[$Pt(N_3)_2(OH)_2(^{15}NH_3)_2$] (3 mM) and 5′-GMP (6 mM) after irradiation with UV light for a) 5 min and b) 30 min. * ^{195}Pt satellites.

Table 6.1 ^{1}H and ^{15}N NMR chemical shifts of Pt^{II} photoproducts after UV irradiation of *cis, trans, cis*-[$Pt(N_3)_2(OH)_2(^{15}NH_3)_2$]

Peaks[a]	δ(^{1}H) / ppm	δ(^{15}N) / ppm	Assignments
70	4.45	-67.47	*cis*-[$Pt(^{15}NH_3)_2$(5′-GMP-*N7*)$_2$]$^{2+}$
71	4.11	-68.68	Pt^{II} photoproduct
72	4.07	-67.95	Pt^{II} photoproduct
73	4.17	-64.92	Pt^{II} photoproduct
74	4.13	-60.55	*trans*-[$Pt(^{15}NH_3)_2$(5′-GMP-*N7*)$_2$]$^{2+}$

a) See Figure 6.4 for peak labels

6.3.1.2 *Trans, trans, trans*-$[Pt(N_3)_2(OH)_2(^{15}NH_3)_2]$ (**3**)

A 3 mM sample of *trans, trans, trans*-$[Pt(N_3)_2(OH)_2(^{15}NH_3)_2]$ (**3**) was irradiated with UVA light in the presence of 2 molar equivalents of 5′-GMP. 1D [^{1}H] and 2D [^{1}H,^{15}N] HSQC NMR spectra were acquired after 0, 1, 5, 15, 30 and 60 min of irradiation with the pH readjusted to 5 each time.[7] As described in section 6.3, the pH rises upon irradiation.

The NMR spectra showed that about 7 % of complex **3** had undergone photoreduction and photosubstitution after only one minute of irradiation. The Pt^{II} product had $\delta(^1H,^{15}N)$ chemical shifts of 4.14, -60.51 ppm, which are characteristic of the bis-GMP adduct *trans*-$[Pt(^{15}NH_3)_2(5'\text{-GMP-}N7)_2]^{2+}$ (**74**) (Figure 6.5).[36] After 1 h, > 75 % of complex **3** had been converted into **74** as the major product (Figure 6.6). After 60 min a peak for *trans*-$[Pt(^{15}NH_3)_2(OH_2)_2]^{2+}$ (**75**) appeared (Table 6.2).[6]

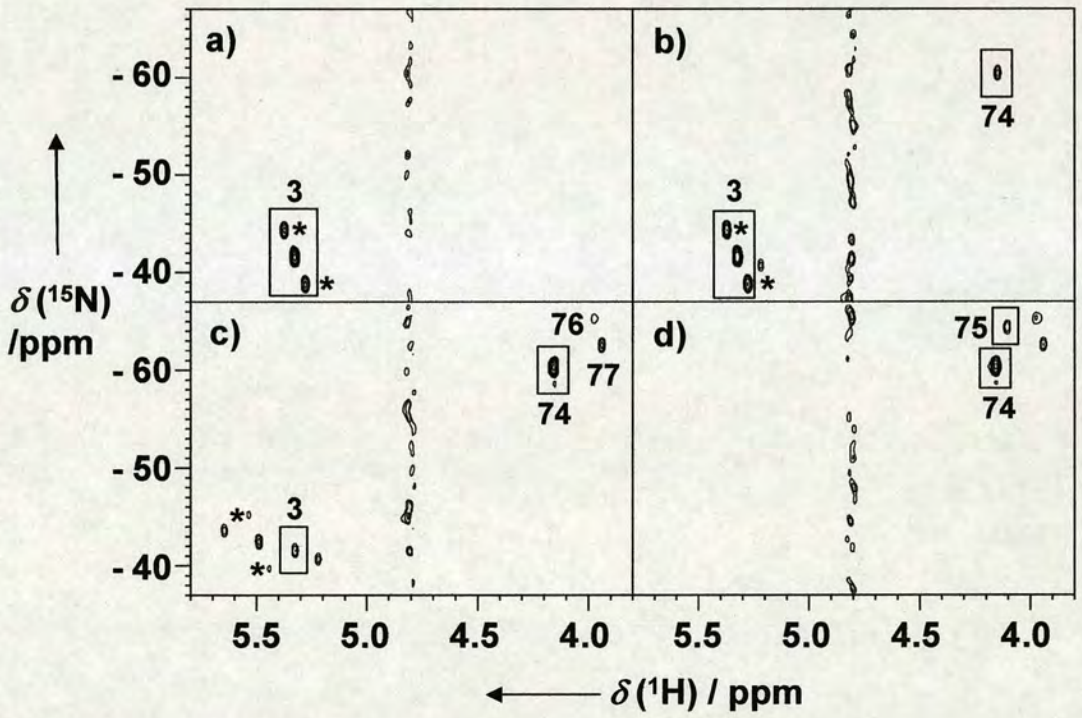

Figure 6.5 2D [^{1}H,^{15}N] HSQC NMR spectra recorded during reaction of *trans, trans, trans*-$[Pt(N_3)_2(OH)_2(^{15}NH_3)_2]$ with 2 mol equiv of 5′-GMP after a) 0 min, b) 1 min c) 30 min, and d) 120 min irradiation. The pH was adjusted to 5 ± 0.2 after every irradiation. * ^{195}Pt satellites.

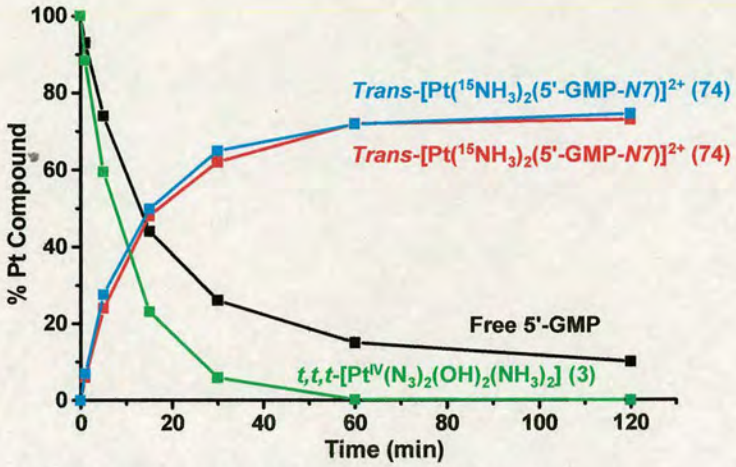

Figure 6.6 The decrease in concentration of *trans, trans, trans*-$[Pt(N_3)_2(OH)_2(^{15}NH_3)_2]$ (—) and free 5′-GMP (—) with time of irradiation based on the integrals of the corresponding peaks in the 2D [^{1}H,^{15}N] and 1D [^{1}H] NMR spectra, respectively. The formation of the product *trans*-$[Pt(^{15}NH_3)_2(5'\text{-GMP-}N7)_2]^{2+}$ (**74**) was followed using both the 1D (—) and 2D (—) spectra.

Table 6.2 ^{1}H and ^{15}N NMR chemical shifts of Pt^{II} photoproducts from irradiation of *trans, trans, trans*-$[Pt(N_3)_2(OH)_2(^{15}NH_3)_2]$.

Peaks[a]	δ(^{1}H) / ppm	δ(^{15}N) / ppm	Assignments
74	4.14	-60.51	*trans*-$[Pt(^{15}NH_3)_2(5'\text{-GMP-}N7)_2]^{2+}$
75	4.10	-63.23	*trans*-$[Pt(^{15}NH_3)_2(OH_2)_2]^{2+}$
76	3.94	-62.65	Pt^{II} photoproduct
77	3.97	-65.30	Pt^{II} photoproduct
78	4.04	-61.42	*trans*-$[Pt(^{15}NH_3)_2(9\text{-EtG})_2]^{2+}$

a) See Figure 6.5 for peak labels

The formation of **74** can be followed by measuring the intensity of the 2D [^{1}H,^{15}N] cross peak or the new H8 peak in the 1D [^{1}H] spectra. These results are plotted in Figure 6.6 and the rates correlate well. A correction for ^{195}Pt satellites (which are broad and therefore not detected) was made by adding 33.8 % to the peak integrals.[7]

Figure 6.7 shows the H8 region for free 5′-GMP (8.11 ppm) and Pt-bound 5′-GMP

(8.79 ppm) in complex **74**. This low-field shift of the H8 signal is characteristic of Pt binding to the N7 position of 5′-GMP.[8]

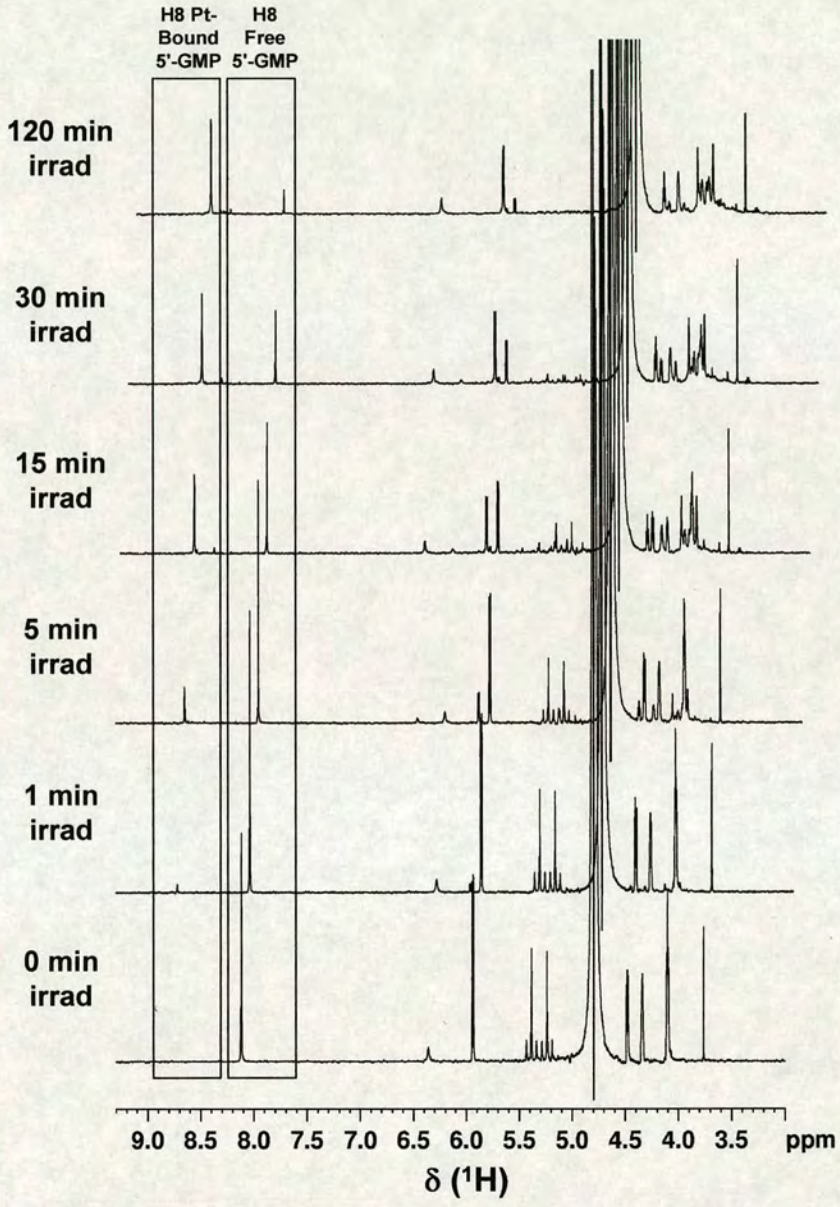

Figure 6.7 ^{1}H NMR spectra of *trans, trans, trans*-$[Pt(N_3)_2(OH)_2(NH_3)_2]$ (3 mM) and 5′-GMP (6 mM) after UVA irradiation for various times. The H8 regions of free and platinum-bound 5′-GMP are boxed. Spectra are offset for clarity.

Binding of Pt^{II} to N7 was further confirmed by a ^{1}H NMR pH titration over the range pH 1 – 11 (Figure 6.8). The H8 chemical shift change associated with the protonation

of N7 of 5′-GMP (pK_a ca. 2.5)[9] was absent for the product (**74**).[10]

A bis adduct *trans*-[Pt($^{15}NH_3$)$_2$(9-ethylguanine-*N7*)$_2$] (**78**; Table 6.2) appeared as a product from the photoreaction of complex **3** with 9-ethylguanine after only 1 min of irradiation. ESI-MS gave a peak at m/z 295.3 assignable to [Pt($^{15}NH_3$)$_2$(9-ethylguanine-*N7*)$_2$]$^{2+}$ (calc. m/z 294.7).

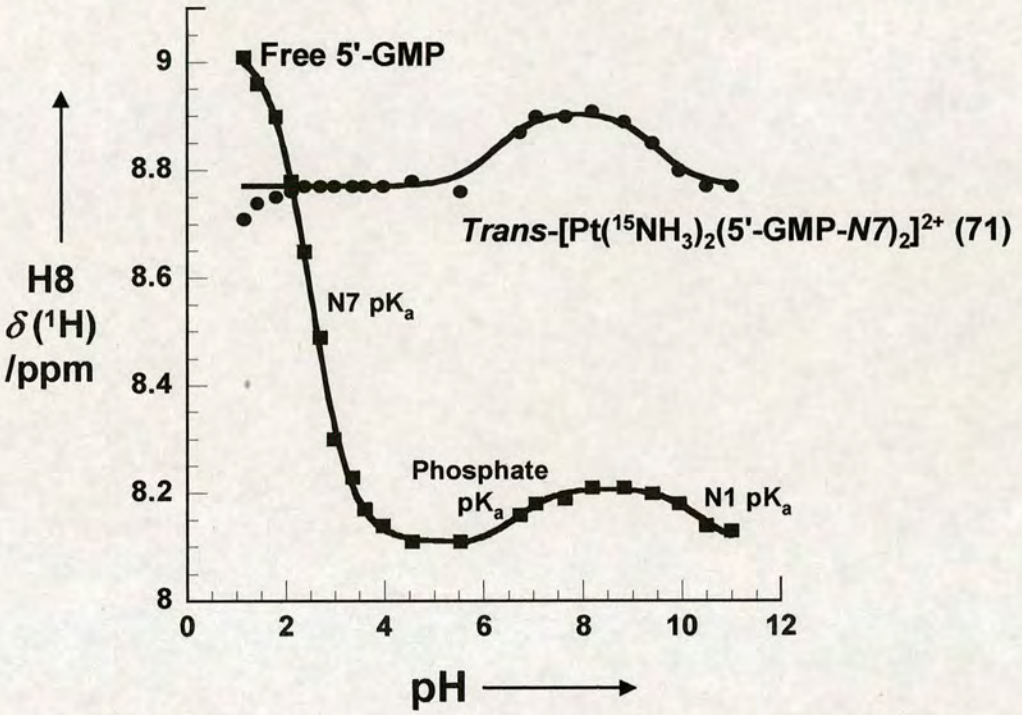

Figure 6.8 Variation with pH of the H8 NMR chemical shift of the major product from irradiation of *trans, trans, trans*-[Pt(N_3)$_2$(OH)$_2$($^{15}NH_3$)$_2$] in the presence of 5′-GMP (**74** *trans*-[Pt($^{15}NH_3$)$_2$(5′-GMP-*N7*)$_2$]), in comparison with free 5′-GMP. The large increase in chemical shift below pH 4 for free 5′-GMP is absent for **74** indicating coordination of Pt to N7.

Interestingly (in view of the deeper tissue penetration of red light), irradiation of complex **3** (3 mM) and 5′-GMP (6 mM) with red light (λ = 647.1 nm, P = 18 mW) also gave rise to a detectable amount of *trans*-[Pt($^{15}NH_3$)$_2$(5'-GMP-*N7*)$_2$]$^{2+}$ (ca. 2% after 90 min; Figure 6.9).[11]

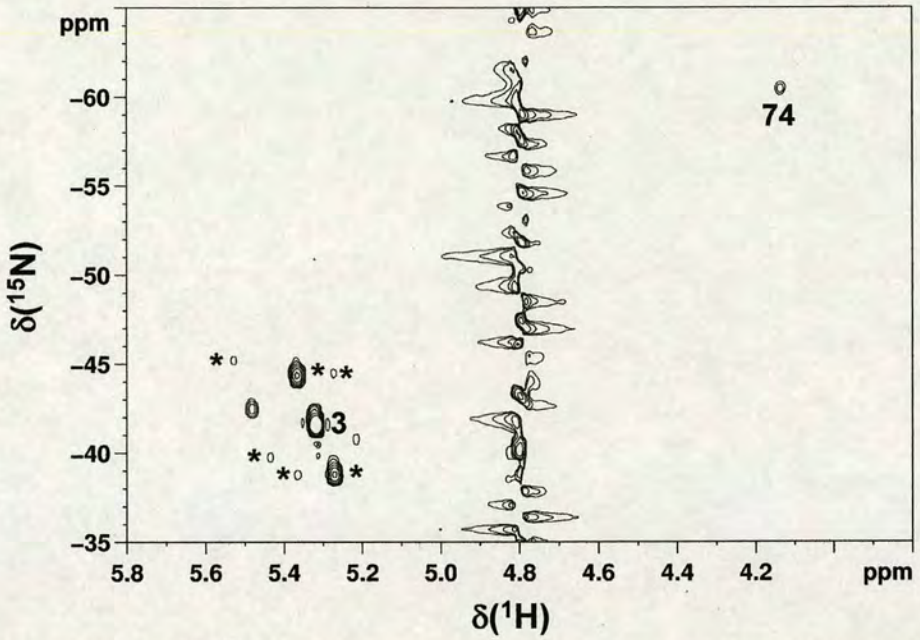

Figure 6.9 2D [^{1}H,^{15}N] NMR spectrum of *trans, trans, trans*-[Pt$(N_3)_2(OH)_2(^{15}NH_3)_2$] after irradiation with red light (λ = 647.1 nm, 18 mW, 90 min) pH 5 * ^{195}Pt satellites.

6.3.1.3 *Trans, trans, trans*-[Pt$(N_3)_2(OH)_2(^{15}NH_3)$(py)] (**4**)

Trans, trans, trans-[Pt$(N_3)_2(OH)_2(^{15}NH_3)$(py)] (3 mM) was irradiated with UV light in the presence of 2 mol equiv of 5′-GMP. The reaction was followed by 1D [^{1}H] and 2D [^{1}H,^{15}N] HSQC NMR spectroscopy, spectra were recorded after 0, 1, 5, 15, 30 and 75 min irradiation, with the pH adjusted to 5.

Initially, by comparison with the photoreaction of complex **3** and 5′-GMP, it was assumed that peak **79** was assignable to the bis-GMP adduct *trans*-[Pt$(^{15}NH_3)$(py)(5′-GMP-*N7*$)_2]^{2+}$ (Figure 6.10).

To confirm this, *trans*-[Pt$(^{15}NH_3)$(py)(5′-GMP-*N7*$)_2]^{2+}$ was synthesised from *trans*-[Pt$(^{15}NH_3)$(py)Cl_2] and analysed by 1D [^{1}H] and 2D [^{1}H,^{15}N] HSQC NMR spectroscopy and mass spectrometry (Figure 6.11). The only peak present after 24 h was **83** (Table 6.3, Figure 6.11); a new 5′-GMP H8 signal had appeared which was shifted to low field (8.86 ppm) compared to free 5′-GMP (8.12 ppm) (Table 6.4). This is characteristic of platinum binding to the N7 position of 5′-GMP. By mass spectrometry this product was confirmed to be *trans*-[Pt$(^{15}NH_3)$(py)(5′-GMP-*N7*$)_2]^{2+}$ (Figure 6.11b).

Table 6.3 ^{1}H and ^{15}N NMR chemical shifts (ppm), coupling constants (Hz) and assignments of Pt^{II} and Pt^{IV} pyridine complexes.

Peak[a]	$\delta(^{1}H)$	$\delta(^{15}N)$	^{1}J ^{195}Pt-^{15}N	^{2}J ^{195}Pt-^{1}H	Assignments
4	5.65	-46.00	282.3	49.5	*t,t,t*-[$Pt^{IV}(N_3)_2(OH)_2(^{15}NH_3)(py)$]
79	4.15	-66.37	-	-	*t*-[$Pt^{II}(^{15}NH_3)(py)(N_3)$(5′-GMP)]
80	4.42	-65.63	-	-	*t*-[$Pt^{II}(^{15}NH_3)(py)$(5′-GMP)$_2$]
81	4.57	-63.77	-	-	Pt^{II} photoproducts
82	4.35	-68.80	-	-	Pt^{II} photoproducts
83	4.42	-65.25	-	-	*t*-[$Pt^{II}(^{15}NH_3)(py)$(5′-GMP)$_2$]
84	4.15	-67.72	-	-	*t*-[$Pt^{II}(^{15}NH_3)(py)Cl$(5′-GMP)]
50	5.56	-45.62	298	50	*t*-[$Pt^{IV}(N_3)(OH)_3(^{15}NH_3)(py)$]
51	5.94	-47.10	290	48	Pt^{IV} photoproducts

a) See Figures 6.10 and 6.11a for peak labels

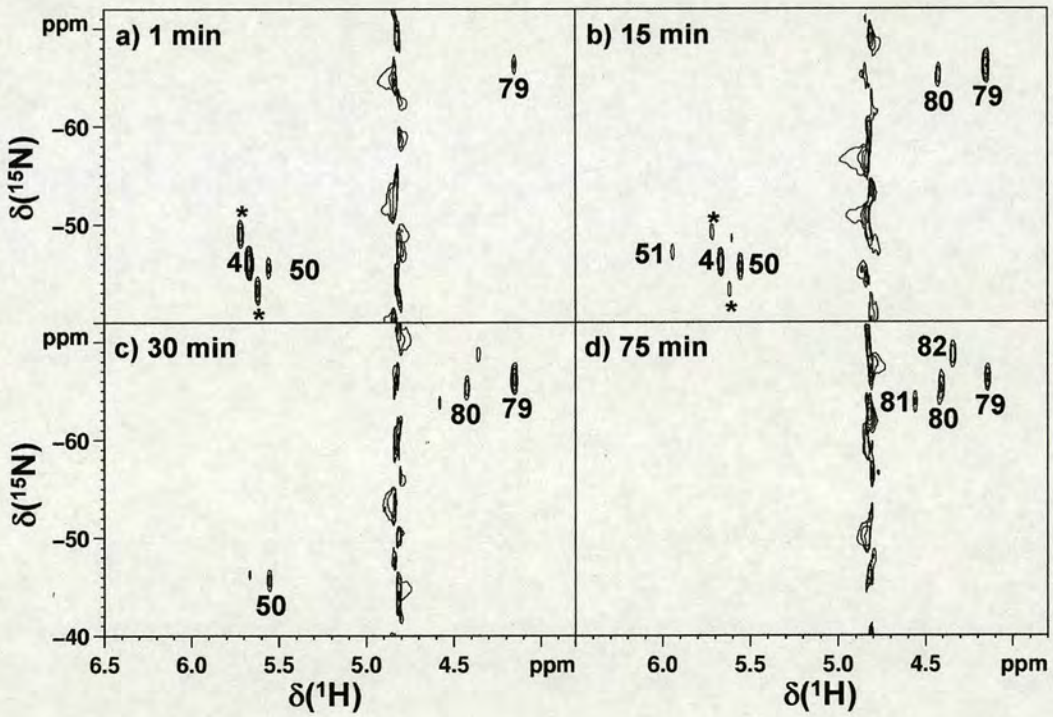

Figure 6.10 2D [^{1}H,^{15}N] HSQC NMR spectra of *trans, trans, trans*-[$Pt(N_3)_2(OH)_2(^{15}NH_3)(py)$] in the presence of 2 mol equiv of 5′-GMP after a) 1 min, b) 15 min, c) 30 min and d) 75 min of irradiation. * ^{195}Pt satellites.

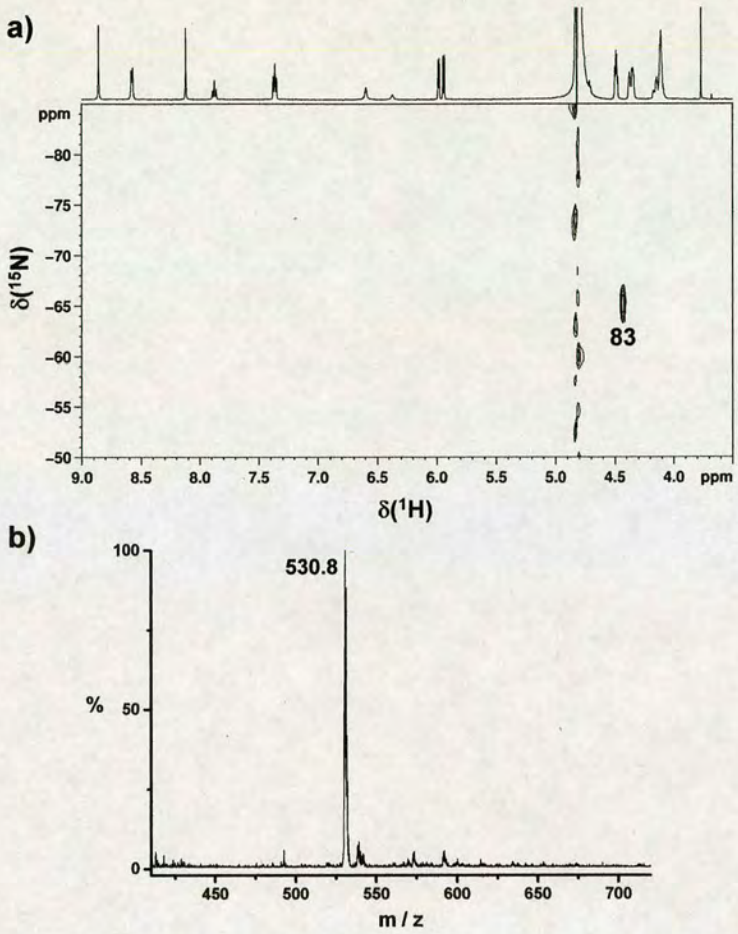

Figure 6.11 NMR and ESI-MS of synthesised *trans*-[Pt($^{15}NH_3$)(py)(5′-GMP-*N7*)$_2$]$^{2+}$. a) 1D [^{1}H] and 2D [^{1}H,^{15}N] HSQC NMR spectra and b) ESI-MS, calculated m/z for {[Pt($^{15}NH_3$)(py)(5′-GMP-*N7*)$_2$]$^{2+}$ − 2H$^+$ + 2 Na$^+$} 531.06

Table 6.4 ^{1}H NMR chemical shifts of pyridine and H8 5′-GMP resonances.

Peaks[a]	δ(^{1}H) / ppm				Assignments
	py-H_o	py-H_p	py-H_m	5′-GMP H8	
4	8.72	8.25	7.78	-	*t,t,t*-[Pt(N_3)$_2$(OH)$_2$($^{15}NH_3$)(py)]
79	8.68	7.94	7.47	8.67	*t*-[Pt^{II}($^{15}NH_3$)(py)(N_3)(5′-GMP)]$^+$
80/83[b]	8.57	7.87	7.36	8.86	*t*-[Pt^{II}($^{15}NH_3$)(py)(5′-GMP)$_2$]$^{2+}$
84	8.63	7.91	7.41	8.74	*t*-[Pt^{II}($^{15}NH_3$)(py)Cl(5′-GMP)]$^+$

a) See Figures 6.10 and 6.11a for peak labels

b) Peak **80** was observed after irradiation of **4** and 5′-GMP. Peak **83** was obtained from synthesised *trans*-[Pt^{II}($^{15}NH_3$)(py)(5′-GMP)$_2$]$^{2+}$. Therefore these peaks are both assigned as *trans*-[Pt^{II}($^{15}NH_3$)(py)(5′-GMP)$_2$]$^{2+}$.

Interestingly this experiment showed that the main photoproduct **79** is not the bis-GMP adduct. The chemical shifts of peak **80** (Table 6.3) agree very well with those of the synthesised *trans*-[Pt($^{15}NH_3$)(py)(5′-GMP-*N7*)$_2$]$^{2+}$ (**83**) and so species **80** is assigned as the bis-GMP adduct.

Peak **79** is believed to be the monoazide species *trans*-[Pt^{II}($^{15}NH_3$)(py)(N_3)(5′-GMP-*N7*)]$^+$ for the following reasons.

- A peak for *trans*-[Pt^{II}($^{15}NH_3$)(py)(N_3)(5′-GMP-*N7*)]$^+$ was detected in the mass spectrum of irradiated samples of **4** containing 5′-GMP.
- Peak **79** decreased in intensity upon further irradiation (Figure 6.12) which would be expected if azide was still bound to platinum.
- The chemical shifts of *trans*-[Pt^{II}($^{15}NH_3$)(py)Cl(5′-GMP)]$^+$ (**84**) are known (Table 6.3). Due to the similar electronic properties of azide and chloride *trans*-[Pt^{II}($^{15}NH_3$)(py)(N_3)(5′-GMP-*N7*)]$^+$ would be expected to have similar ^1H and ^{15}N chemical shifts. Indeed the chemical shifts of **79** and **84** compare well.
- The main Pt^{IV} photoproduct in the presence of 5′-GMP is the monoazide compound *trans, trans, trans*-[Pt(N_3)(OH)$_3$($^{15}NH_3$)(py)] (**50**; Figure 6.10).

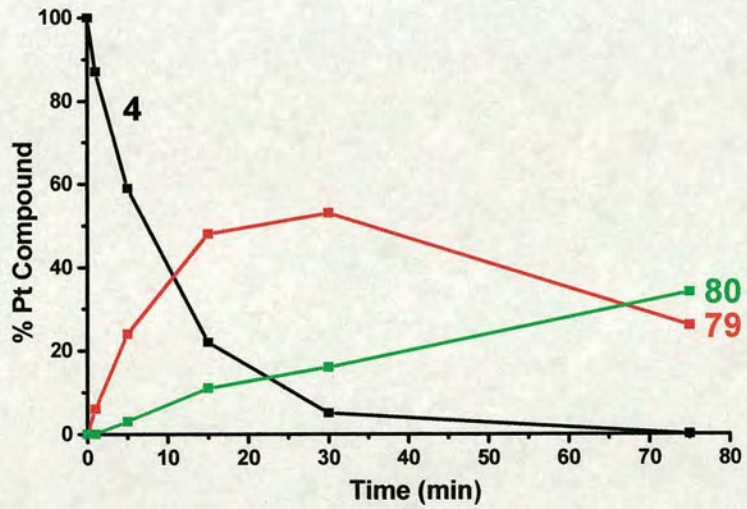

Figure 6.12 The decrease in concentration of complex **4** and formation of complexes **79** and **80** upon irradiation with UVA light based on the integrals of peaks in the 2D [^1H,^{15}N] HSQC NMR spectra.

Peaks **81** and **82** are unassigned, but at least one, if not both, are assignable to species which contain 5′-GMP. One other new H8 peak (8.84 ppm) can be seen in the ^{1}H NMR spectra (Figure 6.13), however it is possible that yet another H8 peak could be masked by the pyridine resonances. There was no evidence for pyridine release during the irradiation of complex **4** in the presence of 5′-GMP.

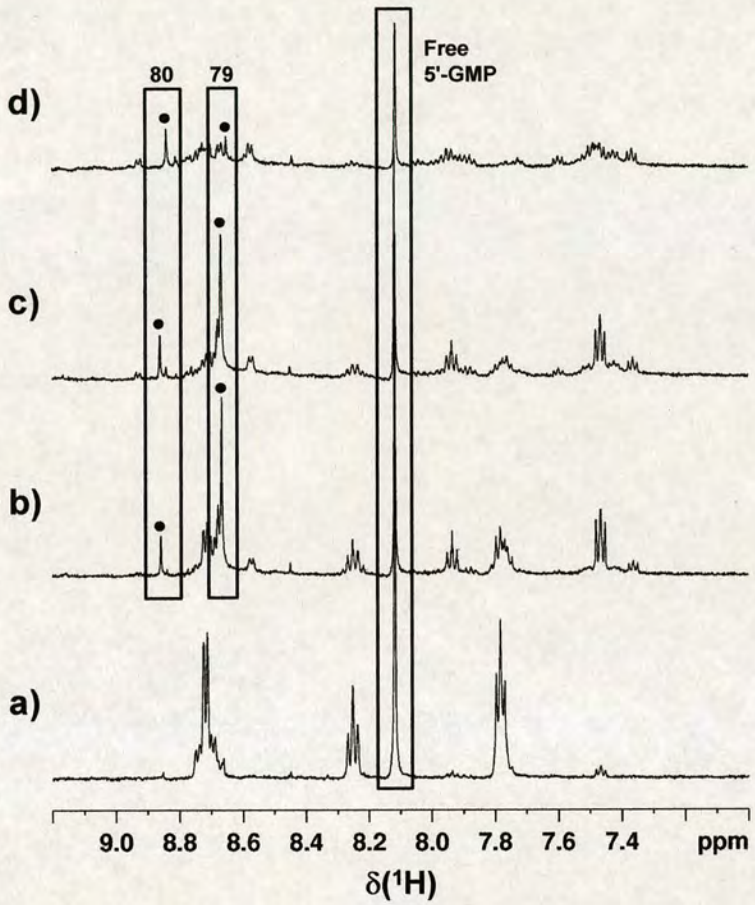

Figure 6.13 ^{1}H NMR spectra for the reaction of *trans, trans, trans*-$[Pt(N_3)_2(OH)_2(^{15}NH_3)(py)]$ in the presence of 2 mol equiv 5′-GMP after irradiation for a) 1 min, b) 15 min, c) 30 min, and d) 75 min. The H8 peaks of 5′-GMP are boxed and highlighted with filled circles (●).

The reaction between complex **4** and 5′-GMP was repeated using red light (647.1 nm, ~15 mW). Peaks corresponding to *trans*-$[Pt(^{15}NH_3)(py)(N_3)(5'\text{-GMP})]$ (**79**) and *trans*-$[Pt(^{15}NH_3)(py)(5'\text{-GMP})_2]^{2+}$ (**80**) appeared after 2.5 h irradiation (Figure 6.14). This is remarkable considering the low power and the weak absorbance of **4** at this wavelength ($\varepsilon_{647} = 3\ M^{-1}cm^{-1}$).

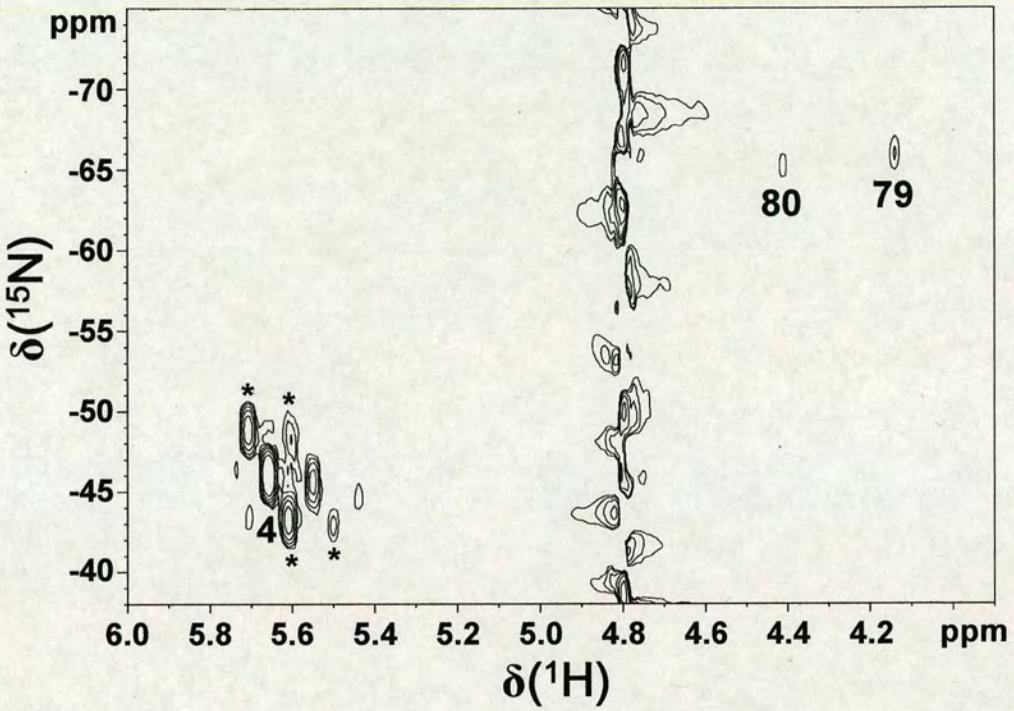

Figure 6.14 2D [^{1}H,^{15}N] HSQC NMR spectra of *trans, trans, trans*-[$Pt(N_3)_2(OH)_2(^{15}NH_3)(py)$] (3 mM) in the presence of 2 mol equiv 5′-GMP after 150 min irradiation with red light (647.1 nm, ~15 mW). * ^{195}Pt satellites.

6.3.2 Photoreactions of Pt^{IV} Azide Complexes with d(GpG)

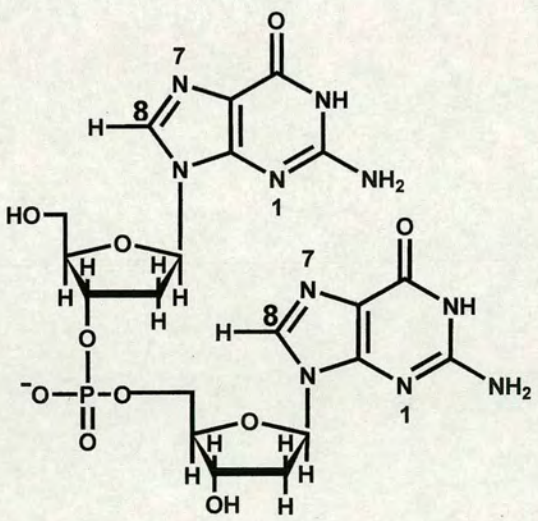

Figure 6.15 Structure of d(GpG).

6.3.2.1 *Cis, trans, cis*-$[Pt(N_3)_2(OH)_2(^{15}NH_3)_2]$ (**1**)

A solution of *cis, trans, cis*-$[Pt(N_3)_2(OH)_2(^{15}NH_3)_2]$ (0.75 mM) and the sodium salt of d(GpG) (0.5 mM) was irradiated with UVA light. 1D [^{1}H] and 2D [^{1}H,^{15}N] NMR spectra were acquired after 0, 3, 6, 11, 16, 26, 36, 46 and 56 min with the pH readjusted to 5.

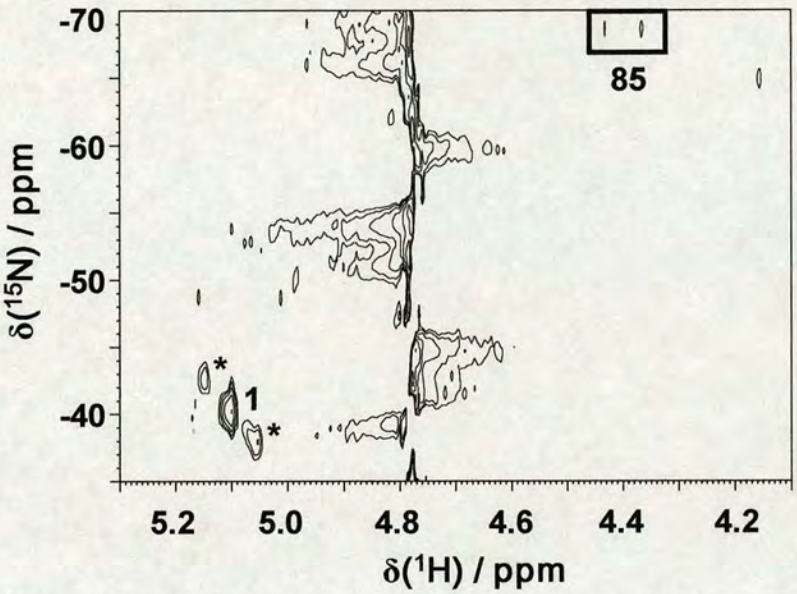

Figure 6.16 2D [^{1}H,^{15}N] HSQC NMR spectrum of *cis, trans, cis*-$[Pt(N_3)_2(OH)_2(^{15}NH_3)_2]$ (0.75 mM) and d(GpG) (0.5 mM) after 11 min of UV irradiation.^{195}Pt satellites are indicated by *.

Figure 6.16 shows a peak for *cis, trans, cis*-$[Pt(N_3)_2(OH)_2(^{15}NH_3)_2]$ and two small peaks which correspond to *cis*-$[Pt(^{15}NH_3)_2)_2(d(GpG)\text{-}N7(1),N7(2))]^{2+}$ δ(^{1}H,^{15}N) (4.45, -68.30 / 4.38, -68.10) (**85**) after 11 min irradiation.[12] These new Pt^{II} peaks first appear after 11 min, but do not significantly increase in intensity upon further irradiation. The concentration of the Pt^{IV} starting material does, however, continue to decrease.

6.3.2.2 *Cis, trans*-$[Pt(^{15}N\text{-}en)(N_3)_2(OH)_2]$

A solution of *cis, trans*-$[Pt(^{15}N\text{-}en)(N_3)_2(OH)_2]$ (0.75 mM) and d(GpG) (0.5 mM) was irradiated with UV light. NMR spectra were acquired after 0, 1, 3, 6, 11, 16, 26, 36 and 46 min. The pH was readjusted to 5 after each irradiation and before NMR analysis.

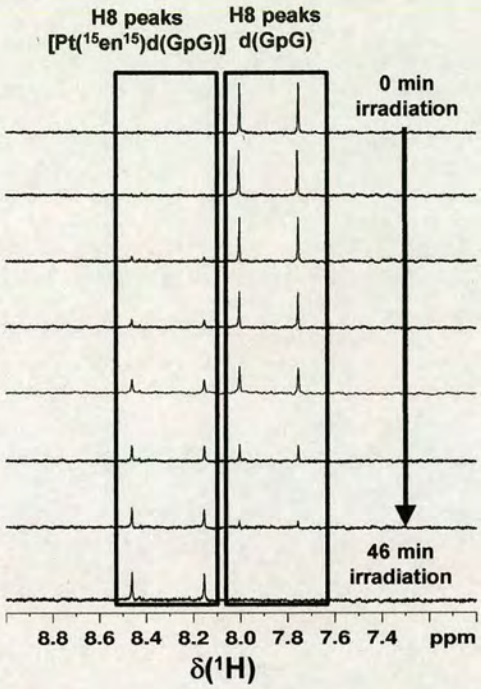

Figure 6.17 [^{1}H] NMR spectra of the H8 region of *cis, trans*-[Pt(^{15}N-en)$(N_3)_2(OH)_2$] (0.75 mM) and d(GpG) (0.5 mM) after irradiation with UV light for various lengths of time.

Figure 6.17 shows peaks assignable to the H8 of free d(GpG) (8.02, 7.78 ppm) and for Pt^{II}-bound (8.48, 8.17 ppm). This low-field shift of about 0.4 ppm of H8 is characteristic of Pt binding to N7 of d(GpG).[13]

The 2D [^{1}H,^{15}N] HSQC NMR spectrum of complex **2** in the presence of d(GpG) (Figure 6.18a) after 26 min irradiation contained a new set of cross-peaks (**86**, 5.64, -31.22 ppm) which consists of four resonances of equal intensity and is separated into two pairs associated with distinct ^{15}N chemical shifts 5.58, 5.62 / -31.47 ppm and 5.66, 5.71 / -31.10 ppm. This is the region where $Pt^{II}(^{15}NH_2)$ *trans* to N peaks are expected,[14] and the shifts agree well with those reported for [Pt(en)(d(GpG)-*N7,N7*)]$^{2+}$ (**86**).[15] These peaks first appear after 3 min of irradiation, and continue to increase in intensity until about 30 min (Figure 6.18b). Only 2 other new peaks (6.30, -8.15 and 6.27, -16.68) were seen during the course of the reaction. These were relatively small and are most likely to be Pt^{IV} substitution photoproducts (Figure 6.18a).

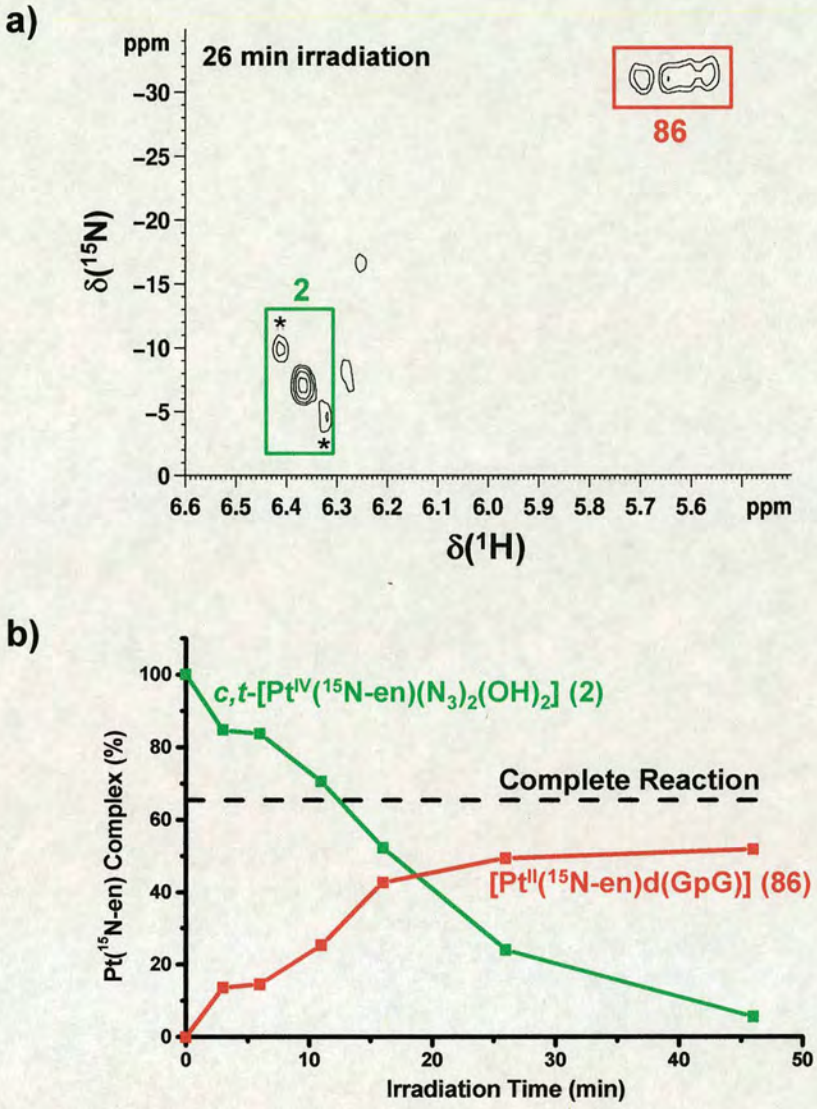

Figure 6.18 Photoreaction of *cis, trans*-[Pt(^{15}N-en)$(N_3)_2(OH)_2$] and d(GpG). a) 2D [^{1}H,^{15}N] HSQC NMR spectrum of *cis, trans*-[Pt(^{15}N-en)$(N_3)_2(OH)_2$] and d(GpG) after irradiation for 26 min. b) Progress of the reaction based on peak integrals for both 1D ^{1}H and 2D [^{1}H,^{15}N] spectra. If the reaction had gone to completion and platinum was bound to all the d(GpG) present, the amount of [Pt(^{15}N-en)(d(GpG)-*N*7(1),*N*7(2))]$^{2+}$ formed would be 67 %, as indicated by the dotted line.

6.3.3 Transcription Mapping of DNA Adducts

Transcription mapping studies on a 212 base pair (bp) fragment of pSP73KB plasmid DNA treated with *cis, trans*-[Pt(en)$(N_3)_2(OH)_2$] and irradiated, were carried out to investigate the selectivity of platination and compare it with that of cisplatin.[16] *In*

vitro RNA synthesis by RNA polymerases on DNA templates which contain several types of bifunctional adducts of platinum complexes, can be prematurely terminated at the level or in the proximity of the adducts.[3,4,17,18] Importantly, monofunctional DNA adducts of several platinum complexes, such as [PtCl(dien)]Cl or $[PtCl(NH_3)_3]Cl$ are unable to terminate RNA synthesis.

Cutting of pSP73KB DNA by *Nde*I and *Hpa*I restriction endonucleases yielded a 212-bp fragment (a substantial part of its nucleotide sequence is shown in Figure 6.19a).[3,4] This fragment contained a T7 RNA polymerase promotor in the upper strand close to its 3' end. The experiments were carried out using this linear DNA fragment, treated with *cis, trans*-$[Pt(en)(N_3)_2(OH)_2]$ at $r_i = 0.5$ (r_i is defined as the molar ratio of free platinum complex to nucleotide phosphates at the onset of incubation with DNA) and cisplatin at $r_b = 0.01$, for RNA synthesis by T7 RNA polymerase.

Two samples of plasmid DNA were treated with *cis, trans*-$[Pt(en)(N_3)_2(OH)_2]$, one was irradiated while the other was kept in the dark. Both samples were precipitated with ethanol, dissolved in 10 mM Tris.HCl plus 0.1 M EDTA (pH 7.2) and then the platinum content estimated by FAAS. The non-irradiated sample contained no platinum, whereas the irradiated sample was modified at a level of $r_b = 0.01$. RNA synthesis on the template modified by *cis, trans*-$[Pt(en)(N_3)_2(OH)_2]$ / irradiation and by cisplatin yielded fragments of defined sizes (Figure 6.19b), which indicates that RNA synthesis on these templates was prematurely terminated. The major stop sites produced by the irradiated template (Figure 6.19b, lane "Irradiated") were similar to those produced by cisplatin (Figure 6.19, lane "Cisplatin"), however no stop sites were produced by the template treated with *cis, trans*-$[Pt(en)(N_3)_2(OH)_2]$ which was not irradiated. The stop sites produced by the irradiated sample and those modified by cisplatin appeared at guanines mainly contained in GG sequences (i.e. at the sites which are preferential DNA binding sites of cisplatin.[2,19]

a)

```
                                  1
                    ●●          ●●          ●          ●
5'  ATTTAGGTGA CACTATAGAA CCAGATCTGA TATCATCGAT
3'  TAAATCCACT GTGATATCTT TGTCTAGACT ATAGTAGCTA

24
●       ●●●     ●●          ●●●             ●●
GAATTCGAGC TCGGATCCTC TAGAGTCGAC CTGCAGGCAT
CTTAAGCTCG AGCCTAGGAG ATCTCAGCTG GACGTCCGTA

64                                        T7
GCAAGCTTCA GCTGCTGCAG GCCGGTCTCC CTATA 3'
CGTTCGAAGT CGACGACGTC CGGCCAGAGG GATAT 5'
```

b)

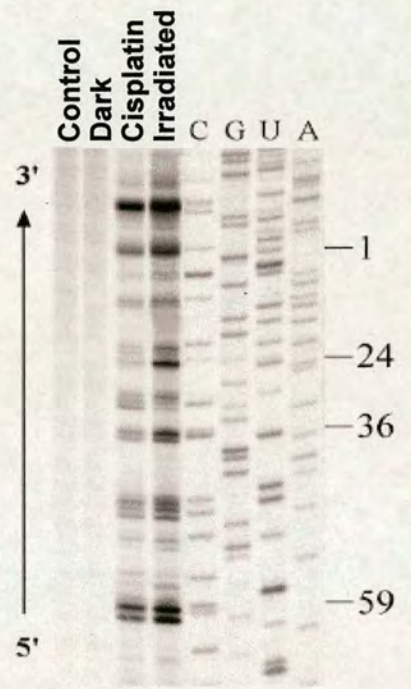

Figure 6.19 Inhibition of RNA synthesis by T7 RNA polymerase on the *Nde*I/*Hpa*I fragment of pSP73KB plasmid modified by *cis, trans*-[Pt(en)$(N_3)_2(OH)_2$] and cisplatin. a) Schematic diagram showing the portion of the nucleotide sequence used to monitor inhibition of RNA synthesis by *cis, trans*-[Pt(en)$(N_3)_2(OH)_2$] and cisplatin. The arrow indicates the start of the T7 RNA polymerase. (•), major stop signals (from 6.19b, lane Irradiated). The numbers correspond to the nucleotide numbering in the sequence map of pSP73KB plasmid. b) Autoradiogram of 6% polyacrylamide / 8 M urea sequencing gel. Lanes: Control - nonmodified template; Dark - the template modified by *cis, trans*-[Pt(en)$(N_3)_2(OH)_2$] and not irradiated; Cisplatin - the template modified by cisplatin; Irradiated - the template modified by *cis, trans*-[Pt(en)$(N_3)_2(OH)_2$] and irradiated.

6.3.4 HPLC Analysis of DNA Adducts

A 40-bp deoxyribooligonucleotide duplex (with a random nucleotide sequence) was treated with *cis, trans*-[Pt(en)$(N_3)_2(OH)_2$] and irradiated, an identical sample was kept in the dark. Both samples treated with *cis, trans*-[Pt(en)$(N_3)_2(OH)_2$] were exhaustively dialyzed against 100 mM $NaClO_4$ in the dark and the content of platinum in these samples was estimated by FAAS. The nonirradiated sample contained no platinum, whereas the irradiated sample was modified at a level of r_b = 0.07. Both samples treated with *cis, trans*-[Pt(en)$(N_3)_2(OH)_2$] and the control (nonmodified) sample were enzymatically digested to mononucleosides. RP-HPLC analysis of enzymatic digests of oligonucleotide duplexes was performed by recording the optical density at 260 nm.

Well-resolved mononucleoside peaks were observed in the profiles, which reflected the proper proportions of the single mononucleosides in the non-modified duplex when integrated and normalized by their extinction coefficients. Digestion of the duplex which was treated with *cis, trans*-[Pt(en)$(N_3)_2(OH)_2$], but not irradiated produced the mononucleoside peaks whose integrated area remained unaffected (not shown). In contrast, digestion of the platinated sample which was irradiated resulted mainly in the decrease of the integrated area of the deoxyriboguanosine peak, and to a markedly smaller extent also in the decrease of the deoxyriboadenosine peak (Figure 6.20). The peaks for deoxyribocytidine and thymidine were not affected. It was verified by FAAS that no product containing platinum co-eluted with the peaks. The platinated products were not retained by the column under the conditions used, so they could not be identified and quantified. The integrated area of the deoxyriboguanosine peak decreased by 58% and that of the deoxyriboadenosine peak by 2%.

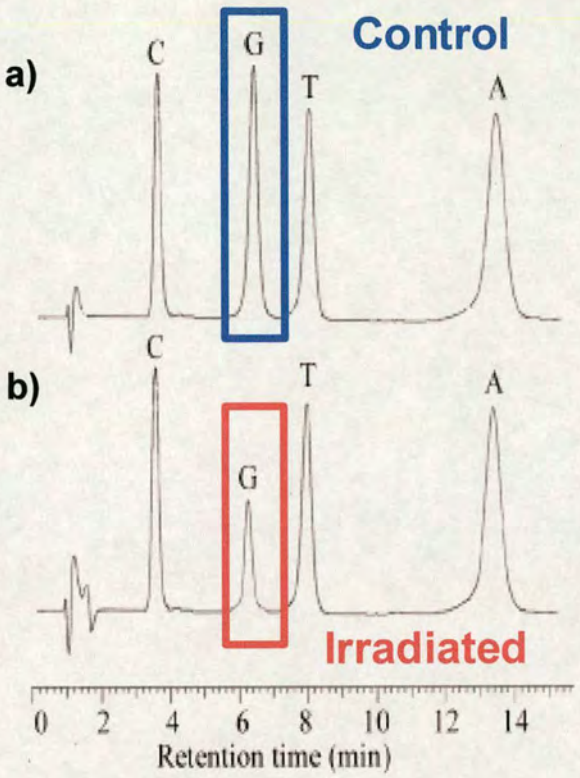

Figure 6.20 Reverse phase C18 HPLC separation of the products of the enzymatic digest of the 40-bp oligonucleotide duplex. a) Control (nonmodified) and b) modified by *cis, trans*-$[Pt(en)(N_3)_2(OH)_2]$ and irradiated.

6.4 Discussion

6.4.1 Photoreactions of Pt^{IV} Azide Complexes with 5′-GMP and 9-Ethylguanine

The target for cisplatin and other related platinum anticancer drugs is DNA,[20] the preferred binding site is the N7 position of guanine bases. The interaction of several Pt^{IV} azide complexes with 5'-GMP and / or 9-EtG upon irradiation was investigated. When the platinum complexes are ^{15}N-labelled this reaction can be followed by 2D [^{1}H,^{15}N] HSQC NMR spectroscopy.

6.4.1.1 *Cis, trans, cis*-$[Pt(N_3)_2(OH)_2(^{15}NH_3)_2]$ (**1**)

The chemical shifts of the new Pt^{II} peaks produced on irradiation at 365 nm of aqueous solutions of *cis, trans, cis*-$[Pt(N_3)_2(OH)_2(^{15}NH_3)_2]$ (**1**) and 5′-GMP, are all in the region for H_3N-Pt *trans* to nitrogen.[14] The main Pt^{II} product can be assigned as *cis*-$[Pt(^{15}NH_3)_2(5'\text{-GMP})_2]^{2+}$ (**70**) from literature values.[6] Interestingly a peak for the

trans isomer *trans*-$[Pt(^{15}NH_3)_2(5'\text{-GMP})_2]^{2+}$ (**74**) also appeared after 5 min. Photoisomerisation could have occurred when the complex was in the Pt^{II} or Pt^{IV} oxidation state, or during the reduction step. Photoisomerisation of platinum compounds has been reported previously.[21,22]

No cross-peaks due to photoproducts such as *cis*-$[Pt(^{15}NH_3)_2(OH/OH_2)_2]^{2+}$ or *cis*-$[Pt(^{15}NH_3)_2(OH/OH_2)(5'\text{-GMP})]^{2+}$ appeared, although they are possible intermediates. Their absence indicates that platinum binding to 5′-GMP is rapid upon loss of the azide ligand(s).

These results compare well with those of a similar reaction carried out with blue light (457.9 nm).[5,12] The same five peaks (**70** – **74**) are observed even though the pH was adjusted to 5 before irradiation but not changed again after. During irradiation with UVA light, the pH was readjusted to 5 after each irradiation (0, 1, 5, 15, 30, 60 and 120 min). The reaction with blue light is much slower, as would be expected due to the much lower absorbance at 457.9 nm (18 $M^{-1}cm^{-1}$), compared to 365 nm (298 $M^{-1}cm^{-1}$).

6.4.1.2 *Trans, trans, trans*-$[Pt(N_3)_2(OH)_2(^{15}NH_3)_2]$ (**3**)

No reaction was observed between *trans, trans, trans*-$[Pt(N_3)_2(OH)_2(^{15}NH_3)_2]$ and 5′-GMP in the dark (Chapter 5, Section 5.3.1.3), but after irradiation for only one minute, 7 % of the starting material underwent photoreduction and photosubstitution to produce *trans*-$[Pt(^{15}NH_3)_2(5'\text{-GMP-}N7)_2]^{2+}$ (**74**; Figure 6.5).[7] This is remarkable as only a very small amount of reduction was seen after 60 min irradiation of *trans, trans, trans*-$[Pt(N_3)_2(OH)_2(^{15}NH_3)_2]$ in the absence of nucleotides (Chapter 5, Section 5.3.2.1c). After 1 h, > 75 % of *trans, trans, trans*-$[Pt(N_3)_2(OH)_2(^{15}NH_3)_2]$ was bound to 5′-GMP as the *trans* bis-G adduct (Figure 6.6).

To confirm that platinum was bound to 5′-GMP in the N7 position a ^1H NMR pH titration over the range pH 1 -11 was carried out. Free 5′-GMP binds two protons at the phosphate group and one at the N7 position (Figure 6.3).[9] The pK_a values of 5′-GMP are listed in Table 6.5.

Table 6.5 pK_a values of 5′-GMP.[9]

Deprotonation	pK_a
-P(O)-$(OH)_2$	0.3 ± 0.2
N7 H	2.48 ± 0.04
-P(O)(O^-)(OH)	6.25 ± 0.02
N1 H	9.49 ± 0.02

Protonation of N1 and N7 of free 5′-GMP cause the H8 ^{1}H NMR signal to shift to lower field, whereas phosphate protonation causes a shift to higher field (Figure 6.8).[10] Figure 6.8 shows that the H8 shift associated with N7 protonation is absent for photoproduct **74** indicating that platinum is bound to 5′-GMP in the N7 position.[7]

Figure 6.6 plots the decay of the 5′-GMP and complex **3** peaks, and the formation of *trans*-[Pt($^{15}NH_3$)$_2$(5′-GMP-*N7*)$_2$]$^{2+}$ upon irradiation. After 120 min there is no *trans, trans, trans*-[Pt(N_3)$_2$(OH)$_2$($^{15}NH_3$)$_2$] left but there is still some free 5′-GMP, and ~74 % has been converted into *trans*-[Pt($^{15}NH_3$)$_2$(5′-GMP-*N7*)$_2$]$^{2+}$. The other ~26 % of Pt-$^{15}NH_3$ is contained in 3 other platinum(II) complexes (**75**, **76** and **77**) which have peaks close to those of **74** (Figure 6.5). Cross-peak **75** has been assigned as *trans*-[Pt($^{15}NH_3$)$_2$(OH_2)$_2$]$^{2+}$ from literature values.[6]

Irradiated solutions of complex **3** and 5′-GMP, as well as ^{15}N-labelled NMR samples, were analysed by ESI-MS in the hope of detecting a peak for **74** (*trans*-[Pt($^{15}NH_3$)$_2$(5′-GMP-*N7*)$_2$]$^{2+}$). However this complex was never observed, which could perhaps be due to the charge on the phosphate groups interfering; this charge depends on the pH. When complex **3** was irradiated in the presence of 9-ethylguanine (9-EtG) (Figure 6.3), [^{1}H, ^{15}N] HSQC NMR spectroscopy showed the major product was a Pt^{II} complex (4.04, -61.42 ppm). Upon analysis by mass spectrometry, a peak for [Pt($^{15}NH_3$)$_2$(9-EtG)$_2$]$^{2+}$ with the appropriate isotope pattern was seen. This result helps to confirm that the major product upon irradiation of complex **3** and 5′-GMP is the bis *trans* GMP adduct **74**, and shows that when there are no phosphate groups present, the product can be detected easily by mass

spectrometry.

After observing the efficiency of the photoreaction of complex **3** and 5′-GMP using UVA light, it was repeated with red light (λ = 647.1 nm). The reason for attempting this reaction is because of the greater depth of penetration into tissue of light with a longer wavelength.[23] After 90 min irradiation (647.1 nm, P = 18 mW), a peak for **74** was present. This is remarkable considering the relatively low power, and the weak absorbance at 647.1 nm ($\varepsilon = 8\ M^{-1}cm^{-1}$).

The formation of a major product (**74**) on irradiation of complex **3** in the presence of 5′-GMP, and absence of the range of side-reactions seen on irradiation of compound complex **3** alone, suggest that 5′-GMP can rapidly trap reactive intermediates produced during the photoexcitation process.[7]

These reactions of **3** with guanine derivatives are remarkable for two reasons. First, platination occurs very rapidly in comparison to reactions of transplatin,[24] and second bis-guanine adducts are readily formed, whereas the progression from mono- to bis-adducts is rarely observed for reactions of transplatin. The lack of ability of transplatin to form bis-G adducts is thought to be responsible for its lack of anticancer activity.[25]

6.4.1.3 *Trans, trans, trans*-$[Pt(N_3)_2(OH)_2(^{15}NH_3)(py)]$ (**4**)

The photoreaction of *trans, trans, trans*-$[Pt(N_3)_2(OH)_2(^{15}NH_3)(py)]$ gave a similar pattern of Pt^{IV} peaks in the 2D [^1H,^{15}N] HSQC spectrum, to those seen upon irradiation of *trans, trans, trans*-$[Pt(N_3)_2(OH)_2(^{15}NH_3)_2]$ (**3**) (Chapter 5). For this reason it was thought that the two compounds acted in a similar way when irradiated. Although this assumption appears to be true for the compounds alone in solution, a different scenario arises when irradiation takes place in the presence of 5′-GMP.

The photoreaction of complex **4** in the presence of 2 mol equiv of 5′-GMP gave unexpected results. The main Pt^{II} photoproduct was not *trans*-$[Pt^{II}(^{15}NH_3)(py)(5'\text{-}GMP)_2]^{2+}$, as for complex **3** for which the main photoproduct was *trans*-

$[Pt(^{15}NH_3)_2(5'\text{-GMP})_2]^{2+}$ (**74**), although this complex did appear after only 5 min irradiation. The main photoproduct is assigned as the Pt^{II} monoazide compound *trans*-$[Pt^{II}(^{15}NH_3)(py)(N_3)(5'\text{-GMP})]^{+}$ (**79**) for reasons described in detail in Section 6.3.1.2. This indicates that Pt^{IV} is probably not reduced only by the azide ligands, which agrees with the previous results where complexes **3** and **4** were not significantly reduced when irradiated on their own. Previous work has shown that 5′-GMP can reduce Pt^{IV} compounds to their Pt^{II} counterparts, and the required electrons are believed to come from the sugar fragment.[26,27] In theory it should be possible to observe such changes by ^1H NMR, however the region of the spectrum which contains the peaks for the 5′-GMP sugar ring contains many peaks and it is not possible to separate and identify them.

Loss of the pyridine ring upon irradiation was originally thought to be the reason for the high *in vitro* phototoxicity of complex **4** (Appendix 2). However, NMR studies have shown that the pyridine ring is not released from the platinum centre in the presence or absence of nucleobases (Section 5.3.2.1 and Figure 6.13). This is interesting as it suggests that pyridine may not be readily released under cell testing conditions.

So-called "non-classical" *trans*-platinum compounds (e.g. *trans*-$[Pt(NH_3)LCl_2]$ where L = e.g. quinoline, pyridine, thiazole) have recently been found to be cytotoxic *in vitro*.[28,29] These compounds interact with DNA in a different way to cisplatin, and their increased activity compared to transplatin is believed to be due to reduced reactivity towards biological thiols.[29,30] Unfortunately these complexes have proved inactive *in vivo*, possibly because of their insolubility,[31] and work is now underway to produce water soluble analogues.[32] Complex **4** contains a planar ligand and has *trans* geometry, but also has the added advantage of being extremely water soluble (>50 mM). This could help to explain the increased activity of complex **4**. However there is not yet any clear evidence that DNA is indeed the main (or only) target for photoactivated Pt^{IV}-azide complexes.

6.4.2 Photoreactions of Pt^{IV} Azide Complexes with d(GpG)

Cis-[$Pt^{II}(NH_3)_2${d(GpG)}] accounts for 60 – 65 % of all cisplatin adducts.[2] Diguanine platinum complexes have therefore been used as simple models of the local structures of an intrastrand cross-link of two adjacent guanines in DNA. NMR and X-ray studies have both shown that platinum is bound to the N7 position of guanine.[33,34]

Binding of *cis, trans, cis*-[$Pt(N_3)_2(OH)_2(^{15}NH_3)_2$] and *cis, trans*-[$Pt(^{15}N$-en)$(N_3)_2(OH)_2$] to d(GpG) upon irradiation with blue light (457.9 nm) has previously been shown.[5,12] These reactions were repeated during this work using UVA light (365 nm).

6.4.2.1 *Cis, trans, cis*-[$Pt(N_3)_2(OH)_2(^{15}NH_3)_2$] (**1**)

The reaction of *cis, trans, cis*-[$Pt(N_3)_2(OH)_2(^{15}NH_3)_2$] with d(GpG) upon irradiation resulted in two new NMR peaks which corresponded to the N7-bound product [$Pt(^{15}NH_3)_2$(d(GpG)-*N7,N7*)] (**85**).[5] These peaks first appeared after 11 min, but did not increase upon further irradiation and were not very intense.

A similar experiment has previously been carried out with blue light (457.9 nm)[5] and all the d(GpG) was bound to platinum after only 0.77 h. The remaining *cis, trans, cis*-[$Pt(N_3)_2(OH)_2(^{15}NH_3)_2$] continued to decrease in concentration and the formation of a yellow precipitate was observed. A peak for NH_4^+ also appeared and increased in intensity with irradiation. Neither a yellow precipitate nor a NH_4^+ peak was observed during the reaction with UVA light.

The main difference between the reactions with blue and UVA light was the pH. The pH was adjusted to 5 before irradiation with 457.9 nm light, but was not adjusted again, whereas the pH was readjusted to 5 after each irradiation with UV light. It seems that changing the pH alters the course of the reaction with d(GpG) in a way that is not seen for the analogous reaction with 5′-GMP. The pK_a of the phosphate group in d(GpG) is low (ca. 1),[33] whereas the 5′-GMP phosphate group has a pK_a between 6 and 7.[9] Therefore perhaps the buffer effect of 5′-GMP is playing a role.

6.4.2.2 *Cis, trans*-[Pt(^{15}N-en)$(N_3)_2(OH)_2$] (**2**)

Irradiation of **2** in the presence of d(GpG) quickly gave rise to new cross-peaks assignable to Pt^{IV} isomers/substitution products and to the Pt^{II} species [Pt(^{15}N-en)d(GpG)-*N7,N7*] (**86**) (Figure 6.18a), an intrastrand GG cross-link of the type formed by cisplatin on DNA.[2] The ^{1}H NMR spectra in Figure 6.17 confirm that binding occurs to N7 of G. Overall the photoreaction can be represented as:

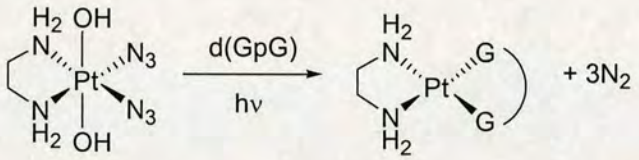

It is notable that platination of DNA can occur more rapidly via this photoactivation pathway than by the usual chemical activation of cisplatin, which is determined by slow rate-limiting hydrolysis steps.[35,36]

There is no significant increase in the intensity of peak **86** after ~30 min of irradiation, although the intensity of complex **2** further decreases.

This experiment has been previously carried out using blue light (457.9 nm, 10 mW).[5,12] The sample was irradiated directly in the NMR probe and the pH adjusted to 5 only at the start. The reaction with blue light was much slower, as expected due to the much lower absorbance of **2** at 457.9 nm (ε = 8 $M^{-1}cm^{-1}$) compared to 365 nm (ε = 298 $M^{-1}cm^{-1}$). No intermediates appeared in the reaction with UVA light, the only new peaks were due to the product **86** and these peaks compared well with those produced upon irradiation with blue light.

6.4.3 Transcription Mapping of DNA Adducts

The profile of DNA platination of a 212-bp fragment of plasmid DNA was determined by transcription mapping of the DNA adducts. Platination was carried out by incubating the DNA fragment with complex **2** and then irradiating. RNA synthesis can be instigated on the fragment by T7 polymerase, but this synthesis is prematurely terminated by bifunctional platinum adducts. Importantly

monofunctional DNA adducts are unable to stop RNA synthesis. The aim of this experiment was to investigate the photoinduced platination of DNA by **2** and compare its base selectivity with that of cisplatin. Complex **2** was chosen for this study because of the efficiency of its reaction with d(GpG) (Section 6.3.2.2), and previous workers have shown that $[Pt^{II}(en)Cl_2]$ forms adducts with DNA which are the same as those formed by cisplatin.[37,38]

Platinum determination by FAAS showed that no platinum binding to DNA occurred in the dark, but platination levels of r_b = 0.01 (one bound Pt per 100 nucleotides) were attained on irradiation. The major stop sites on the irradiated fragment were similar to those produced by cisplatin, and appeared at guanine residues mainly contained in GG sequences (Figure 6.19b). These results demonstrate the high specificity of **2** for G and the preferential formation of predominantly GG intrastrand cross-links is evident. These results were confirmed by HPLC analysis

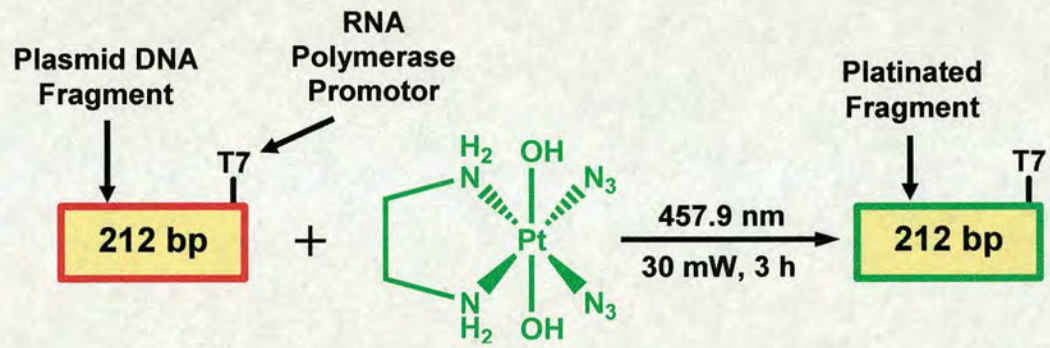

Figure 6.21 Transcription mapping study of a 212-bp fragment of plasmid DNA platinated by *cis, trans*-$[Pt(en)(N_3)_2(OH)_2]$ and irradiated.

6.4.4 HPLC Analysis of DNA Adducts

HPLC analysis of enzymatic digests of a synthetic 40-bp oligonucleotide duplex, irradiated in the presence of complex **2** suggested that the major binding sites involve bifunctional GG adducts which is in agreement with the transcription mapping results.

The r_b of the irradiated sample was 0.07, at this r_b 5.6 or 11.2 guanines would be

platinated depending on whether the adducts were monofunctional of bifunctional, respectively. The 40-bp duplex used in these analyses contained 17 guanine residues. Thus, the decrease of the deoxyriboguanosine peak corresponds to the loss of ~9.9 guanine residues. The peaks corresponding to other nucleosides were unchanged (only deoxyriboadenosine peak decreased by 2%), which implies that guanine residues were preferentially platinated by complex **2** after irradiation and mainly in a bifunctional manner. This confirms the transcription mapping results where the platinum adducts were found at consecutive GG bases.

6.5 Conclusions

One of the main mechanisms of photoactivation of Pt^{IV} azide complexes reported in the literature,[39,40] involves the concerted release of the azide ligands in the form of two azide radicals. Two electrons are transferred to the platinum centre (one from each azide ligand) which results in a reduction from Pt^{IV} to Pt^{II}. The reluctance of the *trans* compounds (**3** and **4**) to photoreduce when irradiated on their own (Chapter 5) hinted that this was not the mechanism of photoactivation (at least for *trans* complexes). The assignment of the main photoproduct from irradiation of **4** plus 5′-GMP as the monoazide complex *trans*-[$Pt(N_3)$(5′-GMP)($^{15}NH_3$)(py)], indicates the formation of azide radicals is definitely not the only mechanism by which azides are lost from this compound. More detailed experiments are required to fully define the photoactivation pathway, which may be different for complex **4** compared to the other Pt^{IV} azide complexes, and may help to explain its high phototoxicity (Appendix 2).

The transcription mapping study and HPLC studies on complex **2** have shown a similar profile of nucleotide platination on duplex DNA (high specificity for G and the formation of predominantly GG intrastrand cross-links), as cisplatin.

Overall the platinum(IV) diazido compounds investigated (**1**-**4**) have shown a remarkable affinity for G bases, whether in the form of nucleotides, nucleosides, duplex DNA or plasmid DNA, but most importantly these reactions have been observed only upon irradiation, and not in the dark.

6.6 References

[1] Bloemink, M.J.; Reedijk, J. *Metal Ions Biol. Syst.* **1996**, *32*, 641.

[2] Fichtinger-Schepman, A.M.J.; Van der Veer, J.L.; Den Hartog, J.H.J.; Lohman, P.H.M.; Reedijk, J. *Biochemistry* **1985**, *24*, 707.

[3] Brabec, V.; Leng, M. *Proc. Natl. Acad. Sci. USA* **1993**, *90*, 5345.

[4] Lemaire, M.A.; Schwartz, A.; Rahmouni, A.R.; Leng, M. *Proc. Natl. Acad. Sci. USA* **1991**, *88*, 1982.

[5] Müller, P. PhD Thesis, University of Edinburgh **2002**.

[6] Berners-Price, S.J.; Frenkiel, T.A.; Ranford, J.D.; Sadler, P.J. *J. Chem. Soc., Dalton Trans.* **1992**, 2137.

[7] Mackay, F.S.; Woods, J.A.; Moseley, H.; Ferguson, J.; Dawson, A.; Parsons, S.; Sadler, P.J. *Chem. Eur. J.* **2006**, *12*, 3155.

[8] Chu, G.Y.H.; Mansy, S.; Duncan, R.E.; Tobias, R.S. *J. Am. Chem.Soc.* **1978**, *100*, 593.

[9] Sigel, H.; Massoud, N.A.; Corfu, J. *J. Am. Chem. Soc.* **1994**, *116*, 2958.

[10] Scheller, K.H.; Scheller-Krattiger, V.; Martin, R.B. *J. Am. Chem. Soc.* **1981**, *103*, 6833.

[11] Berners-Price, S.J.; Frey, U.; Ranford, J.D.; Sadler, P.J. *J. Am. Chem. Soc.* **1993**, *115*, 8649.

[12] Müller, P.; Schroder, B.; Parkinson, J.A.; Kratochwil, N.A.; Coxall, R.A.; Parkin, A.; Parsons, S.; Sadler, P.J. *Angew. Chem. Int. Ed.* **2003**, *42*, 335.

[13] Chu, G.Y.H.; Mansy, S.; Duncan, R.E.; Tobias, R.S. *J. Am. Chem.Soc.* **1978**, *100*, 593.

[14] Berners-Price, S.J.; Sadler, P.J. *Coord. Chem. Rev.* **1996**, *151*, 1.

[15] Berners-Price, S.J.; Ranford, J.D.; Sadler, P.J. *Inorg. Chem.* **1994**, *33*, 5842.

[16] Kašpárková, J.; Mackay, F.S.; Brabec, V.; Sadler, P.J. *J. Biol. Inorg. Chem.* **2003**, *8*, 741.

[17] Kašpárková, J.; Novakova, O.; Vrana, O.; Farrell, N.; Brabec, V. *Biochemistry* **1999**, *38*, 10997.

[18] Zaludova, R.; Zakovska, A.; Kašpárková, J.; Balcarova, Z.; Kleinwächter, V.; Vrana, O.; Farrell, N.; Brabec, V. *Eur. J. Biochem.* **1997**, *246*, 508.

[19] Eastman, A. *Pharmcol. Ther.* **1987**, *34*, 155.

[20] Jamieson, E.R.; Lippard, S.J. *Chem.Rev.* **1999**, *99*, 2467.

[21] Kuroda, R.; Neidle, S.; Ismail, I.M.; Sadler, P.J. *Inorg.Chem.* **1983**, *22*, 3620.

[22] Barnard, C.F.J.; Vollano, J.F.; Chaloner, P.A.; Dewa, S.Z. *Inorg. Chem.* **1996**, *115*, 3280.

[23] Wan, S.; Parrish, J.A.; Anderson, R.R.; Madden, M. *Photochem. Photobiol.* **1981**, *34*, 679.

[24] Natile, G.; Coluccia, M. *Coord. Chem. Rev.* **2001**, *216-217*, 383.

[25] Boudvillain, M. ; Dalbiès, R. ; Aussourd, C. ; Leng, M. *Nucl. Acids Res.* **1995**, *23*, 2381.

[26] van der Veer, J.; Peters, A.R.; Reedijk, J. *J. Inorg. Biochem.* **1986**, *26*, 137.

[27] Choi, S.; Mahalingaiah, S.; Delaney, S.; Neale, N.R.; Masood, S. *Inorg. Chem.* **1999**, *38*, 1800.

[28] Beusichem, M.V.; Farrell, N. *Inorg. Chem.* **1992**, *31*, 634.

[29] Bierbach, U.; Qu, Y.; Hambley, T.W.; Peroutka, J.; Nguyen, H.L.; Doedee, M.; Farrell, N. *Inorg. Chem.* **1999**, *38*, 3535.

[30] Bierbach, U.; Farrell, N. *Inorg. Chem.* **1997**, *36*, 3657.

[31] Farrell, N. *Met. Ions Biol. Syst.* **1996**, *32*, 603.

[32] Bierbach, U.; Sabat, M.; Farrell, N. *Inorg. Chem.* **2000**, *39*, 1882.

[33] Girault, J.-P.; Chottard, G.; Lallemand, J.-Y.; Chottard, J.-C. *Biochemistry* **1982**, *21*, 1352.

[34] Sherman, S.E.; Gibson, D.; Wang, A.H.-J.; Lippard, S.J. *Science* **1985**, *230*, 412.

[35] Bancroft, D.P.; Lepre, C.A.; Lippard, S.J. *J. Am. Chem. Soc.* **1990**, *112*, 6860.

[36] Berners-Price, S.J.; Barnham, K.J.; Frey, U.; Sadler, P.J. *Chem. Eur. J.* **1996**, *2*, 1283.

[37] Eastman, A. *Biochemistry* **1983**, *22*, 3927.

[38] Eastman, A. *Biochemistry* **1986**, *25*, 3912.

[39] Vogler, A.; Kern, A.; Hüttermann, J. *Angew. Chem., Int. Ed. Engl.* **1978**, *17*, 524.

[40] Weber, W.; van Eldik, R. *Inorg. Chim. Acta.* **1986**, *111*, 129.

Chapter 7
Multiphoton Excitation

7.1 Introduction

Multiphoton processes were predicted theoretically in 1931 by Maria Göppert-Mayer,[1] however it was not until 30 years later that the first experimental evidence was reported. In 1961 the two-photon excitation (TPE) of a $CaF_2:Eu^{2+}$ crystal was demonstrated by Kaiser and Garrett using a ruby laser.[2]

TPE relies on two photons being almost simultaneously (ca. 10^{-16} s) absorbed by an atom or molecule, this produces an excitation equivalent to the absorption of a single photon of about twice the energy (Figure 7.1). The intermediate state after absorption of the first photon is referred to as the "virtual state", it need not correspond to any electronic or vibrational energy eigenstate (Figure 7.1b).

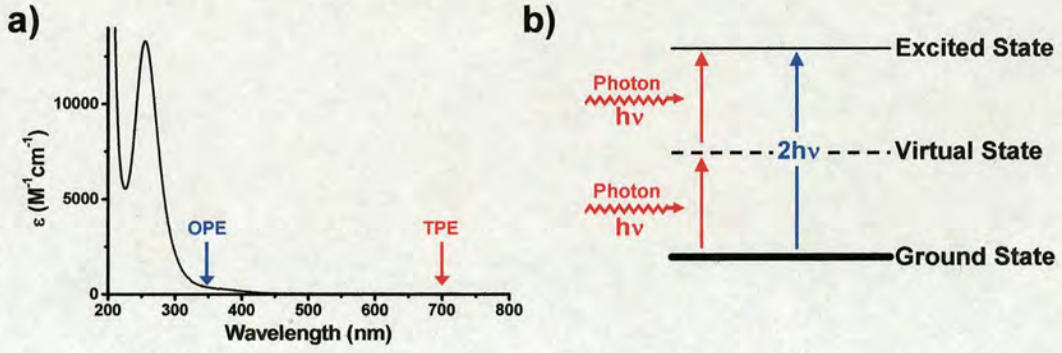

Figure 7.1 Two-photon excitation. a) UV-visible spectrum showing the wavelength of excitation by TPE and OPE. b) Energy level diagram showing that the absorbance of two photons from the red region (700 nm) can excite an atom or molecule to the same state as one photon from the blue region (350 nm).

This theory can also be applied to the absorption of three[3-5] or more photons.[6-8] Research into multiphoton excitation is a rapidly expanding area due to the recent availability of commercial pulsed femtosecond lasers, and also because of the discovery of practical applications, such as 3D data storage,[9-12] fluorescence microscopy,[13-15] and photodynamic therapy (PDT).[16-18]

PDT is a cancer treatment which involves the activation of a photosensitizing drug with light, the mechanism of action is described in more detail in Chapter 1. One of

the main problems associated with PDT is the wavelength of absorbance of most of the drugs; this is the same problem as that encountered with Pt^{IV}-azide compounds. A great deal of work has been done in an attempt to extend the wavelength of absorption of photosensitizers.[19,20] For this reason, attention has turned to the activation of PDT drugs by two-photon excitation.[16,18]

An important property of a molecule undergoing TPE is its two-photon cross-section.[21,22] The one-photon cross-section of a molecule is another way of expressing the extinction coefficient; it is not really related to molecular dimensions, rather it is the strength of the optical transitions and selection rules which are most important. It is expressed as a cross-section because it is easy to imagine a relative capture area. Two-photon cross-sections are similar, but are expressed in units of cm^4s (i.e. the product of two areas and time) because two photons have to be "captured simultaneously". It can also be described as a quantitative measure of the probability of a two-photon absorption.[15] It is possible (although by no means simple) to measure two-photon cross-sections.[23]

TPE depends on two photons interacting with a molecule almost simultaneously, and so has a quadratic dependence on the light intensity. Conventional one-photon excitation (OPE) has a linear dependence on light intensity. TPE probabilities are extremely small and focusing the beam increases the local intensity at the focus point. This can be achieved by placing an objective lens in the path of the beam and ensuring the focal point is within the sample. Away from the focus TPE probability drops off rapidly.

Pulsed lasers are used to further increase the likelihood of two-photons simultaneously interacting with a molecule; this means the "average" power can still be kept relatively low. In the following sections, a mode-locked Ti:Sapphire laser is used to induce two-photon excitation. The term "mode-locked" is used to describe a laser operating with only a certain set of frequencies (modes) propagating in the laser cavity. The phase between these modes is locked, so that there is destructive interference between the propagating frequencies everywhere in the cavity, except at

one point where the waves add constructively.[24] This results in a single short pulse of light travelling in the cavity, with the repetition rate dictated by the distance between the two cavity end mirrors and the speed of light. Femtosecond Ti:Sapphire lasers require a relatively large number of intracavity frequencies to achieve 150-fs pulses, therefore the pulses have a significantly large spectral bandwidth. The Ti:Sapphire laser is capable of TPE in the wavelength range 700 – 1000 nm.

The main advantage of using TPE for the photoactivation of drugs is clearly the accessibility of longer wavelengths. Most porphyrins currently used in PDT are excited between 620 and 690 nm, where the maximum tissue penetration depth is ca. 1 cm.[25] In comparison, a 10-fold increase in the depth of penetration can be achieved by near infrared (NIR) light (750 – 1400 nm).[17] NIR light also minimizes the effects of laser-induced hyperthermia as it has reduced absorption in tissues. The small excitation volumes, which can potentially be confined to the order of ca. 1 μm^3 are also an advantage. The point of activation can be controlled in three dimensions and the problem of absorption all along the beam associated with OPE is overcome.

One of the main problems associated with Pt^{IV}-azide compounds is their wavelength of absorbance. The intense ligand-to-metal charge transfer (LMCT) bands ($N_3 \rightarrow Pt$) are centred in the UV region generally between 250 and 300 nm, at these wavelengths there is virtually no tissue penetration.[26] Attempts to shift this LMCT band and improve absorption in the visible region by synthetic means are discussed in Chapter 3. However, another approach is to use multiphoton excitation, this would enable the use of red or NIR light to activate the compounds.

7.2 Experimental

The platinum compounds *cis, trans*-$[Pt(en)(N_3)_2(OH)_2]$, *trans, trans, trans*-$[Pt(N_3)_2(OH)_2(NH_3)_2]$, *cis, trans*-$[Pt(^{15}N\text{-}en)(N_3)_2(OH)_2]$, *trans, trans, trans*-$[Pt(N_3)_2(OH)_2(^{15}NH_3)(py)]$ and *trans, trans, trans*-$[Pt(N_3)_2(OH)_2(^{15}NH_3)_2]$ were synthesised as described in Chapter 3. *Cis, trans*-$[Pt(en)I_2(OAc)_2]$ was prepared by Dr. Phillipe Müller using the literature method.[27] Azobenzene (99 %), d_6-benzene, d_6-DMSO, DMSO and D_2O were purchased from Aldrich, and 5′-GMP was

purchased from Acros. Azo-dye **1** was supplied by DyStar UK Ltd. and was used without further purification (86 % azo-dye, 14 % NaCl and water).

Irradiations with the argon-krypton laser were carried out as described in Chapter 4. NMR spectra were recorded on a Bruker DMX500 spectrometer and UV-visible spectra were recorded on a Cary 300 Perkin-Elmer photospectrometer. This equipment is described in detail in Chapter 2. A UV lamp was employed for one-photon excitations in the ultraviolet region (365 nm) (Chapter 2). The UV quartz cuvettes used were Hellma cells supplied by Aldrich and were either standard (3.5 mL) or ultra micro (100 μL).

Two-photon excitation was performed with a 10 W Verdi and Mira Ti:Sapphire laser (Coherent) producing pulses of *ca.* 150 fs at 76 MHz, with a full-width half-maximum (FWHM) at 740 nm of 5.6 nm. The pulse width and spectrum were measured with an autocorrelator (Mini, APE) and spectrometer (Wavescan, APE). The laser spectrum was continuously monitored to ensure pulse stability. The laser power was varied with neutral density filters and measured with a power meter (Fieldmaster with LM10 head, Coherent). The laser was focused with a ×4, NA = 0.1, objective lens. For the samples which were irradiated in NMR tubes, the alignment was checked by observing the two-photon fluorescence of a solution of fluorescein in an identical tube, this tube was then replaced with that containing the sample. By approximating the square of the illuminating point spread function as a 3D Gaussian volume,[15] the estimated focal volume was ca. 30 pL.

For two-photon excitation at wavelengths below 700 nm an optical parametric oscillator (OPO) (APE, Berlin) that was synchronously pumped by a modelocked femtosecond Ti:Sapphire laser was used. It was operated in the ring-cavity configuration, which has a single resonant OPO and intracavity SHG (second harmonic generation), and covers the range 525-680 nm, which fills the gap between the Ti-Sapphire output (700-1000nm) and its frequency doubled signal (350 – 500 nm).

The Ti-sapphire laser and optical parametric oscillater were operated by Dr. Stephen Magennis who helped set-up all multiphoton experiments, and also carried out the kinetic calculations in Section 7.3.2.1. Sample preparation, NMR analysis and all other work was carried out by the author.

7.3 Results

7.3.1 *Cis, trans*-[Pt(en)(N_3)$_2$(OH)$_2$]

Initially, the OPE of *cis, trans*-[Pt(en)(N_3)$_2$(OH)$_2$] using the Ti:Sapphire laser (457 nm, 1.5 mW) was investigated. The reaction was followed by observing the change in absorbance at 330 nm (Figure 7.2a). Irradiations were also carried out with the Argon-Krypton laser (457.9 nm, 40 mW) for comparison (Table 7.1). Similar rates of reaction were seen with both lasers (Figure 7.2b). Controls were placed beside the irradiating samples during excitation, but kept in the dark and then treated identically.

TPE using the same set-up did not result in any photoactivation. Many different conditions were tried (Table 7.10) and the samples analysed by UV-visible or NMR spectroscopy.

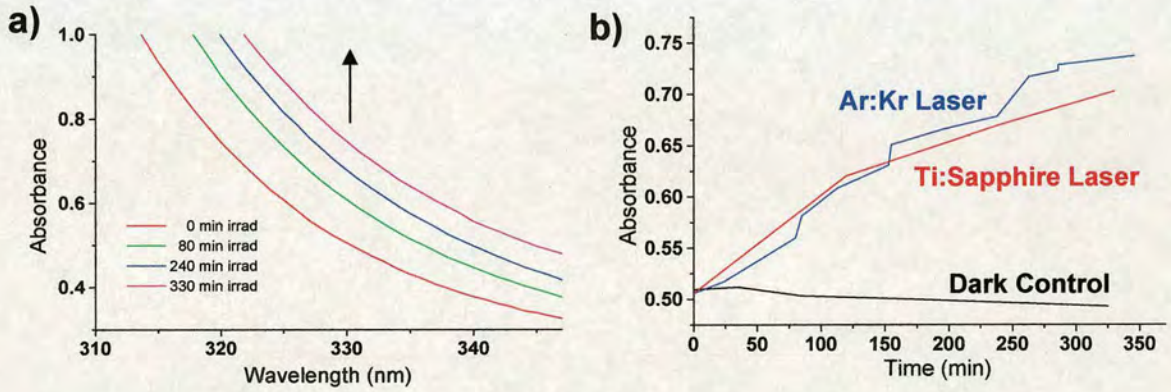

Figure 7.2 One-photon excitation of *cis, trans*-[Pt(en)(N_3)$_2$(OH)$_2$]. a) Change in absorbance at 330 nm upon irradiation of a 1 mM sample in H_2O (Ar-Kr laser 457.9 nm, 40 mW). b) A comparison of the rate of reaction using two different lasers, Ar-Kr laser (457.9 nm, 40 mW) and Ti-Sapphire laser (457 nm, 1.5 mW).

Table 7.1 Experimental conditions for one- and two-photon excitation of *cis, trans*-$[Pt(en)(N_3)_2(OH)_2]$.

λ (nm)	Power (W)	Solvent	Irrad. Vessel	Conc. (mM)	Time (h)	Vol. (mL)	Analysis	Laser
457.9	0.04	H_2O	Cuvette (3.5mL)	1	Various	3	UV-vis	Ar-Kr 1-Photon
457	0.0015	H_2O	Cuvette (3.5mL)	1	2, 4, 5.5	3	UV-vis	Ti-sapphire 1-Photon
914	0.75	H_2O	Cuvette (3.5mL)	1	2	3	UV-vis	Ti-sapphire 2-Photon
800	1.4	H_2O	Cuvette (3.5mL)	1	1	3	UV-vis	Ti-sapphire 2-Photon
800	1.4	H_2O	Cuvette (3.5mL)	1	3.5	1	UV-vis	Ti-sapphire 2-Photon
800	1.4	H_2O	Cuvette (3.5mL)	1	1, 2	1	UV-vis	Ti-sapphire 2-Photon
750	1.4	H_2O	Cuvette (3.5mL)	1	1.5, 3.5	1	UV-vis	Ti-sapphire 2-Photon
760	1	D_2O	Cuvette (100μL)	3	5	0.1	NMR	Ti-sapphire 2-photon
760	1	D_2O	Cuvette (100μL)	0.07	3	0.1	NMR	Ti-sapphire 2-photon
720	0.7	D_2O	Cuvette (100μL)	3	4.5	0.1	NMR	Ti-sapphire 2-photon

7.3.2 Azo-Dye

Photoisomerisation of the azo-dye **1** (Figure 7.3) from *trans* to *cis* can easily be followed by NMR spectroscopy. The ^{1}H NMR spectrum of the *trans* isomer (Figure 7.4a) consists of two singlets, each of relative intensity 1, at 8.67 and 8.40 ppm (H1 and H4, respectively), two doublets, each of intensity 1, at 8.31 and 8.16 ppm (H5 and H7, respectively, ^2J = 1.7 Hz), a doublet of intensity 2 at 8.01 ppm (H3′ and H5′, ^1J = 8.7 Hz), and a doublet of intensity 2 at 7.61 ppm (H2′ and H6′). The *cis* isomer (Figure 7.4b) also consists of two singlets, each of relative intensity 1, at 7.47 and 8.26 ppm (H1 and H4, respectively), two doublets each of intensity 1 at 8.16 and 8.03 ppm (H5 and H7, respectively, ^2J = 1.7 Hz) a doublet of intensity 2 at 7.24 ppm (H3′ and H5′, ^1J = 8.7 Hz), and a doublet of intensity 2 at 7.16 ppm (H2′ and H6′).

Two-photon excitation (740 nm, 0.75 W) of a d_6-DMSO solution of **1** in an NMR tube (14 mM, 0.6 mL) led to the appearance of *cis* isomer peaks in the NMR spectrum. This result was achieved after only 90 min irradiation; it was assumed to be due to TPE as **1** has no measurable absorbance at 740 nm (Figure 7.5). The effect

of changing several experimental variables was investigated in an attempt to optimise the set-up.

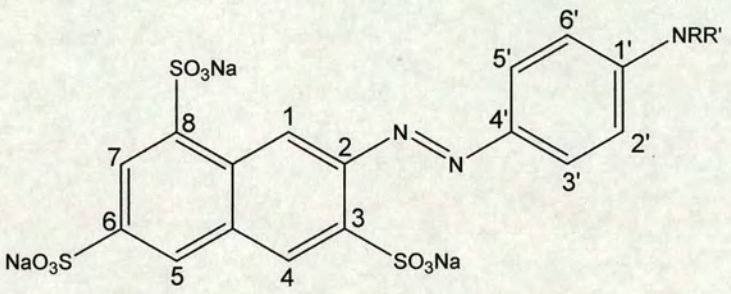

Figure 7.3 Structure of azo-dye **1**

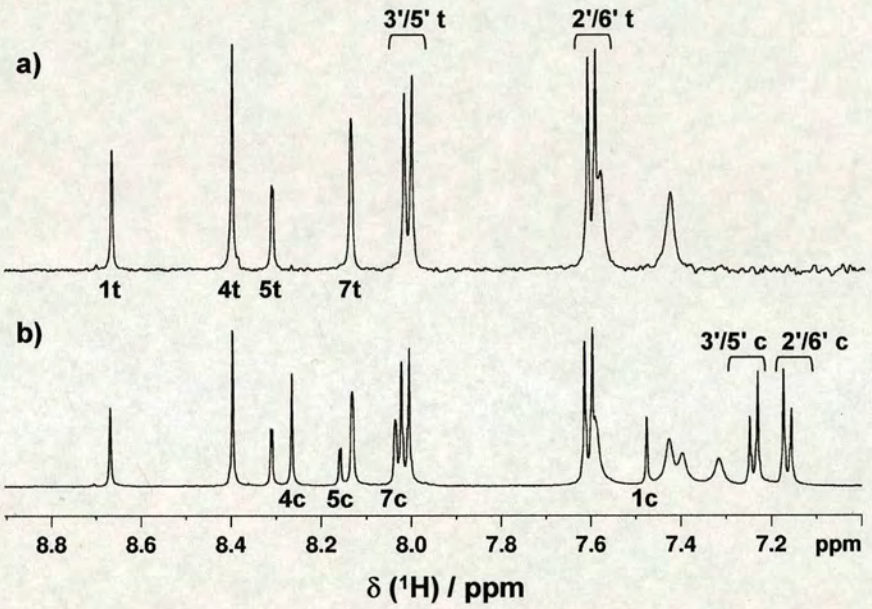

Figure 7.4 ^{1}H NMR spectra of azo-dye **1** in d_6-DMSO (14 mM) a) before irradiation (100 % *trans*) and b) at the photostationary state (54 % *trans* : 46 % *cis*). The peaks are assigned according to the numbered structure in Figure 7.3 with c or t denoting the *cis* and *trans* forms respectively.

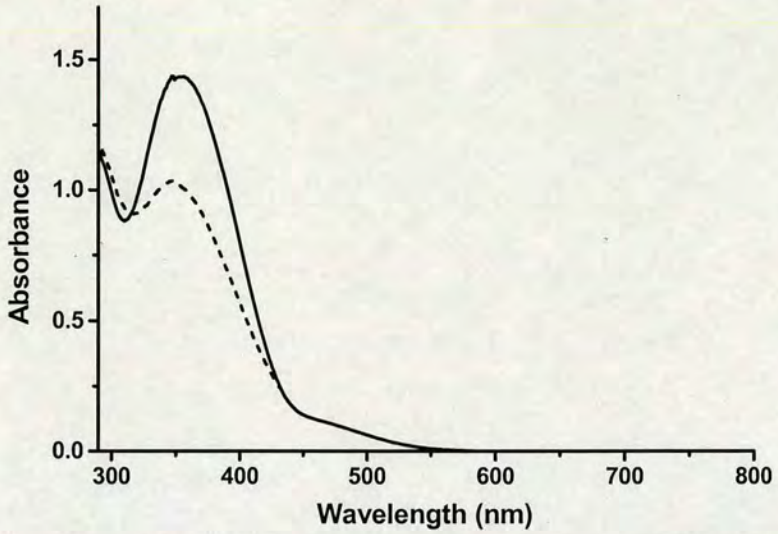

Figure 7.5 Electronic absorption spectrum of azo-dye **1** in DMSO (7×10^{-5} M) before irradiation (solid line) and after one-photon irradiation at 457 nm to the photostationary state (dashed line).

The effects of varying volume and concentration were determined together. A 50 μL, 69 mM sample in d_6-DMSO in an NMR tube was irradiated at 880 nm for 1.5 h, and compared to a 600 μL, 10 mM sample treated identically. A significantly larger proportion of the smaller more concentrated sample was converted to the *cis* isomer (13 % cf. 22 %). Whether mixing was essential was determined by irradiating (740 nm, 0.55 W) two identical samples (150 μL, 14 mM) for 5 min but only stirring one. The stirred sample was found to contain 6.0 % of the *cis* isomer, whereas the static sample only had 4.0 % *cis*. This experiment was repeated with a lower power (285 mW) and again the stirred sample had a larger proportion of the *cis* isomer (1.2 % cf. 0.60 %). Stirring appears to accelerate the reaction but is not essential. As expected the excitation wavelength was found to have a large effect on the level of photoisomerisation. Irradiation at 740 nm (1 W) produced a much larger amount of the *cis* isomer than irradiation at 880 (1 W) for the same length of time (Figure 7.6). The conditions used for TPE of **1** described hereafter were as follows.

- Small volume ≤ 150 μL
- High concentration ≥ 14 mM
- Stirred in an NMR tube (with magnetic stirrer bars 2 mm)
- λ = 740 nm

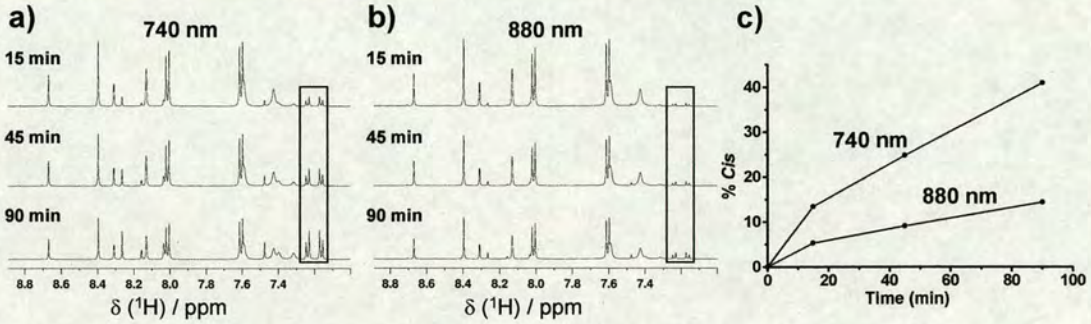

Figure 7.6 Dependence of the two-photon wavelength on the rate of photoisomerisation. ^{1}H NMR spectra of **1** in d_6-DMSO after irradiation at a) 740 nm and b) 880 nm for 15, 45, 90 min. The boxed areas highlight some of the emerging *cis* isomer peaks. c) Comparison of the percentage of *cis* isomer produced at the two different wavelengths.

7.3.2.1 Rate of Reaction

The photostationary state (PSS) is the point where the forward ($k_1(h\nu)$) and backward ($k_{-1}(h\nu, \Delta)$) reaction rates are equal, and further irradiation does not change the *cis:trans* ratio. It can be expressed according to equation **1**.

$$trans \underset{k_{-1}(h\nu, \Delta)}{\overset{k_1(h\nu)}{\rightleftharpoons}} cis \qquad (\mathbf{1})$$

The rate constants $k_1(h\nu)$ and $k_{-1}(h\nu)$ are rate constants for the photoisomerisation process, the combined process of photoexcitation (absorption) followed by excited state isomerization. The integrated rate law for approach to the PSS is given by equation **2**,

$$[cis](t) = [cis](\text{PSS}) - [[cis](\text{PSS}) - [cis](0)] \exp(-k_p t) \qquad (\mathbf{2})$$

where $[cis](t)$, $[cis](0)$ and $[cis](\text{PSS})$ are the concentrations of the *cis* form present at time t, at time 0, and at the PSS, respectively, and the rate constant k_p is the sum of the rate constants for the forward and reverse reactions, $k_1(h\nu)$ and $k_{-1}(h\nu, \Delta)$.

Seven samples (150 μL, 14.2 mM) were irradiated at 740 nm (1.1 W) for various lengths of time (1, 5, 10, 20, 52, 85 and 116 min). As analysis of the samples by NMR spectroscopy required the addition of 450 μL of d_6-DMSO, it was not possible to irradiate, analyse, then continue irradiation, so each point was measured starting from 0 h with a fresh sample. The time course results were plotted (Figure 7.7)[28] and fitted to the rate law (Equation **2**), giving values of [*cis*](PSS) = 54 % and k_p = 7.594 × 10^{-4} s^{-1}. The value of $k_{-1}(\Delta)$ has been previously determined[29] by monitoring the reversion of the PSS to the thermal equilibrium (100 % *trans*), it was found to be 2.4 × 10^{-6} s^{-1} and so makes a negligible contribution to k_p. Since there was no evidence of any additional thermal effects during irradiation, which is most likely due to the lack of one-photon absorption at the excitation wavelength, k_p is the sum of the photochemical rate constants only. The equilibrium constant at the PSS, $k_1(h\upsilon)$ / $k_{-1}(h\upsilon)$ is 0.54 / 0.46, and so the photochemical rate constants are $k_1(h\upsilon)$ = 4.1 × 10^{-6} s^{-1} and $k_{-1}(h\upsilon)$ = 3.5 × 10^{-6} s^{-1}.

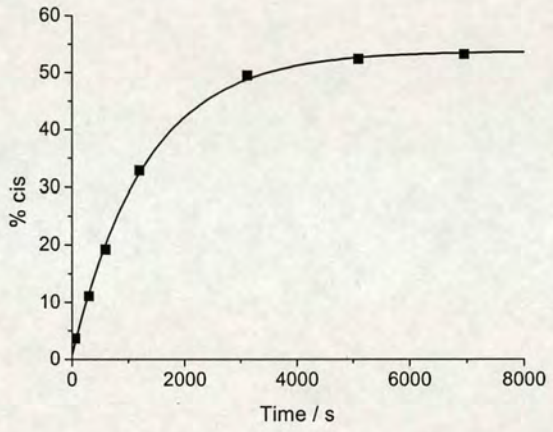

Figure 7.7 Time course of two-photon photoisomerisation upon irradiation at 740 nm (1.1 W) as determined by ^{1}H NMR spectroscopy. The solid curve is the fitted integrated rate law (Equation **2**).

7.3.2.2 Two-Photon or One-Photon Excitation?

Confirmation that the observed photoisomerization was definitely due to the absorption of two photons (not OPE at 740 nm) was provided in two ways.[28] The first method involved irradiating two identical samples (100 μL, 22 mM) under the same conditions (740 nm, 1.2 W), except that for one the Ti:Sapphire laser was

operated in continuous-wave mode (i.e. one-photon mode). For this sample no conversion to the *cis* isomer was seen whereas 3.5 % *cis* isomer was seen for the sample irradiated by the laser while mode-locked.

The second method involved monitoring the initial rate of photoisomerisation as a function of the laser power. For two-photon processes the initial rate has a nonlinear dependence upon the power, and plotting a logarithmic graph of the results will give a straight line with a gradient of two.[15] The initial rate of photoisomerisation was measured at 7 different powers on 14 mM (150 μL) samples. The results were plotted as described above (Figure 7.8) and fitting a straight line gave a gradient of 1.7 ± 0.1. However, using only the data for low power excitation (up to ca. 400 mW), the slope of the ln–ln plot is 2. Samples were irradiated in an NMR tube for 1.5 - 50 min to give < 5 % conversion in each case (typically 2 - 4 %). The low conversion ensured that initial rate conditions were applicable. The relative conversion was then calculated by normalizing the data with respect to irradiation time.

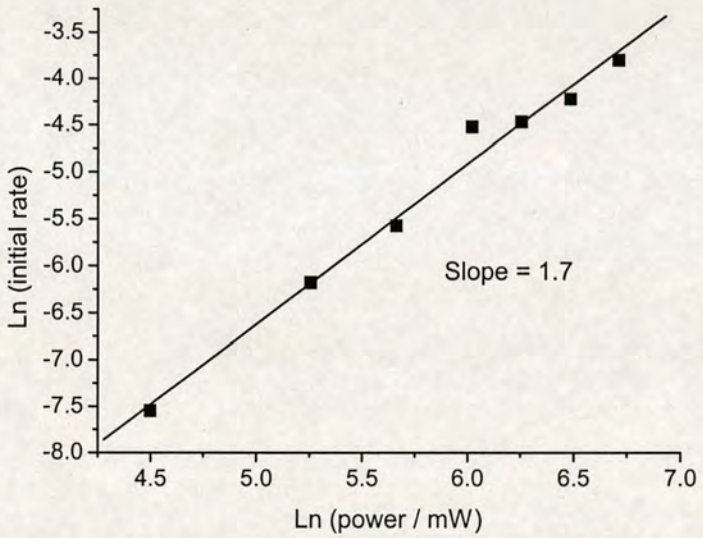

Figure 7.8 Dependence of the initial rate of *cis* isomer formation on the average laser power at 740 nm, as monitored by ^{1}H NMR spectroscopy. For a 160 fs pulse, at a repetition rate of 76 MHz, an average power of 100 mW corresponds to an instantaneous peak power of 10 kW. The solid line shows the best straight line fit to the data ($R = 0.99$).

7.3.3 Pt^{IV} Complexes

7.3.3.1 *Trans, trans, trans*-$[Pt(N_3)_2(OH)_2(NH_3)_2]$

Activation of *trans, trans, trans*-$[Pt(N_3)_2(OH)_2(NH_3)_2]$ by two-photon irradiation was attempted in both UV cuvettes and NMR tubes. No reaction was seen for TPE of samples contained in cuvettes.

Irradiations in NMR tubes were carried out using the set-up and conditions optimised for azo-dye **1** (i.e. small volume, high concentration and stirring). The Pt^{IV} compound was labelled with ^{15}N-ammonia to enable the reaction to be followed by 1D [^1H] and 2D [^1H,^{15}N] HSQC NMR spectroscopy. A 14 mM (100 μL) sample in 90 % H_2O / 10 % D_2O was irradiated at 720 nm (0.2 W) for 6 h, 395 μL H_2O, 55 μL D_2O and 2 μL dioxane were added before analysis. New Pt^{IV} peaks were observed after the pH was adjusted to 5. This reaction was repeated with 2 molar equivalents of 5′-GMP added, the power was increased to 400 mW and the sample irradiated for 5.5 h. Analysis by NMR spectroscopy showed 3 new Pt^{II} peaks, 10 % of *trans, trans, trans*-$[Pt(N_3)_2(OH)_2(NH_3)_2]$ had been reduced and bound to 5′-GMP.

7.3.3.2 *Cis, trans*-$[Pt(en)I_2(OAc)_2]$

TPE of *cis, trans*-$[Pt(en)I_2(OAc)_2]$ (Figure 7.9a) was followed by both UV-visible and NMR spectroscopy. A sample (0.4 mM, 0.5 mL) in methanol was irradiated in a cuvette at 796 nm (650 mW). The absorbance band centred at 400 nm (Figure 7.9b) decreased indicating that a reaction had taken place. The spectra were measured after 2 h and 3.5 h. A dark control was treated identically and placed beside the irradiated sample during irradiation, no decrease of the absorbance band was seen for this sample.

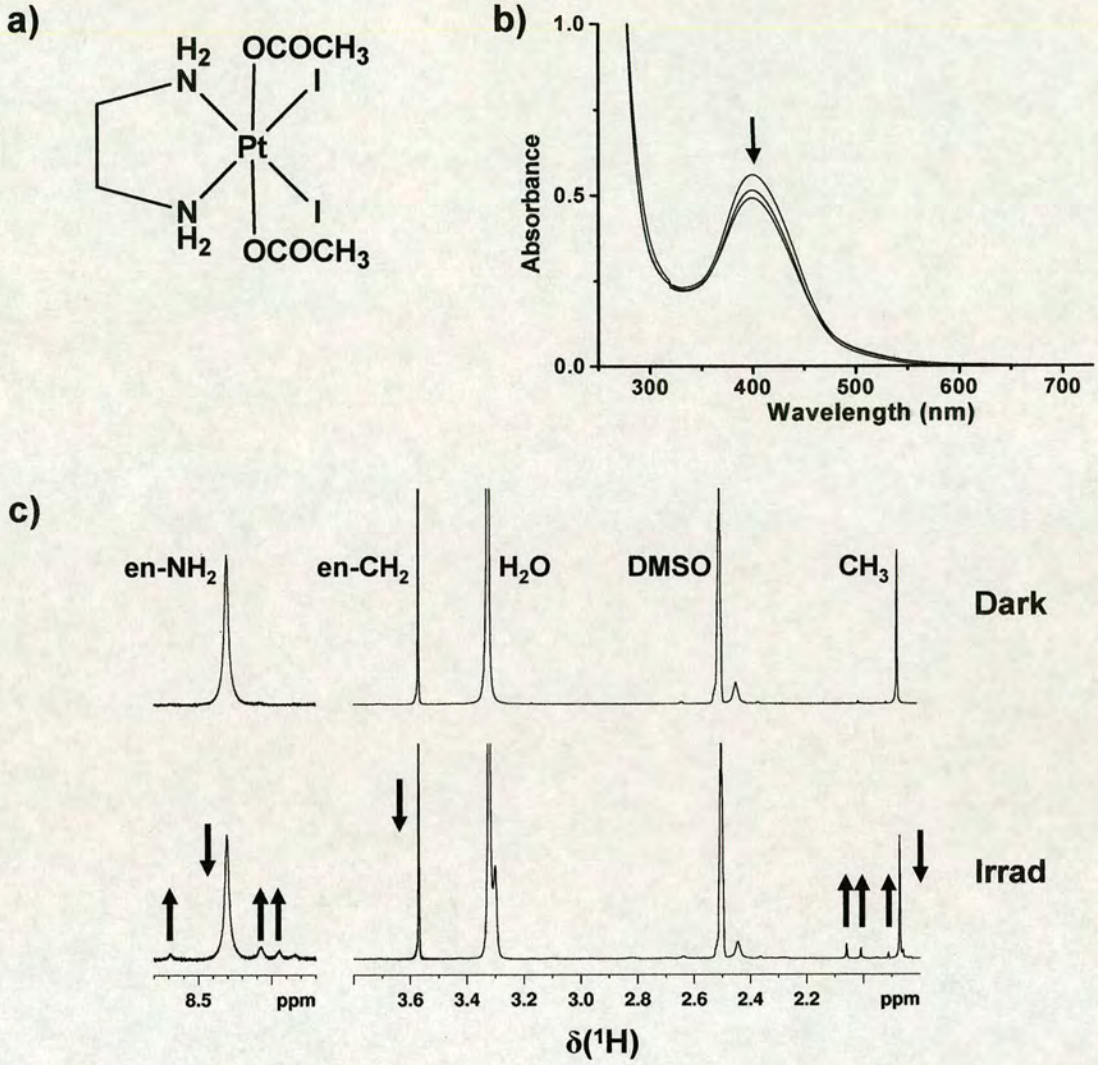

Figure 7.9 Two-photon excitation of *cis, trans*-[Pt(en)I_2($OAc)_2$]. a) Structure of *cis, trans*-[Pt(en)I_2($OAc)_2$] b) UV-visible spectrum in methanol, the LMCT (I → Pt) band at ~ 400 nm decreases upon irradiation. c) NMR spectra in d_6-DMSO, a decrease of the CH_2, CH_3 and NH_2 peaks can be seen after irradiation, new peaks in the CH_3 and NH_2 region are also visible.

Cis, trans-[Pt(en)I_2($OAc)_2$] in d_6-DMSO (4.7 mM, 150 μL) was irradiated at 790 nm (0.7 W) in an NMR tube for 134 min whilst stirring. A dark control was placed beside the sample being irradiated. Figure 7.9 shows new peaks have appeared in the irradiated sample; these peaks are in the same position as those produced by OPE (results not shown).

To determine whether the observed photoreactions were definitely a result of TPE, two identical samples were irradiated (720 nm, 0.75 W, 3 h) one with the laser in continuous-wave mode (OPE) and the other with the laser mode-locked (TPE). Upon analysis by 1D [^{1}H] NMR spectroscopy it was found that both samples had undergone a reaction and produced new species in the same amounts. A dark control was also set-up but this sample contained no new peaks after 3 h. This means that the photoreactions observed so far for the platinum complexes are probably more likely to be a result of one-photon absorption at longer wavelengths.

7.3.4 Three-Photon Excitation

7.3.4.1 *Trans, trans, trans*-[$Pt(N_3)_2(OH)_2(py)(^{15}NH_3)$]

Three-photon excitation of *trans, trans, trans*-[$Pt(N_3)_2(OH)_2(^{15}NH_3)(py)$] (8.4 mM) in the presence of 2 molar equivalents of 5′-GMP was attempted with the OPO laser. Irradiation of 150 μL at 900 nm (0.7 W) was carried out for 7 h, the sample was made up to 0.6 mL with a 90 % H_2O / 10 % D_2O solution containing 2 μL dioxane (1 %) and analysed by 1D [^{1}H] and 2D [^{1}H,^{15}N] HSQC NMR spectroscopy. No new peaks were seen indicating that no photoreaction has taken place.

7.3.4.2 *Trans, trans, trans*-[$Pt(N_3)_2(OH)_2(^{15}NH_3)_2$]

The above reaction was repeated with *trans, trans, trans*-[$Pt(N_3)_2(OH)_2(^{15}NH_3)_2$] (9.9 mM) and 2 molar equivalents of 5′-GMP, but again no photoactivation was observed.

7.3.4.3 *Cis, trans*-[$Pt(^{15}N\text{-en})(N_3)_2(OH)_2$]

Three-photon excitation of *cis, trans*-[$Pt(^{15}N\text{-en})(N_3)_2(OH)_2$] (3 mM) and 5′-GMP (6 mM) was also attempted as described above but again was unsuccessful.

7.4 Discussion

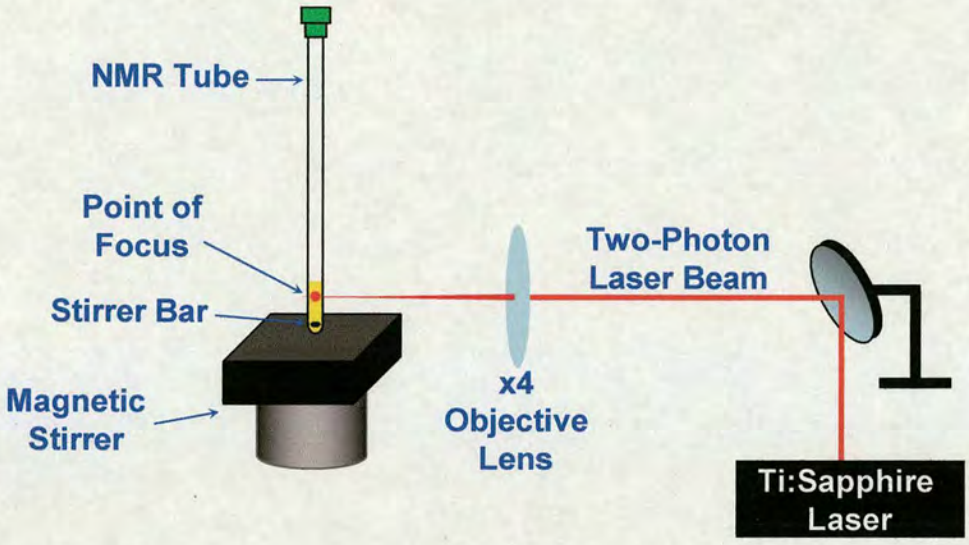

Figure 7.10 Experimental set-up for two-photon excitation of a sample in an NMR tube, using the Ti:Sapphire laser.

7.4.1 *Cis, trans*-[Pt(en)$(N_3)_2(OH)_2$]

Cis, trans-[Pt(en)$(N_3)_2(OH)_2$] was chosen over *cis, trans, cis*-[Pt$(N_3)_2(OH)_2(NH_3)_2$] for these studies due to its slightly higher extinction coefficient (ε_{max} = 14,300 cf. 13,700 $M^{-1}cm^{-1}$). The first experiment involved the OPE of *cis, trans*-[Pt(en)$(N_3)_2(OH)_2$] with the Ti:Sapphire laser. The rate of reaction was compared with that achieved using the argon:krypton laser.

There was a large difference in the powers used, and a possible reason why roughly the same effect can be seen is that the Ar:Kr laser is equipped with a fibre optic. This is used to deliver the light into the sample, and may mean the beam is not as focussed as that of the Ti:Sapphire laser and therefore power is being lost

All two-photon irradiations of *cis, trans*-[Pt(en)$(N_3)_2(OH)_2$] were unsuccessful. Many different experimental conditions were tried (Table 7.1), and samples were analysed by both UV-visible and NMR spectroscopy. The 2-photon cross sections for these types of complexes are not known. However if they are low, smaller sample

volumes would be needed to observe the photochemistry. Also 2-photon absorption may not occur at double the one-photon wavelength, although a range of wavelengths was tried.

7.4.2 Azo-Dye

As TPE of various *cis, trans*-[Pt(en)$(N_3)_2(OH)_2$] samples had failed, attention was turned to a new system. The *trans*-to-*cis* photoisomerisation of azo molecules is a well known reaction[30] which involves the conversion of the thermally stable *trans* structure to the *cis* form. Initially the excitation of azo-dye **1** was intended as a quick check on whether the experimental set-up was adequate, however due to some interesting results a more in-depth study was carried out.

The photosimerisation of **1** is reversible, and the back reaction occurs both photochemically and thermally (Equation **1**).[31] The photostationary state is reached when the forward and backward reaction rates are equal. Several studies on azo containing materials using non-resonant excitation have recently been reported,[32-38] however the nature of the photogenerated species, the identity of the excited states involved, and the efficiency of the photoinduced process were not established. The photoisomerisation of azo-dyes is easily followed by ^{1}H NMR spectroscopy as demonstrated by Tait et. al.,[39] and this technique also enables the unambiguous identification of the photoproducts.

Azo-dye **1** (Figure 7.3) was chosen for these studies for several reasons: 1) the one-photon photochemistry had already been investigated, 2) it has a very high absorbance in the required wavelength range (λ_{max} 353 nm), and 3) the half-life ($t_{½}$) of the *cis* isomer is ca. 115 h. The NMR spectra were always recorded immediately after irradiation and a large $t_{½}$ means the amount of thermal reversion to the *trans* state is negligible.

The structure of **1** (Figure 7.3) consists of an azo unit with a substituted phenyl group attached to one azo nitrogen, and a substituted naphthyl group on the other azo nitrogen. R is a methyl group, and R' is a typical "reactive" group to enable the

attachment of the dye to textile fibres. These substituents are not expected to significantly alter the photochemical properties of the parent dye molecule, and they do not interfere with the signals of interest in the ^{1}H NMR spectrum.

TPE was generally carried out at 740 nm where there is no measurable absorbance, however there is a significant one-photon absorbance at 370 nm due to intense π–π^* transitions. Upon irradiation new peaks appear which can all be assigned to the *cis* isomer, indicating no other species are produced. The *cis* peaks are all shifted up-field relative to those of the *trans* isomer. This is because the position of the rings in the *trans* structure means the protons encounter only a local deshielding within the ring plane; however in the *cis* structure the rings are much closer and so the protons are now subject to the additional shielding effect of the other aromatic ring (Figure 7.11).[39]

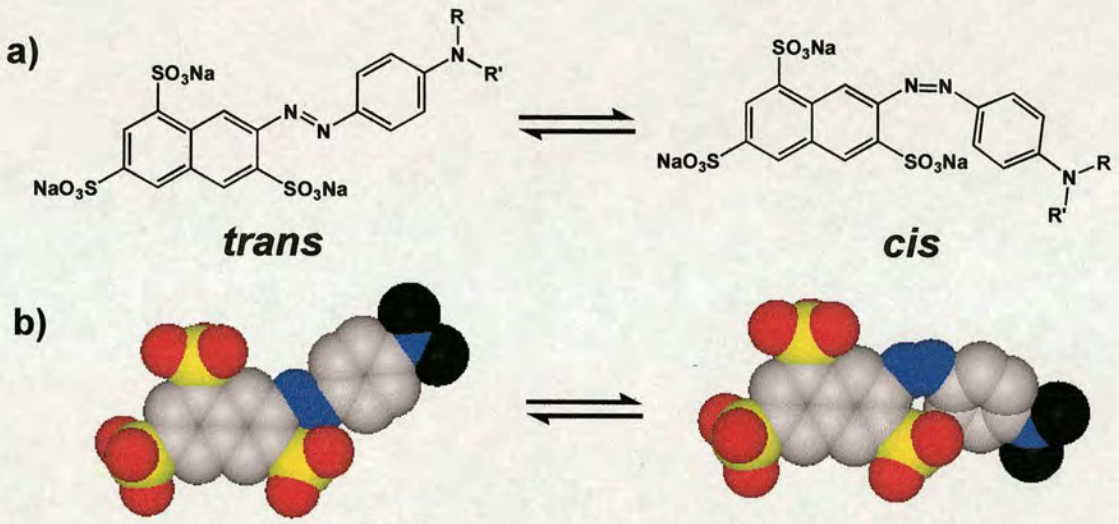

Figure 7.11 *Cis-trans* isomerisation of azo-dye **1**. a) Chemical structure diagram, b) space-fill model which shows the twisting of the phenyl ring in the *cis* structure.

7.4.2.1 Rate of Reaction

The rate of two-photon induced photoisomerisation was determined by measuring the amount of *cis* isomer after various irradiation times. The results were fitted to the integrated rate law (Equation **2**) and compared to those obtained by one-photon irradiation (457 nm, 10 mW) (Table 7.2).

Table 7.2 Data relating to the one- and two-photon induced isomerisation of azo-dye **1**.

Parameter	One-Photon	Two-Photon
λ	457 nm	740 (370) nm
[*cis*](PSS)	29 %	54 %
k_1(hν)	50×10^{-4} s^{-1}	4.1×10^{-4} s^{-1}
k_{-1}(hν)	120×10^{-4} s^{-1}	3.5×10^{-4} s^{-1}
ε_{cis} / ε_{trans}	1	0.3
k_p	170×10^{-4} s^{-1}	7.59×10^{-4} s^{-1}

From the absorbance at 370 and 457 nm, which are taken from the spectra in Figure 7.5, the ratio of the one-photon molar absorption coefficients of the *cis* and *trans* isomers (ε_{cis} / ε_{trans}) were calculated as 1 at 457 nm and 0.3 at 370 nm. If the *trans* isomer is 3.3 times more absorbent at 370 nm than the *cis* isomer, the forward reaction rate will also be increased by the same amount so k_1(hν) will now be 167×10^{-4} s^{-1} and k_p 287×10^{-4} s^{-1}. The expected amount of *cis* isomer which would be produced by one-photon irradiation at 370 nm is therefore 58 %. This is very similar to the value of 54 % obtained by two-photon irradiation, which indicates the ratio of the two-photon cross sections of the two isomers is essentially equivalent to the ε ratio. From these results it is clear the same photochemical mechanism is operating in the two different excitation regimes; this suggests that the same excited states are accessed by both OPE and TPE.

7.4.2.2 Two-Photon or One-Photon Excitation?

To ensure that the *trans-cis* photoisomerisations were due to the absorption of two-photons, the laser was operated in continuous-wave mode at 740 nm. Although the average power was the same as for mode-locked operation, the laser was not pulsed, so the peak laser power was low. Therefore, "simultaneous" absorption of two photons was unlikely. The reaction was carried out as normal and NMR analysis showed no evidence of photoisomerisation.

This result was confirmed by a power-rate study where the initial rate of reaction was measured as a function of power. The initial rate of a two-photon process has a quadratic dependence on the power[1] (initial rate $\propto$ power^2) and therefore the

logarithmic plot has a gradient of 2 (ln(initial rate) $\propto$ 2ln(power)).[31,40] A ln-ln plot of the results (Figure 7.8) gave a slope of 1.7 ± 0.1, however using the data for low power excitation (up to ca. 400 mW) the slope is 2 within error. The small deviation at higher laser powers is most likely due to competing processes, such as saturation.[23]

These results are significant as they have shown by the unambiguous identification of the photoproducts, and measurement of the kinetic parameters that the two-photon reaction closely mimics the one photon process. The photochemical reaction pathways are the same, and the efficiencies of photoisomerisation are similar.[28]

As well as finding widespread use in synthetic dyes and pigments,[31] and photoresponsive biomolecular[41] and supramolecular systems,[42,43] azo molecules are increasingly being used in phototonic-based materials.[44] In particular, polymers doped with azo dyes or containing azo units are promising materials for optical storage,[45] holography,[46] optical switching[47] and non-linear optics.[48] The desirable properties of these materials arise predominantly from photoinduced motions resulting from photoisomerisation of the azo groups. The advantages of using TPE to induce these reactions are similar to those described for PDT. The longer wavelength allows an increased depth of penetration into materials, while the small focal volume can potentially give complete 3D control.

7.4.3 Pt^{IV} Complexes

Now that a successful method had been designed for TPE, attention was turned back to the platinum complexes. Irradiations were generally carried out in NMR tubes on small, concentrated samples (100 – 150 μL, > 14 mM).

Photoactivation of a platinum compound was finally successful for *trans, trans, trans*-$[Pt(N_3)_2(OH)_2(^{15}NH_3)_2]$. Evidence of new Pt^{IV} peaks were observed by 2D [^1H,^{15}N] HSQC NMR spectroscopy, and by repeating the reaction in the presence of 5'-GMP Pt^{II} peaks were seen. Unfortunately, as this reaction was so slow, no time was available to check whether it was definitely TPE by operating the laser in

continuous wave mode. However, in Chapter 6 the photoactivation of this compound was achieved with red light (647.1 nm) and was shown to be relatively efficient (1.5 % reduced and bound to 5′-GMP, 19 mW, 90 min) considering the low absorbance (ε_{647} = 6 $M^{-1}cm^{-1}$) at this wavelength. Therefore these results must be treated as preliminary until they can be confirmed as due to TPE.

Photoactivation of a similar compound, *cis, trans*-$[Pt(en)I_2(OAc)_2]$, was also observed by both NMR and UV-visible spectroscopy. This reaction was faster and so it was possible to operate the laser in both the mode-locked (TPE) and continuous-wave (OPE) state to confirm whether the photoproducts produced were due to TPE. Unfortunately the two different samples both showed evidence of new species in the same amounts, a control sample contained no new products. This means all the photoreactions of *cis, trans*-$[Pt(en)I_2(OAc)_2]$ so far are due to the absorption of one-photon at 720 nm.

These results are perhaps not surprising since *cis, trans*-$[Pt(en)I_2(OAc)_2]$ has a LMCT (I → Pt) band centred at 400 nm (Figure 7.9), which tails out into the red region. Reduction of *trans, trans, trans*-$[Pt(N_3)_2(OH)_2(NH_3)_2]$ with red light has previously been demonstrated and this compound has its LMCT (N_3 → Pt) band at 286 nm.

7.4.4 Three-Photon Excitation

As two-photon excitation of platinum compounds was proving difficult to acheive, a few three-photon excitation experiments were attempted. The advantage of using three photons is that excitation directly into the LMCT (N_3 → Pt) band is possible, a wavelength of 900 nm was used which corresponds to an absorbance at around 300 nm. The extinction coefficients at 300 nm of the two compounds, *trans, trans, trans*-$[Pt(N_3)_2(OH)_2(NH_3)(py)]$ and *trans, trans, trans*-$[Pt(N_3)_2(OH)_2(NH_3)_2]$, are 15,000 and 13,000 $M^{-1}cm^{-1}$ respectively.

The experiments were carried out in the same way as the two-photon excitations, but no photoreactions were observed.

7.5 Conclusions

The reason for the failure to activate Pt^{IV} compounds by two-photon excitation is not known. As the same experimental set-up was successfully used to irradiate azo-dye **1** this is unlikely to be the problem. It is possible that absorbance at the two-photon wavelength (370 nm) was not high enough, TPE is also a much less efficient process than OPE. The two-photon cross-section could also be a problem for these small molecules, alterations of the structure are required to investigate this. However, the incorporation of aromatic chelating ligands, such as bipyridine and phenanthroline (Chapter 3), might help to increase the probability of capturing two photons simultaneously.

New laser systems which are more powerful and efficient are constantly being developed. Indeed it is now possible to obtain lasers which can carry out TPE at low wavelengths (< 300 nm) with very high peak power. Therefore, the activation of platinum-azide compounds could still be achieved by two-photon excitation in the near future.

Two-photon excitation of azo-dye **1** produced some exciting results. By the unambiguous identification of the photoproducts and measurement of the kinetic parameters, it was shown that the two-photon induced reaction closely mimics the one-photon process. This is significant as it demonstrates that TPE using commercial Ti:Sapphire lasers is a practical alternative to the conventional OPE of azo materials.

7.6 References

[1] Göppert-Mayer, M. *Ann. Phys.* **1931**, *9*, 273.

[2] Kaiser, W.; Garrett, C.G.B. *Phys. Rev. Lett.* **1961**, *7*, 229.

[3] He, G.S.; Markowicz, P.P.; Lin, T.-C.; Prasad, P.N. *Nature* **2002**, *415*, 767.

[4] Benec'h, S.; Bachau, H. *J. Phys. B – At. Mol. Opt.* **2004**, *37*, 3521.

[5] Song, H.; Sun, B.; Wang, T.; Lu, S.; Yang, L.; Chen, B.; Wang, X.; Kong, X. *Solid State Commun.* **2004**, *132*, 409.

[6] Hernandez, F.E.; Belfield, K.D.; Cohanoschi, I.; Balu, M.; Schafer, K.J. *Appl. Optics* **2004**, *43*, 5394.

[7] Markowicz, P.P.; He, G.S.; Prasad, P.N. *Opt. Lett.* **2005**, *30*, 1369.

[8] Gryczynski, I.; Piszczek, G.; Gryczynski, Z.; Lacowicz, J.R. *J. Phys. Chem. A* **2002**, *106*, 754.

[9] Parthenopoulos, D.A.; Rentzepis, P.M. *J. Appl. Phys.* **1990**, *68*, 5814.

[10] Dvornikov, A.S.; Rentzepis, P.M. *Opt. Commun.* **1995**, *119*, 341.

[11] Ma, W.; Wu, Y.; Gu, D.; Gan, F. *P. Soc. Photo-Opt. Inst.* **2005**, 5966.

[12] Chon, J.W.M.; Zijlstra, P.; Gu, M.; van Embden, J.; Mulvaney, P. *Appl. Phys. Lett.* **2004**, *85*, 5514.

[13] Denk, W.; Strickler, J.H.; Webb, W.W. *Science* **1990**, *248*, 73.

[14] Denk, W. *Proc. Natl. Acad. Sci. USA* **1994**, *91*, 6629.

[15] Zipfel, W.R.; Williams, R.M.; Webb, W.W. *Nat. Biotechnol.* **2003**, *21*, 1369.

[16] Bhawalkar, J.D.; Kumar, N.D.; Zhao, C.-F.; Prasad, P.N. *J. Clin. Laser Med. Sur.* **1997**, *15*, 201.

[17] Goyan, R.L.; Cramb, D.T. *Photochem. Photobiol.* **2000**, *66*, 141.

[18] Dichtel, W.R.; Serin, J.M.; Edder, C.; Fréchet, J.M.J.; Matuszewski, M.; Tan, L.-S.; Ohulchanskyy, T.Y.; Prasad, P.N. *J. Am. Chem. Soc.* **2004**, *126*, 5380.

[19] Wu, T.; Xu, S.J.; Shen, J.Q.; Song, A.M.; Chen, S.; Zhang, M.H.; Shen, T. *Anticancer Drug Des.* **2000**, *15*, 287.

[20] Lee, H,-Y.; Zhou, Z.-X.; Chen, S.; Zhang, M.-H.; Shen, T. *Dyes Pigments* **2006**, *68*, 1.

[21] Albota, M.; Beljonne, D.; Brédas, J.-L.; Ehrlich, J.E.; Fu, J.-Y.; Heikal, A.A.; Hess, S.E.; Kogej, T.; Levin, M.D.; Marder, S.R.; McCord-Maughon, D.; Perry,

J.W.; Röckel, H.; Rumi, M.; Subramaniam, G.; Webb, W.W.; Wu, X.-L.; Xu, C. *Science* **1998**, *281*, 1653.

[22] Karotki, A.; Kruk, M.; Drobizhev, M.; Rebane, A.; Nickel, E.; Spangler, C.W. *IEEE J. Quantum Electron.* **2001**, *7*, 971.

[23] Xu, C.; Webb, W.W. *J. Opt. Soc. Am. B* **1996**, *13*, 481.

[24] Hopkins, J.; Sibbett, W. *Sci. Am.* **2000**, *283*, 73.

[25] Cheong, W.-F.; Prahl, S.A.; Welch, A.J. *IEEE J. Quantum Electron.* **1990**, *26*, 2166.

[26] Wan, S.; Parrish, J.A.; Anderson, R.R.; Madden, M. *Photochem. Photobiol.* **1981**, *34*, 679.

[27] Kratochwil, N.A.; Zabel, M.; Range, K.-J.; Bednarski, P.J. *J. Med. Chem.* **1996**, *39*, 2499.

[28] Magennis, S.W.; Mackay, F.S.; Jones, A.C.; Tait, K.M.; Sadler, P.J. *Chem. Mater.* **2005**, *17*, 2059.

[29] Tait, K.M. PhD Thesis, University of Edinburgh. **2004**.

[30] Griffiths, J. *J. Chem. Soc. Rev.* **1972**, *1*, 481.

[31] Christie, R.M. *Colour Chemistry*; Royal Society of Chemistry, London, **2001.**

[32] Zhao, J.; Dong, F.; Qu, H.; Ye, P.; Fu, X.; Qiu, L.; Shen, Y. *Appl. Phys. B* **1995**, *61*, 377.

[33] Churikov, V.M.; Lin, J.T.; Wu, H.H.; Lin, J.H.; Huang, T.-H.; Hsu, C.-C. *Opt. Commun.* **2002**, *209*, 451.

[34] Si, J.; Qiu, J.; Zhai, J.; Shen, Y.; Hirao, K. *Appl. Phys. Lett.* **2002**, *80*, 359.

[35] Si, J.; Qiu, J.; Guo, J.; Qian, G.; Wang, M.; Hirao, K. *Appl. Opt.* **2003**, *42*, 7170.

[36] Guo, J.; Si, J.; Qian, G.; Qiu, J.; Wang, M.; Hirao, K. *Chem. Phys. Lett.* **2003**, *378*, 553.

[37] Qian, G.; Guo, J.; Wang, M.; Si, J.; Qiu, J.; Hirao, K. *Appl. Phys. Lett.* **2003**, *83*, 2327.

[38] Xingsheng, X.; Hai, M.; Pei, W.; Zhongcheng, L.; Qijin, Z. *J. Opt. A.: Pure Appl. Opt.* **2002**, *4*, 5.

[39] Tait, K.M.; Parkinson, J.A.; Bates, S.P.; Ebenezer, W.J.; Jones, A.C. *J. Photochem. Photobiol.: A* **2003**, *154*, 179.

[40] Kim, H.-C.; Kreiling, S.; Greiner, A.; Hampp, N. *Chem. Phys. Lett.* **2003**, *372*, 899.

[41] Willner, I. *Acc. Chem. Res.* **1997**, *30*, 347.

[42] Hugel, T.; Holland, N.B.; Cattani, A.; Moroder, L.; Seitz, M.; Gaub, H.E. *Science* **2002**, *296*, 1103.

[43] Balzani, V.; Credi, A.; Marchioni, F.; Stoddart, J.F. *Chem. Commun.* **2001**, *18*, 1860.

[44] Natansohn, A.; Rochon, P. *Chem. Rev.* **2002**, *102*, 4139.

[45] Natansohn, A.; Xie, S.; Rochon, P. *Macromolecules* **1992**, *25*, 5531.

[46] Lagugné, Labarthet, F.; Bruneel, J.L.; Buffeteau, T.; Sourisseau, C. *J. Phys. Chem. B* **2004**, *108*, 6949.

[47] Ikeda, T.; Tsutsumi, O. *Science* **1995**, *268*, 1873.

[48] Yesodha, S.K.; Pillai, C.K.S.; Tsutsumi, N. *Prog. Polym. Sci.* **2004**, *29*, 45.

Appendices

Appendix 1 Structures and Numbering of Platinum Azide Complexes.

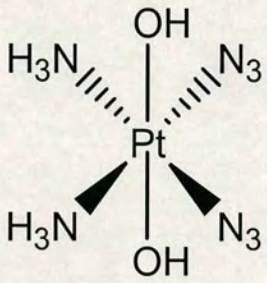

1

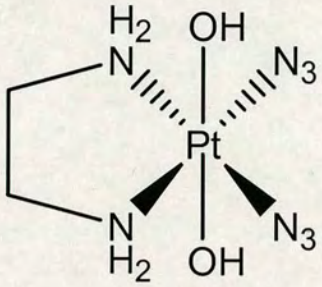

2

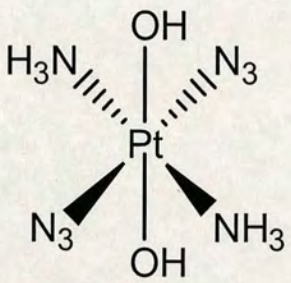

3

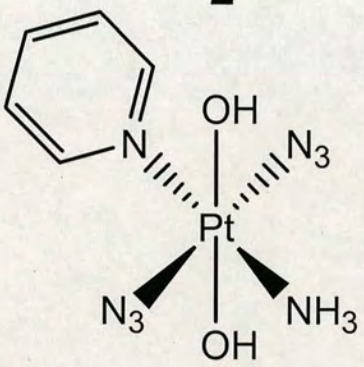

4

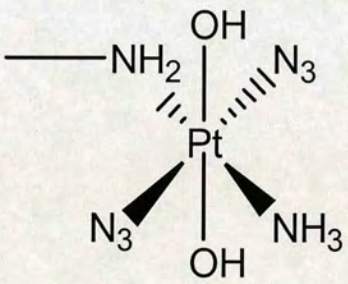

5

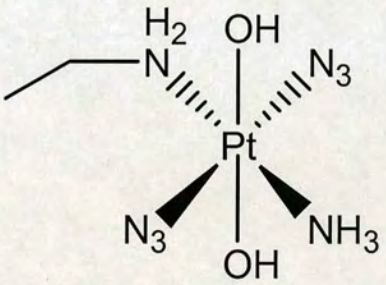

6

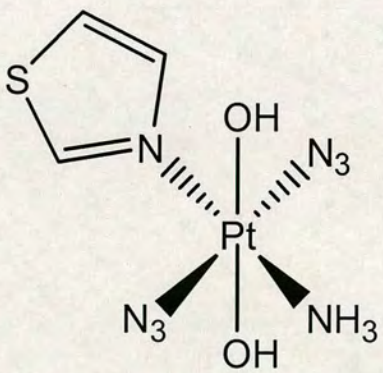

7

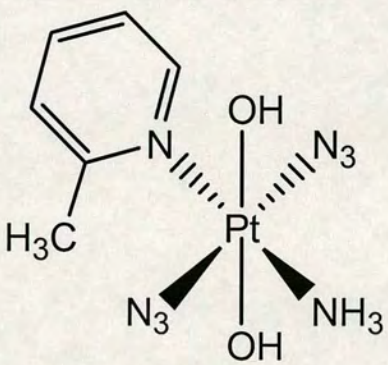

8

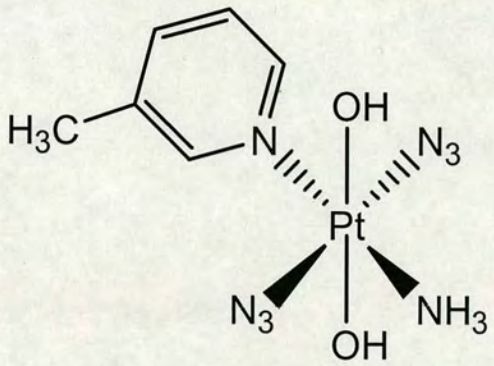

9

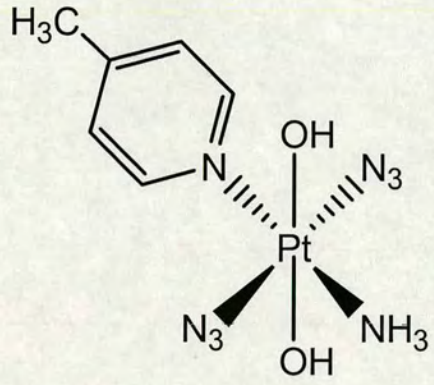

10

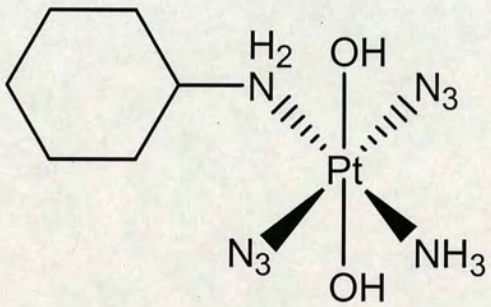

11

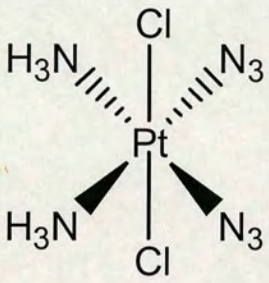

12

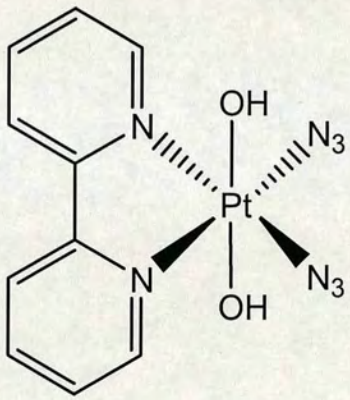

13

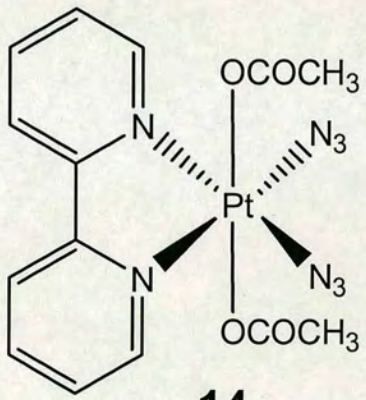

14

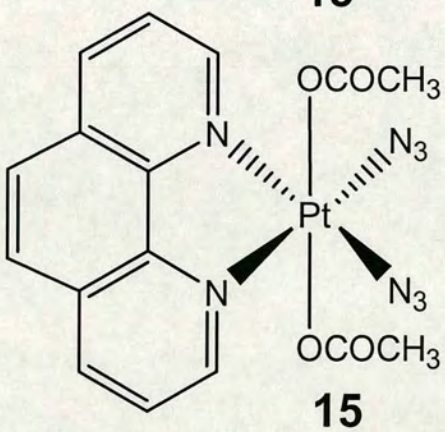

15

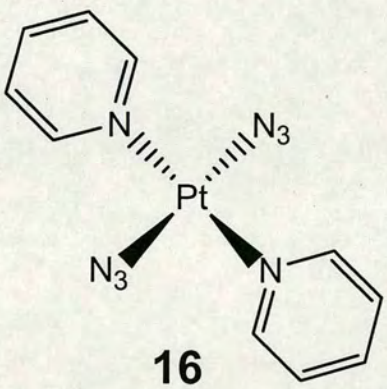

16

Appendix 2 *In Vitro* Phototoxicity Data

Complex	**IC_{50} Value (μM)[a]**					
	HaCaT		**A2780**		**A2780cis**	
	Light	**Dark**	**Light**	**Dark**	**Light**	**Dark**
Complex **1**	174.2	> 288.0[b]	133.3	> 288.0	204.8	> 288.0
Complex **2**	> 267.9	> 267.9	>267.9	> 267.9	>267.9	> 267.9
Complex **3**	154.1	> 288.0	99.1	> 288.0	163.9	> 288.0
Complex **4**	6.1	> 244.3	1.9	> 244.3	16.9	> 244.3
Complex **5**	60.3	> 276.8	39.9	> 276.8	128.7	> 276.8
Complex **6**	68.2	> 266.5	58.4	> 266.5	90.1	> 266.5
Complex **7**	5.8	> 241.0	5.4	187.0	16.1	> 241.0
Complex **8**	55.3	> 236.2	51.0	> 236.2	59.8	> 236.2
Cisplatin	144.0	173.3	151.3	152.0	261.0	229.0
Transplatin	250.0	> 333.3	60.8	131.5	>333.3	> 333.3
Chlorpromazine	9.0	239.7	5.7	193.9	4.9	112.0

a) IC_{50} Value: Concentration of complex that reduced neutral red dye uptake by 50%.

b) > No IC_{50} value determined within concentration range used.

All *in vitro* phototoxicity testing was carried out by Dr. Julie Woods and Dr. Karen Harper at the Photobiology Unit in Ninewells Hospital, Dundee.

Phototoxicity testing was carried out on three different cell lines, HaCaT keratinocytes, A2780 cells and A2780cis cells. HaCaT keratinocytes are a human skin cell line, A2780 cells are a human ovarian carcinoma cell line and the A2780cis cells are a human ovarian carcinoma cell line which is resistant to cisplatin.

For cell irradiation, 2 x 6ft Cosmolux RA Plus (Cosmedico), 15500/100W light sources were used, each filtered to attenuate UVB/UVC wavelengths. Immediately before use, the compounds were dissolved in warm Earle's Balanced Salt Solution (EBSS), sonicated and vortexed to assist dissolution. For experiments, cells were seeded at densities of 3 or 5 x 10^4 cells/cm^2. After overnight incubation, washed cells

were incubated with test compounds in EBSS for 1 h at 310 K / 5%CO_2. Cells were then irradiated with 5 J cm^{-2} glass filtered UVA (1.77 mW cm^{-2}: λ_{max} 365 nm) for 50 min. Test compounds were removed and cells incubated with complete medium for 24 h before assessing phototoxicity. Control plates were treated identically to the test plates and sham irradiated.

Phototoxicity was monitored by measuring the uptake of neutral red dye into viable cells. Briefly, after irradiation cells were washed and then incubated with DMEM containing 5% FCS, 1% NEAA and 50 μg ml^{-1} neutral red dye for 3 h at 310 K/5%CO_2. After this time, cells were rapidly washed with formaldehyde containing 1 % (w/v) $CaCl_2$, and solubilised in 50 % EtOH containing 1 % acetic acid. Absorbance was read at 540 nm against a solubilisation solution as blank. The IC_{50} value was defined as the concentration of compound that inhibited dye uptake by 50% and was calculated using non-linear regression (Graphpad Prism). Goodness of fit was determined from the R^2 values of the curves and 95 % confidence intervals.

Chlorpromazine, cisplatin and transplatin were used as references. Chlorpromazine is an antipsychotic drug which is a member of the phenothiazine family. Phenothiazines are known to have antimutagenic activity upon exposure to light.

The cell test results showed that generally complexes with azides in the *trans* position were more phototoxic than the corresponding *cis* compounds. This is the reason that this work has focussed on developing new complexes with *trans* geometry. One complex has shown remarkable phototoxicity while remaining inactive in the dark, *trans, trans, trans*-[$Pt(N_3)_2(OH)_2$(pyridine)(NH_3)] (**4**). The phototoxic effects of complex **4** are shown in Figure A2.1.

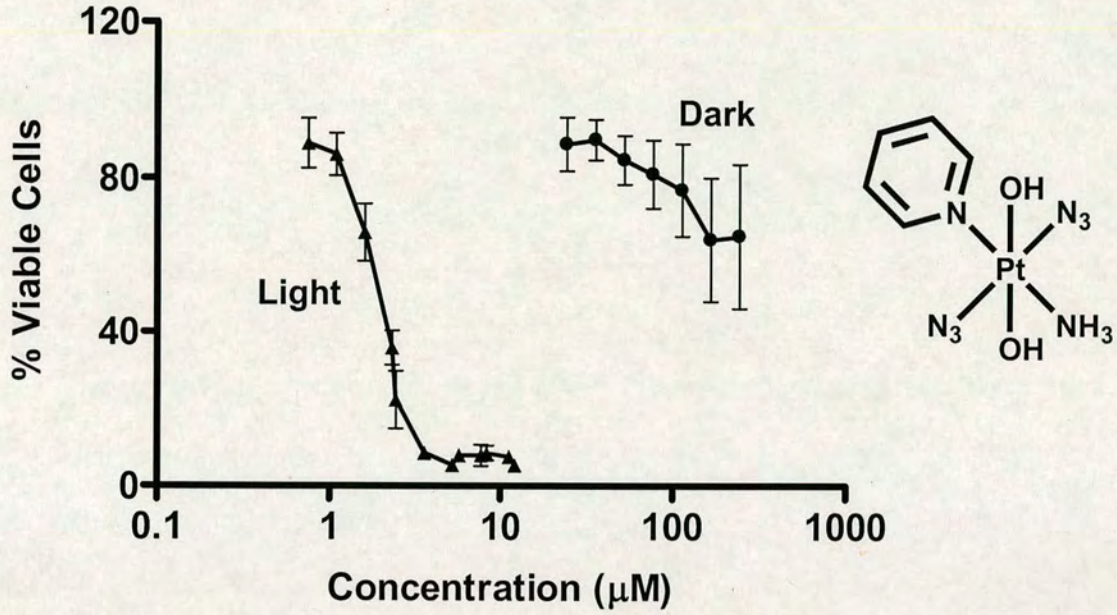

Figure A2.1 Phototoxicity of *trans, trans, trans*-$[Pt(N_3)_2(OH)_2(py)(NH_3)]$ (**4**) towards A2780 human ovarian cancer cells upon irradiation (365 nm) and in the dark.

Appendix 3 Stability Study Results

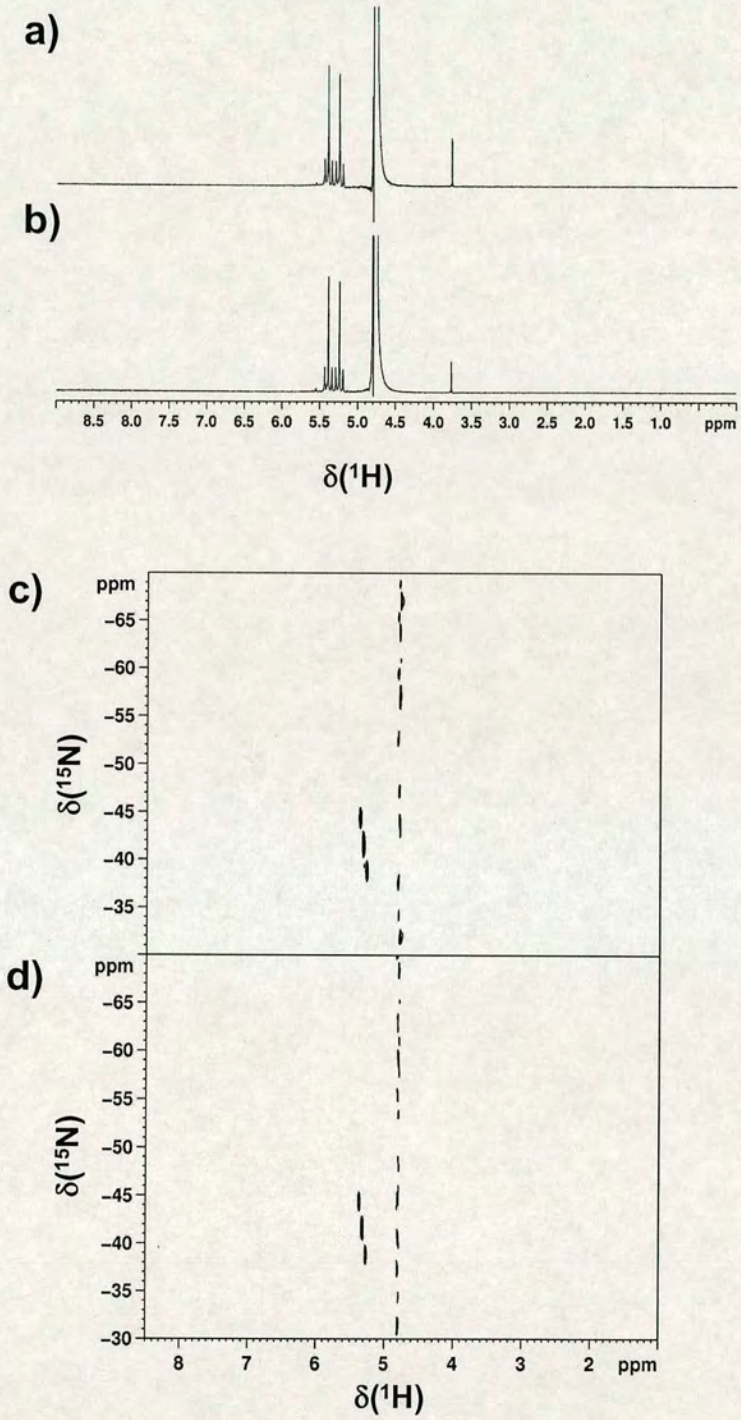

Figure A3.1 1D ^{1}H and 2D [^{1}H,^{15}N] HSQC NMR spectra of *trans, trans, trans*-[$Pt(N_3)_2(OH)_2(^{15}NH_3)_2$] (**3**) (3 mM) in 90 % H_2O / 10 % D_2O were acquired after a, c) 0 h and b,d) 154 d.

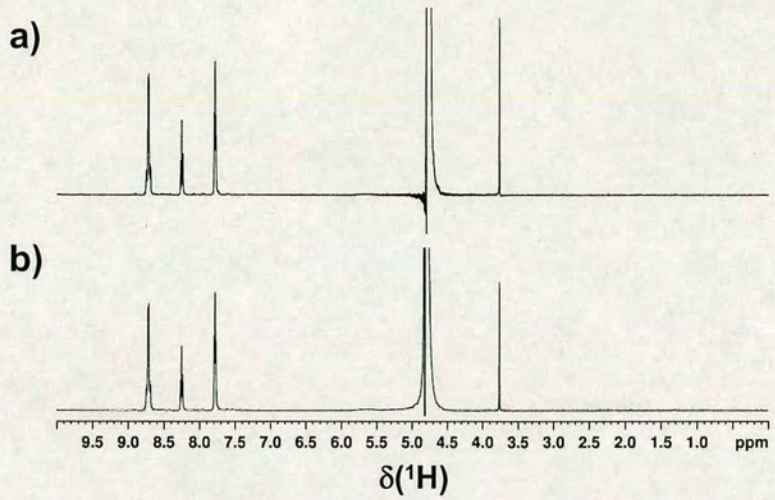

Figure A3.2 1D ^{1}H NMR spectra of *trans, trans, trans*-[$Pt(N_3)_2(OH)_2(NH_3)(py)$] (**4**) (3 mM) in 90 % H_2O / 10 % D_2O were acquired after a) 0 h and b) 154 d.

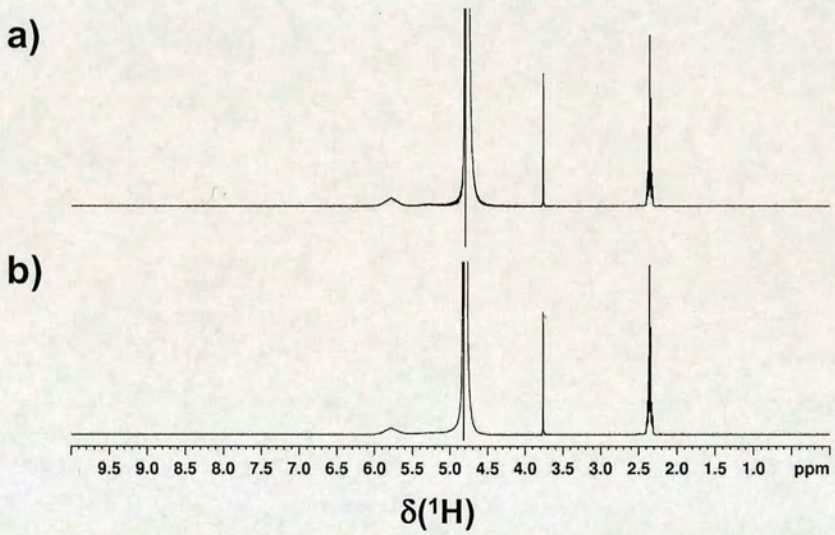

Figure A3.3 1D ^{1}H spectra of *trans, trans, trans*-[$Pt(N_3)_2(OH)_2(NH_3)(MeNH_2)$] (**5**) (3 mM) in 90 % H_2O / 10 % D_2O were acquired after a) 0 h and b) 154 d.

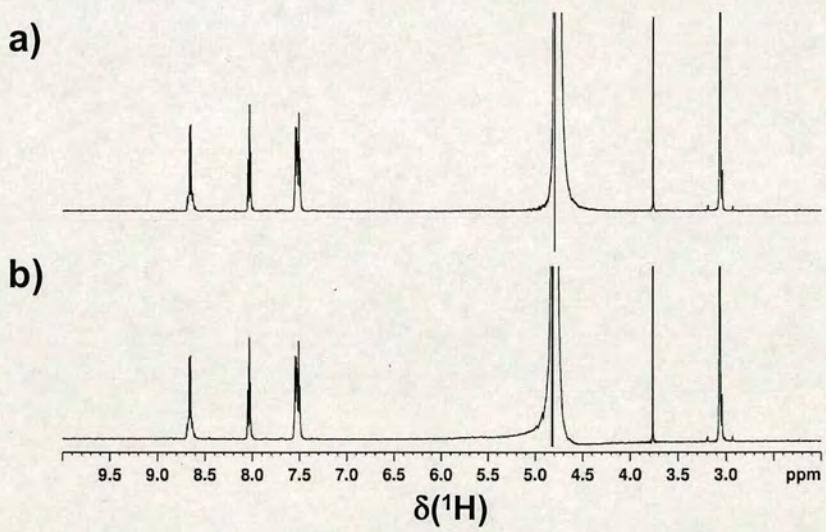

Figure A3.4 1D ^{1}H NMR spectra of *trans, trans, trans*-[$Pt(N_3)_2(OH)_2(NH_3)$(2-pic)] (**8**) (3 mM) in 90 % H_2O / 10 % D_2O were acquired after a) 0 h and b) 154 d.

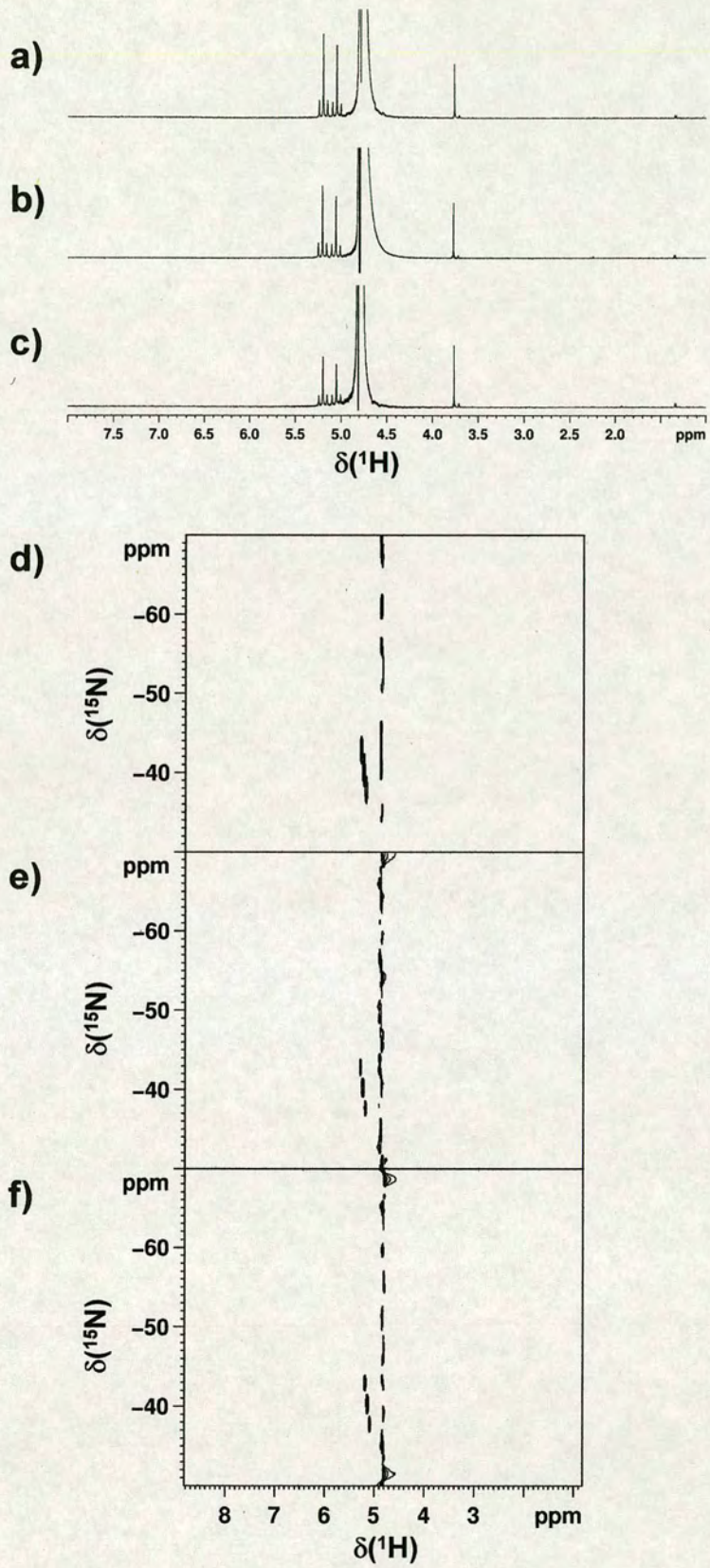

Figure A3.5 1D ^{1}H and 2D [^{1}H,^{15}N] NMR spectra of *cis, trans, cis*-$[Pt(N_3)_2(OH)_2(NH_3)_2]$ (**1**) (3 mM) in the presence of NaCl (100 mM) were acquired after a,d) 0 h, b,e) 12 h and c,f) 154 d.

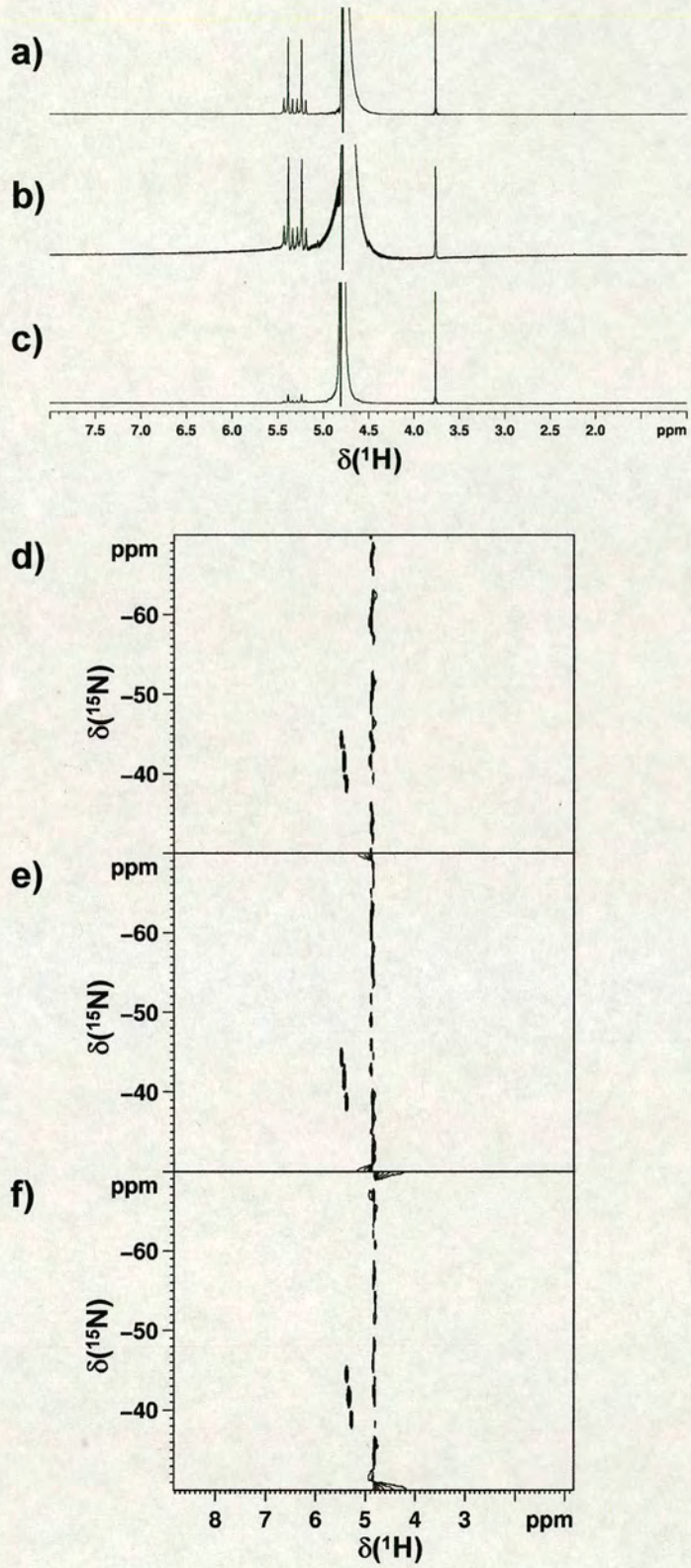

Figure A3.6 1D ^{1}H and 2D [^{1}H,^{15}N] NMR spectra of *trans, trans, trans*-[$Pt(N_3)_2(OH)_2(NH_3)_2$] (**3**) (3 mM) in the presence of NaCl (100 mM) were acquired after a,d) 0 h, b,e) 6 h and c,f) 154 d.

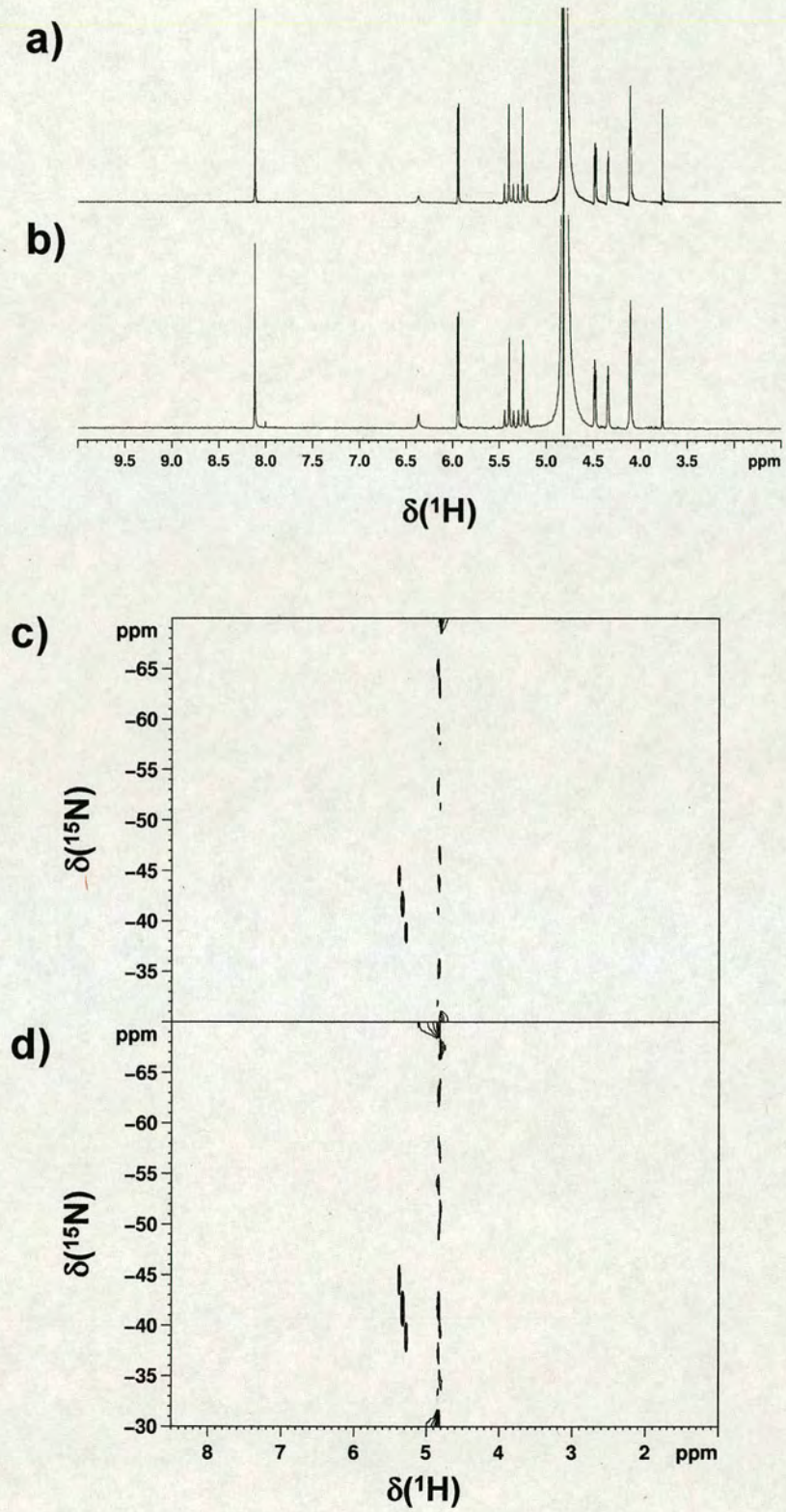

Figure A3.7 1D ^{1}H and 2D [^{1}H,^{15}N] NMR spectra of *trans, trans, trans*-[$Pt(N_3)_2(OH)_2(NH_3)_2$] (**3**) (3 mM) in the presence of 5′-GMP (6 mM) were acquired after a,c) 0 h and b,d) 47 h.

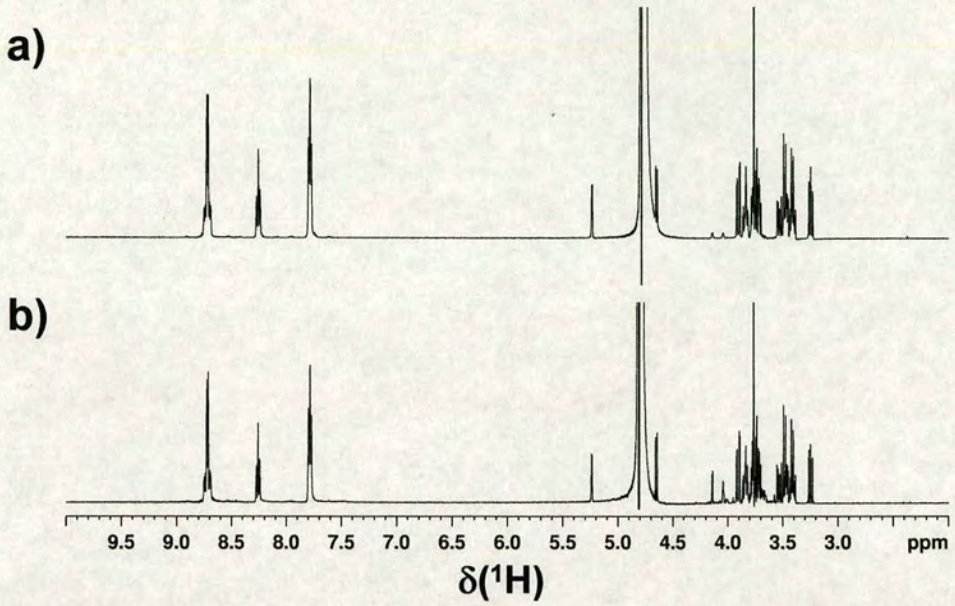

Figure A2.8 1D ^{1}H NMR spectra of *trans, trans, trans*-$[Pt(N_3)_2(OH)_2(NH_3)(py)]$ (**4**) (3 mM) in 90 % EBSS / 10 % D_2O were acquired after a) 0 h and b) 154 d.

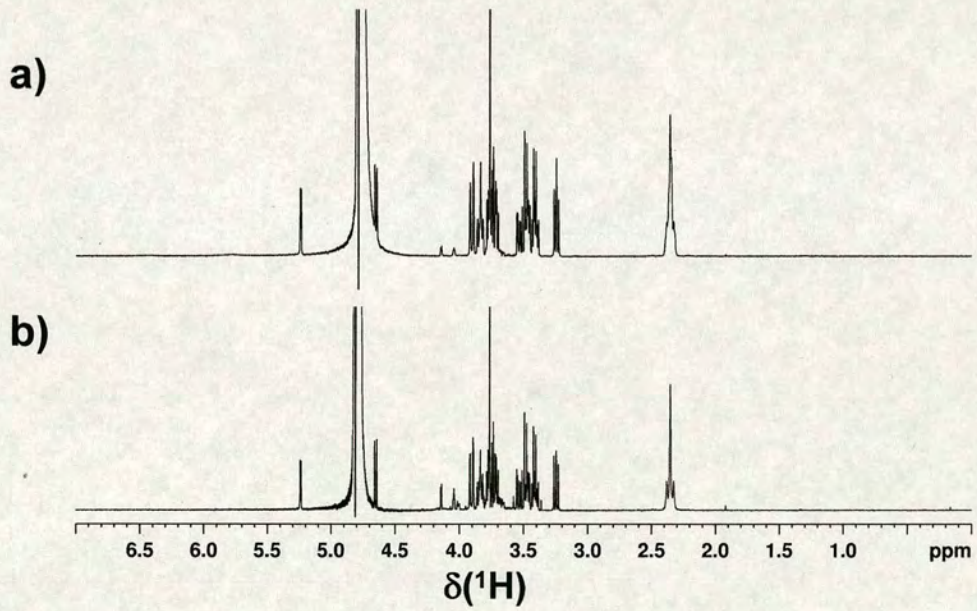

Figure A3.9 1D ^{1}H spectra of *trans, trans, trans*-$[Pt(N_3)_2(OH)_2(NH_3)(MeNH_2)]$ (**5**) (3 mM) in 90 % EBSS / 10 % D_2O were acquired after a) 0 h and b) 154 d.

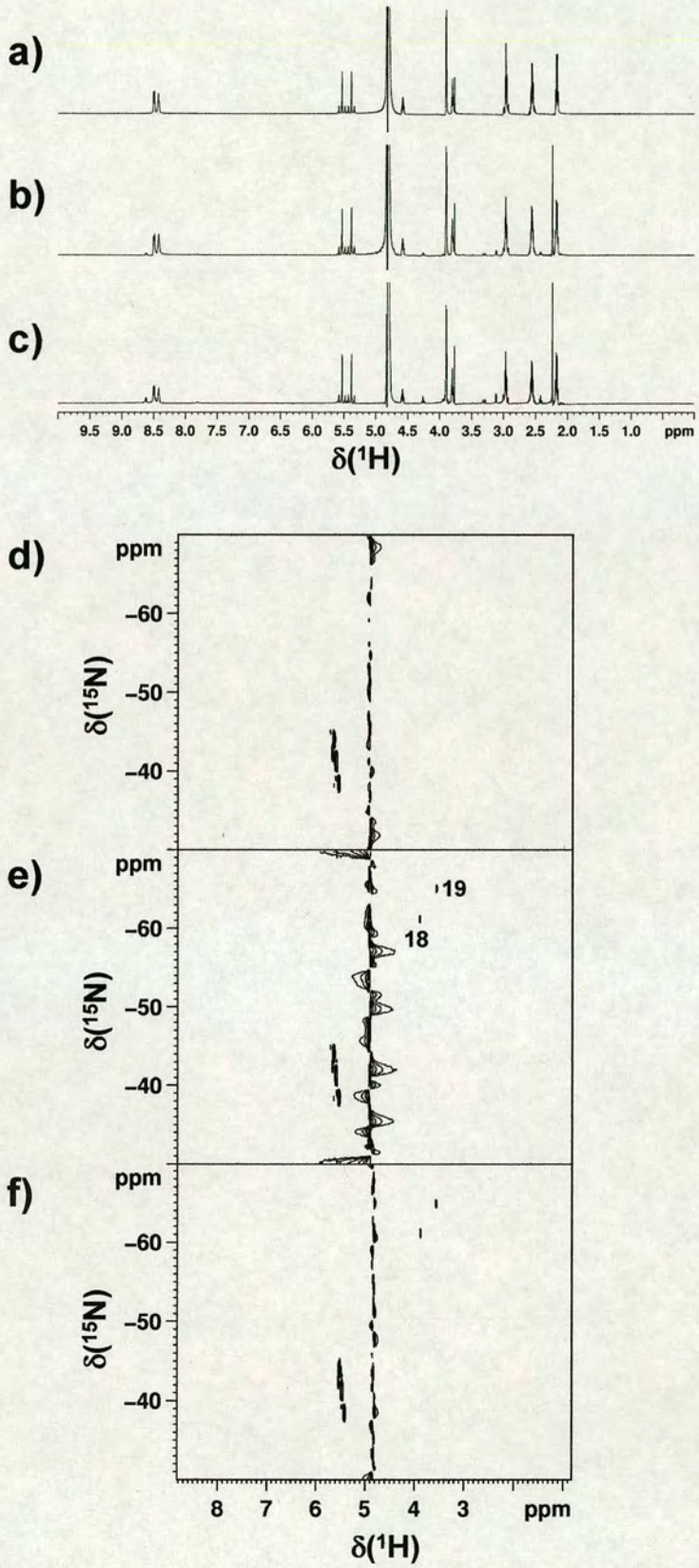

Figure A3.10 1D ^{1}H and 2D [^{1}H,^{15}N] NMR spectra of *trans, trans, trans*-[$Pt(N_3)_2(OH)_2(NH_3)_2$] (**3**) (3 mM) in the presence of reduced glutathione (6 mM) were acquired after a,d) 0 h, b,e) 24 h and c,f) 21 d.

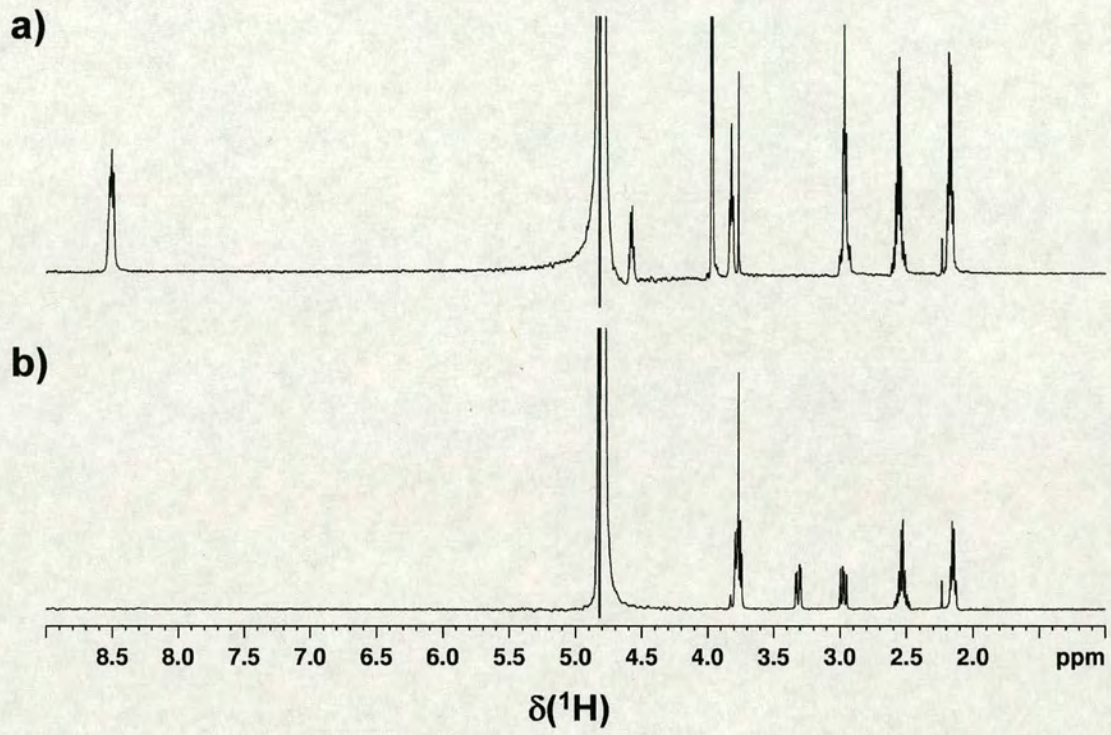

Figure A3.11 1D ^{1}H NMR spectra of a) reduced and b) oxidised glutathione.

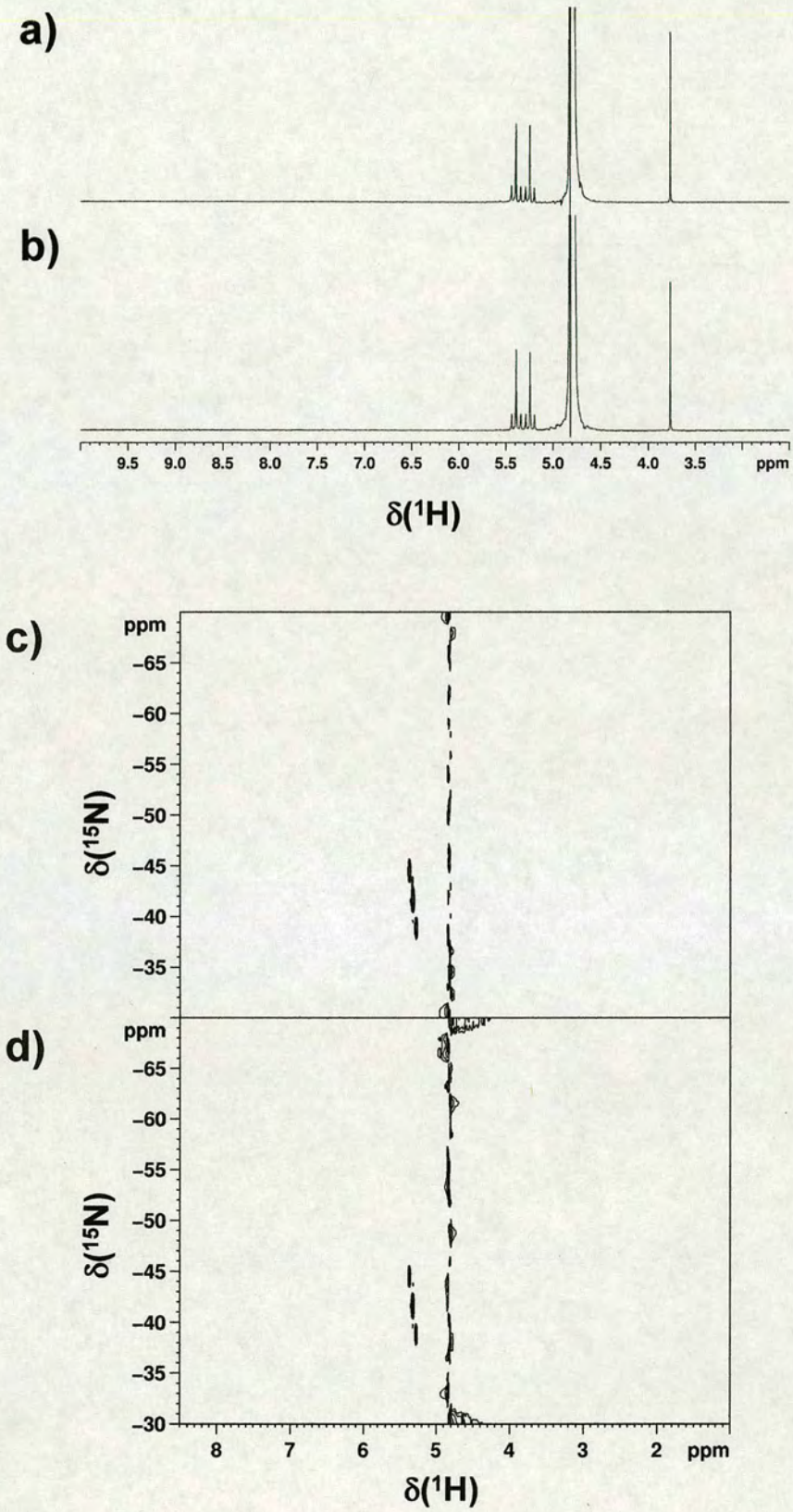

Figure A3.12 1D ^{1}H and 2D [^{1}H,^{15}N] HSQC NMR spectra of *trans, trans, trans*-[$Pt(N_3)_2(OH)_2(^{15}NH_3)_2$] (**3**) (3 mM) in 90 % H_2O / 10 % D_2O at 310 K were acquired after a, c) 0 h and b,d) 21 d.

Courses Attended

1) Transferable skills courses: UNIX I, introduction to HTML, introduction to Excel.
2) Postgraduate NMR spectroscopy lecture course, 2003.
3) Postgraduate Synthesis lecture course, 2003.
4) Laser Safety Course, 2002.
5) Weekly Inorganic Section Seminars during term time, 2002 – 2005.

Conferences Attended

1) 37th USIC conference, University of Strathclyde, UK, September 2003 (poster presentation).
2) 9th International Symposium on Platinum Coordination Compounds in Cancer Chemotherapy, New York, USA, October 2003 (poster presentation).
3) RSC Symposium on Inorganic Chemistry, University of Edinburgh, UK, March 2004 (poster presentation).
4) Scipharm International Pharmaceutical Industry Conference, Edinburgh, March 2004 (poster presentation).
5) European COST programme D20 Conference, Garmisch-Partenkirchen, Germany, September 2004 (oral presentation).
6) 7th European Biological Inorganic Chemistry Conference, Garmisch-Partenkirchen, Germany, September 2004 (poster presentation).
7) 12th International Conference on Biological Inorganic Chemistry, Ann-Arbor, Michigan, August 2005 (poster presentation).
8) 39th USIC conference, University of Glasgow, UK, September 2005 (poster presentation).
9) SET for Britain Annual Presentations, House of Commons, UK, March 2006 (poster presentation).

Publications

Formation of platinated GG cross-links on DNA by photoactivation of a platinum(IV) azide complex.

Jana Kašpárková, Fiona S. Mackay, Viktor Brabec and Peter J. Sadler

Journal of Biological Inorganic Chemistry **2003**, *8*, 741.

Two-Photon-Induced Photoisomerization of an Azo Dye.

Steven W. Magennis, Fiona S. Mackay, Anita C. Jones, Katrina M. Tait and Peter J. Sadler

Chemistry of Materials **2005**, *17*, 2059.

Light-Activated Destruction of Cancer Cell Nuclei by Platinum Diazide Complexes.

Patrick J. Bednarski, Renate Grünert, Michael Zielzki, Anja Wellner, Fiona S. Mackay and Peter J. Sadler

Chemistry and Biology **2006**, *13*, 61.

A Photoactivated *trans*-Diammine Platinum Complex as Cytotoxic as Cisplatin.

Fiona S. Mackay, Julie A. Woods, Harry Moseley, James Ferguson, Alice Dawson, Simon Parsons and Peter J. Sadler

Chemistry – A European Journal **2006**, *12*, 3155.

Photoactivatable Platinum Complexes.

Patrick J. Bednarksi, Fiona S. Mackay and Peter J. Sadler

Current Medicinal Chemistry **2006** (in press).